A SplitCas9-based Screen identifies an Essential Actin-dependent Golgi Protein in *Toxoplasma gondii*

Janessa Christine Grech

Dissertation der Fakultät für Biologie,

Ludwig Maximilians Universität

München, 2023

Statutory Declaration

I hereby declare under oath that the submitted dissertation was written independently and without unauthorized aids. This dissertation was not submitted in whole or in part to any other examination board. I have never previously attempted to submit a dissertation or take a doctoral exam.

Eidesstattliche Erklarung

Ich versichere hiermit an Eides statt, dass die vorgelegte Dissertation selbstständig und ohne unerlaubte Hilfsmittel angefertigt worden ist. Die vorliegende Dissertation wurde weder ganz noch teilweise bei einer anderen Prüfungskommission vorgelegt. Ich habe noch zu keinem früheren Zeitpunkt versucht, eine Dissertation einzureichen oder an einer Doktorprüfung teilzunehmen.

Janessa Christine Grech

Munich, 17.01.2023

Erster Gutachter: Prof. Dr. Michael Boshart

Zweiter Gutachter: Prof. Dr. Markus Meißner

Datum der Abgabe: 17.01.2023

Datum der mündlichen Prüfung: 20.06.2023

Table of Contents

Statutory Declaration I

List of Figures VII

List of Tables IX

List of Abbreviations XI

Abstract XV

Chapter 1. Introduction 1

1.1. *Toxoplasma gondii* 1

1.1.1. Taxonomy 1

1.1.2. The health impact of *Toxoplasma gondii* 2

1.1.3. The lifecycle 2

1.1.4. The asexual tachyzoite – structure and unique features 5

1.1.5. Motility 10

1.1.6. Invasion 11

1.1.7. Replication 12

1.1.8. Egress 14

1.2. Actin and actin-regulatory proteins 14

1.2.1. Actin in model Eukaryotes 15

1.2.2. Actin in Apicomplexan parasites 17

1.3. Vesicular trafficking 20

1.3.1. Vesicular trafficking in model eukaryotes 20

1.3.2. Vesicular trafficking in *Toxoplasma gondii* 24

1.4. Tools to study the parasite 26

1.4.1. The DiCre system 27

1.4.2. CRISPR/Cas9 and the splitCas9 system 28

1.5. Aims of the project 32

Chapter 2. Materials and Methods 35

2.1. Equipment 35
2.2. Computer software 36
2.3. Consumables, and biological and chemical reagents 38
2.4. Microbiology methods 48
2.4.1. Liquid cultures and cryopreservation of bacterial stocks 48
2.4.2. Transformation of bacteria 48
2.5. Molecular biology methods 49
2.5.1. Polymerase chain reaction 49
2.5.2. Agarose gel electrophoresis 51
2.5.3. DNA restriction 51
2.5.4. DNA purification 52
2.5.5. sgRNA preparation 52
2.5.6. Gibson assembly 52
2.5.7. DNA ligation 53
2.5.8. Plasmid DNA isolation from bacteria 53
2.5.9. Preparation of DNA for *Toxoplasma* transfections 54
2.5.10. Genomic DNA isolation from *Toxoplasma* 54
2.5.11. DNA sequencing 54
2.6. Biochemistry methods 55
2.6.1. Indirect immunofluorescence Assays 55
2.6.2. Western Blots 56
2.6.3. TurboID pulldowns 57
2.7. Cell culture 60
2.7.1. Host cell and *Toxoplasma gondii* culture 60
2.7.2. Cryopreservation of *Toxoplasma* 60
2.7.3. *Toxoplasma* transfections 61
2.7.4. Generation of *Toxoplasma* strains 62

2.7.5. splitCas9 and DiCre induction in *Toxoplasma* 64
2.7.6. Basic phenotypic assays 65
2.8. Microscopy 67
2.8.1. Widefield microscopy 67
2.8.2. Time-lapse video microscopy 67
2.8.3. Confocal microscopy and STED microscopy 68
2.8.4. Electron Microscopy 68
2.8.5. Image analysis 68
2.9. Bioinformatics 69
2.9.1. Design of screen sgRNAs 69
2.9.2. Design of sgRNAs for targeted insertion of constructs 69
2.9.3. Design of primers for repair template generation 70
2.9.4. Design of primers for genotyping 70
2.10. Statistics 70
Chapter 3. Results 71
3.1. Screen 71
3.1.1. Establishment of the main parental line 71
3.1.2. Screening of the library and selection of the candidates 73
3.1.3. Analysis of candidates with an egress phenotype 79
3.1.4. Analysis of candidates with a potential F-actin/apicoplast phenotype 81
3.2. Characterisation of TGGT1_301410 83
3.2.1. Database research of TGGT1_301410 83
3.2.2. Subcellular localisation 85
3.2.3. The lytic cycle – invasion, replication, egress, essentiality 91
3.2.4. Knockout phenotypes 94
3.2.5. Endocytosis and secretion 105
3.2.6. TurboID proximity labelling 107

Chapter 4. Discussion 119
4.1. The actin and egress phenotypic screens 119
4.1.1. The setup of the screens 120
4.1.2. Outcome of the actin screen 121
4.1.3. Outcome of the egress screen 123
4.1.4. Limitations of the screen and recommendations for future screens 123
4.2. TGGT1_301410 – ENTH Domain-containing Protein (TgEDP) 126
4.2.1. Subcellular localisation of TgEDP 126
4.2.2. Essentiality of TgEDP 127
4.2.3. TgEDP within the context of vesicular trafficking 127
4.2.4. TgEDP interactors 128
4.2.5. TgEDP within the context of actin dynamics 129
4.2.6. TgEDP's possible role in parasite nutrition 130
4.2.7. Looking at the bigger picture and the outlook 131
4.3. General outlook and concluding thoughts 137
References 141
Appendix 175
Supplementary results 175
Oligos 184
Acknowledgements 207
Curriculum Vitae 209

List of Figures

Figure 1.1 – The lifecycle of *Toxoplasma gondii* 3
Figure 1.2 – The lytic cycle of *Toxoplasma gondii* 5
Figure 1.3 – The cell structure of *Toxoplasma gondii* 6
Figure 1.4 – The micropore in *Toxoplasma gondii* 7
Figure 1.5 – The apical complex of *Toxoplasma gondii* 10
Figure 1.6 – Replication of *Toxoplasma gondii* 13
Figure 1.7 – Actin dynamics involve different actin-regulatory proteins 15
Figure 1.8 – Actin filament distribution in intracellular *Toxoplasma* tachyzoites 18
Figure 1.9 – The process of vesicle budding and fusion 21
Figure 1.10 – An overview of the endosomal-lysosomal system in a typical Eukaryotic cell 23
Figure 1.11 – The DiCre system 28
Figure 1.12 – CRISPR/Cas9-induced double-strand breaks and subsequent DNA repair 30
Figure 1.13 – The splitCas9 in *Toxoplasma gondii* 31
Figure 2.1 – Scheme showing endogenous tagging and floxing strategy 63
Figure 2.2 – Scheme showing strategy for targeted insertion 64
Figure 3.1 – Validation of the splitCas9 system in *Toxoplasma* 72
Figure 3.2 – Knockout phenotypic screen to select for altered actin dynamics, apicoplast segregation and egress mutants 75
Figure 3.3 – Parasites with super-aberrant phenotypes were observed 77
Figure 3.4 – Control genes identified from the screen 78
Figure 3.5 – Egress factors SLF (TGGT1_208420) and CGP (TGGT1_240380) localise to the apical region and are essential 80
Figure 3.6 – Mutants with observable changes to F-actin and apicoplast distribution 82
Figure 3.7 – The phylogeny of TGGT1_301410 as predicted using STRING-db 84
Figure 3.8 – *Tg*EDP (TGGT1_301410) localises close to the *trans*-Golgi 86
Figure 3.9 – Colocalisation of *Tg*EDP (TGGT1_301410) with post-Golgi markers 88
Figure 3.10 – *Tg*EDP (TGGT1_301410) is present within the cytoplasm 90
Figure 3.11 – *Tg*EDP (TGGT1_301410) is essential for parasite survival 93
Figure 3.12 – Knockout of *Tg*EDP (TGGT1_301410) results in *trans*-Golgi fragmentation, but does not affect *cis*-Golgi 96
Figure 3.13 – Knockout of *Tg*EDP (TGGT1_301410) results in the swelling of the Golgi 97

Figure 3.14 – Knockout of *Tg*EDP (TGGT1_301410) results in the fragmentation of some post-Golgi compartments 98
Figure 3.15 – Knockout of *Tg*EDP (TGGT1_301410) does not affect the localisation of micronemes, rhoptries, dense granules, IMC, or apicoplast 100
Figure 3.16 - Knockout of TgEDP (TGGT1_301410) results in altered CPL localisation 102
Figure 3.17 – Knockout of *Tg*EDP (TGGT1_301410) causes mitochondrial fragmentation 103
Figure 3.18 – CPL accumulation is the first phenotype evident upon knockout of *Tg*EDP 104
Figure 3.19 – Dual labelling of SAG1-Halo shows no effect on endocytosis or secretion upon *Tg*EDP knockout 106
Figure 3.20 – Biotinylated proteins in parasites expressing TurboID-tagged *Tg*EDP 109
Figure 3.21 – PCA plot showing the clustering for all TurboID sample replicates 110
Figure 3.22 – Biotinylated proteins identified by mass-spectrometry 113
Figure 3.23 – *Tg*EDP moves along actin filaments 114
Figure 3.24 – Knockout of *Tg*EDP impacts MyoF and actin filaments but not formin2 ... 116
Figure 3.25 – Knockout of formin2 does not affect *Tg*EDP (TGGT1_301410) localisation 117
Figure 4.1 – Strains for future screens 125
Figure 4.2 – Predicted structures of *Tg*EDP, tepsin, and the AP-4 epsilon subunits of *Toxoplasma* and *Homo sapiens* 134
Figure 4.3 – Proteins clustering with CPL within *Toxoplasma* as detected by hyperLOPIT 136
Figure 4.4 – Model illustrating the hypothesised function of *Tg*EDP 139
Figure A.1 – Genotyping and knockout of *Tg*EDP (TGGT1_301410) 179
Figure A.2 - Colocalisation of *Tg*EDP with AP-4 181
Figure A.3 - TGGT1_213392 does not colocalise with TGGT1_301410 182

List of Tables

Table 2.1 – Equipment used during this study 35
Table 2.2 – Computer software and online resources 36
Table 2.3 – Consumables used during this study 38
Table 2.4 – Commercial kits used during this study 38
Table 2.5 – Buffers, solutions, and media prepared or modified in-house 39
Table 2.6 – Commercial chemical and biological reagents 41
Table 2.7 – Primary antibodies used for immunofluorescence assays 42
Table 2.8 – Secondary antibodies used for immunofluorescence assays 43
Table 2.9 – Antibodies used for Western blotting 43
Table 2.10 – Dyes used during this study 44
Table 2.11 – Drugs used during this study 44
Table 2.12 – Plasmids used during this study 45
Table 2.13 – Bacterial strains used during this study 45
Table 2.14 – Mammalian cell lines used during this study 46
Table 2.15 – *Toxoplasma gondii* strains used during this study 46
Table 2.16 – Electroporation settings used 48
Table 2.17 – Q5 PCR reaction mix 50
Table 2.18 – Q5 PCR reaction conditions 50
Table 2.19 – *Taq* PCR reaction mix 50
Table 2.20 – Taq PCR reaction conditions 51
Table 2.21 – Gibson assembly reaction mix 52
Table 2.22 – DNA ligation mix 53
Table 2.23 – Plasmid sample preparations for sequencing 55
Table 2.24 – PCR product preparations for sequencing 55
Table 2.25 – Transfection mix preparations 61
Table 2.26 – Drugs used for drug selection 61
Table A.1 - Table of phenotypes observed during the phenotypic screen 175
Table A.2 - List of screen candidates followed up 178
Table A.3 - Highest enriched proteins obtained from TurboID experiment, selected based on phenotypic score, predicted localisation, and domain prediction (listed in ascending order of phenotypic score) 180

Table A.4 - List of proteins clustering with CPL according to hyperLOPIT, arranged in ascending order of phenotypic score 183
Table A.5 - Curated library of sgRNAs used for the phenotypic screen..... 184
Table A.6 - List of sgRNAs used for downstream characterisation of the screen candidates 198
Table A.7 - List of oligos designed for downstream characterisation of the screen candidates 199

List of Abbreviations

Abbreviation	Meaning
ADF	Actin Depolymerising Factor
AP	Accessory Proteins
AQP	Aquaporin
ASP3	Aspartyl protease 3
ATG	Autophagy related protein
ATP	Adenosine Triphosphate
BDCP	BEACH domain-containing protein
BFA	Brefeldin A
bp	base pairs
CbEm	Chromobody-Emerald Fluorescent Protein
CbEmerald	Chromobody-Emerald Fluorescent Protein
CGP	Conoid Gliding Protein
CI	Calcium Ionophore
COG	Conserved Oligomeric Golgi complex
COPI	Coat Protein complex I
COPII	Coat Protein complex II
CORVET	C core vacuole/endosome tethering complex
CPB	Cathepsin B
CPL	Cathepsin L
CRISPR/Cas9	Clustered Regularly Interspaced Short Palindromic Repeats/ CRISPR-Associated protein 9
CRT	Chloroquine Resistance Transporter
CTCF	Corrected Total Cell Fluorescence
DHFR	Dihydrofolate Reductase
DIC	Differential Interference Contrast
DiCre	Dimerisable Cre recombinase
DMSO	Dimethyl Sulfoxide
DNA	Deoxyribonucleic Acid
DrpB	Dynamin B
EDP	ENTH Domain-containing Protein

ELC	Endosome-Like Compartment
ENTH	Epsin N-terminal Homology
ER	Endoplasmic Reticulum
FACS	Fluorescence-Activated Cell Sorting
FH	Formin Homology
FKBP	FK506 Binding Protein
FNR	Ferredoxin-NADP(+) Reductase
FRB	FKBP–Rapamycin Binding
FRM	Formins
GAC	Glideosome-Associated Connector
GAP	Gliding-Associated Protein
GAPM	Glideosome-Associated Protein with Multiple-membrane spans
GARP	Golgi-Associated Retrograde Protein
GC	Guanylate Cyclase
GFP	Green Fluorescent Protein
GMP	Guanosine Monophosphate
GPI	Glycosylphosphatidylinositol
GRA	Dense Granule protein
GRASP	Golgi Reassembly Stacking Protein
HDR	Homology-Directed Repair
HFF	Human Foreskin Fibroblasts
HOPS	Homotypic fusion and vacuole Protein Sorting
hpi	hours post-induction
IFA	Immunofluorescence assay
IMC	Inner Membrane Complex
INDEL	Insertion or Deletion mutations
LC-MS/MS	Liquid Chromatography with tandem mass spectrometry
MIC	Micronemes
MLC	Myosin Light Chain
MTOC	Microtubule Organising Centre
Myo	Myosin
NA	Numerical Aperture
NCBI	National Center for Biotechnology Information
NEB	New England Biolabs Inc.

NHEJ	Non-Homologous End-Joining
NIH	National Institutes of Health
PA	Phosphatidic acid
PAM	Protospacer Adjacent Motif
PCA	Principal Component Analysis
PCR	Polymerase Chain Reaction
PFA	Paraformaldehyde
PLV	Plant-Like Vacuole or Vacuolar Compartment
ProM2AP	M2AP pro-peptide
Rapa	Rapamycin
RFP	Red Fluorescent Protein
RNA	Ribonucleic Acid
RON	Rhoptry neck protein
ROP	Rhoptry bulb protein
SAG	Surface Antigen
sCas9	Split Cas9
sgRNA	Single Guide RNA
SLF	Signalling Linking Factor
SortLR	Sortilin-Like Receptor
STED	Stimulated Emission Depletion
Tg	*Toxoplasma gondii*
TGN	Trans-Golgi Network
TOM	Translocase of the Outer Mitochondrial membrane
t-SNARE	target Snap-Receptor
UPRT	Uracil Phosphoribosyl Transferase
VAC	Vacuolar Compartment
VHS	VPS-27, Hrs and STAM
VP1	Vacuolar Proton pyrophosphatase
Vps	Vacuolar Protein Sorting
v-SNARE	vesicle Snap-Receptor
WASP	Wiskott–Aldrich Syndrome protein
WHO	World Health Organisation
WT	Wildtype
YFP	Yellow Fluorescent Protein

Abstract

The acto-myosin system of *Toxoplasma gondii* has been shown to be critically involved in transport of vesicular material within this apicomplexan parasite. The filamentous actin network has also been observed to maintain a connection between parasites within a parasitophorous vacuole thus allowing communication between parasites. In an effort to further understand this acto-myosin system and possibly identify novel actin-binding proteins, a knockout phenotypic screen was carried out using an inducible Cas9 system and the actin chromobody as a marker.

In addition to the identification of two novel proteins essential for egress, another protein chosen from this screen is currently being characterised. This protein, TGGT1_301410, localises in close proximity to the *trans*-Golgi and therefore one of the actin polymerisation centres. While it has not yet been shown to be a direct interactor of actin, this protein was observed to be essential for parasite survival. Results suggest that knockout parasites replicate slower despite not having an outright replication defect. TGGT1_301410 was also observed to be crucial for the maintenance of the structure of the *trans*-Golgi body and post-Golgi compartments, its absence leading to the fragmentation of these structures. This fragmentation, however, was curiously not observed to have an impact on the localisation of secreted proteins like the micronemes and rhoptries, with the primary phenotype appearing to be an altered cathepsin L localisation. Biotinylation experiments also showed that this protein comes within close proximity to the parasite's micropore, the hypothesised site of endocytosis. This, in conjunction with altered cathepsin L localisation and mitochondrial fragmentation, seems to suggest a starvation phenotype.

Chapter 1. Introduction

1.1. Toxoplasma gondii

Toxoplasma gondii is an obligate intracellular parasite that is capable of infecting any nucleated cell within a warm-blooded animal (Robert-Gangneux & Dardé, 2012). This chapter will provide an introduction to the parasite, its biology, its impact on global health, and the molecular tools which have been employed to facilitate its study.

1.1.1. Taxonomy

Toxoplasma gondii is classified as a parasite within the Superphylum Alveolata, Phylum Apicomplexa, Class Conoidasida, Order Eucoccidiorida, and Family Sarcocystidae (Adl et al., 2007, 2019; Ruggiero et al., 2015). As it is the only known species within the Genus Toxoplasma, *Toxoplasma gondii* will occasionally be referred to simply as *Toxoplasma* henceforth.

The phylum Apicomplexa consists of more than 6000 known species (Adl et al., 2007). The families within this phylum are Hematozoa, Coccidia, Gregarines and Cryptosporidium. All Alveolates possess an alveolar membrane system around their periphery, directly beneath their plasma membrane (Gould et al., 2008; Harding et al., 2019; Tosetti et al., 2020). In the case of apicomplexans, this alveolar system is referred to as the Inner Membrane Complex, or IMC, and will be discussed in a later section of this introduction chapter.

All apicomplexan species are known to be unicellular parasitic protozoa whose ancestors initially had a symbiotic lifestyle (Arisue & Hashimoto, 2015; van Dooren & Striepen, 2013; Woo et al., 2015a). However, while all apicomplexans are parasites, not all species within the Superphylum Alveolata are parasitic. Other members of this Superphylum include ciliates and dinoflagellates (Adl et al., 2019).

Many apicomplexan parasites cause diseases in a range of host species, including poultry, livestock, and humans. The diseases these parasites cause, including coccidiosis (caused by Coccidia) and besnoitiosis (caused by *Besnoitia spp*.), are therefore both of medical and veterinary relevance, and are also an economic burden (Blake et al., 2020; Cortes et al., 2014; Gilbert et al., 2020; Zintl et al., 2003).

Other parasites with severe health impacts on humans include *Cryptosporidium spp*., a waterborne opportunistic parasite which causes diarrhoea that may even lead to death in small children and immunocompromised individuals (Striepen, 2013), and *Plasmodium spp.,* which is the most lethal apicomplexan to humans and is the cause of malaria (Cowman et al., 2016; White et al., 2014). Toxoplasmosis, the disease caused by *Toxoplasma*, is also of medical and veterinary importance, as is discussed in the next section.

1.1.2. The health impact of Toxoplasma gondii

It is estimated that one third of the human population is infected with *Toxoplasma*. This infection is usually contracted via contaminated foods such as under-cooked meat, or from the parasite's definitive host, the cat (Robert-Gangneux & Dardé, 2012). The majority of post-natal infections in immunocompetent individuals are non-life-threatening, with symptoms being mild and influenza-like. However, there are two contexts in which a relatively harmless infection can become serious; in the case of immunocompetent individuals becoming immunocompromised, and when an acute infection occurs during pregnancy. In the former case, problems arise because latent parasitic cysts become reactivated, and may result in life-threatening toxoplasmic encephalitis. In the latter case, congenital infection can occur in the foetus, leading to potential retinal damage, deafness (De Castro Corrêa et al., 2018; McAuley, 2014), mental retardation (Jones et al., 2003), and miscarriages. It is important to also note, that while common infections do not typically pose a serious risk to the life of individuals, *Toxoplasma* can also cause ocular disease (Park & Nam, 2013). Despite *Toxoplasma* being of such medical importance, no human vaccinations exist, and current treatment has its limitations due to drug resistance and an inability for the body to clear *Toxoplasma* cysts from an infected brain (Konstantinovic et al., 2019).

1.1.3. The lifecycle

Toxoplasma has a dixenous lifecycle, which means that it requires specific hosts for it to carry out its whole lifecycle to completion. The asexual stages of the lifecycle can occur within any warm-blooded intermediate host, while the sexual stages of the lifecycle are only possible within the definitive hosts, felids (Hill & Dubey, 2002; Hunter & Sibley, 2012;

Robert-Gangneux & Dardé, 2012). Transmission is not necessarily restricted to intermediate and definitive hosts. In fact, since it can also occur between intermediate hosts, this is one of the main routes of infection for humans (Robert-Gangneux & Dardé, 2012).

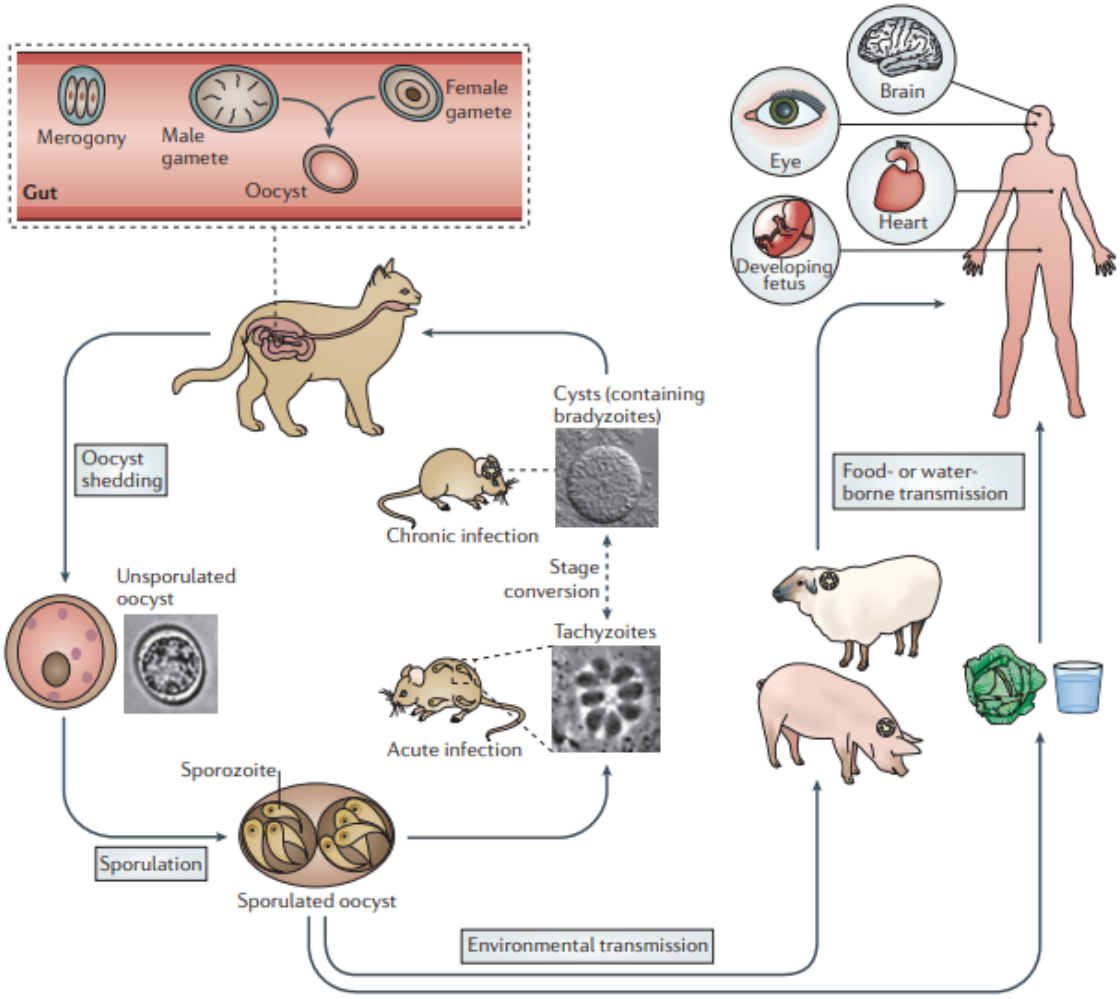

Figure 1.1 – The lifecycle of *Toxoplasma gondii*
Sexual reproduction of *Toxoplasma* gondii takes place in felids, whereas asexual reproduction takes place within the intermediate hosts. Sexual reproduction occurs in the gut epithelium of the felids, wherein the male and female gametes fuse to form oocysts. These oocysts are shed into the environment and depending on the environmental conditions, these oocysts then sporulate. These sporulated oocysts are taken up by intermediate hosts via food- or water-borne transmission, and the sporozoites are released. These invade the gut epithelia of the hosts, differentiate into tachyzoites, and initiate the acute infection. These tachyzoites then disseminate throughout the whole body, eventually differentiating into cyst-forming bradyzoites within different organs, thus developing the chronic infection. Uptake of any of these cysts by felids results in merogony, consequently restarting the lifecycle. Image from Hunter & Sibley, (2012).

The sexual stage

Felids, both domesticated or otherwise, are the definitive host of *Toxoplasma*. They become infected by either consuming other animals carrying the parasite cysts within their flesh, or by coming in contact with faecal material from another feline which is shedding cysts. Following ingestion of contaminated material, these cysts rupture within the cats' digestive systems, and the parasites then replicate via merogony, resulting in both male and female gametes. These gametes are eventually fertilized, creating diploid oocysts which are shed into the environment via the gastro-intestinal tract (Hill & Dubey, 2002; Hunter & Sibley, 2012; Robert-Gangneux & Dardé, 2012).

The environmental stage

The wall of the shed oocysts is multi-layered (Ferguson et al., 1975; Speer et al., 1998), offering enough protection to the encysted parasites that it allows them to survive for months to years, depending on their external environment (Belli et al., 2006; Yilmaz & Hopkins, 1972). This high survivability allows these parasites to infect a multitude of hosts, both intermediate as well as definitive (Hill & Dubey, 2002; Robert-Gangneux & Dardé, 2012). Contamination of water systems has been known to cause outbreaks of toxoplasmosis in humans (Benenson et al., 1982; Bowie et al., 1997). Upon exposure to the external environment, the oocysts sporulate and form sporozoites (Robert-Gangneux & Dardé, 2012). When oocysts are ingested, the released haploid sporozoites infect the host's digestive tract and replicate to form tachyzoites, thus starting in the acute stage of the infection.

The asexual acute and chronic stages

During the acute stage of the infection, the parasites carry out what is known as the lytic cycle. The tachyzoites actively enter host cells, establish a parasitophorous vacuole, and undergo several rounds of replication, with one parasite ultimately resulting in approximately 64-256 parasites. These parasites then egress from the infected host cell, and proceed to glide to, and reinvade, neighbouring host cells, thus initiating a new lytic cycle (Black & Boothroyd, 2000).

When the parasites experience stress as the host immune system attempts to clear the acute infection, the tachyzoites develop into bradyzoites. These bradyzoites are the slow-dividing stage which form cysts in the brain, muscles, and other organs, thus establishing the chronic infection (Blader et al., 2015; Robert-Gangneux & Dardé, 2012). It is this asymptomatic chronic stage which can potentially reactivate and cause encephalitis if the host were to become immunocompromised.

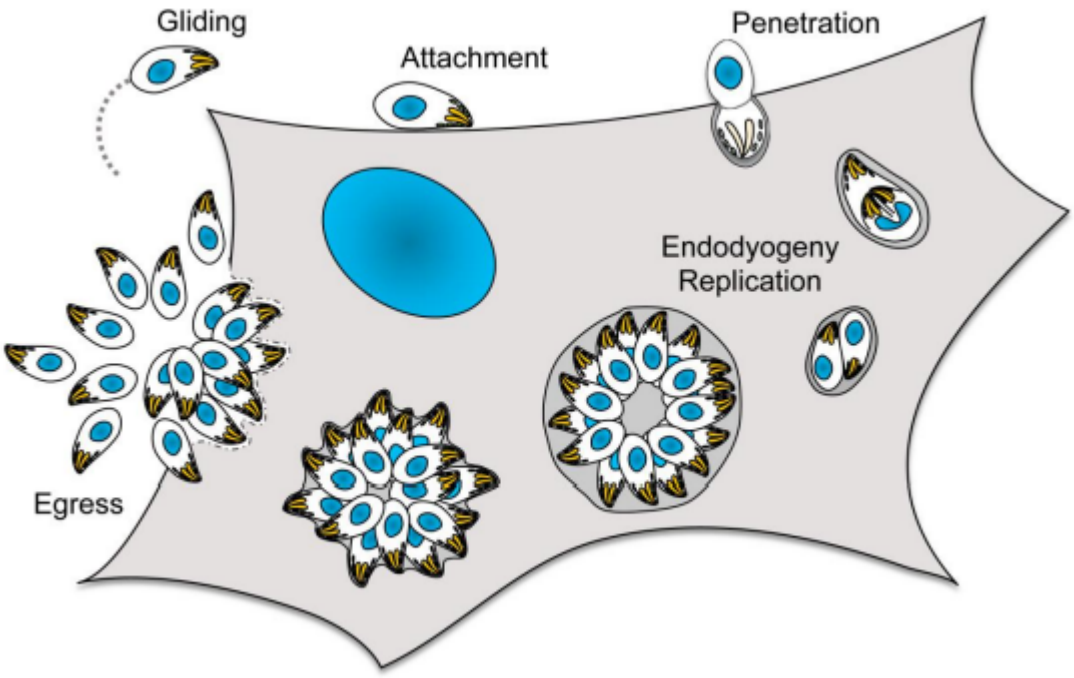

Figure 1.2 – The lytic cycle of *Toxoplasma gondii*
Free gliding parasites disseminating within the host's body invade a host cell via active invasion, resulting in the formation of a parasitophorous vacuole. The parasites replicate within the vacuole via endodyogeny over a period of approximately 48hr. Egress of these parasites is then induced via both intrinsic as well as extrinsic signalling. These newly-released parasites then proceed to invade fresh host cells. Image from Whitelaw, (2017)

1.1.4. The asexual tachyzoite – structure and unique features

The parasites cultured and studied in the Meissner lab are tachyzoites. It is for this reason that everything discussed henceforth will only be applicable to tachyzoites, unless otherwise stated. It is also for this reason, and for the purposes of brevity, that this introduction section will now only discuss tachyzoites.

Tachyzoites are crescent-shaped cells, with a more pointed anterior end and a more rounded posterior end. These cells are around 2 μm in width and 7 μm in length (Dubey et al., 1998). Like other eukaryotes, *Toxoplasma* tachyzoites have a nucleus, with an internal nucleolus. Surrounding the nucleus, these parasites have an endoplasmic reticulum which leads to the Golgi body. A single, typically lasso-shaped mitochondrion is also present in every cell, the shape of this organelle varying depending on which stage of the lytic cycle the parasite is in (Ovciarikova et al., 2017).

In addition to these typical eukaryotic organelles, *Toxoplasma* has several specialised organelles which are specifically adapted to allow it to carry out its parasitic lifestyle. These are further discussed in the following sections.

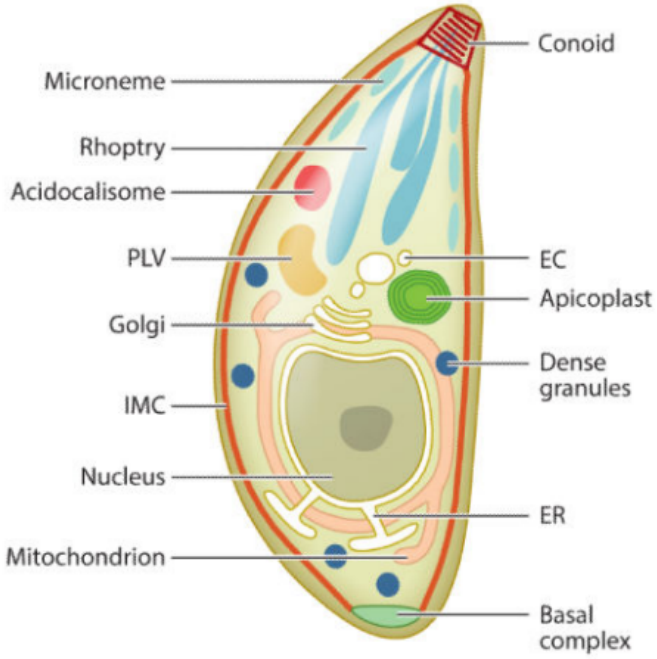

Figure 1.3 – The cell structure of *Toxoplasma gondii*
Toxoplasma tachyzoites have a pointed apical end where the apical complex localises. This complex consists of the conoid and the secretory organelles; the micronemes and rhoptries. Microtubules also form part of the apical complex, these connecting to the apical polar ring and extending downwards, providing structure to the parasite (Koreny et al., 2021; Leung et al., 2017). The parasites also possess a nucleus surrounded by the endoplasmic reticulum which leads to the Golgi body, an apicoplast, a lasso-shaped mitochondrion, and a plant-like vacuole (PLV). Acidocalcisomes are also present, these being the sites of calcium storage and therefore responsible for ion flux. Image from Blader et al., (2015).

The Inner Membrane Complex

The Inner Membrane Complex (or IMC) is composed of flattened alveolar sacs (or alveoli) present just underneath the parasite's plasma membrane. These sacs are sutured together in a similar fashion to a quilt (Anderson-White et al., 2012; Morrissette & Sibley, 2002a). Present at the sutures at the boundary of the IMC sacs, among other essential proteins (Chen et al., 2017), is a 'micropore' hypothesised to facilitate endocytosis as shown in Figure 1.4 (Koreny et al., 2022).

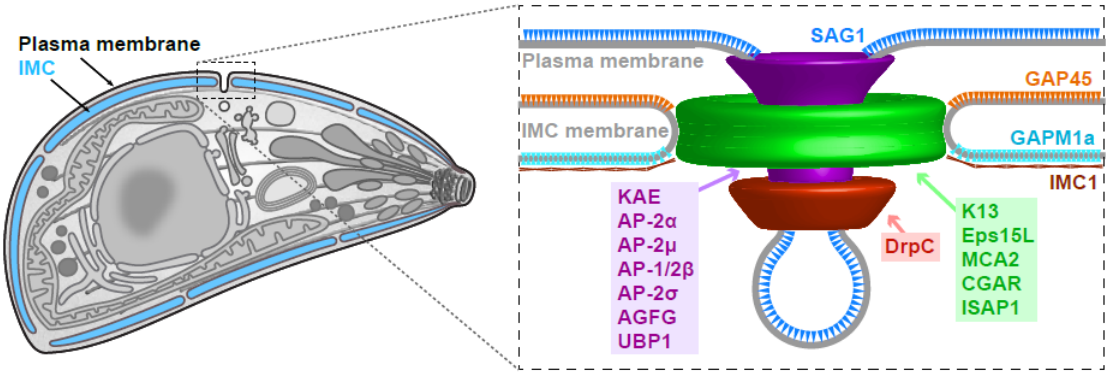

Figure 1.4 – The micropore in *Toxoplasma gondii*
The micropore localises within the sutures between the IMC plates. It is via this pore that the parasites are hypothesised to carry out endocytosis. Image from Koreny et al., (2022)

The IMC is divided into three main parts; the apical cap, the central part, and the basal part. The space between the plasma membrane and the IMC is where the gliding motor, which is largely responsible for the parasites' motility, is hypothesised to be. Connecting the IMC to the microtubules underneath is the alveolin network, a network composed of intermediate filament-like proteins which span the entire length of the IMC (Gould et al., 2008; Mann & Beckers, 2001; Tosetti et al., 2020). The IMC has been observed to be essential with regards to maintaining the shape of the parasites. It also helps organise parasite replication, and, due to its anchoring of the gliding motor, is also important for motility and invasion (Egarter et al., 2014; Harding et al., 2016).

The apicoplast

The apicoplast is an organelle which is the result of secondary endosymbiosis, and therefore can be observed to have genetic material surrounded by four membranes. It is present anterior to the nucleus, and its presence is essential to the parasites as it is involved in biosynthesis pathways such as those which produce fatty acids, haem, and isoprenoid (Mazumdar et al., 2006; Nair et al., 2011; Van Dooren et al., 2012). Proteins destined for the apicoplast are trafficked via the secretory system, with some having been observed to travel directly from the endoplasmic reticulum (ER) to the apicoplast, and others travelling via the Golgi body (Aparna & Swati, 2021; Bouchut et al., 2014; Marilyn et al., 2007; Prasad et al., 2021; Tomova et al., 2009; Waller et al., 2000).

The secretory organelles

Like other apicomplexans, *Toxoplasma* has specialised secretory organelles; the micronemes, the rhoptries, and the dense granules.

Micronemes are small rod-shaped organelles which are present at the apical end of the parasites. Proteins within the micronemes are secreted, and via integration of secreted adhesins into the parasite plasma membrane, facilitate adhesion to the substrate, gliding motility, host cell invasion, and egress (Alexander et al., 2005; Kessler et al., 2008; Soldati et al., 2001). Micronemes have been observed to originate both via *de novo* synthesis as well as via inheritance from mother cells (Kremer et al., 2013; Morlon-Guyot et al., 2015, 2018; Periz et al., 2019; Venugopal et al., 2017).

Rhoptries are larger, more elongated organelles. These structures are composed of the rhoptry neck, the elongated part of the entire rhoptry which contains RON proteins, and the rhoptry bulb, the basal part of the entire rhoptry which contains ROP protein (Dubremetz, 2007). Similar to micronemes, rhoptries have also been observed to be critical for invasion, with some having been observed to localise to the moving junction during invasion (Besteiro et al., 2009; Lebrun et al., 2005; Straub et al., 2011). Other secreted rhoptry proteins have also been seen to be critical for host cell infection by allowing the parasite to evade the host immune system (Butterworth et al., 2022; Hakimi et al., 2017; Lima & Lodoen, 2019; Niedelman et al., 2012). The mechanism involved in signaling rhoptries to discharge their

contents still remains unknown but hypotheses involving micronemal proteins have been put forward (Singer et al., 2023; Sparvoli et al., 2022).

Dense granules are vesicles within the parasite cytoplasm. These vesicles contain GRA proteins which, once secreted, either localise to the parasitophorous vacuole lumen, are inserted into the parasitophorous vacuole membrane, localise to the membranous network present in the parasitophorous vacuole, or leave the parasitophorous vacuole to enter the host cell (Bougdour et al., 2013; Gold et al., 2015; Joshua et al., 2022; Mercier et al., 2002). GRA proteins mainly function to maintain the infection within the host cell and have been observed to be involved in a multitude of processes, from nutrient uptake to host immune evasion and recruitment of host organelles to the parasitophorous vacuole. Details of dense granule biogenesis, trafficking, and function have been nicely summarised in the review by Griffith et al., (2022).

The apical complex

The apical complex is a structure that is conserved throughout the phylum Apicomplexa (Koreny et al., 2021), and is composed of the conoid complex, and the micronemes, and rhoptries. All of these structures are enclosed under the apical cap, a cone-shaped IMC plate (Beck et al., 2010). The conoid is a barrel-like structure made up of tubulin-rich fibres (Hu et al., 2002). Associated with the conoid are two rings, the apical polar ring 1 and 2, the first of which marks the margin of the IMC, while the second functions to organise the subpellicular microtubules and is therefore also termed the microtubule organising centre (MTOC) (Morrissette & Sibley, 2002b; Russell & Burns, 1984). Inside the conoid are two intraconoidal microtubules which connect to two preconoidal rings (Morrissette et al., 1997; Nichols & Chiappino, 1987). The conoid complex made up of the conoid barrel, the intraconoidal microtubules, and the preconoidal rings is enclosed under the apical cap in intracellular parasites, but is extruded beyond the apical polar ring during invasion (Del Carmen et al., 2009). Multiple components of the conoid and pre-conoidal rings have been studied. These have been observed to serve different functions, with some being critical for the structural integrity of the conoid, for conoid extrusion, and for invasion and egress (Dos Santos Pacheco et al., 2022; Munera Lopez et al., 2022). The dynamics of this extrusion has been observed to be dependent on the acto-myosin system (Graindorge et al., 2016).

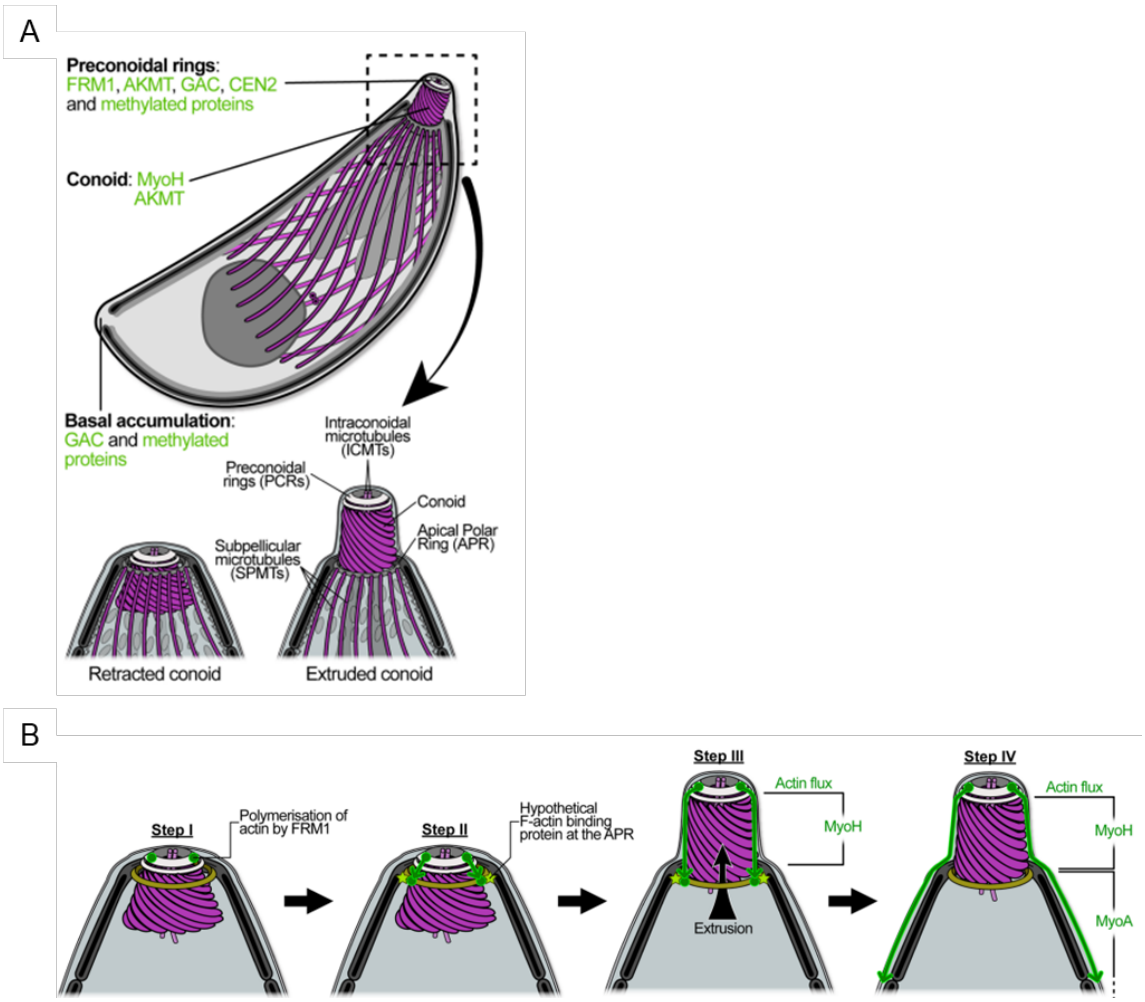

Figure 1.5 – The apical complex of *Toxoplasma gondii*

(**A**) Numerous proteins have been localised to different sub-compartments within the apical complex. (**B**) Formin1, which localises to the pre-conoidal rings, produces actin filaments which are bound by a hypothetical protein at the apical polar ring (APR) and then used by MyoH to extrude the conoid. Following this extrusion, these actin filaments are then moved towards the back of the parasites and are critical for subsequent parasite motility. Images adapted from Dos Santos Pacheco et al., (2022).

1.1.5. *Motility*

Tachyzoite movement has been observed in a 2-dimentional environment and described as being of three types; rotating, upright twirling, and circular gliding (Håkansson et al., 1999). While many key molecules involved in gliding motility and invasion have been identified, their precise mode of action is still under debate. It has long been hypothesised to be controlled by an acto-myosin motor complex, as reviewed in Frénal, Dubremetz, et al., (2017). To summarise briefly, according to this hypothesis, this complex is present

between the IMC and the parasite plasma membrane. It is hypothetically anchored to the stable IMC via GAP proteins. The tail of the myosin MyoA is also linked to the IMC via MLC1, while the MyoA head interacts with actin. Micronemes are secreted from the apical tip of the parasites and thus adhesins are delivered to the parasite plasma membrane. These adhesins span the membrane, interacting with the extracellular substrate while also being connected to the parasite actin via the glideosome-associated connector (GAC) (Jacot et al., 2016). Motility is thus brought about by a rearward translocation of the adhesins interacting with the substrate, propelling the parasite forwards.

While many of the components of the acto-myosin motor have been observed to be critical for parasite motility (Frénal et al., 2010; Meissner et al., 2002), parasite strains lacking some components were seen to be viable (Andenmatten et al., 2013; Egarter et al., 2014; Gras et al., 2017; Whitelaw et al., 2017). In addition to this, recent studies on parasite motility in a 3D environment have shown that while this motor model predicts the formation of a continuous force moving rearward along the parasite, the force observed is actually periodic, localised to specific areas on the parasite surface, and pointing inwards (Stadler et al., 2022). It is therefore likely that an alternative or additional gliding and invasion mechanism exists (Gras et al., 2019).

1.1.6. *Invasion*

The ability to successfully invade host cells is critical for an obligate intracellular parasite, both in order to feed, as well as a means of evading the host immune system. In order for *Toxoplasma* to carry out this seconds-long process effectively and efficiently, it has developed specialised secretory organelles; the micronemes, rhoptries, and dense granules. Parasites initially attach to the host cell substrate, after which they orient themselves so as to point the apical end towards the host cell of interest, thus permitting invasion. Secretion of micronemes, which act as adhesins, occurs in a Ca^{2+}-dependent manner. These proteins are then translocated towards the back of the parasite and eventually shed (Carruthers et al., 1999; Garcia-Réguet et al., 2000; Opitz et al., 2002).

After microneme secretion, several rhoptry proteins are also secreted. The function of these rhoptries varies, with some binding to the previously discharged micronemes, thus creating the moving junction through which the parasite pushes in order to enter the cell (Alexander et al., 2005; Besteiro et al., 2009; Lebrun et al., 2005). This propulsion of the parasite into

the host cell is driven by the acto-myosin motor as discussed above (Frénal, Dubremetz, et al., 2017). The invaginated host cell plasma membrane is what ultimately becomes the parasitophorous vacuole membrane (Suss-Toby et al., 1996). Other rhoptry proteins are discharged into the host cytoplasm, or are targeted towards the parasitophorous vacuole membrane. In both cases, these act to maintain a successful infection within the host cell (Alexander et al., 2005; Beckers et al., 1994; Lentini et al., 2021; Sinai & Joiner, 2001).

1.1.7. *Replication*

Toxoplasma replicates via endodyogeny, wherein two daughter cells are formed within the mother cell via internal budding (Sheffield & Melton, 1968). This entire process is highly regulated, with each step occurring sequentially, and it typically takes between two or three hours to complete. All parasites within a single parasitophorous vacuole undergo synchronous endodyogeny (Anderson-White et al., 2012; Nishi et al., 2008).

During replication, the Golgi and centrosomes are the first structures to duplicate. The apicoplast starts to elongate as the centrosomes separate and divide (Anderson-White et al., 2012; Nishi et al., 2008). As this is occurring, DNA in the mother cell undergoes one single replication cycle, after which the nuclei also divide. Unlike in the case of other eukaryotes, during this DNA replication and nuclear division, the chromosomes do not condense and the nuclear membrane is never disassembled (Francia & Striepen, 2014; Gubbels et al., 2008). Throughout this entire process of organellar division, *de novo* daughter conoids and IMC start to assemble at the apical end of the daughter buds and extend downwards towards the basal end of the daughter cells, the components of the basal complexes accumulating at the leading edge. This downward extension of the IMC occurs at the same time as the duplicated organelles start to divide and migrate into the individual daughter cells. Maternal material such as vesicular material is either degraded or inherited into the daughter cells (Periz et al., 2019) with more material also being synthesized *de novo* (Nishi et al., 2008). Mitochondrial partitioning into the daughter cells is one of the last steps to occur prior to daughter cell emergence. The daughter buds then emerge, with the mother plasma membrane becoming incorporated onto the daughters. Any remaining maternal material then moves towards the back of the daughter parasites and becomes the residual body, connecting the now mature cells within the parasitophorous vacuole (Attias et al., 2019; Frénal, Jacot, et al., 2017; Periz et al., 2017).

Countless proteins have been observed to be essential for parasite replication to occur. Many of these essential proteins have been observed to be components of the parasite microtubule cytoskeleton or the IMC. The absence of these proteins was seen to result in a number of phenotypes; from improper division or segregation of the nucleus, to an inability for the parasites to even form an IMC and successfully form daughter cell buds (Beck et al., 2010; Harding et al., 2016). It is interesting to note that while actin has been observed to be critical for division and segregation of the apicoplast, it has been observed to be non-essential for parasite division itself. Parasites lacking actin divide and segregate successfully, albeit doing so asynchronously and resulting in morphologically aberrant parasites (Periz et al., 2017).

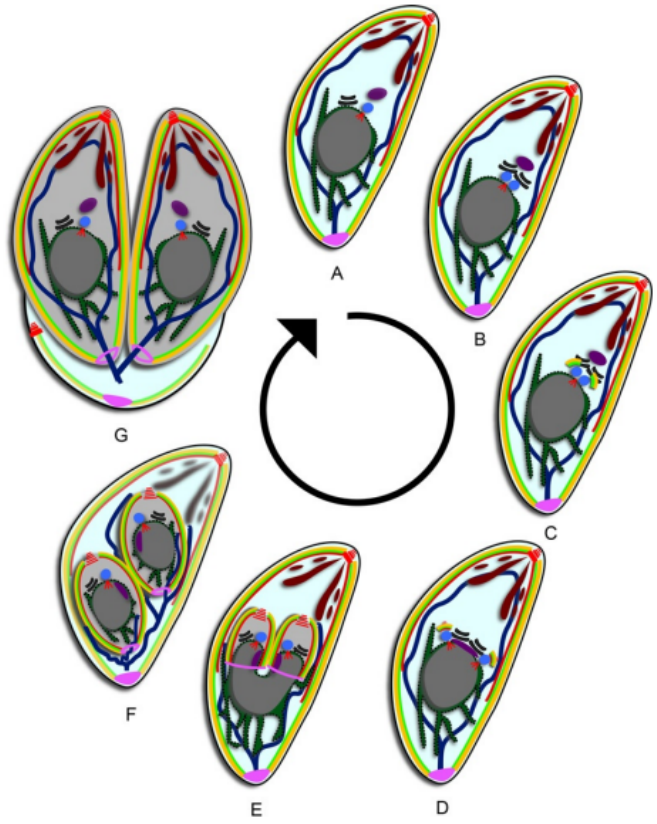

Figure 1.6 – Replication of *Toxoplasma gondii*

Toxoplasma divides by forming internal buds inside the mother cell (**A**). (**B**) The centrosome (blue) and Golgi apparatus (black) are the first to divide. (**C**) Early components of the IMC then appear (yellow alveoli and green IMC). (**D**) The spindle pole (in red) then duplicates and the (dark purple) apicoplast elongates. (**E**) The organelles and dividing nucleus (grey) start to partition into the elongating daughter cells. (**F**) Material from the mother starts to degrade as the daughter cells start to close at the basal end. (**G**) The mitochondrion (in dark blue) is pulled

into the daughter cells and these emerge from the mother cell as the mother cell plasma membrane is incorporated onto the daughters. Image from Anderson-White et al., (2012).

1.1.8. *Egress*

Egress is the final step in the lytic cycle, without which parasite dissemination is impossible. Parasite egress is possible through any stage of parasite replication, this exit being dependent on either internal or external cues (Bisio & Soldati-Favre, 2019; Lourido et al., 2012; Vella et al., 2021; Ye et al., 2022). Parasites detect these cues, and this initiates a signalling cascade which culminates in their egress. The exact signalling mechanisms controlling this process have not yet been elucidated. Recent reports have suggested that phosphatidic acid (PA) regulates parasite egress via a guanylate cyclase (GC) signalling complex (Bisio et al., 2019). In addition to this, two molecules which have been observed to be essential for activation of the signalling pathway are cyclic GMP and calcium ions (Arrizabalaga & Boothroyd, 2004; Borges-Pereira et al., 2015; Lourido et al., 2012; Vella et al., 2021). In fact, calcium ionophore is commonly used to chemically induce egress within a laboratory context (Caldas et al., 2007; Endo et al., 1982).

While it is currently known that egress is controlled by a signalling cascade which eventually leads to the secretion of micronemes, it is also known that egress requires initiation of motility. It has been observed that for successful egress and parasite dissemination to occur, the actin filament network connecting all the parasites within the parasitophorous vacuoles needs to disassemble (Li et al., 2022). In addition to this, it has been observed that knockout of actin-regulatory factors has a negative impact on successful egress (Mehta & Sibley, 2011). It is, therefore, safe to say that while actin may not be a direct egress factor, its proper dynamics are crucial for this step.

1.2. Actin and actin-regulatory proteins

Actin is a crucial component of a cell's cytoskeletal system, and this is no different in the case of apicomplexan parasites. As mentioned briefly in the above section overviewing the parasite lytic cycle, actin plays a key role in all steps of the cycle. Therefore, it is of critical importance that this protein and the systems regulating it are investigated.

1.2.1. *Actin in model Eukaryotes*

Actin is a highly abundant protein that is critical for a multitude of processes within a eukaryotic cell, including cellular motility, vesicular trafficking, and cytokinesis (Pollard & Cooper, 2009). Actin is present in two different states; the globular form and the filamentous form (Oda et al., 2009). The polymerisation of globular actin to form filamentous actin is a process that is ATP-dependent (Baum et al., 2006; Wegner, 1976). In addition to this necessity for ATP, a critical concentration of globular actin is required for polymerisation to take place (Pollard & Borisy, 2003). The presence of a vast repertoire of actin regulatory proteins further facilitates and/or controls actin dynamics within the cell (Pollard, 2016).

Actin-regulatory proteins

Several actin-regulatory proteins exist in eukaryotes. The functions of these proteins vary widely, as can be observed in Figure 1.7. For the purposes of this thesis, only a subset of these proteins will be briefly discussed.

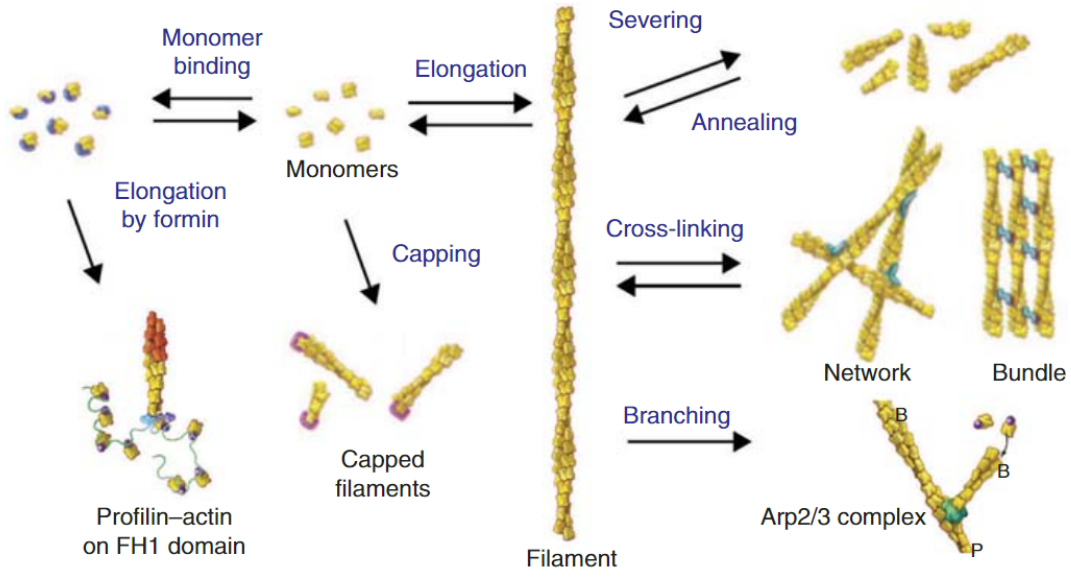

Figure 1.7 – Actin dynamics involve different actin-regulatory proteins
There are countless canonical eukaryotic actin-modulating proteins. Different families of proteins are involved in different actin-modulating processes, including elongation, branching, cross-linking, bundling, depolymerisation, and capping. Actin-dependent motor proteins such as myosins are not included in this depiction. Image from Pollard, (2016).

One of the main processes wherein actin-binding proteins are involved is actin nucleation and polymerisation. For this process to take place, many factors are involved. Some of these factors are actin depolymerising factor (ADF), and cofilins. These factors bind to actin filaments and act to destabilise and severe these filaments, thus increasing the pool of globular actin monomers present within the cell (Moon & Drubin, 1995; Yeoh et al., 2002). This generation of available actin monomers is essential as it allows the critical concentration of actin to be reached, thus allowing new filament elongation and/or formation (Pollard & Borisy, 2003). Another factor which works to maintain this critical actin concentration is profilin, a protein which binds and sequesters actin monomers (Baum et al., 2006; Pollard, 2016). In addition to this, profilin acts in conjunction with formins, proteins which are involved in actin nucleation (Kovar, 2006; Romero et al., 2004).

Actin filament formation involves three different classes of proteins; the aforementioned formins, proteins belonging to the Arp2/3 complex, and Spire (Goode & Eck, 2007). The Arp2/3 complex is known to interact with already formed actin filaments, resulting in the formation of actin branches (Mullins et al., 1997; Welch et al., 1997). Formins, on the other hand, possess two domains; the formin homology domains 1 and 2 (FH1 and FH2) (Breitsprecher & Goode, 2013; Castrillon & Wasserman, 1994). The FH1 domain supposedly interacts with profilin whereas the FH2 domain is used for filament assembly (Evangelista et al., 1997; Pruyne et al., 2002; Sagot et al., 2002). Spire promotes actin filament formation via four WASP homology 2 domains (WH2) (Quinlan et al., 2005).

Myosins are actin-dependent molecular motors which are involved in numerous processes; from co-ordination of muscle contractions within a body to transport of cargo within a single eukaryotic cell (Mermall et al., 1998). These motors are generally made up of a heavy chain and a light chain. The heavy chain is composed of a head domain, a neck domain, and a tail domain. The head domain is highly conserved and binds and releases actin in an ATP-dependent manner (Itakura et al., 1993; Kühner & Fischer, 2011). The neck domain binds the myosin light chain and functions to regulate ATP-binding by adjusting the ATP-binding site (Heissler & Sellers, 2014). The structure of the tails, on the other hand, are variable, with this part of the protein being involved in binding different cargo (Hartman & Spudich, 2012; Sellers, 2000).

1.2.2. Actin in Apicomplexan parasites

Actin is encoded by a single gene in *Toxoplasma*. This single gene shares about 93% sequence similarity with *Plasmodium falciparum* actin, but only around 80% similarity with other eukaryotic actins (Baum et al., 2006; Dobrowolski et al., 1997). For a time, *Toxoplasma* actin was not believed capable of forming long filaments. The critical concentration for actin polymerisation was estimated to be lower than that for conventional actin, thus supporting the idea that *Toxoplasma* actin formed very short, unstable filaments which were capable of rapid assembly and disassembly due to their high turnover rate (Sahoo et al., 2005; Skillman et al., 2013). Stabilisation of actin via the actin-modulating drug Jasplakinolide reduced the parasites' motility, also hypothetically supporting the idea that the presence of actin filaments is unlikely in *Toxoplasma* (Poupel & Tardieux, 1999; Skillman et al., 2011). Actin filaments were also not very clearly visible using either actin antibodies or the classical actin-labelling technologies such as LifeAct and phalloidin (Periz et al., 2017).

Bearing all of this in mind, the ability to visual actin filaments using the actin chromobody was therefore revolutionary for the field of apicomplexan actin (Periz et al., 2017). Not only did the chromobody prove that actin filaments are present within the parasites, but it allowed further investigations into actin and its many functions. It was observed that individual parasites within the parasitophorous vacuole are all connected to each other via actin filaments, and it is via these actin filaments that material is transported, both within each parasite and from one parasite to another (Periz et al., 2017, 2019).

The idea that trafficking within the parasites is actin and myosin-dependent is not new as this observation had also been made prior to the establishment of the actin chromobody, when it was observed that dense granule trafficking is dependent on actin and myosins (Heaslip et al., 2016; Whitelaw et al., 2017), as is also the case for Golgi and post-Golgi trafficking (Carmeille et al., 2021). Actin has also been seen to be important for all processes involving motility. Actin depletion resulted in inhibited egress and reduced gliding and invasion - although it is important to note that a percentage of the knockout parasites were still able to glide and invade (Egarter et al., 2014; Whitelaw et al., 2017). Additionally, while actin has not been observed to be critical for parasite division, it was noted that endodyogeny in the absence of actin occurs asynchronously, parasites lack the typical rosette arrangement within the parasitophorous vacuole, and some parasites experience apicoplast loss (Andenmatten et al., 2013; Periz et al., 2017; Whitelaw et al., 2017).

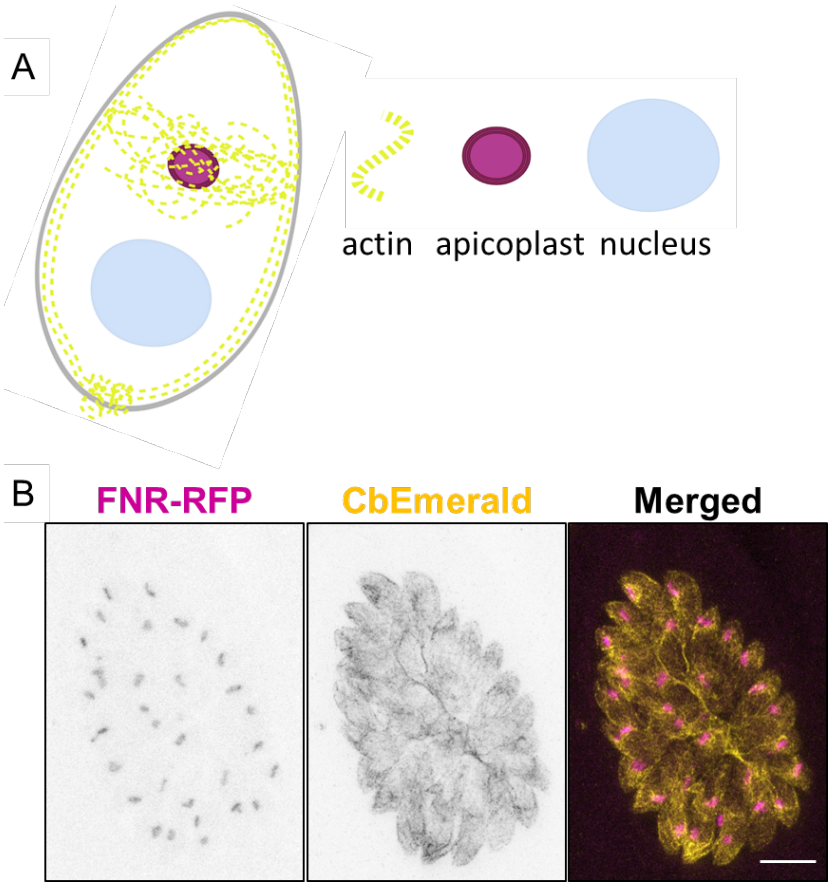

Figure 1.8 – Actin filament distribution in intracellular *Toxoplasma* tachyzoites
(**A**) Schematic of actin filament distribution within *Toxoplasma gondii* tachyzoites. Image was generated using BioRender, adapted from Stortz et al., (2019). (**B**) Thick bundles of actin filaments labelled with the Chromobody-emerald (shown in yellow) can be seen connecting the parasites towards the centre of the parasitophorous vacuole. Filaments can also be seen within each parasite, with a higher density being around the apicoplast (labelled with FNR-RFP in magenta). Images were taken by the author using STED for actin, and confocal mode for the apicoplasts. Scale bar is 5 µm.

Actin-regulatory proteins

While there are tens if not hundreds of canonical actin-modulating proteins in eukaryotic cells, few of these are present in apicomplexans (Baum et al., 2006). In stark contrast to human's 5 profilin genes, 14 adf/cofilin genes, and 16 formin genes, *Toxoplasma* only has one profilin, three formins and one gene for adf (Baum et al., 2006). In addition to this, *Toxoplasma* does not have the Arp2/3 and Spire actin nucleating factors (Baum et al., 2006; Gordon & Sibley, 2005), seemingly leaving actin nucleation to be entirely dependent on the three formins (Tosetti et al., 2019).

ADF, which localises to the cytoplasm (Haase et al., 2015; Mehta & Sibley, 2011), has been observed to be important for gliding, invasion, and egress as its deletion results in an abnormal accumulation of actin filaments (Mehta & Sibley, 2011). Similarly, work on formin1 has also shown it to be important for gliding, invasion, and egress (Daher et al., 2010; Tosetti et al., 2019). Its localisation is still a matter of some debate as although its localisation at the conoid has been well documented, other data showing its possible localisation at the IMC and along subpellicular microtubules cannot be ruled out (Baum et al., 2008; Tosetti et al., 2019). Formin2, on the other hand, was seen to localise near to the Golgi body and the apicoplast (Stortz et al., 2019; Tosetti et al., 2019). While it has not been observed to be critical for invasion or egress (Tosetti et al., 2019), its knockout was seen to cause a disruption in actin dynamics, with more prominent filaments connecting the individual parasites but a lack of filaments around the Golgi region within each parasite (Stortz et al., 2019). A defect in apicoplast segregation was also observed (Stortz et al., 2019). Unlike formin1 and formin2, formin3 was deemed to be unessential for *Toxoplasma* tachyzoites. It localises to the basal pole and the residual body, and is hypothesised to be involved in parasite-parasite communication (Tosetti et al., 2019).

The function of profilin in *Toxoplasma* is believed to be divergent from that of profilin in yeasts. While profilin in yeasts is known to be involved in formin-mediated actin polymerisation (Sagot et al., 2002), in vitro evidence seems to suggest that *Toxoplasma* actin polymerisation is inhibited by profilin (Skillman et al., 2012). It is therefore hypothesised that *Toxoplasma* profilin acts to sequester actin monomers. This hypothesis is in agreement with the phenotype observed in profilin knockout parasites, wherein more prominent filaments are observed compared to wildtype (as shown in Figure 3.4). Profilin has been shown to be critical for the parasite's lytic cycle, the knockdown mutants suffering a defect in gliding, invasion, and egress in its absence (Plattner et al., 2008).

In addition to the actin-regulatory proteins found in *Toxoplasma*, several other actin-binding proteins are also present. For the purposes of this thesis, I will be focussing on the myosins. Many myosins present in apicomplexans are classified into class XIV superfamily. In the case of *Toxoplasma*, this class includes MyoA, MyoB/C, MyoD, MyoE, and MyoH (Foth et al., 2006). Of these, myosin A is the most commonly investigated, and most well-characterised due to its involvement with the acto-myosin motor complex responsible for parasite gliding (Frénal, Dubremetz, et al., 2017). Myosins B and C are encoded by the same gene, the expression of these myosins being dependent on alternative gene splicing.

MyoB is expressed in bradyzoites, whereas MyoC is expressed in tachyzoites and is hypothesised to be involved in daughter cell formation (Delbac et al., 2001). Both MyoD and MyoE are expressed in bradyzoites (Delbac et al., 2001). MyoH has been observed to localise to the conoid, and a role in conoid extrusion has been suggested (Dos Santos Pacheco et al., 2022; Graindorge et al., 2016).

In addition to the mentioned myosins, *Toxoplasma* also possesses myosin F which contains WD40 repeats (Foth et al., 2006), and unlike the other myosins mentioned, is classified as a class XXVII myosin (Odronitz & Kollmar, 2007). This myosin has been observed to be critical for the lytic cycle of *Toxoplasma*, with its functions being related to centrosome positioning, apicoplast inheritance, and maintenance of Golgi structural integrity, and vesicular trafficking (Carmeille et al., 2021; Heaslip et al., 2016; Jacot et al., 2013).

1.3. Vesicular trafficking

Trafficking is a crucial process within any living cell. It is via this mechanism that all products produced within said cell reach their final destination. It is also via this process that material outside of cells is taken up to be used for nutrition, and material within the cell is secreted.

1.3.1. Vesicular trafficking in model eukaryotes

Trafficking involves a number of structures and organelles which communicate via transport of vesicles. In a typical cell, as shown in Figure 1.10, these structures include the plasma membrane, the endoplasmic reticulum (ER), the Golgi body, and a number of post-Golgi compartments such as the early and late endosomes, and the lysosomes.

Biosynthesis of cellular products takes place within the ER which is present adjacent to the nucleus and forms a continuum with the outer nuclear membrane. These products are transported to the Golgi body, which acts as one central sorting station that is organised into sub-compartments from where products are packaged to reach their final, specific destination (M. C. S. Lee et al., 2004). These packages are then either secreted via secretory vesicles, or transferred to the endosomes, and eventually reach the lysosome (M. C. S. Lee et al., 2004). Reverse transport of material is possible at a number of these steps (Béthune et al., 2006; Hsu et al., 2009; M. C. S. Lee et al., 2004; Rohn et al., 2000).

While this simplified overview of the trafficking pathway is generally taken to be the model, it is important to note that the endosomal-lysosomal pathway in eukaryotes is highly divergent as a result of adaptations to the different needs of the varied biological systems. These modifications have resulted in a loss of components in some species, and gain of components in others (Schlacht et al., 2014; Woo et al., 2015b). However, despite these differences in key players taking part, the overall mechanism of how transport of material is possible remains the same. This mechanism centres around vesicle budding and fusion.

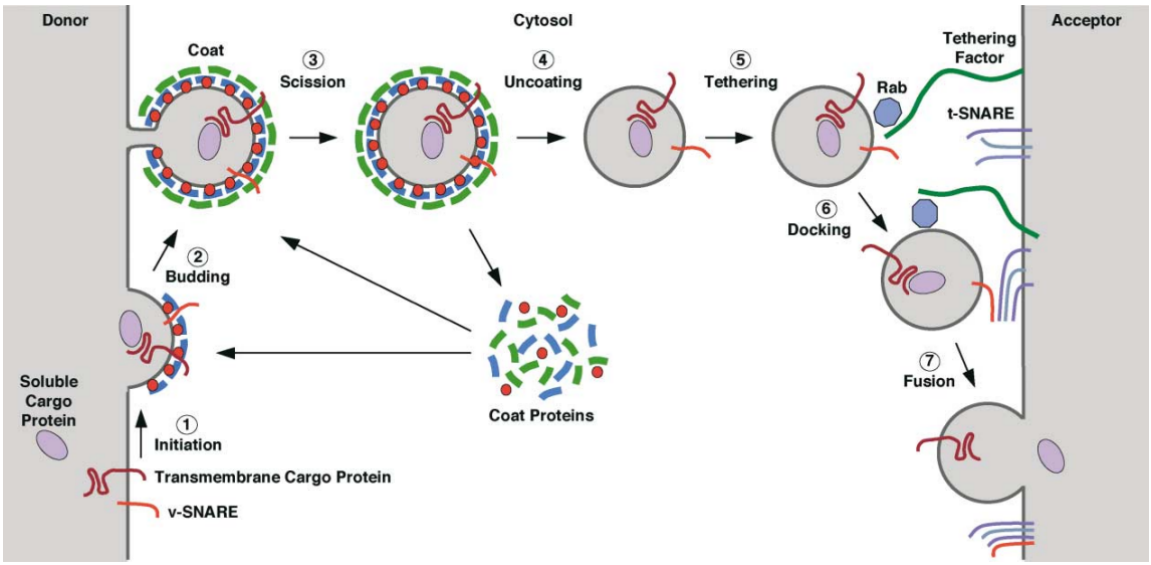

Figure 1.9 – The process of vesicle budding and fusion
Coat proteins associate with the membrane of the donor compartment either directly, or via accessory proteins. These alter the membrane curvature to induce bud formation. Scission, either by the coatomer itself or via other proteins, causes the vesicle to bud off. The coat proteins are then removed from the surface of the vesicle. As the vesicle moves closer to the target compartment, it associates with tethering factors and Rab GTPases which bring it closer to allow v-SNARE and t-SNARE proteins to interact and the vesicle to fuse. Image from Bonifacino & Glick, (2004).

The first step of vesicle formation involves the recruitment of coat proteins to the site of budding. These coat proteins, which vary depending on the compartment from which the vesicles are budding, form complexes which induce membrane curvature causing a large bud to form (Figure 1.9). Examples of such coat complexes are COPII complexes which function to transport material from the ER to the Golgi, or COPI complexes which are involved in the reverse pathway, trafficking material from the Golgi back to the ER (M. C. S.

Lee et al., 2004). Clathrin is also a well-known coatomer which facilitates membrane budding both at the Golgi and endosomes, as well as at sites of endocytosis (Rohn et al., 2000; Schmid, 1997; C. J. Smith & Pearse, 1999). These coat complex members are recruited to the site of budding via interactions with membrane-associated GTPases and either associate with the cargo directly, or, in the case of clathrin, with the aid of accessory proteins (APs) (Pucadyil & Schmid, 2009; Rohn et al., 2000). The budding vesicles which form with the aid of the coatomers contain SNARE proteins on the membrane as well as transmembrane cargo proteins, and soluble cargo proteins. The bud is separated from the 'donor' compartment either by the coatomer itself, or via the action of other accessory proteins such as dynamins (Pucadyil & Schmid, 2009). After the vesicle buds off, it then moves towards the target compartment and is detected by means of tethering factors on the target compartment which interact with Rab GTPases present on the vesicle surface (Stenmark, 2009). Different tethering factors are present at different sites of vesicle reception, with the most well-known being the class c core vacuole/endosome tethering factor (CORVET) complex which acts between the Golgi body and the endosomes, and the homotypic fusion and vacuole protein sorting (HOPS) complex which acts at the late endosomes (Balderhaar & Ungermann, 2013; Chou et al., 2016). This interaction between tethering factors and Rab GTPases is critical as it allows for both the recognition of the correct vesicles for fusion, as well as brings the vesicle closer to the target compartment thus permitting the v-SNAREs on the vesicle and the t-SNAREs on the target compartment to interact. It is this interaction between the SNARE proteins which pulls the vesicle in such proximity to the target compartment that the membranes of both vesicle and compartment fuse, resulting in the release of the vesicle cargo into the compartment (Han et al., 2017).

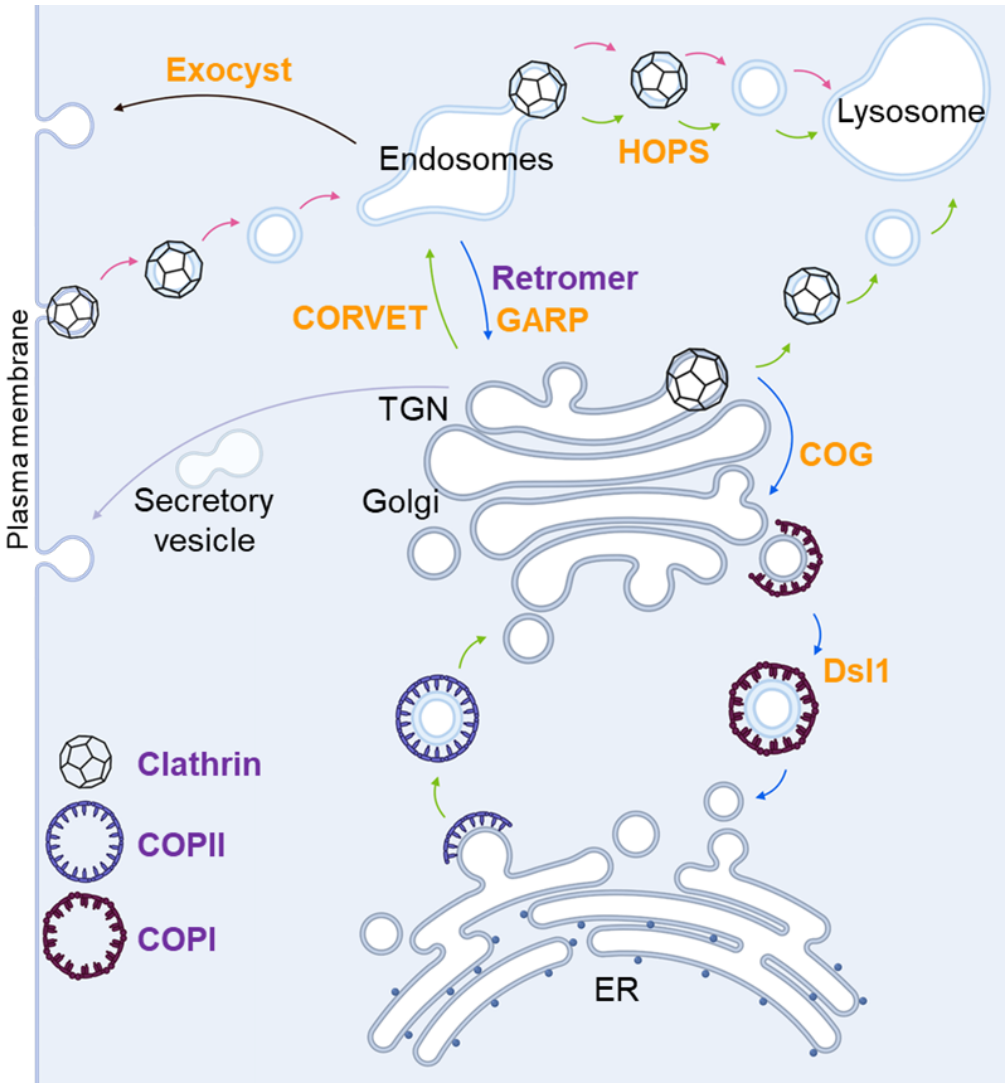

Figure 1.10 – An overview of the endosomal-lysosomal system in a typical Eukaryotic cell

Proteins are trafficked from the ER to the Golgi body, after which they are either secreted or transferred to the endosomes and eventually to the lysosomes. Material from the endosomes can also be secreted, or trafficked back to the Golgi and to the ER. Endocytosed material is typically transported to the early then late endosomes (not differentiated here), after which it goes to the lysosome. This overview of the endosomal-lysosomal system shows some of the different components involved in trafficking. The coatomers are labelled in purple whereas tethering factors are labelled in orange. Image generated using BioRender, adapted from Hsu et al., (2009); Munson, (2009); Xu & Esko, (2009).

1.3.2. Vesicular trafficking in Toxoplasma gondii

The organellar compartments involved

To briefly summarise, *Toxoplasma*'s vascular trafficking system is similarly composed of the endoplasmic reticulum which is surrounding the nucleus. Adjacent to the ER but posterior to the apicoplast is the Golgi body, which comprises a single Golgi-stack consisting of the typical organisation; the *cis*-Golgi and the *trans*-Golgi, the former being the closest to the ER. The *trans*-Golgi stacks then lead to a series of post-Golgi compartments.

Unfortunately, unlike in the case of other eukaryotes, the *Toxoplasma* endosomal system is not well understood. One of the main problems with studying this trafficking system is the fact that the many Golgi and post-Golgi compartments are primarily identified using a number of marker proteins. Since many of these marker proteins are overlapping and can be found in multiple post-Golgi compartments, this has resulted in some disagreements within the literature with regards to the identity of these compartments. As a result of this, many compartments, including the early and late endosomes as well as all vesicles in between, are now broadly referred to as 'endosome-like compartment' (ELC) (Jackson et al., 2013; Stasic et al., 2022).

In addition to the ER, Golgi body and endosome-like compartment, *Toxoplasma* also possesses a plant-like vacuole (PLV), or vacuolar compartment (VAC). This vacuole is present as a large compartment in extracellular parasites which fragments and becomes diffused throughout the cytoplasm upon parasite invasion into host cells (Miranda et al., 2010; Parussini et al., 2010). The VAC contains cathepsin proteases which function to degrade material of both internal as well as external origin, and it is for this reason that this organelle is generally considered the equivalent of a lysosome (Stasic et al., 2022). *Toxoplasma* possesses five known cathepsin proteases, two of which (cathepsin L, CPL, and cathepsin B, CPB) localise to the vacuolar compartment (Dou et al., 2013; Miranda et al., 2010; Parussini et al., 2010). These are trafficked here as prepeptides which eventually mature within the VAC's acidic environment thanks to CPL acting as a maturase for both (Dou et al., 2013; Parussini et al., 2010). A number of components of the VAC's membrane have been characterised, including a pore protein, VP1, whose knockout disrupted microneme localisation, secretion and subsequence attachment and invasion (Liu et al., 2014). An aquaporin, AQP, has also been investigated, and was seen to be non-essential (Miranda et al., 2010; Stasic et al., 2022). The chloroquine resistance transporter (CRT), a

transporter also localising to the VAC membrane has also been noted as being critical for export of digested material, thus maintaining the proper functioning of this compartment. Knockdown of this transporter, although not lethal to the parasites, was observed to result in an enlarged VAC (Thornton et al., 2019; Warring et al., 2014). This phenotype has also been observed when investigating one of the cathepsins inhabiting the VAC, CPL.

Pathways and adaptation to an intracellular parasitic lifestyle

One could argue that some of the most crucially secreted material in *Toxoplasma* are the micronemes, rhoptries, and dense granules, all of which are critical for a successful invasion and occupancy within a host cell. Upon translation, these proteins are trafficked and processed in the Golgi body and ELC prior to secretion. Bioinformatics approaches have identified a number of orthologs for components of the CORVET and HOPS complexes in *Toxoplasma* (Morlon-Guyot et al., 2015). A number of orthologs of endosome-associated Rab GTPases have also been identified, including Rab5 orthologs, classically associated with the early endosomes, and which are involved in trafficking material from the endosome-like compartment in *Toxoplasma* (Kremer et al., 2013; Sakura et al., 2016). Both Rabs 5a and 5c have been observed to be critical for correct trafficking of rhoptries and a subset of microneme proteins, but were seen to be non-essential for micronemal processing and ELC organisation, suggesting that their function is downstream of the ELC (Kremer et al., 2013). Rab7, typically associated with the late endosomes, was seen to be involved in trafficking between the endosome-like compartment and the VAC in *Toxoplasma* (Miranda et al., 2010; Parussini et al., 2010). Disruption of Rab7 was not seen to have an impact on trafficking to secretory organelles (Kremer et al., 2013). Along this same vein, other components and interactors of the CORVET and HOPS complexes were also seen to be essential for proper formation localisation of the secretory organelles as well as the VAC, including Vps11, Vps8, and TgBDCP (Morlon-Guyot et al., 2015, 2018). Clathrin heavy chain, dynamin B (DrpB), and the sortilin-like receptor (SortLR) are likewise also critical for exocytic trafficking, the perturbation of which resulting in a loss of the secretory organelles (Breinich et al., 2009; Pieperhoff et al., 2013; Sloves et al., 2012). Components of the VAC are also involved, with disruption of V-ATPase, *T. gondii* aspartyl protease 3 (*Tg*ASP3), and CPL negatively affecting the localisation, processing, or secretion of a number of microneme and rhoptry proteins (Dogga et al., 2017; Parussini et al., 2010; Stasic et al., 2019).

Following successful invasion into a host cell, *Toxoplasma* then uses endocytosis to satisfy its nutritional needs. In typical model eukaryotic cells such as mammalian and yeast cells, the endocytic process occurs as follows; clathrin-mediated endocytosed material is trafficked to the early endosomes, followed by the late endosomes, finally reaching the end destination by fusing with mature lysosomes (Galvez et al., 2012). This system, however, differs in plants. Here, the material taken up by the cells is first taken to the *trans*-Golgi, before being taken to the early endosomes (Viotti et al., 2010). Although not much is known about the process of endocytosis in *Toxoplasma* as of yet, a recent pre-print has demonstrated that a protein complex at the pellicle of the parasites forms a pore through which endocytosis occurs (Koreny et al., 2022). It has also been shown that extracellular parasites are capable of taking up exogenous lipids, later trafficking this material to the ER, Golgi body, and VAC (Gras et al., 2019). McGovern et al., (2018) have also observed that host proteins ingested by the parasites also end up localising to, and digested in, the VAC. Functional ablation of proteases within the VAC, either genetically or with the use of the protease inhibitor LHVS, was not observed to be lethal for tachyzoites, but resulted an accumulation of endocytosed host-derived GFP (Dou et al., 2014). Disruption of normal CPL function was also observed to be detrimental to the chronic stage of the parasites, with an accumulation of undigested organelles within the VAC (Di Cristina et al., 2017).

1.4. Tools to study the parasite

Toxoplasma is a haploid organism, meaning that genetic modifications are possible with relatively little difficulty (Sibley et al., 2009). In addition to this, both targeted as well as non-targetted mutations within the parasite genome are possible with ease, via the use of different parasite strains. These are possible since the parasite's primary means of DNA strand break repair seems to be non-homologous end-joining, thus facilitating random integration of constructs within the genome as well as allowing for easy knockouts via targeted double-strand breaks (Fox et al., 2009). In situations where a targeted integration of a construct is necessary, a strain wherein the ku80 gene is knocked out (Δku80), thus making the parasite deficient in non-homologous end-joining, is used (Huynh & Carruthers, 2009). Both the wildtype strain as well as the Δku80 strain were used extensively throughout this project as it is these repair mechanisms which oftentimes affected experimental design.

The molecular tools available to investigate the biology of the parasite are varied, with each technology having its own benefits and pitfalls (Jiménez-Ruiz et al., 2014). The main technologies which are used to alter protein levels, thus allowing for functional characterisation, fall under three main categories; those that allow alteration of the gene of interest within the genome (splitCas9, DiCre), those which control expression on the transcriptional level, and those which control the expression at the protein level. The choice of technology highly depends on the protein being investigated. Strategies which control protein expression on a transcriptional level or a protein level include those wherein the protein under investigation is knocked down, either via promoter replacement and downregulation of expression (Meissner et al., 2002; Sheiner et al., 2011), degradation of transcripts (Pieperhoff et al., 2015), or conditional protein destabilisation and subsequent degradation (Brown et al., 2018; Herm-Götz et al., 2007; Serpeloni et al., 2016). Techniques involving protein destabilisation and degradation are known to be very fast-acting and are therefore ideal when looking to elucidate the primary phenotype from any downstream ones, whereas strategies which depend on transcriptional regulation have the benefit of being reversible. One of the main drawbacks to these systems, however, is their tendency to be not very tightly regulated, sometimes exhibiting background expression (Jiménez-Ruiz et al., 2014). In addition to this, the system involving transcriptomic regulation necessitates that the gene of interest not be under the effect of the endogenous promoter anymore, thus possibly unintentionally altering the non-induced strain's behaviour (Jiménez-Ruiz et al., 2014). In the case of protein-level regulation, the working efficiency is heavily dependent on the accessibility of the protein of interest to the proteasome to which it is targeted (Smith et al., 2022). It was for this reason that the two systems used during this project, the DiCre system and the CRISPR/Cas9 system, both involved gene knockouts rather than protein regulation.

1.4.1. *The DiCre system*

The DiCre system involves expressing the Cre recombinase enzyme in two separate subunits within the parasite. One subunit is fused to FKBP domain, while the other is fused to FRB domain. In addition to the two Cre recombinase subunits, the target sequence to be deleted is flanked by two loxP sequences, that is, floxed (Andenmatten et al., 2013). Upon addition of rapamycin to the parasites expressing the Cre recombinase and floxed DNA

sequence, the FKBP and FRB subunits join together, reconstituting a functional enzyme which then excises the floxed DNA sequence.

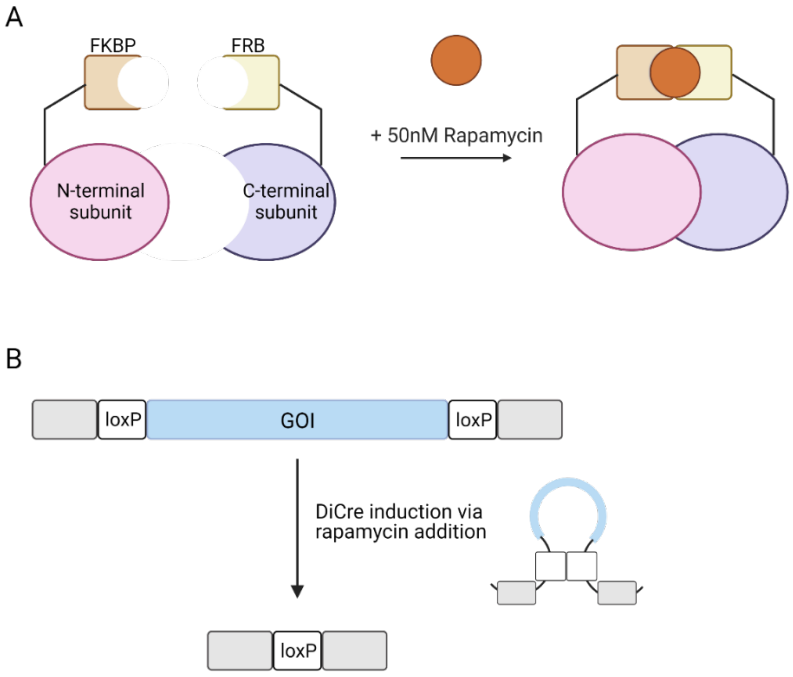

Figure 1.11 – The DiCre system
(**A**) The Cre recombinase enzyme subunits are expressed separately, with the N-terminal subunit fused to FKBP, and the C-terminal subunit of the enzyme fused to FRB. Upon addition of rapamycin, both the FKBP and FBR bind to the drug, bringing the two enzyme subunits together thus reconstituting a functional enzyme. (**B**) A functional Cre recombinase results in the excision of the floxed gene of interest, leaving behind a single loxP sequence. Image created using BioRender, adapted from Andenmatten et al., (2013).

1.4.2. *CRISPR/Cas9 and the splitCas9 system*

Genetic modifications using CRISPR/Cas9 (**c**lustered **r**egularly **i**nterspaced **s**hort **p**alindromic **r**epeats) involve the use of the Cas9 endonuclease (Jinek et al., 2012). This endonuclease is guided by a single guide RNA (sgRNA), a sequence of RNA complementary to the target sequence to be cleaved (Garneau et al., 2010; Hale et al., 2009; Jinek et al., 2012). This sgRNA sequence is fused to a recognition sequence which is recognised by, and thus bound to, the Cas9 enzyme. A protospacer adjacent motif (PAM) proximal to the target sequence is also necessary for the Cas9 enzyme to be able to cut the DNA, this cut normally occurring three nucleotides upstream of the PAM (Garneau et al., 2010; Jinek et al., 2012). Upon binding to the target sequence, the Cas9 induces a

double-strand break. This double-strand break is caused when each of the two nuclease domains present in the Cas9 enzyme cleaves one of the DNA strands (Gasiunas et al., 2012; Jinek et al., 2012). This break is typically repaired in one of two ways; either via non-homologous end-joining, or via the incorporation of donor DNA. The former repair mechanism has a high probability of generating indel mutations, resulting in a frameshift and the likelihood of a gene knockout. The use of the second repair mechanism, however, is useful for generating specific mutants. Both of these strategies for genome modification have been successfully used in *Toxoplasma* research (Shen et al., 2014; Sidik et al., 2014). In 2016, a critical genome-wide CRISPR/Cas9 screen was carried out to identify fitness conferring genes (Sidik et al., 2016, 2018).

Since the successful implementation of CRISPR/Cas9, multiple research groups have attempted to generate an inducible Cas9 system by splitting the enzyme into two subunits which are dimerisable upon induction (Nihongaki et al., 2015; Polstein & Gersbach, 2015) or chemicals (Zetsche et al., 2015). This has since been also implemented in *Toxoplasma* (Li et al., 2022). By fusing the rapamycin-binding domains FKBP and FRB, to the two Cas9 subunits and targeting them to different locations within the parasite, the Cas9 was rendered inactive. Similar to the aforementioned DiCre system, the activity of the Cas9 enzyme is then reconstituted upon addition of rapamycin, where the Cas9 subunits then come together within the parasite nucleus, and are able to create a double-strand break (Li et al., 2022).

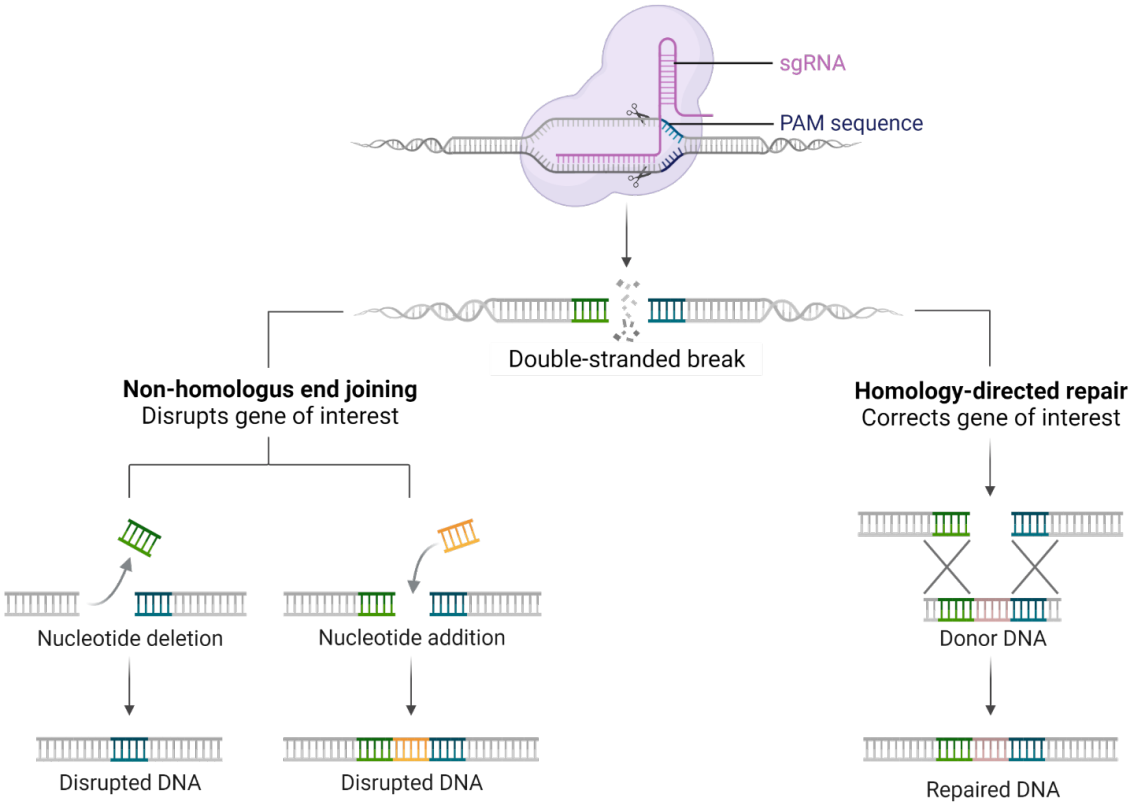

Figure 1.12 – CRISPR/Cas9-induced double-strand breaks and subsequent DNA repair

Interaction between the Cas9 enzyme and the guideRNA directs the endonuclease to the target site to be cut. The double-strand break occurs three nucleotides downstream of the PAM sequence. After the double-strand break occurs, the cut is either repaired via non-homologous end-joining or homology-directed repair. Non-homologous end-joining likely results in the addition or deletion of nucleotides, leading to a frameshift, and therefore a gene knockout. Homology-directed repair requires the presence of donor DNA which is flanked by regions homologous to the regions of the site of the double-strand break. The use of homology-directed repair results in specifically designed mutations. Reprinted from “CRISPR/Cas9 Gene Editing”, by BioRender.com (2022). Retrieved from https://app.biorender.com/biorender-templates

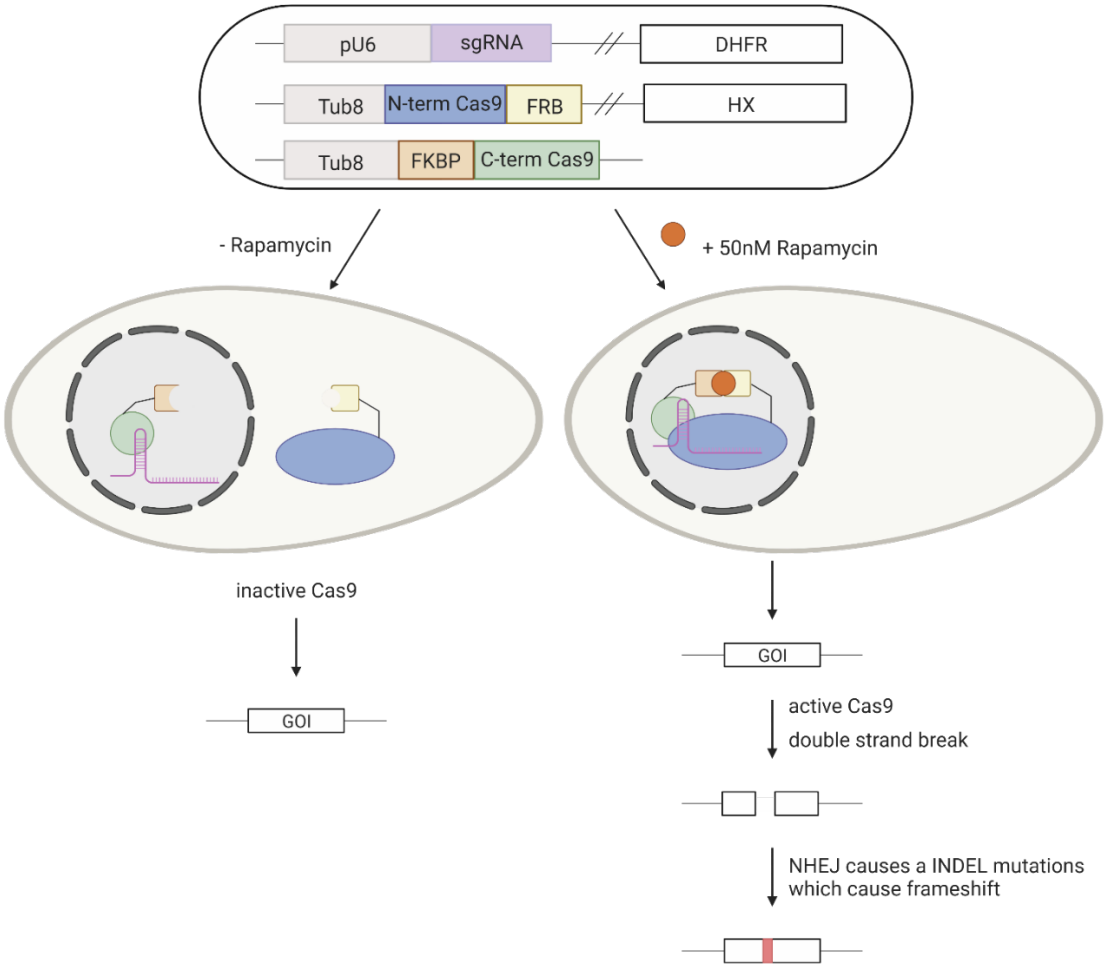

Figure 1.13 – The splitCas9 in *Toxoplasma gondii*

The splitCas9 system is similar to the DiCre system in that the two enzyme subunits are expressed separately, with one fused to FKBP domain and the other fused to FRB domain. The N-terminal subunit fused to FRB also includes a nuclear export sequence whereas the C-terminal-FKBP fusion also includes a nuclear import sequence, thus ensuring spatial separation within the cell and reducing the chances of system 'leakiness'. The constructs coding for these subunits are inserted into parasites via random integration and so also include drug-resistance cassettes for downstream selection and clone isolation. Upon addition of rapamycin, the FKBP and FRB domains join to reconstitute a functional Cas9 enzyme. The enzyme then binds with the sgRNA to cause a double-strand break which is repaired via non-homologous end-joining. Image created using BioRender, adapted from (Li et al., 2022).

1.5. Aims of the project

Despite the fact that multiple actin-binding proteins have been investigated in apicomplexan parasites, there still seems to be a lack of many actin-regulatory proteins which are typically found in other eukaryotic cells, including multiple proteins involved in nucleation, and proteins involved in actin filament bundling (Baum et al., 2006; Gordon & Sibley, 2005). Given how crucial actin is for parasite survival, proteins that serve these functions can still be expected to exist. It is this belief which has led to the formation of the original hypothesis of this project, this being that either a) conserved actin regulatory proteins are still present but have significantly diverged from their orthologs present in other eukaryotes to the point that they are no longer recognisable by bioinformatic approaches, or b) these conserved proteins have been altogether lost in apicomplexan parasites, and a unique set of actin-regulatory proteins have developed to fulfil the need left by these 'lost' proteins.

This project takes advantage of the work of a former PhD student in the Meissner lab, Dr. Johannes Stortz. In his project, Dr. Stortz generated a parasite line with the intention of using it for a phenotypic screen. In addition to the parasite strain expressing the Chromobody-emerald as a marker for actin filaments within *Toxoplasma*, he also created the splitCas9 constructs for *Toxoplasma*. In his project, he validated the use of this splitCas9 system and tested its efficacy by knocking out a number of well-known genes and analysing the phenotypes obtained. In addition to the efficacy of the splitCas9, Dr. Stortz also investigated its bystander effect and confirmed that while it does have unintended side-effects, it is still good for use in the context of a phenotypic screen.

With all of the above in mind, the overarching aim of this project was to use a knockout phenotypic screen to identify potential novel actin-regulatory or binding proteins in *Toxoplasma*. The main research objectives going into the project were to:

1. generate a curated guide RNA library that could be used for the purposes of carrying out knockout screens in pool.
2. use the generated guide RNA library and a parasite strain expressing the splitCas9, the actin chromobody, and an apicoplast marker to phenotypically screen for potential novel actin-regulatory proteins.
3. functionally characterise the candidates identified as potential actin-binding proteins.

After achieving these aims and obtaining a list of candidates, a candidate was picked for further characterisation based on its localisation at the Golgi body. The aims of the project then became:

1. to accurately localise the protein of interest.
2. to determine the essentiality of the protein.
3. to elucidate the biological function the protein of interest serves and the mechanism by which it is carrying out this function.
4. to understand its relevance to the acto-myosin system.
5. to understand its importance to the parasite biological system as a whole.

Chapter 2. Materials and Methods

2.1. Equipment

Table 2.1 – Equipment used during this study

Instrument	Manufacturer
4D-Nucleofector™ electroporation unit	Lonza
-86°C ULT freezer	Haier Biomedical
Agarose Gel Electrophoresis equipment	Bio-Rad, Avantor®
Analytical Balance	Sartorius, KERN
Centrifuge - 5810R & 5910R	Eppendorf
Centrifuge - Mini	Roth
Centrifuge - Pico™ 21 microcentrifuge, Mikro 200R, 5425R	Thermo Scientific™, Hettich, Eppendorf
Dynamag™-2 magnet	Thermo Scientific™
FACSAria™ III Cell Sorter	BD Biosciences
FastGene Blue/Green LED Transilluminator	Nippon Genetics
Fridge	Siemens, Bosch
Heating Block - Genius dry bath incubator	Major Science
Heating Block – ThermoMixer® C & ThermoMixer® Comfort	Eppendorf
Incubator - UM300	Memmert
Incubator – Heracell™ 240i	Thermo Scientific™
Incubator - Innova™ 4200	New Brunswick Scientific
Laminar Flow Hood - HERAsafe HS15	Thermo Heraeus
Laminar Flow Hood - ENVAIReco® Comfort Plus	ENVAIReco®
Microscope - 3D STED	Abberior

Microscope - Axiovert A1	Zeiss
Microscope - DMi8	Leica
Microscope - Primovert	Zeiss
Microwave	Sharp
NanoDrop® ND-1000 spectrophotometer	ThermoFisher Scientific
Neubauer Hemocytometer	Roth
Odyssey CLx	LI-COR Biosciences
pH meter	Mettler Toledo
Pipette controller - Accujet® Pro	BrandTech®
Pipettes - Multichannel	Eppendorf, Pipetman®
Pipettes - Single	Eppendorf, StarLab, Gibson
Printer P93D	Mitsubishi
Rotator SB2	Stuart
SDS-PAGE system, blotting apparatus	BioRad
Shaker - Titertek	Flow Laboratories
Thermal Cycler - Vapo.Protect Mastercycler® Pro	Eppendorf
Vacuum pump	A. Hartenstein
Vortex	Scientific Industries, Bender & Hobein GmbH
Water bath WB-12	Phoenix Instruments

2.2. Computer software

Table 2.2 – Computer software and online resources

Software / Website	**Source**
Adobe Acrobat Reader	Adobe Systems Inc.
AlphaFold	EMBL-EBI – (Jumper et al., 2021; Varadi et al., 2022) https://alphafold.ebi.ac.uk/
ApE Plasmid Editor	University of Utah (by M. Wayne Davis, v.2.0.53c)
bioRENDER	bioRENDER https://biorender.com/

Basic Local Alignment search tool (BLAST)	National Institute for Biotechnology Information (NCBI) https://blast.ncbi.nlm.nih.gov/Blast.cgi
Clustal Omega	EMBL-EBI – (Sievers et al., 2011) https://www.ebi.ac.uk/Tools/msa/clustalo/
DOG (Domain Graph, v. 2.0)	(Ren et al., 2009)
Eukaryotic Pathogen sgRNA Design Tool (EuPaGDT)	University of Georgia – (Peng & Tarleton, 2015) http://grna.ctegd.uga.edu/
Graphpad Prism 8.2.1.	GraphPad Software
Fiji (ImageJ) software v.2.1.0	National Institutes of Health (NIH) – (Schindelin et al., 2012)
Imspector 16.3.14274	Abberior Instruments
InterPro	EMBL-EBI – (Blum et al., 2021) https://www.ebi.ac.uk/interpro/
LasX software (v. 3.4.2.183668)	Leica Microsystems
LI-COR Image Studio software	LI-COR Biosciences – GmbH
Mendeley	Mendeley Ltd.
Perseus 1.6.15.0	Max Planck Institute of Biochemistry
STRING v11.5	(Szklarczyk et al., 2011) https://string-db.org/
NEB tools™ - Tm Calculator	New England Biolabs (NEB) https://tmcalculator.neb.com/#!/main
ToxoDB Toxoplasma Informatics Resources	National Institute of Allergy and Infectious Diseases (NIAID) – (Gajria et al., 2008) https://toxodb.org/toxo/app
Windows 10, Microsoft Office 2019	Microsoft Corporation
TMHMM 2.0	Technical University of Denmark – (Krogh et al., 2001) https://services.healthtech.dtu.dk/service.php?TMHMM-2.0
HHPred	MPI Bioinformatics Toolkit – (Gabler et al., 2020; Zimmermann et al., 2018) https://toolkit.tuebingen.mpg.de/tools/hhpred

2.3. Consumables, and biological and chemical reagents

Consumables

Table 2.3 – Consumables used during this study

Source	Product
Eppendorf	Eppendorf tubes
Faust	Cryotubes; Cell scrapers; Falcon tubes; TPP cell culture dishes, plates, and flasks; Vacuum filtration system
A. Hartenstein	Pipette controller filters; Coverslips
ibidi	Glass bottom 96 well plates; µSlide 8well Glass Bottom
IBL	Glass bottom dish with 20 mm micro-well #1.5 cover glass
Roth	Bacteria cell spreaders; Sterile Filter Nylon 0,2 µm; Microscope slides; Parafilm
Sarstedt	Aspirators; Serological pipettes
Merck	Membrane filters 3um; Amersham™ Protran® Western blotting membranes 0,45 µm 300 mm x 4 m; Whatman® cellulose chromatography papers
SMS Medipool	Sterile needles; Gloves; Sterile syringes
StarLab	Pipette tips
VWR	PCR tubes; Petri dishes; Reaction reservoirs

Kits

Table 2.4 – Commercial kits used during this study

Company	Kit
Blirt	ExtractMe Genomic DNA kit, ExtractMe Plasmid Mini kit, ExtractMe DNA Clean-Up and Gel-out kit
Qiagen	Plasmid Plus Midi kit
Lonza	P3 Primary Cell 4D-NucleofectorTM X Kit L

Buffers, solutions, and media

Table 2.5 – Buffers, solutions, and media prepared or modified in-house

Solutions or media	Components	Use
LB medium	10 g/L tryptone, 5 g/L yeast extract, 10 g/L NaCl	Bacterial culture
LB agar	1.5% agar (w/v) in LB medium	Bacterial culture
50% glycerol	50% glycerol (v/v) in ultrapure water	Bacterial culture
Supplemented DMEM	500 mL DMEM, 10% FCS (v/v), 4 mM L-glutamine, 20 µg/mL gentamicin	Cell Culture
2X Freezing medium	50% FCS (v/v), 20% DMSO (v/v), 30% supplemented DMEM (v/v)	Cell Culture
Supplemented DMEM FluoroBrite	500 mL DMEM FluoroBrite, 10% FCS (v/v), 4 mM L-glutamine, 20 µg/mL gentamicin	Cell Culture
2.5% Glutaraldehyde	1:20 50% Glutaraldehyde in PBS	Electron Microscopy
1X TAE	1:50 50X TAE in water	Gel electrophoresis
Agarose	0.8-2% (w/v) agarose in 1X TAE	Gel electrophoresis
4% PFA	1:5 20% PFA in PBS	Immunofluorescence assays
Blocking buffer	3% BSA (w/v) in PBS	Immunofluorescence assays
Permeabilising buffer	0.2% (v/v) Triton TX-100 in blocking buffer	Immunofluorescence assays
Annealing buffer	10 mM Tris-base pH 7.5-8, 50 mM NaCl, 1 mM EDTA	Plasmid preparation
Tris-HCl	50 mM Tris-HCl (pH 8)	TurboID pulldowns

RIPA buffer	50 mM Tris-HCl (pH 8), 0.5% sodium deoxycholate, 150 mM NaCl, 1 mM EDTA, 0.1% SDS, 1% Triton TX-100	Western Blotting/ TurboID pulldowns
Orange protein loading buffer	125 mM Tris-HCl pH 6.5, 50% glycerol (v/v), 4% SDS (w/v), 0.2% Orange G (w/v)	Western Blotting
Running buffer (10X)	250 mM Tris-base, 1.92 M glycine, 1% SDS (w/v)	Western Blotting
Transfer buffer (10X)	480 mM Tris base, 390 mM glycine, 10-20% methanol (v/v)	Western Blotting
Tris-buffered saline (10X) (TBS)	152 mM Tris-HCl, 46 mM Tris-base, 1.5 M NaCl	Western Blotting
TBST	1X TBS, 0.2% Tween-20	Western Blotting
PBST	1X PBS, 0.2% Tween-20	Western Blotting
Ponceau S Stain	0.1% (w/v) Ponceau S, 5% (v/v) acetic acid	Western Blotting
Blocking buffer	1X TBS, 0.1% (v/v) Tween-20, 5% (w/v) non-fat milk powder	Western Blotting

Table 2.6 – Commercial chemical and biological reagents

Source	Product
Biochrom	Trypsin/EDTA 0,05% / 0,02%
BioRad	4–20% Mini-PROTEAN® TGX™ Precast Protein Gels
Biotrend	GelRed® Nucleic Acid Gel Stain, 10,000X
Biozym	Sieve GeneticPure Agarose
A. Hartenstein	Incuwater-Clean™ ; Yeast extract; Agar; Tryptone
Heirler Cenovis	Skimmed milk powder
LI-COR Biosciences	Odyssey® Blocking Buffer (TBS); Chameleon Duo Pre-stained Protein Ladder
Life Technologies	Hoechst 33342 solution 20 mM
Merck	Hemacolor® Rapid blood smears sol. 2; Hemacolor® Rapid blood smears sol. 3; NaOH; Ampicillin Sodium Salt; Biotin >99% (HPLC) lyophilized powder; BSA; Dulbecco′s Modified Eagle′s Medium - high glucose; DMSO anhydrous; DNA Ladder 250bp; EDTA; Brefeldin A; FBS; Gentamycin; H_2O sterile; Hydrochloric acid 37%; Calcium Ionophore A23187; Potassium chloride; L-Glutamine 200 mM; Magnesium chloride anhydrous >98%; Sodium chloride; Orange G sodium, mol.biol. Grade; Dulbecco's phosphate buffered saline; Poly-L-lysine solution 0,1% (w/v) in H_2O; Pyrimethamine; Rapamycin; Sodium Acetate; Sodium deoxycholate; Tris-HCl; Tris base; Tween 20; 5-Fluoro-2'-Desoxyuridine (FUDR)
NEB	NEBuffer 3.1; AseI; BsaI-HFv2; CutSmart Buffer; 1kb DNA Ladder; 1kb Plus DNA Ladder; DNA Ladder 100bp; Deoxynucleotide (dNTP) Solution Mix; Gibson Assembly® Master Mix; Gel loading Dye Blue 6X; NsiI-HF; PacI; Q5 High-Fidelity DNA Polymerase; Quick-Load Purple 1kb Plus DNAs Ladder; T4 DNA Ligase; Taq DNA Polymerase
NIPPON	Midori Green Advance
Roth	Acetic acid 100%; Ethanol; Glycerol 99.7%; Iso-Propanol; Methanol HPLC Gradient; pH 10.00 buffer; pH 4.00 buffer; pH

	7.00 buffer; Ponceau S; SDS 99% Blotting Grade; TAE Buffer 50X; Triton X-100
Electron Microscopy Science	Glutaraldehyde EM quality, 50% aqueous solution; 20% Paraformaldehyde
Thermo Fisher	ProLong™ Gold Antifade Mountant; Proteinase K; Dynabeads™ MyOne™ Streptavidin T1; FluoroBrite™ DMEM; Pierce™ Protease Inhibitor Mini Tablets
Zeiss	Immersion oil 518F

Antibodies

Table 2.7 – Primary antibodies used for immunofluorescence assays

Antibody	Origin	Dilution	Source
CPL	Rabbit	1:1000	Vern Carruthers
DrpB	Rat	1:1000	Peter Bradley
GAP45	Rabbit	1:1000	Dominique Soldati
GFP	Mouse	1:1000	Roche #11841460001
GFP	Rabbit	1:1000	Abcam #AB290
Gra1	Mouse	1:500	BIOTEM BIO.018.4 Clone TG 17-3
G2-Trx	Rabbit	1:500	Lilach Sheiner
HA	Rat	1:1000	Roche #1187431001
IMC1	Mouse	1:1000	Gary Ward
Mic2 6D10	Mouse	1:500	Vern Carruthers
Mic3 T82C10	Mouse	1:300	
Mic8	Rabbit	1:500	
Pro-M2AP	Rabbit	1:1000	Vern Carruthers
RFP	rabbit	1:1000	Rockland 600-401-379
Rop2,4 T34A7	Mouse	1:500	
SAG1	Mouse	1:1000	Sebastian Lourido
TOM40	Rabbit	1:2000	Giel Van Dorreen
Streptavidin, Alexa Fluor™ 594 conjugate	N/A	1:1000	Thermofisher #S11227

Table 2.8 – Secondary antibodies used for immunofluorescence assays

Antibody	Origin	Dilution	Source
anti-Rat IgG (H+L) Alexa Fluor™ 488	Goat	1:2000	Invitrogen #A-11006
abberior STAR 580, anti-rat IgG	Goat	1:2000	Abberior #ST580-1007-500UG
abberior STAR RED, anti-rat IgG	Goat	1:2000	Abberior #STRED-1007-500UG
anti-Rabbit IgG (H+L) Alexa Fluor™ 350	Goat	1:2000	Invitrogen #A-11046
anti-Rabbit IgG (H+L) Alexa Fluor™ 488	Goat	1:2000	Invitrogen #A-11008
abberior STAR 580, anti-rabbit IgG	Goat	1:2000	Abberior #ST580-1002-500UG
abberior STAR 635P, anti-rabbit IgG	Goat	1:2000	Abberior #ST635P-1002-500UG
anti-Mouse IgG (H+L) Alexa Fluor™ 488	Goat	1:2000	Invitrogen #A-11001
abberior STAR 580, anti-mouse IgG	Goat	1:2000	Abberior #ST580-1001-500UG
abberior STAR 635P, anti-mouse IgG	Goat	1:2000	Abberior #ST635P-1001-500UG

Table 2.9 – Antibodies used for Western blotting

Antibodies	Origin	Dilution	Source
Aldolase	Rabbit	1:10,000	David Sibley
IRDye680RD anti-Rabbit IgG	Donkey	1:10,000	LI-COR Biosciences, 925-68073
IRDye 800CW Streptavidin	N/A	1:20,000	LI-COR Biosciences, 926-32230

Dyes

Table 2.10 – Dyes used during this study

Dye	Concentration	Source & Cat. No.
HaloTag Oregon Green	0.2 µM	Promega, G280B
Janelia Fluor HaloTag ligand 549	200 nM	Promega, GA111A
Janelia Fluor HaloTag ligand 646	20 nM	Promega, GA112A
SNAP-Cell 647-SiR	1 µM	Biolabs, S9102S

Drugs

Table 2.11 – Drugs used during this study

Drug	Stock concentrations	Use
Ampicillin (1000x)	100 mg/mL in H_2O	Bacterial culture
Ci A23187 (1000x)	2 mM in DMSO	Egress assays
Brefeldin A (1000x)	100 µg/mL in DMSO	Golgi disruption IFA
Rapamycin (1000x)	50 µM in DMSO	Knockout induction
Pyrimethamine (1000x)	1 mM in ethanol	*Toxoplasma* drug selection
Mycophenolic acid (MPA) (500x)	39 mM in methanol	*Toxoplasma* drug selection
Xanthine (XAN) (500x)	115 mM in 1M KOH	*Toxoplasma* drug selection
FUDR (5000x)	5 mM in H20	*Toxoplasma* drug selection

Oligonucleotides & Library sgRNAs

Please refer to appendix for full tables.

Plasmids

Table 2.12 – Plasmids used during this study

Name	Information	Purpose	Source
Cas9_YFP plasmid	pTub_Cas9-YFP/pU6_ccdB_tracrRNA	Generation of Cas9_sgRNA plasmid	Curt-Varesano et al., 2016
Cas9_YFP_sgRNA plasmid	pTub_Cas9-NLS-YFP/pU6_sgRNA	Induce double strand break in target sequence	This study
Chromobody Emerald plasmid	pDHFR_chromobody_Emerald	Amplification for UPRT locus replacement	Periz et al., 2017
GFP-Nanobody plasmid	pCMV_SNAP_CRY2_VHH(GFP)	Generation of GFP-NB_Halo plasmid	addgene plasmid 58370
GFP-Nanobody_Halo plasmid	p5RT70_Halo_GFP-Nanobody_HXGPRT	Detection of cytosolic GFP	This study
GRASP-RFP plasmid	pTub_GRASP55_RFP	Amplification for UPRT locus replacement	Pfluger et al., 2005
HA plasmid	pUC19_LIC_3HA_LoxP	Amplification of tag	Meissner Lab
Halo plasmid	pUC19_LIC_Halo-LoxP	Amplification of tag	Meissner Lab
Library	pU6_Library_DHFR	Library	This study
mCherry plasmid	pUC19_LIC_mcherry-LoxP	Amplification of tag	Meissner Lab
p5RT70_DDmycGFP	p5RT70_DD_myc_GFP_HXGPRT	Generation of GFP-Nb_Halo plasmid	Herm-Götz et al., 2007
pU6_DHFR	pU6_DHFR	Generation of sCas9 library	Sidik et al., 2016
SNAP plasmid	pGEM _LIC_SNAP_ LoxP	Amplification of tag	Meissner Lab
SYFP2 plasmid	pUC19_LIC_SYFP2-LoxP	Amplification of tag	Meissner Lab
TurboID plasmid	pGEM_LIC_TurboID_ LoxP	Amplification of tag	Meissner Lab

Cell strains and cell lines

Table 2.13 – Bacterial strains used during this study

Strain	Competence	Source
DH5α	Chemically competent	NEB®
E. cloni® EXPRESS	Electrocompetent	Lucigen®

Table 2.14 – Mammalian cell lines used during this study

Line	Source	Origin
Human Foreskin Fibroblasts (HFFs)	ATCC® SCRC-1041™	*Homo Sapiens*

Table 2.15 – *Toxoplasma gondii* strains used during this study

Strain Ref. No.	Strain	Resistance	Source / Parental strain
1	RH ΔKu80 DiCre	*cat*/Δ*hxgprt*	Hunt et al., 2019
2	RH sCas9/Cb_Emerald/FNR_RFP	*cat*/Δ*hxgprt* */dhfr*	Dr. Elena Jimenez Ruiz
3	RH sCas9/Cb_Emerald/FNR_RFP/SAG1_sgRNA	*cat*/Δ*hxgprt* */dhfr*	Strain #2
4	RH sCas9/Cb_Emerald/FNR_RFP/Act1_sgRNA	*cat*/Δ*hxgprt* */dhfr*	Strain #2
5	RH sCas9/Cb_Emerald/FNR_RFP/DrpA_sgRNA	*cat*/Δ*hxgprt* */dhfr*	Strain #2
6	RH sCas9/Cb_Emerald/FNR_RFP/library	*cat*/Δ*hxgprt* */dhfr*	Strain #2
7	RH sCas9/Cb_Emerald/HSP60_RFP	*cat*/Δ*hxgprt* */dhfr*	Dr. Elena Jimenez Ruiz
8	RH sCas9/YFP-IMC1/MIC8_RFP	*cat*/Δ*hxgprt* */dhfr*	Dr. Elena Jimenez Ruiz
9	RH ΔKu80 DiCre/248490_3HA	*cat*/Δ*hxgprt*	Strain #1
10	RH ΔKu80 DiCre/229460_SYFP2	*cat*/Δ*hxgprt*	Strain #1
11	RH ΔKu80 DiCre/286790_3HA	*cat*/Δ*hxgprt*	Strain #1
12	RH ΔKu80 DiCre/255920_3HA	*cat*/Δ*hxgprt*	Strain #1
13	RH ΔKu80 DiCre/210490_3HA	*cat*/Δ*hxgprt*	Strain #1
14	RH ΔKu80 DiCre/294930_SYFP2	*cat*/Δ*hxgprt*	Strain #1
15	RH ΔKu80 DiCre/269700_mCherry	*cat*/Δ*hxgprt*	Strain #1
16	RH ΔKu80 DiCre/249970_3HA	*cat*/Δ*hxgprt*	Strain #1
17	RH ΔKu80 DiCre/263680_3HA	*cat*/Δ*hxgprt*	Strain #1
18	RH ΔKu80 DiCre/259720_mCherry	*cat*/Δ*hxgprt*	Strain #1

19	RH ΔKu80 DiCre/226320_SNAP	*cat*/Δ*hxgprt*	Strain #1
20	RH ΔKu80 DiCre/301410_SYFP2	*cat*/Δ*hxgprt*	Strain #1
21	RH ΔKu80 DiCre/floxed301410_SYFP2	*cat*/Δ*hxgprt*	Strain #18
22	RH ΔKu80 DiCre/floxed301410_mCherry	*cat*/Δ*hxgprt*	Strain #1
23	RH ΔKu80 DiCre/301410_SNAP	*cat*/Δ*hxgprt*	Strain #1
24	RH ΔKu80 DiCre/floxed301410_mCherry/SortLR_Halo	*cat*/Δ*hxgprt*	Strain #20
25	RH ΔKu80 DiCre/floxed301410_SYFP2/GRASP55_RFP	*cat*/Δ*hxgprt* /Δ*uprt*	Strain #19
26	RH ΔKu80 DiCre/floxed301410_mCherry/Syn6_Halo	*cat*/Δ*hxgprt*	Strain #20
27	RH ΔKu80 DiCre/floxed301410_mCherry/GFP-Nb_Halo	*cat*/Δ*hxgprt* /Δ*uprt*	Strain #20
28	RH ΔKu80 DiCre/floxed301410_SYFP2/GFP-Nb_Halo	*cat*/Δ*hxgprt* /Δ*uprt*	Strain #19
29	RH ΔKu80 DiCre/floxedFRM2_SYFP2/GFP-Nb_Halo	*cat*/Δ*hxgprt* /Δ*uprt*	Stortz et al., 2019
30	RH ΔKu80 DiCre/floxedSAG1_YFP/GFP-Nb_Halo	*cat*/Δ*hxgprt* /Δ*uprt*	Dr. Mirko Singer
31	RH ΔKu80 DiCre/301410_TurboID	*cat*/Δ*hxgprt*	Strain #1
32	RH ΔKu80 DiCre/floxed301410_mCherry/Cb_Emerald	*cat*/Δ*hxgprt* /Δ*uprt*	Strain #20
33	RH ΔKu80 DiCre/floxed301410_mCherry/MyoF_Halo	*cat*/Δ*hxgprt*	Strain #20
34	RH ΔKu80 DiCre/floxed301410_mCherry/FRM2_SYFP2	*cat*/Δ*hxgprt*	Strain #20
35	RH ΔKu80 DiCre/floxedFRM2_SYFP2/301410_Halo	*cat*/Δ*hxgprt*	Stortz et al., 2019
36	RH ΔKu80 DiCre/floxed301410_mCherry/SAG1_Halo	*cat*/Δ*hxgprt*	Strain #20
37	RH Δku80 DiCre/floxed301410_SYFP2/213390_Halo	*cat*/Δ*hxgprt*	Strain #19

38	RH Δku80 DiCre/CbEmerald/213390_mCherry	*cat*/Δ*hxgprt*	Strain #1
39	RH ΔKu80 DiCre/floxed301410_mCherry/AP-4ε_Halo	*cat*/Δ*hxgprt*	Strain #20

2.4. Microbiology methods

2.4.1. Liquid cultures and cryopreservation of bacterial stocks

Bacteria streaked or spread across an agar plate were incubated for a period of between 14 and 18 hours at 37°C. A single isolated colony was then picked and added to LB broth containing the required antibiotic depending on the plasmid being amplified, after which the broth was incubated overnight at 37°C while shaking.

Glycerol stocks were prepared by mixing the grown bacterial liquid cultures with filtered freezing medium (50% v/v glycerol in deionised water) at a ratio of 2:1. The bacterial glycerol stocks were stored at -80°C.

2.4.2. Transformation of bacteria

Transformation of electrocompetent bacteria

Transformations into electrocompetent bacteria were made for the purpose of generating the plasmid library, as was done in Sidik et al., (2018). The ElectroSquarePorator™ ECM® 830 (BTX) was used with the following settings:

Table 2.16 – Electroporation settings used

Setting	**Value**
Choose mode	LV
Set voltage	500 V
Set pulse length	17 ms
Set number of pulses	1
Electrode type	BTX Disposable Cuvettes Model #610 (1mm gap)
Desired Field Strength	5.0 kV/cm

A total volume of 50 µL was used. Plasmids assembled using Gibson assembly were transformed in two batches and allowed to grow to log phase. The plasmids were then extracted, purified, pooled, and 200ng retransformed to further amplify the library. Library complexity was estimated by using serial dilutions to calculate the number of transformed bacteria. The complexity was assumed to have been maintained based on the fact that; 1. The number of obtained colonies exceeded that recommended in Sidik et al., (2018) ($3.2x10^4$ were needed to maintain complexity, $3x10^6$ colonies were obtained), and 2. The random isolation and sequencing of colonies showed that 77% of those isolated were unique.

Transformation of chemically competent bacteria

Transformations were done according to manufacturer instructions, with some amendments. In short, DH5α competent cells were thawed on ice, after which 5 ng of plasmid or 5 µl of freshly ligated chilled plasmid mixture were added to about 50 µl of competent cells in a microcentrifuge tube and gently mixed by pipetting. The tube was placed on ice for 30 minutes, heat shocked at 42°C for 30 seconds, and placed on ice again for 5 minutes. The transformation mixture was then spread onto a prewarmed agar plate containing the required antibiotic and incubated for a period of between 14 and 18 hours at 37°C.

2.5. Molecular biology methods

2.5.1. Polymerase chain reaction

PCR was done in order to amplify DNA fragments to be used for multiple purposes, including ligations, transfections and for analytical purposes. Q5® high-fidelity DNA polymerase was used in situations where the prevention of mutations was of utmost importance, including the generation of repair DNA to be used for transfections, whereas standard *Taq* polymerase was used for analytical purposes. The PCR mixes and thermal profiles for both types of polymerases were prepared as in the tables below. The annealing temperatures used depended on the melting temperatures of the primers used, and were calculated using the online NEB Tm calculator. The length of the elongation period during

the amplification steps depended on the length of the fragments being amplified, as detailed in the tables below. All reagents were mixed well by pipetting prior to mixture preparations.

Table 2.17 – Q5 PCR reaction mix

Component	volume / 25 µl reaction	Final concentration
5X Q5 reaction buffer	5 µl	1X
10 mM dNTPs	0.5 µl	200 µM
10 mM forward primer	1.25 µl	0.5 µM
10 mM reverse primer	1.25 µl	0.5 µM
5X Q5 high GC enhancer	5 µl	1X
Q5® high-fidelity DNA polymerase	0.25 µl	0.5 units
nuclease-free water	variable	
Template DNA	variable	<1000 ng

Table 2.18 – Q5 PCR reaction conditions

Step	Temperature/ °C	Time
Initial denaturation	98	30 sec
30 cycles	98	10 sec
	variable	30 sec
	72	30 sec/kb
Final extension	72	2 mins
Hold	4	∞

Table 2.19 – *Taq* PCR reaction mix

Component	volume / 25 µl reaction	Final concentration
10X standard *Taq* Reaction Buffer	2.5 µl	1X
10 mM dNTPs	0.5 µl	200 µM
10 mM forward primer	0.5 µl	0.2 µM
10 mM reverse primer	0.5 µl	0.2 µM
Taq DNA polymerase	0.125 µl	0.75 units
nuclease-free water	variable	
Template DNA	variable	<1000 ng

Table 2.20 – Taq PCR reaction conditions

Step	Temperature/ °C	Time
Initial denaturation	95	30 sec
30 cycles	95	30 sec
	variable	40 sec
	68	1 min/kb
Final extension	68	5 mins
Hold	4	∞

2.5.2. Agarose gel electrophoresis

Agarose gel electrophoresis was used both for analytical purposes as well as to separate DNA fragments for downstream uses. The concentration of the agarose in 1X TAE buffer used depended on the size of fragments being separated, the concentration ranging between 0.8% and 2%. GelRed Nucleic acid stain was generally used to allow visualisation using UV light. In cases where the DNA fragments separated needed to be used further, Midori Green was used as DNA stain instead of GelRed Nucleic acid stain. The NEB 6X loading dye was used to facilitate loading of the DNA onto the gel. Different DNA ladders were used to determine the size of the DNA fragments being separated, the type of ladder used depending on the size of the DNA fragments in question.

2.5.3. DNA restriction

Restriction enzymes were used according to manufacturer's instructions. DNA restriction incubation times and the amount of enzyme added varied depending on the amount of DNA being digested and the concentration of the enzyme being used. In the case of analytical digests, the amount of DNA digested was always less than 1 µg, generally making the total reaction volume less than 10 µL. For preparative restriction reactions which were done prior to transfection, 10 µg were typically digested for a minimum of 6 hours.

2.5.4. DNA purification

DNA purification from both PCR mixes as well as from agarose gels was done using the ExtractMe DNA Clean-Up Kit (Blirt) according to manufacturer's instruction. During DNA collection, DNA was incubated with elution buffer for 5 minutes at room temperature prior to centrifugation to maximise yield.

2.5.5. sgRNA preparation

Oligos ordered were resuspended according to manufacturer's instructions to make up a stock solution of 100 µmoles. 2 µL of both the forward and reverse primer were mixed with 16 µL of annealing buffer and placed in a heating block at 95°C for 5 minutes. The heat was then switched off and the mixtures allowed to cool gradually to room temperature, after which they were either used for ligation or stored at -20°C until use.

2.5.6. Gibson assembly

Gibson assembly was used to both generate the library plasmids by ligating the sgRNAs into the vector, as was done in Sidik et al. (2018), as well as generate the plasmid encoding the GFP-nanobody-Halo construct. In both cases, the protocol was done according to manufacturer's instructions. The reaction mixtures were prepared as follows:

Table 2.21 – Gibson assembly reaction mix

Component	Library mixture	Nanobody mixture
Total amount of fragments	0.02 – 0.5 pmols X µL	10 µL
Gibson assembly master mix (2X)	10 µL	10 µL
Deionised water	10-X µL	0 µL
Total volume	20 µL	20 µL

The reaction mixtures were incubated in a thermal cycler at 50°C for 15 minutes, after which they were either used for transformations or stored at -20°C until use.

2.5.7. DNA ligation

Ligations were done in order to generate new plasmids. The inserts used for the ligations were prepared in one of two ways; either by PCR amplification of the construct of interest, introducing sticky ends via the primers, or by primer annealing as explained in the subheading above.

Ligations were done using the T4 DNA ligase (NEB). The ligation mixtures were prepared as follows:

Table 2.22 – DNA ligation mix

Component	Amount
T4 DNA ligase buffer (10X)	2 µL
Vector DNA	50 ng
Insert DNA	37.5 ng
T4 DNA ligase	1 µL
Nuclease-free water	Up to 20 µL

All reagents were mixed well via pipetting up and down prior to the preparation of the mixture. The ligation mixtures were incubated at room temperature overnight.

2.5.8. Plasmid DNA isolation from bacteria

Plasmid DNA was generally isolated from liquid bacterial cultures using ExtractMe Plasmid Mini kit (Blirt) according to manufacturer's instructions. During the final step, DNA was incubated with elution buffer for 5 minutes at room temperature prior to centrifugation to maximise yield.

In the case of the sgRNA library, the plasmid library was extracted from liquid bacterial cultures using the QIAGEN Plasmid Plus Midi kit (Qiagen) according to manufacturer's instructions.

2.5.9. Preparation of DNA for Toxoplasma transfections

DNA was prepared for transfections using ethanol precipitation. The required amount of DNA was mixed with 100% ice-cold ethanol and sodium acetate (3M, pH5) at ratios of 1:3 and 10:1 respectively. The mixture was then incubated at -80^{o}C for a minimum of 30 minutes, after which the DNA was pelleted at maximum speed at 0^{o}C for one hour. The DNA was subsequently washed with 70% ethanol and pelleted at maximum speed at 0^{o}C for 10 minutes twice. The DNA pellet was finally air dried under sterile conditions for approximately 5 minutes, after which it was either eluted in P3 buffer for immediate transfection (using the Amaxa© system), or in 10 µl of ultrapure water for storage (at -20^{o}C) and later transfection.

2.5.10. Genomic DNA isolation from Toxoplasma

To extract genomic DNA from *Toxoplasma*, approximately 500 µl of freshly lysed tachyzoites were first centrifuged at 1500 g for 5 minutes. DNA from the parasite pellet was then extracted using the ExtractMe Genomic DNA kit (Blirt) according to manufacturer's instructions.

In order to carry out rapid genotyping of parasite clones from the library 96-well plates, DNA was extracted by first gently resuspending the parasites in the well by pipetting, and then centrifuging 100 µl at 1500 g for 5 minutes. The supernatant was removed and 18 µl of elution buffer and 2 µl of proteinase K from the above-mentioned kit (Blirt) were added to the parasite pellet, after which this mixture was incubated at 50^{o}C for 20 minutes and then at 95^{o}C for 10 minutes. This mixture was then used for genotyping PCRs.

2.5.11. DNA sequencing

DNA sequencing was done by Eurofins Genomics. The DNA to be sequenced, whether plasmid DNA or PCR products, along with the primers for sequencing, were prepared according to the company's requirements.

The plasmids and purified PCR products and their associated primers were prepared as follows:

Table 2.23 – Plasmid sample preparations for sequencing

Sample type	Sample concentration	Volume / reaction
Plasmid	100 ng/µL	20 µL
Purified PCR products	5 ng/µL	35 µL
Primer	10 pmol/µL	20 µL

In the case of the unpurified PCR products obtained from amplification of the sgRNAs integrated in the screen clones, these were prepared by first estimating the DNA concentration of the PCR products via gel electrophoresis. The DNA concentration was normalised across the plates and the plates and primers prepared as follows:

Table 2.24 – PCR product preparations for sequencing

Sample type	Sample concentration	Volume / reaction
Primer	10 pmol/µL	15 µL (+5 µL for every subsequent reaction)
Purified PCR products	Minimum 10 ng/µL	15 µL

The final well of every plate was left empty for the company to run an internal quality control.

2.6. Biochemistry methods

2.6.1. Indirect immunofluorescence Assays

Parasites were used to inoculate a fresh monolayer of HFFs. These were then incubated at 37°C and 5% CO_2 for the desired length of time, after which they were either imaged live or fixed with 4% paraformaldehyde (PFA) for 15 mins at room temperature. Live imaging was generally done for parasites which expressed proteins tagged with self-labelling tags such as SNAP-tag and Halo-tag. For this labelling, synthetic dyes were added according to manufacturer's instructions. In the case of samples expressing Halo- or SNAP-tagged proteins which required fixation, the synthetic dyes were added prior to fixation.

In the case of fixed IFA slides, the cells were washed thrice with PBS following fixation. These were then permeabilised and blocked for 45mins at room temperature with 3%

bovine serum albumin (BSA), and 0.2% Triton X-100 in PBS. Subsequently, the cells were labelled for 1 hour at room temperature with primary antibodies diluted in the blocking/permeabilising buffer according to Table 2.7. Following this incubation, the cells were again washed thrice with PBS, and then labelled for 1 hour at room temperature in the dark with secondary antibodies diluted in the blocking/permeabilising buffer according to Table 2.8. After labelling with the secondary antibodies, the cells were then incubated with 0.4 µM Hoechst for 5 minutes at room temperature in the dark, and then finally washed thrice with PBS and mounted with ProLong™ Gold antifade mountant (ThermoFisher Scientific).

Brefeldin A (BFA) was used during IFAs in order to disrupt Golgi trafficking, redirecting all Golgi material back to the ER (Sciaky et al., 1997). For these experiments, 100 µg/mL BFA was added for 1 hour prior to fixation.

For IFAs done in order to visualise the biotinylated proteins, 150 µM biotin was added for either 30 minutes or 6 hours prior to fixation.

2.6.2. Western Blots

Sample Preparation

HFFs were infected with parasites and incubated for the desired length of time, after which they were harvested. The parasites were washed with PBS and then counted and the equal number of parasites were aliquoted. These were pelleted at 1500 g for 5 minutes, after which the PBS was aspirated and the pellets frozen at -80°C until use.

The pellets were lysed with 8 µL of lysis buffer and incubated for 5 minutes on ice. The lysis material was then centrifuged at full speed for 4 minutes at 0°C, after which 7.8 µL of the supernatant taken and mixed with 3 µL 4X loading dye and 1.2 µL 10X DTT (to a final concentration of 50 mM) and boiled at 95°C for 10 minutes. In the case of TurboID control samples, 10 µL of 100 µM biotin were also added to the mixture prior to boiling.

Protein Migration

12 µL of the boiled sample were loaded onto a precast gel, alongside 4 µL of Chameleon Duo Marker. The proteins were migrated at 100 V in 1X running buffer (Table 2.5) until the bands reached the bottom of the gel.

Protein Transfer

20% methanol was added fresh to the 1X transfer buffer (Table 2.5), and cooled at -20°C for the duration of the protein migration. The gel, nitrocellulose membrane, and Whatman® paper (3 for each side of the sandwich) were equilibrated in the transfer buffer prior to the assembly of the sandwich. The sandwich assembly was done carefully to avoid air bubbles and the transfer done at 4°C at 400 mA for 1 hour.

Labelling

The membranes were blocked for 1 hour with shaking at room temperature. Blocking was done using the Odyssey® Blocking Buffer (Table 2.6) when carrying out western blots of TurboID samples, and using blocking buffer containing milk (Table 2.5) for all other samples. After blocking, the membranes were incubated in a wet chamber in the presence of the primary antibody diluted in blocking buffer with 0.2% Tween-20 for 1 hour. The primary antibodies were washed off three times with 0.1% Tween-20 TBS/PBS for 5 minutes with shaking. The membranes were then incubated for 1 hour at room temperature in the dark in the presence of secondary antibodies also diluted in blocking buffer with 0.2% Tween-20. The secondary antibodies were washed off three times with 0.1% Tween-20 TBS/PBS for 5 minutes with shaking, after which the membranes were washed three times with TBS/PBS while shaking for 5 minutes. The membranes were then imaged using the Odyssey-CLx imaging system.

2.6.3. TurboID pulldowns

Sample Preparation

Parasites were used to infect and replicate in fresh HFFs for a period of 36-42 hours. Biotin was added to the cells at a concentration of 150 µM for either 30 minutes or 6 hours, after which the parasites were egressed manually and filtered using 3 µm filters on ice. The

egressed parasites were centrifuged at 1500 g for 5 minutes at 0°C and washed with cold PBS. The washing step was repeated thrice on ice, after which the parasites were counted and the desired number of parasites aliquoted, pelleted, and frozen at -80°C until use. For the 30-minute timepoint, $3x10^7$ parasites were used, whereas for the 6-hour timepoint, $2x10^7$ parasites were used. Input control samples (10^6 parasites) were also collected to be run on Western blots.

Bead preparation

Dynabeads™ MyOne™ Streptavidin T1 bead preparation was done as recommended by the manufacturer (Invitrogen). The beads in the vial were resuspended well by vortexing for more than 30 seconds, after which the desired volumes of beads were aliquoted. 50 µL of beads were used for the 30-minute timepoint whereas 85 µL were used for the 6-hour timepoint. 1 mL volumes of PBS were used to washed the beads three times. The DynaMag™ magnet was used to be able to separate the beads from the washing solution. The beads were then left resuspended in PBS until use.

Sample lysis and pulldown

Pierce™ protease inhibitor was added to RIPA buffer at a concentration of 1:10. The pellets prepared were lysed in 100 µL RIPA buffer with 1% SDS. Lysis was done on ice for 45 minutes, after which the mixture was diluted with more RIPA buffer to bring the SDS concentration down to 0.1% and this diluted mixture was further incubated on ice for 10 minutes. The lysis mixture was centrifuged at maximum speed at 0°C for 4 minutes, and the supernatant then used to resuspend the prepared beads. The lysis pellets were stored at -80°C for Western blot controls. The lysis-bead mixture was incubated at room temperature for 30 minutes while rotating. After incubation, the samples were always kept on ice to prevent protein degradation. The beads were washed with 1 mL RIPA buffer without Triton X-100 for five times, using the DynaMag™ magnet to separate the beads from the supernatant. The beads were then washed with 1 mL 50 mM (pH 8) Tris-HCL three times. After the final wash, the beads were resuspended in 200 µL of Tris-HCL and transferred to a clean new Eppendorf tube, and 10% of the resuspended beads kept for Western blot controls. The beads were centrifuged at full speed at 0°C, the Tris-HCl was

aspirated, and the beads were stored dry at -80^{o}C until they were sent for mass spectrometric analysis.

Mass spectrometry

The beads were sent to Dr. Ignasi Forné at the Department of Molecular Biology of the LMU Munich, at the Biomedical Centre Munich. The protocol done was as in Singer et al., (2023). Briefly, the beads were incubated with 10 ng/µL of trypsin in 1 M urea and 50 mM of NH_4HCO_3 for 30 minutes. These were then washed with 50 mM of NH_4HCO_3 and the supernatant collected was then digested overnight with 1 mM DTT. The digested peptides were alkylated and desalted, after which these were then injected into an Ultimate 3000 RSLCnano system (Thermo). The peptides were separated via HPLC using a 15cm analytical column (75 µm ID with ReproSil-Pur C18-AQ 2.4 µm from Dr. Maisch) with a gradient going from 4 to 40% acetonitrile in 0.1% formic acid for 50 minutes. The resulting effluent of the HPLC was then electrosprayed into a Qexactive HF (Thermo) which was used in a data-dependent mode in order to automatically switch between full scan MS and MS/MS acquisition. Survey full scan MS spectra (from m/z 375–1600) with resolution R=60,000 at m/z 400 (AGC target of $3x10^6$) were acquired. The 10 most intense peptide ions having charge states between 2 and 5 were then isolated to a target value of $1x10^5$, and fragmented at 27% normalized collision energy. The conditions used for mass spectrometry were as follows: 1.5 kV spray voltage, no sheath and auxiliary gas flow, 250^{o}C heated capillary temperature, 33.000 counts ion selection threshold.

MaxQuant 1.6.14.0 was used to identify proteins and quantification by iBAQ was done using the following parameters: UP000005641_T. gondii_20220321.fasta; MS tol: 10 ppm; MS/MS tol: 20 ppm Da; Peptide FDR: 0.1; Protein FDR: 0.01 min. peptide length: 7; Variable modifications: Oxidation (M); Fixed modifications: Carbamidomethyl I; Peptides for protein quantitation: razor and unique; Min. peptides: 1; Min. ratio count: 2. The MaxQuant iBAQ Z-score normalised values of the identified proteins were plotted on a volcano plot using Perseus (Tyanova et al., 2016). Any missing values were replaced (width: 0.3 and downshift: 4), the false discovery rate (FDR) was set to 0.05, and the S0 value was set to 0.1. The t-test was used.

2.7. Cell culture

2.7.1. Host cell and Toxoplasma gondii culture

Human foreskin fibroblasts (HFF) were grown in Dulbecco's modified Eagle's medium (DMEM) supplemented with 10% fetal calf serum, 2 mM L-glutamine and 10 mg/mL gentamycin. Cell culture was maintained at 37°C and 5% CO_2. HFF cells were obtained from ATCC®. Cell culture was maintained by Marzena Broniszewska. Fully confluent cells were washed with pre-warmed PBS prior to the addition of trypsin/EDTA. These were then allowed to detach during a 10-minute incubation at 37°C and 5% CO_2, after which fully supplemented media was added, and the culture split at a 1:4 concentration into new culture vessels.

Toxoplasma tachyzoites were grown on a monolayer of HFF cells under the same conditions until complete lysis of the monolayer, after which the parasites were transferred onto a new fresh monolayer for maintenance. A complete list of *Toxoplasma* strains used in this project can be found in Table 2.15. Any parasite culture which was observed to be crashing, such as those undergoing drug selection, were egressed manually by scratching and syringing using a 26G needle and passaged onto new fresh HFF cells.

2.7.2. Cryopreservation of Toxoplasma

Long-term storage of parasite and host cell strains was achieved via cryopreservation. Parasite strains were generally frozen inside cryovials, or as 96-well plates in the case of the library strains. In the former case, heavily infected HFF cells containing large vacuoles of intracellular parasites were scraped off the culture vessel and, along with fresh supplemented DMEM, were transferred into a cryovial with 2X freezing medium (Table 2.5) at a ratio of 1:1. In the case of the library 96-well plates, the heavily-infected HFF monolayer was allowed to lyse, after which the plates were centrifuged at 1500 g for 5 minutes, the medium changed to fresh 1X freezing medium, and the plate wells sealed with a foil seal. In both cases, the parasites were frozen at -80°C immediately after the addition of the freezing medium. Long-term storage of parasites in cryovials was then done in liquid nitrogen, whereas the 96-well plates were kept at -80°C.

When thawing cryopreserved parasites, cryovials were thawed at 37°C and then immediately transferred onto fresh HFF cells, whereas plates were thawed at room

temperature and also immediately transferred onto fresh HFF cells. In both cases, the parasites were allowed to invade overnight, after which the medium was changed to fresh supplemented DMEM.

2.7.3. Toxoplasma transfections

The Amaxa© 4D-Nucleofector system was used for all transfections. The transfection mixtures were prepared according to the Amaxa© protocol – a total volume of 100 µL of P3 buffer was used for transfection in cuvettes. The programme FI-158 was used for electroporation.

The amount of DNA and parasites used for different transfections were as in the below table:

Table 2.25 – Transfection mix preparations

Purpose of transfection	**Volume of parasites from a freshly-lysed 6cm dish**	**Amount of DNA**
Random integration of library plasmids	1000 µL	60 µg (divided into 3 transfections)
Targeted modifications	1000 µL	10 µg of plasmid + amplified repair DNA / oligo

For transfections which necessitated drug selection in order to obtain stable integration of the required genetic material, drugs at the below-specified concentrations were added 24hr post-transfection with fresh supplemented DMEM.

Table 2.26 – Drugs used for drug selection

Selection marker	**Drug/s**	**Concentration**
UPRT deletion	FUDR (5000x)	5 mM
DHFR	Pyrimethamine (1000x)	1 mM

2.7.4. Generation of Toxoplasma strains

The preparation of *Toxoplasma* strains was done differently depending on the strain being manipulated and the nature of the manipulations being made. The three types of modifications made throughout this project and the course of action employed in order to carry out these modifications were as explained below.

Insertion of exogenous material via random integration

This primarily involved the insertion of the library plasmids which carried the sgRNAs and scaffolds, along with the DHFR resistance cassette. All plasmids which were to be used for random integration were linearised prior to ethanol precipitation, after which this DNA was then transfected according to the above procedure.

Modification of endogenous material

All endogenous material was modified using Cas9 as described in Stortz et al., (2019), as shown in Figure 2.1. Plasmids coding for both Cas9-YFP as well as a sgRNA targeting the region of interest were transfected into RHΔku80DiCre tachyzoites (created by Hunt et al., 2019). For endogenous tagging of genes and the insertion of loxP sequences, the sgRNAs were designed to target the C-terminal region and N-terminal region of the gene of interest respectively. The loxP sequence upstream of the genes were introduced via an oligo which consisted of 33 base pairs of homology on either side of the loxP sequence. In the case of the C-terminal tagging repair templates, these were amplified from template plasmids by PCR. The primers for these PCRs were designed in such a way to utilise a LIC sequence as a linker between the protein and the tag being inserted. A loxP sequence was also inserted downstream of the tag using the reverse primer. These primers amplifying the tags were flanked by 50 base pairs of homology to facilitate homologous recombination. Transfection mixes were typically done as explained in the table above. However, in the case of transfections done with the purpose of eventually obtaining a floxed gene, these were generally initially attempted simultaneously, that is, 10 µg of Cas9 plasmid targeting the 5’ end and 10 µg of Cas9 plasmid targeting the 3’ end of the gene of interest were transfected along with PCR-amplified repair templates and oligos. In the cases where clones carrying both modifications could not be obtained in one transfection event, these

modifications were then done sequentially. For information on primer design, please refer to Section 2.9.

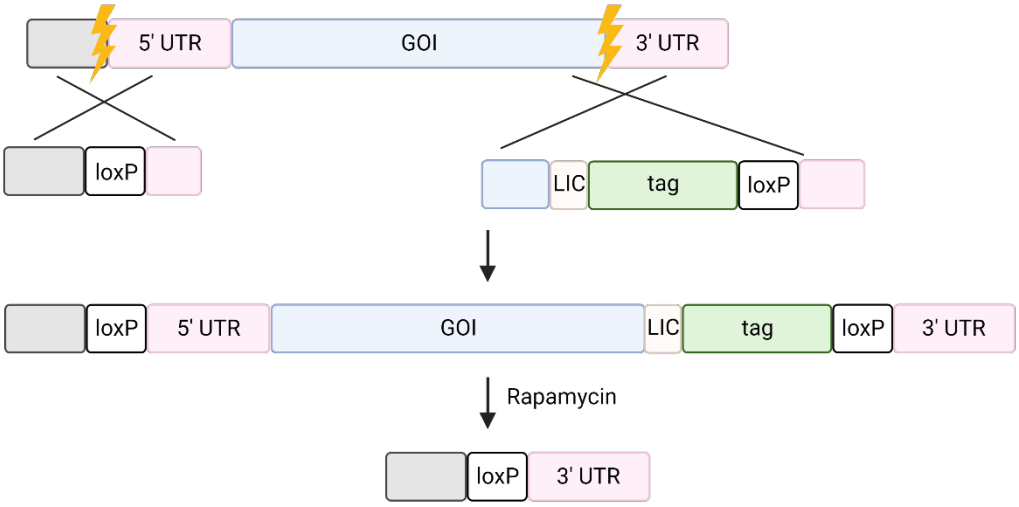

Figure 2.1 – Scheme showing endogenous tagging and floxing strategy

sgRNAs targeting upstream and downstream of the gene of interest were designed. Donor DNA for 5' loxP insertion was provided in the form of an oligo, whereas that for 3' tag insertion was provided as a PCR amplicon. LIC sequences were included upstream of all tags inserted as a form of linker. Downstream loxP sequences were also inserted with the tag to allow the generation of knockout mutants via rapamycin-induced DiCre-mediated excision. Scheme was made using BioRender.

Insertion of exogenous material via targeted integration

Insertion of any exogenous material into RHΔku80DiCre parasites was also done using Cas9-YFP as explained above, as shown in Figure 2.2. The genes which were inserted via this protocol included the Chromobody-Emerald amplified from the plasmid used in Periz et al, (2017), GRASP-RFP amplified from a gifted plasmid (Pfluger et al., 2005), and a GFP-nanobody-Halo construct amplified from a plasmid generated during this study. In these cases, the target locus was the UPRT locus (Donald & Roos, 1995; Shen et al., 2014) which was disrupted using a sgRNA targeting the first exon. The primers used to amplify the sequences being inserted were designed in such a way as to have 50 base pairs of homology upstream of the cutsite and downstream of the UPRT gene, thus replacing the gene but retaining the UPRT 5' and 3' UTRs. The genes inserted into the locus were always amplified from plasmids in a way so as to also include the promoter and 3' UTR. The transfection mixtures were prepared the same as when tagging endogenous genes.

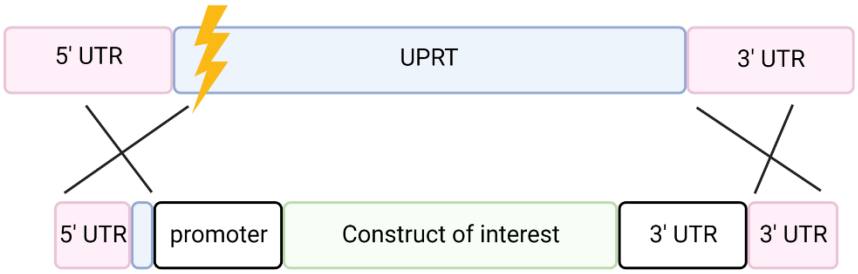

Figure 2.2 – Scheme showing strategy for targeted insertion

A sgRNA targeting the first exon of the UPRT locus was designed. Primers to amplify the construct of interest were designed in such a way as to include flanking sequences homologous to the genomic DNA directly upstream of the cut, and downstream of the UPRT stop codon. The construct of interest amplified also included the associated promoter and 3' UTR so as to ensure sufficient expression. Scheme was made using BioRender.

Isolation of Toxoplasma strain clones

Following transfections, the parasites were allowed to invade a new HFF monolayer in fresh supplemented DMEM. Depending on the type of strain being generated, these parasites were then either allowed to replicate for around 40 hours, after which they were mechanically egressed, filtered through 3 µm filters, and sorted for transient Cas9-YFP expression using a cell sorter (FACSAria IIIu, BD Biosciences) into 96-well plates, or else put under drug selection post-transfection, after which they were cloned in 96-well plates by means of serial dilution and examination for plaque formation after 7 days of undisturbed incubation. Parasite clones obtained were typically analysed and confirmed by PCR and IFA. In the cases where confirmation of genetic modification could not be done by IFA, this was confirmed by genetic sequencing. Depending on the strain generated, analytical primers were designed to either bind the genome flanking targeted insertions, or to bind the plasmid which was randomly inserted.

2.7.5. splitCas9 and DiCre induction in Toxoplasma

Conditional knockouts were generated by incubating the strains of interest, whether DiCre or splitCas9, in the presence of 50 nM rapamycin. The parasite knockouts were 'synchronised' by inducing for 1 hour, after which the media was exchanged for fresh,

supplemented, rapamycin-free supplemented DMEM. DMSO was always used as vehicle control.

2.7.6. Basic phenotypic assays

Plaque assay

Parasites were counted and used to infect 6-well plates at a concentration of $5x10^2$ parasites per well. 50 nM of rapamycin per well was used for induction of the knockouts, while an equal volume of DMSO was used as the non-induced vehicle control. The plates were left to incubate undisturbed for 7 days, after which the cells were fixed with 100% ice cold methanol for 20 minutes at room temperature, and washed with PBS. The cells were then stained with Hemacolor® Rapid Staining for Blood Smear solution 2 for 1 minute, and solution 3 for 2 minutes, and finally washed thoroughly with water. Images of the plaque assays were taken using a 10x objective on a Leica Dmi8 widefield microscope attached to a Leica DFC9000 GTC camera and the associated LasX Navigator software. A 12x12 field area at the centre of the wells was chosen. Focus maps and autofocus settings were employed. Following the acquisition of the images, the 'mosaic merge' function on the LasX software was used to generate a merged image from the multiple fields of view imaged. Three biological replicates were done.

Invasion assay

$3x10^6$ parasites were incubated for 48 hours in dishes in the presence of 50 nM rapamycin, the length of time necessary for the protein of interest to no longer be visible via IFA. These were then egressed manually, after which $5x10^5$ parasites were used to infect fully confluent coverslips. The 24well plates inoculated with parasites were incubated on ice for 10 minutes to allow the parasites to settle on the cells, after which these were then incubated at 37°C for 30 minutes, to allow the parasites to invade. The coverslips were then fixed with 4% PFA, after which the parasites were stained to allow visualisation and distinction between the invaded and extracellular parasites. Extracellular parasites were labelled by incubating the slides with antibodies against SAG1 diluted in PBS and 3% BSA for 1 hour at room temperature. The cells were then washed and labelled with secondary antibodies for 1 hour in the dark. Following the labelling of extracellular parasites, the intracellular parasites were labelled by following the IFA protocol in section 2.6.1, labelling the parasites with anti-

GAP45 antibodies. The slides were mounted, imaged, and a minimum of 100 total vacuoles per replicate were counted. Three biological replicates were done.

Replication assay

Parasites were prepared in the same way as for invasion assays. $5x10^5$ parasites were used to infect fully confluent coverslips, after which these were allowed to invade for one hour at 37°C. The coverslips were then washed thoroughly thrice using fresh supplemented DMEM, after which the parasites were allowed to replicate for 24 hours. Following this incubation, the cells were fixed using 4% PFA, and the parasites labelled as in section 2.6.1 using anti-GAP45 antibodies. The slides were mounted, imaged, and a minimum of 100 total vacuoles per replicate were counted. Three biological replicates were done.

Egress assay

Parasites were incubated in the presence or absence of 50 nM rapamycin or DMSO for 24 hours. Following this incubation, they were egressed manually, after which $1x10^5$ parasites were used to infect IFA slides. The parasites were allowed to invade for 4 hours, after which the slides were washed thrice with fresh media to remove any uninvaded parasites. After an incubation period of 36 hours, egress was induced or not induced via the addition of 2 µM calcium ionophore (Ci A23187) in supplemented DMEM without FCS. Induction of egress was done for 5 minutes at 37°C, after which the slides were fixed in 4% PFA for 15 minutes. Staining for egressed parasites was done as was done for invasion assays. The slides were mounted, imaged, and a minimum of 100 total vacuoles per replicate were counted. Three biological replicates were done.

SAG1 uptake and secretion assay

The SAG1 uptake assay was done as has been described in Koreny et al., (2022). Briefly, SAG1 was tagged with a Halo-tag upstream of the GPI-anchor using primers designed by Dr. Mirko Singer. Parasites were incubated in the presence or absence of 50 nM rapamycin for 24 hours, after which these were then incubated in the presence of Janelia Fluor HaloTag ligand 646 for a further 24 hours. The parasites were then washed thoroughly to remove any unbound ligand, after which these were allowed to invade fresh HFFs and

replicate for 24 hours. Oregon Green dye was then added to saturate any *de novo* SAG1. Endocytic activity was assessed by the presence of vesicles containing both 'old' as well as *de novo* SAG1. Successful secretion was observed via the presence of *de novo* SAG1 at the plasma membrane. IFAs were done in triplicate.

2.8. Microscopy

2.8.1. Widefield microscopy

Widefield microscopy was used for both carrying out the phenotypic screen as well as for the characterisation of proteins of interest, and was done using a Leica Dmi8 widefield microscope attached to a Leica DFC9000 GTC camera.

In the case of the phenotypic screen, the plates were imaged using a 20x objective. The automated imaging was set up on the LasX navigator by first choosing the correct carrier depending on the glass-bottom 96-well plates used. The plates were then aligned and three random images were taken from each well using the 'on demand' adaptive autofocus setting. The images acquired were all screened by eye by myself and another investigator, and the phenotypes observed were taken note of and the severity of said phenotypes ranked. The candidates with the strongest phenotypes exhibiting aberrant morphologies and F-actin network were then selected for further investigation.

For phenotype characterisation, Z-stack images were obtained using the same microscope and a 100x objective. When taking images for phenotype quantification purposes, a 63X object was used to take single images, and no image processing was done.

2.8.2. Time-lapse video microscopy

All live imaging was done using the Leica Dmi8 widefield microscope attached to a Leica DFC9000 GTC camera. Parasites were placed in a pre-heated chamber at 37°C and 5% CO_2. Fully supplemented DMEM FluoroBrite was used.

2.8.3. Confocal microscopy and STED microscopy

Confocal and STED microscopy were performed using the Abberior 3D STED microscope, equipped with 3 colour STED. Imaging settings were adjusted according to the signal strength of every sample in order to optimise signal to noise and resolution. Typically, 60x60x250 nm sampling was performed for confocal mode, while 30x30x250 nm was done for 2D STED.

2.8.4. Electron Microscopy

Parasites were incubated in the presence or absence of 50 nM rapamycin for 48 or 72 hours, after which these were fixed using 2.5% glutaraldehyde in 0.1 M phosphate buffer pH 7.4. The parasites were then taken to Dr. Andreas Klingl at the Faculty for Biology of the LMU Munich, at the Biomedical Centre Munich. The samples were washed thrice with PBS, after which these were post-fixed with 1% (w/v) osmium tetroxide for 1 hour. After washing with PBS and water, the samples were then stained en bloc with 1% (w/v) uranyl acetate in 20% (v/v) acetone for 30 minutes and dehydrated in a series of graded acetone and embedded in Epon 812 resin. Sections of 60 nm thickness were cut using a diamond knife on a Reichert Ultracut-E ultramicrotome. These sections were then mounted on collodium-coated copper grids, stained with 80 mM lead citrate (pH 13), and imaged using an EM 912 transmission electron microscope (Zeiss, Oberkochen, Germany) equipped with an integrated OMEGA energy filter operated in the zero-loss mode at 80 kV. Images were taken using a 2k x 2k slow-scan CCD camera (Tröndle Restlichtverstärkersysteme, Moorenweis, Germany).

2.8.5. Image analysis

Leica LasX software and Imspector were used for image acquisition at the Leica widefield microscope and at the Abberior 3D STED microscope respectively. LI-COR Image Studio was used to acquire Western Blot images. All subsequent image processing and analysis was done using Fiji (ImageJ) software v.2.1.0 (Schindelin et al., 2012).

Relative fluorescence or Corrected Total Cell Fluorescence (CTCF) was calculated was follows:

$$CTCF = Integrated\ Density - (area\ of\ selection \times mean\ fluorescence\ of\ background)$$

2.9. Bioinformatics

2.9.1. Design of screen sgRNAs

The sgRNAs used for the screen were designed and prepared by a former PhD student, Dr. Johannes Stortz, who picked 320 genes based on their ToxoDB annotation in the ToxoDB 30 release. These genes were picked based on their prediction to be apicomplexan-specific, and to not have signal peptides, and only genes with a phenotypic score of -1.5 or less were chosen (Sidik et al., 2016). One sgRNA per target gene was selected from the genome-wide screen (Sidik et al., 2016), the sgRNA chosen having been the one that showed the strongest phenotype in said screen. The sgRNA oligo pool was then synthesised by CustomArray.

2.9.2. Design of sgRNAs for targeted insertion of constructs

The sequence of the gene of interest was downloaded from toxodb.org, including 1000bp upstream of the start codon and 1000bp downstream of the stop codon. The sequence was pasted in ApE and the UTRs and coding region annotate accordingly. In the case of 5' loxP insertion or 3' tagging, the distance from neighbouring genes was checked via the synteny function on toxodb.org. A sgRNA was designed by copying 50bp from the region where the cut site is desired, and pasting this into grna.ctegd.uga.edu. The 'RNA guided nuclease selection' was chosen to be 'SpCas9: 20nt sgRNA, NGG PAM on 3'end' and the 'Genome' option was chosen to be 'T.gondii GT1 ToxoDB-32'. The best sgRNA was chosen to be the one closest to the ideal cutsite location (for example, in the case of 3' tagging, the closest to the stop codon), and which was not likely to cause off-target cutting. The latter was checked by using the 'Blast' function of toxodb.org, comparing the sgRNA including PAM sequence with the genome of *Toxoplasma gondii* GT1, and ensuring that there is only one perfect match within the whole genome. After ensuring this, the primers were designed with sticky ends matching the vector to be ligated into as follows:

AAGTTsgRNAsequenceG (without PAM) (a "G" was added at the beginning of the sgRNA if there was no "G" or "A already)

AAAACgRNAsequenceA (without PAM, reverse complement of the gRNA) (if a “G” was added, then a “C” at the end of the sgRNA sequence was also added)

2.9.3. Design of primers for repair template generation

The design of the primers for repair template generation for 3’ tagging was dependent on the location of the Cas9 cutsite with respect to the stop codon. In the cases where the cutsite was located downstream of the stop codon, the forward primer was designed in a way to incorporate the fifty nucleotides present upstream of the stop codon, was well as the sequence GCTAAAATTGGAAGTGGAGG coding for the LIC sequence used as a linker between the gene of interest and the tag being inserted. The reverse primer was designed in a way to incorporate the reverse complement of the fifty nucleotides downstream of the cutsite as well as the sequence ATAACTTCGTATAATGTATGCTATACG coding for loxP. On the other hand, in the cases where the cutsite was designed in such a way as to be upstream of the stop codon, the forward primer was designed to incorporate fifty nucleotides upstream of the cutsite as well as the entire recodonised sequence until the stop codon, and finally the LIC sequence. The reverse primer was designed to include the reverse complement of the fifty nucleotides downstream of the cutsite and the loxP sequence. In all cases, if the homology sequences were to include the sgRNA sequence, these were also recodonised so as to prevent repeat cutting by the Cas9.

2.9.4. Design of primers for genotyping

Primers for genotyping were designed to bind around 100 nucleotides upstream and downstream of the regions of interest, with the reverse primer being in reverse complement. If possible, the primers were designed to have a ‘G’ or a ‘C’ at the 3’ end, and the annealing temperature estimated to be around 58^{o}C. The primers were also designed in such a way as to result in a wildtype PCR product that is a minimum of 200bp long.

2.10. Statistics

Data and statistics were prepared using Graphpad Prism 8.2.1. One-tailed analysis of variance (ANOVA) and multiple comparison t-test or unpaired two-tailed Student’s t-test were performed as required.

Chapter 3. Results

3.1. Screen

This section of this chapter describes the work that directly led to the publication of Li et al., (2022). For this, a novel dimerisable Cas9 system was used within the context of a knockout phenotypic screen with the aim of identifying novel actin and egress-related factors. From this screen, two new egress factors which impact actin dynamics were discovered and characterised. While the reader is encouraged to refer to the publication for a more cohesive and rounded story, this section will detail my contribution towards the publication and summarise the contributions other authors have made. Ongoing work that is yet unpublished will also be described in a later section.

As described in Chapter 1, numerous apicomplexan actin-binding proteins have already been the subject of investigation. Despite this, a number of canonical eukaryotic actin-regulatory proteins, including those involved in filament bundling and branching, still seem to be missing from these parasites (Baum et al., 2006; Gordon & Sibley, 2005). Given how essential actin is for parasite survival, our hypothesis going into this project was that these 'missing' proteins are present but have either a) become so divergent from the canonical ones that they are no longer recognisable via bioinformatic approaches, or b) have been replaced with a new set of apicomplexan-specific proteins. In order to find these hypothetically novel actin-binding proteins, the approach taken was to carry out a phenotypic knockout screen.

3.1.1. *Establishment of the main parental line*

In order to carry out the screen, a parental parasite line was generated by a previous PhD student, Dr. Johannes Stortz, wherein the Chromobody-emerald was expressed as a marker for actin filaments (Periz et al., 2017). He also integrated into this parasite strain constructs which code for the two subunits involved in the inducible dimerisable Cas9 system (splitCas9/sCas9) (Figure 1.13). A construct labelling the apicoplast via the expression of FNR-RFP was also inserted into this parasite line by Dr. Elena Jimenez Ruiz (Striepen et al., 2000) (Figure 3.1A). This was also done as a marker for altered actin dynamics since defects in apicoplast segregation and localisation have been observed

when knocking out actin and multiple actin-regulatory proteins (Jacot et al., 2017; Stortz et al., 2019; Tosetti et al., 2019; Whitelaw et al., 2017). The use of this strain was validated, and the efficiency of the inducible Cas9 system was tested by Dr. Stortz by knocking out a number of well-known genes and analysing the phenotypes obtained. A number of positive control genes relating to actin were targeted, these being actin itself, ADF, and formin2 (Figure 3.1C). DrpA was also targeted as a positive control for an apicoplast-related phenotype. SAG1 was also targeted as a negative control (Figure 3.1B).

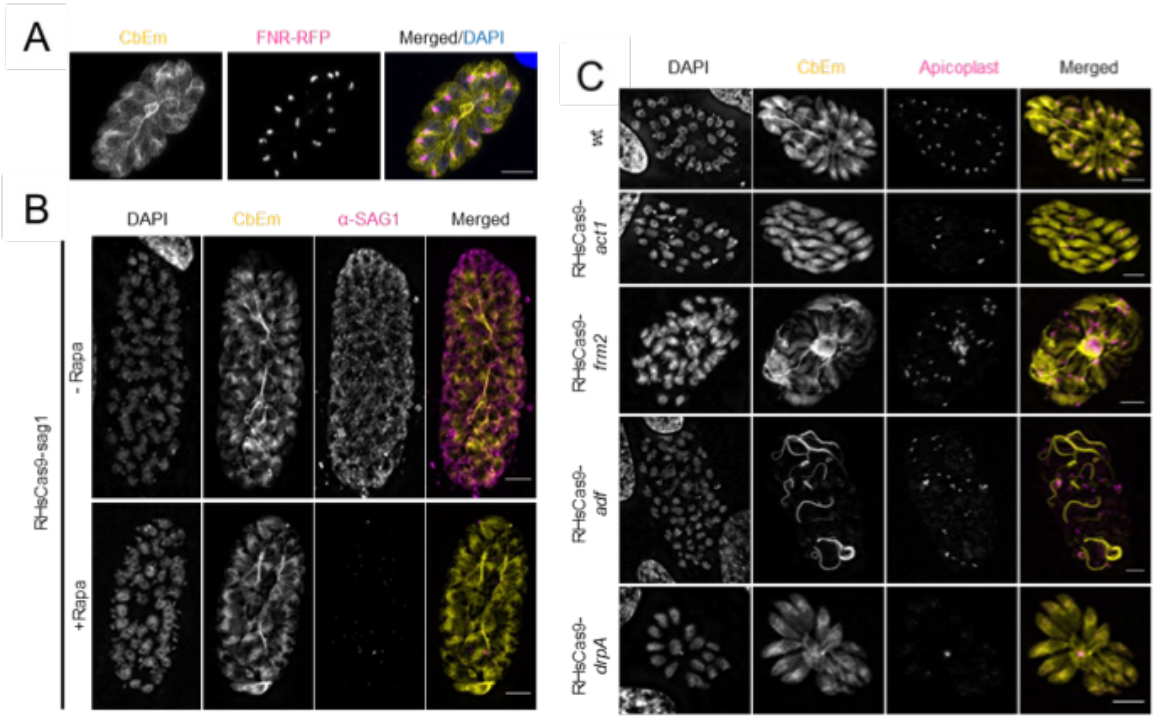

Figure 3.1 – Validation of the splitCas9 system in *Toxoplasma*

(**A**) The indicator parental strain used for the phenotypic screen expresses the Chromobody-emerald as a marker for the actin filaments (in yellow), and FNR-RFP as a marker for the apicoplasts (in magenta). (**B**) Immunofluorescence analysis of the parasite strain wherein SAG1 was knocked out using the splitCas9 system, as in Figure 1.13. The actin filaments were seen to be unaffected. (**C**) immunofluorescence analysis of parasites wherein actin, ADF, formin2, and DrpA were knocked out. All knockouts disrupt apicoplast segregation. Knockout of actin, ADF, and formin2 also affect the formation of typical actin filaments, with the former resulting in no filament formation, and the latter two resulting in abnormally thick filaments. All scale bars are 5 μm. Images in (B) and (C) were generated by Dr. Stortz. Figure adapted from Li et al., (2022).

Knockout of SAG1 was not observed to have an impact on the actin filaments whatsoever (Figure 3.1B). On the other hand, as expected, knockout of actin was seen to result in a

complete lack of actin filaments, as well as disrupted apicoplast inheritance leading to some parasites not possessing this organelle (Figure 3.1C). Similarly, knockouts of ADF and formin2 also resulted in disrupted apicoplast inheritance, with the latter seemingly causing the apicoplasts to collect close to the residual body (Figure 3.1C). These knockouts of ADF and formin2 also showed a lack of actin filaments at the actin nucleation region within the individual parasites, but showed thicker filaments connecting the parasites within the vacuoles. Knockout of DrpA was seen to also negatively impact apicoplast division, with the parasites being observed to lack this organelle (Figure 3.1C). In this case, the actin distribution within the vacuole was seen to be unaffected.

3.1.2. Screening of the library and selection of the candidates

In order to carry out the phenotypic screen, a library of target genes was curated. These genes were chosen based on the three criteria; their annotation on ToxoDB (version 30) (Gajria et al., 2008) as being apicomplexan-specific and lacking a signal peptide, and their predicted essentiality (phenotypic score **≤** −1.5) based on the phenotypic score obtained from the genome-wide screen conducted a few years ago (Sidik et al., 2016). In addition to the genes following these three criteria, GAP40 and profilin were also included in the library as internal positive controls for a 'nuclear/replication' phenotype and an 'F-actin' phenotype respectively. This curation resulted in a library of sgRNAs targeting total of 320 genes (full table can be found in the appendix).

As described in Figure 3.2A, following the synthesis of the sgRNA library, it was subsequently cloned into the recipient vectors. This library was transformed into bacteria and the number of bacteria obtained from the transformation calculated as a means of estimating whether the complexity of the library was conserved during preparation. According to Sidik et al., (2018), in order to ensure the conservation of library complexity, the number of bacteria obtained from the transformation is to exceed the complexity of the library by 100-fold. In the case of this project, the library complexity was 320 genes while the number of bacteria obtained was 3×10^6 c.f.u., showing that the complexity of the library was successfully maintained. To further confirm this, 35 random bacterial colonies were picked and the plasmid sequenced. 83% (or 29), of these colonies were determined to have unique sgRNAs. The plasmid library was purified prior to transfection of the parasite indicator strain. After transfection, the pool of library parasites underwent drug selection for

3 weeks, at which point fluorescence-activated cell sorting was used in order to obtain single parasite clones in a 96-well plate format. 608 clonal populations were obtained. The generation of knockouts was induced via the addition of rapamycin for 48 and 72 hours, and these were then imaged (Figure 3.2B).

Images were analysed independently by two researchers, and 99 clones were picked for having a detectable phenotype. These selected clones were classified based on the phenotype they were deemed to have shown upon knockout. The types of phenotypes observed were classified as follows; ‘no phenotype’, ‘nuclear/replication’, ‘F-actin phenotype’, ‘apicoplast segregation’, and an ‘egress phenotype’ (Figure 3.2B). The phenotypes of these selected clones were then graded depending on their relative strength. Due to a non-specific nuclear phenotype being an inherent caveat of using Cas9 in *Toxoplasma*, clonal populations classified as having the ‘nuclear/replication’ phenotypes were chosen based on whether the phenotype was observed in a relatively higher percentage of the parasitic vacuoles (>70%) compared to controls that also showed the non-specific nuclear phenotype (Figure 3.2B).

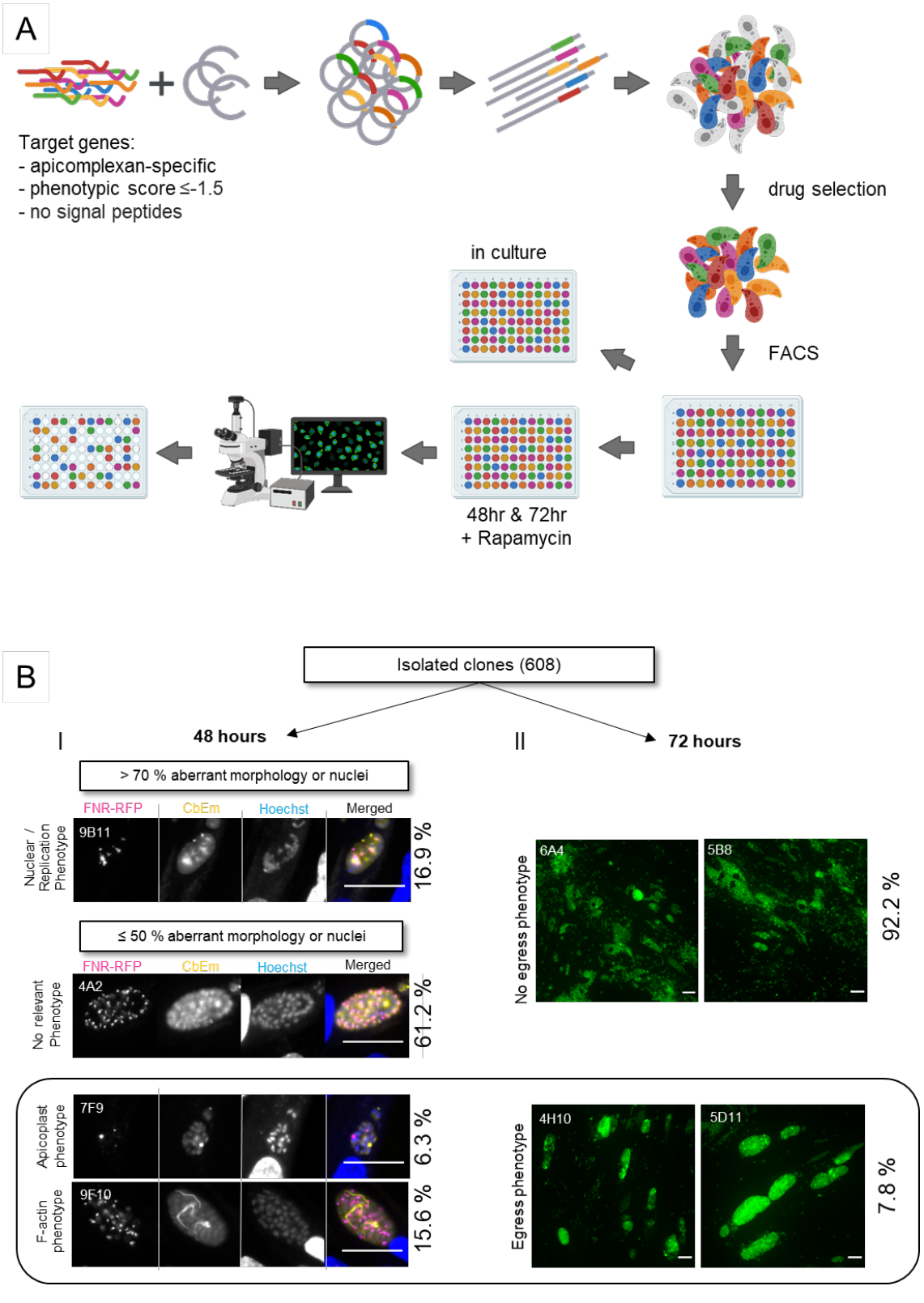

Figure 3.2 – Knockout phenotypic screen to select for altered actin dynamics, apicoplast segregation and egress mutants

Figure 3.2 – Knockout phenotypic screen to select for altered actin dynamics, apicoplast segregation and egress mutants (previous page)
(**A**) shows a scheme of the experimental workflow. The pool of sgRNAs were amplified by PCR and ligated by Gibson assembly into digested plasmids carrying a promoter and a DHFR cassette. This pool of plasmids was then purified, and transfected into the indicator strain. The parental strain expressing the splitCas9, Chromobody-emerald, and FNR-RFP, was transfected with the sgRNA library. Following transfection, the parasites underwent drug selection using pyrimethamine. The parasites were then sorted into 96-well plates for the purposes of obtaining clonal populations. These 96-well plates were divided into four sets of replicate plates; one for culturing, two with 50 nM rapamycin, and the final set was the non-induced control. Double-strand breaks were induced for 48 and 72hr, after which the plates were imaged at 20x magnification, screened by eye, and the mutants of interest selected. Scheme adapted from Li et al., (2022) created using BioRender. (**B**) the images of the mutants obtained were analysed by two independent researchers and classified according to their perceived phenotype. **i**) shows representative images of knockout mutants after 48 hr of induction. Clones wherein more than 70% of the population were seen to have an aberrant morphology or nuclear phenotype were classified as having a replication phenotype and were not investigated any further. Clones wherein less than 50% of the population showed an aberrant nuclear phenotype, and which also showed an altered F-actin distribution or apicoplast morphology were selected for downstream analysis. Scale bars are 25 μm. **ii**) shows representative images of knockout mutants after 72 hr of induction. These were classified as either having, or not having, an egress phenotype. Clones with a perceived deficiency in egress were selected for downstream analysis. Scale bars are 30 μm. Figure adapted from Li et al., (2022).

All of the clones which exhibited a phenotype were sent for sequencing and the gene knockouts responsible for the respective phenotypes identified. The full list can be found in the Appendix. In addition to the above-listed main phenotypes, a number of clones which showed a ‘super aberrant’ phenotype were also selected (Figure 3.3). The knockout parasites which exhibited the ‘super aberrant’ phenotype contained multiple copies of the library plasmid meaning that the phenotype was caused by the disruption of multiple genes. Consequently, these candidates were dismissed. However, also included in the list of 99 potential candidates were GAP40, identified for having a ‘nuclear/replication phenotype’, and profilin, which was identified as having the strongest ‘F-actin phenotype’ of all (Figure 3.4). The isolation and identification of these two positive controls based on their perceived phenotype served as a good indication of the success of this screening strategy.

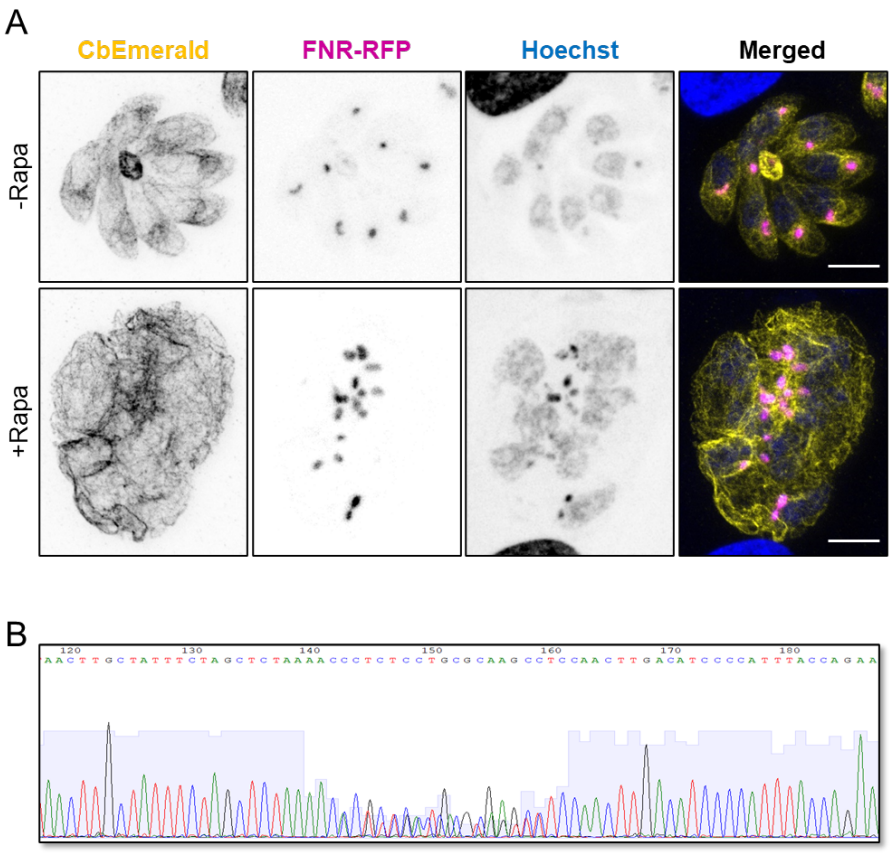

Figure 3.3 – Parasites with super-aberrant phenotypes were observed
(**A**) Images show an isolated clone treated with 50 nM rapamycin for 48hr. Parasites were fixed with 4% PFA. Actin is seen in yellow, apicoplasts are in magenta, and nuclei were stained with Hoechst. The aberrant phenotype is a result of multiple plasmids carrying guide RNA integrating into the parasite genome, leading to multiple gene knockouts upon addition of rapamycin. Scale bars are 3 µm. Image from Li et al., (2022). (**B**) The mixed sequence indicates the presence of multiple guide RNAs in the clone imaged in (A). This mixed sequence shows that integration of multiple sgRNAs occurred in the parasite, leading to multiple simultaneous gene disruptions upon addition of rapamycin.

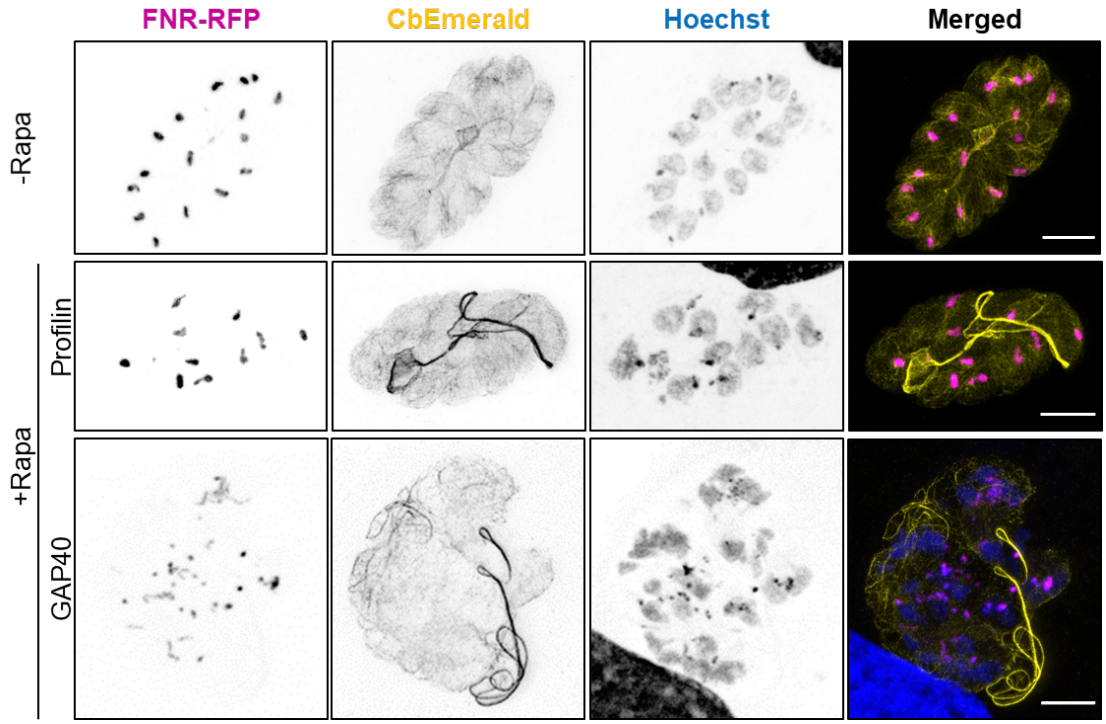

Figure 3.4 – Control genes identified from the screen

Clones were identified as having a thick intravacuolar network. Upon further investigation, these were seen to have integrated a sgRNA targeting profilin, the actin-regulatory protein included in the screen as a control. Parasites which had integrated the sgRNA targeting GAP40 were also identified as having a nuclear/replication phenotype. The actin labelled with CbEmerald shown in yellow was imaged using STED, whereas the FNR shown in magenta and Hoechst in blue were imaged using confocal microscopy. Scale bars are 5 µm. Figure from Li et al., (2022).

Following sequencing and the identification of the candidates of interest, the project split in two avenues, with the parallel project led by Li Wei focusing on clones which were seen to have an egress phenotype. Since some clones listed as having an 'F-actin phenotype' were also observed to have an egress phenotype, these was investigated by her and their characterization has since been published (Li et al., 2022). An overview of the characterisation of these egress candidates can be found in the next section.

As for this project, priority was given to candidates which were marked as having an 'F-actin' or an 'apicoplast segregation' phenotype (Section 3.1.4).

3.1.3. Analysis of candidates with an egress phenotype

Images of the knockout mutants generated from the phenotypic screen were analysed after both 48 hr and 72 hr of induction (Figure 3.2). At 48 hr, some mutants were seen to have mild alterations in the F-actin network, and no effect on apicoplast segregation and localisation. However, at 72 hr, these mutants did not lyse the host cells. Following their identification, and validation of the egress phenotype via egress assays, two candidates stood out. These were endogenously C-terminally tagged in the RHΔKu80DiCre strain (called Δku80 DiCre from here onwards), and loxP sequences inserted flanking the genes of interest to validate the screen phenotype using an alternate knockout strategy; the DiCre system (Figure 3.5B). TGGT1_240380 (named Conoid Gliding Protein, or CGP) localised to the apical tip, whereas TGGT1_208420 (named Signalling Linking Factor, or SLF) localised to the apical region and residual body (Figure 3.5C-D). Both were observed to be critical for the parasite's lytic cycle, as evidenced by plaque assays. SLF was seen to be a critical component of the signalling complex necessary for the induction of egress (Bisio et al., 2019). CGP, on the other hand, was observed to act later during the egress process, with its role being that of activating gliding motility. Further information on their role in egress can be found in Li et al., (2022).

Figure 3.5 – Egress factors SLF (TGGT1_208420) and CGP (TGGT1_240380) localise to the apical region and are essential (next page)

(**A**) After 48 hr of knockout induction, STED imaging of the mutants' actin filaments (in yellow) showed slight changes in the F-actin network, while confocal imaging of the apicoplasts (in magenta) showed no effect on this organelle. (**B**) The tagging approach employed made use of CRISPR/Cas9 and homology directed repair (as in Figure 2.1). sgRNAs targeting upstream and downstream of the gene of interest were designed. Donor DNA for 5' loxP insertion was provided in the form of an oligo, whereas that for 3' tag insertion was provided as a PCR amplicon. LIC sequences were included upstream of all tags inserted as a linker. Downstream loxP sequences were also inserted with the tag to allow the generation of knockout mutants via rapamycin-induced DiCre-mediated excision (Andenmatten et al., 2013) thus permitting downstream characterisation. Scheme was made using BioRender. (**C**) Endogenous C-terminal tagging of CGP with Halo (in magenta) showed that it localises to the apical tip, whereas (**D**) shows that endogenous C-terminal tagging of SLF with mCherry (in magenta) showed that it localises both to the apical region as well as the residual body. IMC1 (in yellow) was labelled to denote the parasite shape. The corresponding plaque assays for both CGP and SLF confirm that following induction with rapamycin, the knockout parasites are not viable. Scale bars are 5 μm in all IFA images, and 1.5 mm in the plaque assays. IFA images and plaque assays generated by Li Wei. Figure adapted from Li et al., (2022).

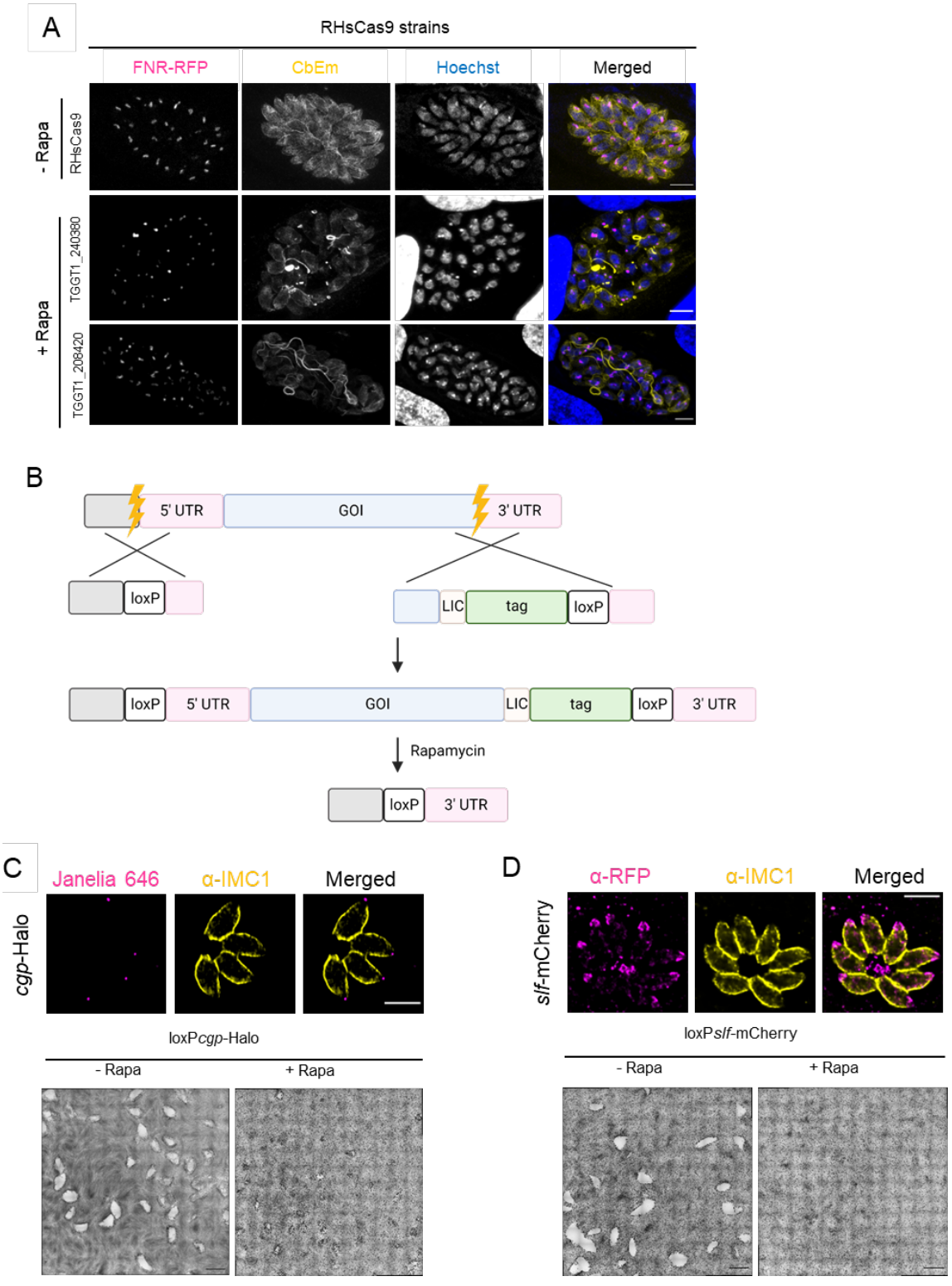

Figure 3.5 – Egress factors SLF (TGGT1_208420) and CGP (TGGT1_240380) localise to the apical region and are essential

3.1.4. Analysis of candidates with a potential F-actin/apicoplast phenotype

The most prominent F-actin phenotype was seen to have been a result of knocking out profilin, the screen positive control. Nevertheless, to follow up on candidates which exhibited an 'F-actin' phenotype, priority was given to those which were graded as also having a prominent phenotype. These identified candidates were endogenously tagged in order to narrow down the candidate list based on their localisation. Fluorescent or epitope tags were inserted at the 3' end of the genes of interest, thus tagging the proteins at the C-terminus. As shown in Figure 3.5B, this was done via the induction of a double-strand break using Cas9 in a Δku80DiCre parasite strain deficient in non-homologous end-joining (Huynh & Carruthers, 2009). A double strand break was induced at the 3' end of all the genes using Cas9-YFP, after which sequences coding for the tags flanked by homology arms were integrated by the parasites via homology-directed repair. While some proteins could not be tagged, the localisation of the majority was determined (Figure 3.6).

The proteins of interest localised to a variety of compartments within the cell, with the majority localising to either the nucleus or to the mitochondria. Others were seen to localise to the micronemes, or localising to the Golgi body.

Two of the proteins tagged were seen to have already been described in the literature. The first, TGGT1_263300, is a voltage-dependent anion channel which localises to the mitochondria and is believed to be essential for metabolite and protein import into the organelle, as well as maintaining mitochondrial-ER contact sites (Mallo et al., 2021). TGGT1_249970, on the other hand, is a protein localising to the micronemes which was observed to be essential for microneme secretion and therefore for invasion and egress (Bullen et al., 2016).

Two of the candidates (TGGT1_301410 and TGGT1_259720) localised adjacent to the nucleus, in proximity to a known F-actin polymerisation centre (Periz et al., 2019), indicating a potential role in F-actin dynamics. TGGT1_259720 was resilient to efficient genetic manipulation and therefore subsequent analysis focused on TGGT1_301410.

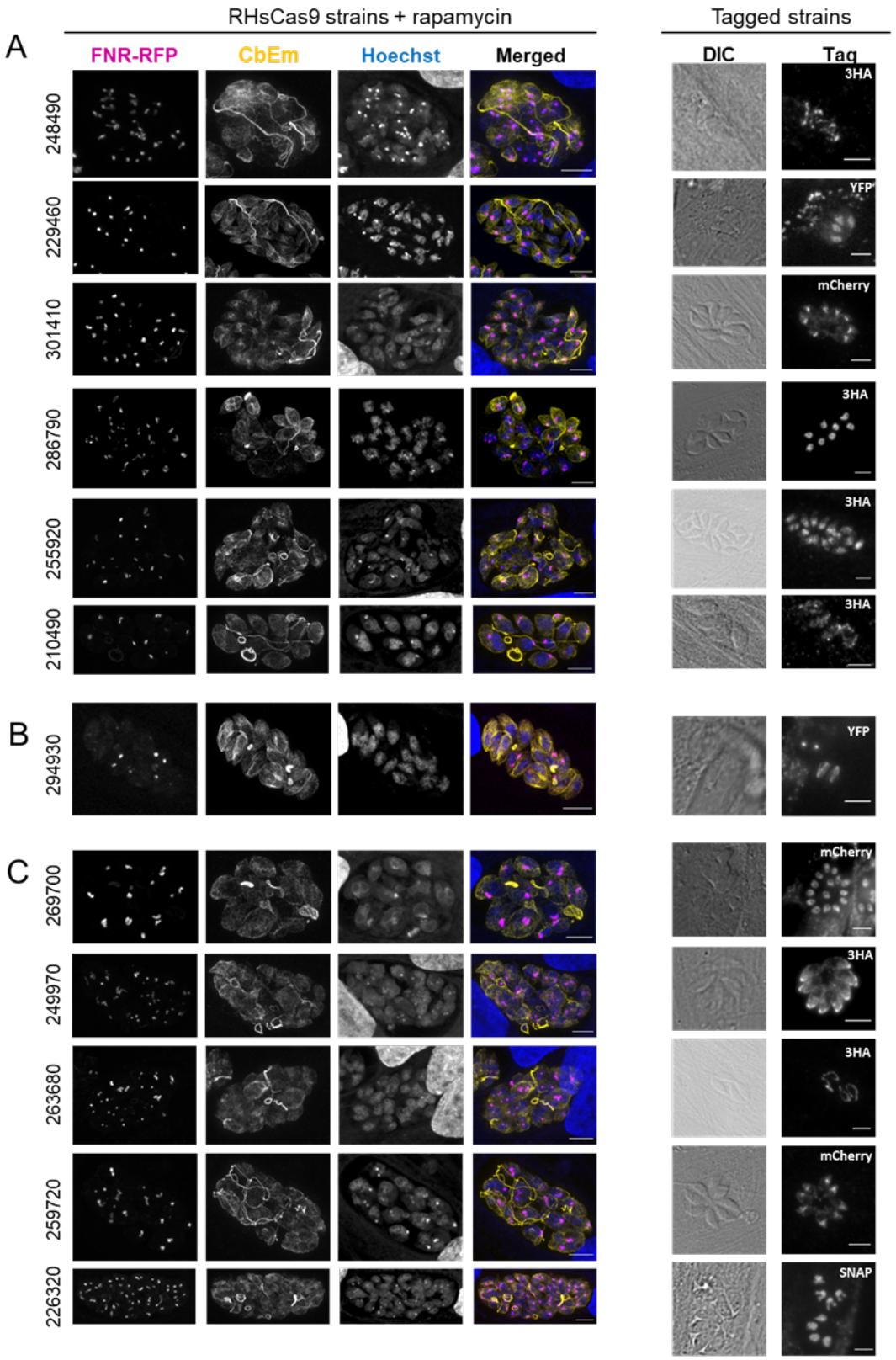

Figure 3.6 – Mutants with observable changes to F-actin and apicoplast distribution

Figure 3.6 – Mutants with observable changes to F-actin and apicoplast distribution (previous page)
(**A**) shows mutants with an F-actin phenotype, while (**B**) shows a mutant with an apicoplast phenotype. (**C**) shows mutants with both an F-actin as well apicoplast phenotype. The images on the left show the splitCas9 clones containing the sgRNAs isolated from the library. Parasites were induced with rapamycin for 48hr, after which they were fixed and imaged. The CbEmerald shown in yellow was imaged using STED, whereas the FNR shown in magenta and Hoechst in blue were imaged using confocal microscopy. The numbers on the far left are the accession numbers of the corresponding genes as can be found on ToxoDB (Gajria et al., 2008). The images on the right are widefield images of RHΔku80 DiCre parasites wherein the gene identified was endogenously tagged. Scale bars are 5 μm. Figure from Li et al., (2022).

3.2. Characterisation of TGGT1_301410

Following the completion of the phenotypic screen, this project proceeded to focus on the characterization of one of the candidate proteins identified from the screen, TGGT1_301410. A manuscript focusing on the analysis of TGGT1_301410 is currently in preparation.

3.2.1. Database research of TGGT1_301410

The information present in this section is information which is currently available on the ToxoDB database (version 59) (Gajria et al., 2008).

TGGT1_301410 is predicted to be 1033 amino acids long, with a molecular weight of 106kDA. The protein is not predicted to have a signal peptide, as expected based on the criteria chosen for inclusion into the curated sgRNA library from which it was picked. The protein is also not predicted to have any transmembrane domains. The only domain annotated was an ENTH domain from amino acids 1 to 150 (Figure 3.7A). Due to the presence of this domain, it has now been given the name “ENTH domain-containing protein” or *Tg*EDP.

*Tg*EDP is not predicted to be a particularly well-conserved protein in eukaryotes, seemingly only being present in the superphylum Alveolata (Figure 3.7B) (Szklarczyk et al., 2011; von Mering et al., 2003). It is predicted to have a phenotypic score of -4.6 based on the genome-wide Cas9 screen (Sidik et al., 2016), suggesting that it is fitness-conferring to the *Toxoplasma* tachyzoite stage on which the screen was carried out. Transcript levels for this gene have been observed to be comparable between the GT1 strain as well as the ME49

strain, both for tachyzoites as well as the corresponding bradyzoites induced via compound 1 or high pH (Behnke et al., 2008). In addition to this, a study by Behnke et al., (2010) also suggests that this gene is expressed throughout the cell cycle, with expression levels being slightly reduced during the G1 phase.

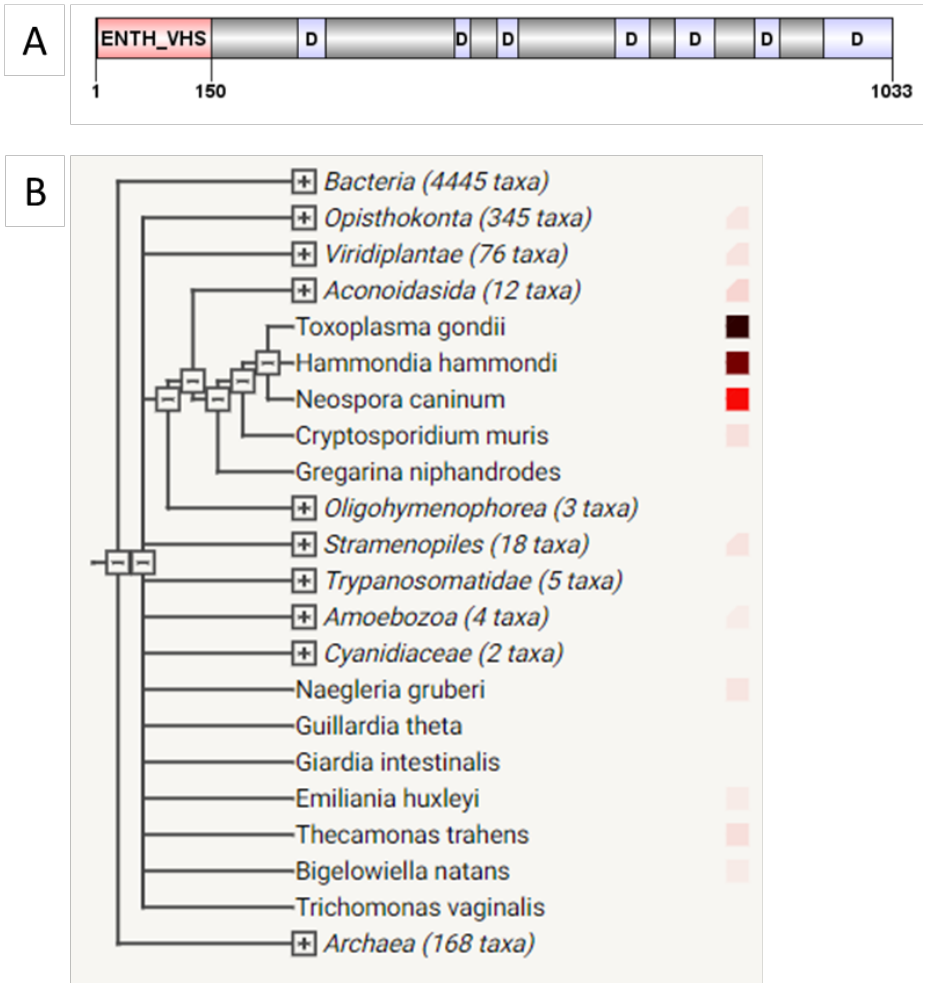

Figure 3.7 – The phylogeny of TGGT1_301410 as predicted using STRING-db
(**A**) The protein of interest was predicted to have an ENTH_VHS domain. Apart from disordered regions marked with a 'D', the protein is not annotated as having any other regions of note. Graphic generated using DOG 2.0 (Ren et al., 2009). (**B**) STRING-db is an online tool which predicts the phylogeny of proteins in addition to their possible interactors based on public text mining as well as published experimental data (Szklarczyk et al., 2011; von Mering et al., 2003). The darker the shade of the box on the far right of the graphic indicates a stronger conservation of the protein within that specific phylogenetic group. STRING-db suggests that TGGT1_301410 or its homologues may be found in other phylogenetic groups, with a strongly conservation within Alveolata.

3.2.2. Subcellular localisation

*Tg*EDP was endogenously C-terminally tagged with mCherry, SYFP2, and SNAP-tag. Upon tagging, the protein appeared to localise to a compartment between the nucleus and the apicoplast. Signal which seems to be distributed throughout the cytoplasm was also observed. While HyperLOPIT data predicts the protein to be a resident of the nucleus (Barylyuk et al., 2020), all tagged clones localised to the same compartment, regardless of the tag used. Since no phenotypes were observed upon C-terminal tagging of the protein, it was concluded that it is fully functional and therefore the detected localisation was interpreted as genuine.

Colocalisation studies

The first steps taken were to accurately identify where the protein localises. Widefield images suggested that the protein is present at the Golgi body. Upon further investigation via colocalisation studies with GRASP-RFP, a marker for the *cis*-Golgi (Pfluger et al., 2005), and SortLR-Halo, a marker for the *trans*-Golgi (Sloves et al., 2012), it was concluded that the protein of interest likely resides in close proximity to the *trans*-Golgi (Figure 3.8A-B). Confocal images, orthogonal views, and profile plots confirm that while the protein is present within very close proximity of the *trans*-Golgi, it does not perfectly colocalise with SortLR (Figure 3.8C-F). The mean Pearson Correlation coefficient of *Tg*EDP with SortLR of 6 parasitophorous vacuoles was found to be 0.546. To confirm that *Tg*EDP is a part of the Golgi body, Brefeldin A (BFA) was used to disrupt the Golgi body. BFA is a drug which causes the contents of the Golgi body to relocate to the ER (Helms & Rothman, 1992; Sciaky et al., 1997). As seen below (Figure 3.8G), BFA redirects the protein of interest to the ER, further supporting its Golgi body localisation.

Further colocalisation IFAs using markers for the endosome-like compartment, Dynamin B (DrpB) (Breinich et al., 2009), and syntaxin6 (Jackson et al., 2013) (Figure 3.9) were also done since these have been documented to occupy different post-Golgi compartments (Carmeille et al., 2021). The endosome-like compartments were labelled using an antibody against proM2AP (Harper et al., 2006). An antibody was also used against DrpB, whereas syntaxin6 was endogenously C-terminally tagged. Once again, confocal data and profile plots showed no perfect colocalisation, with the *Tg*EDP only residing in close proximity to these compartments.

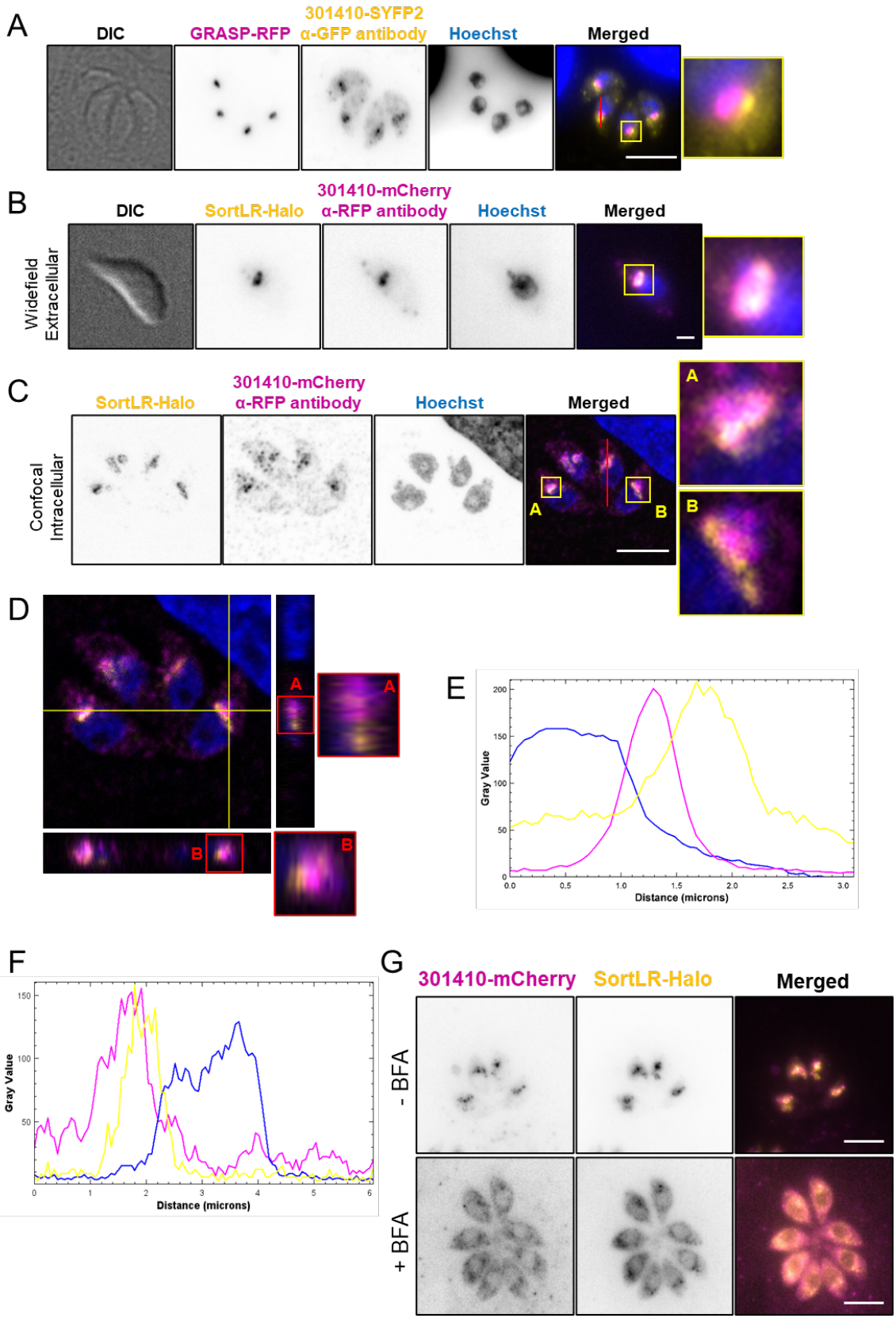

Figure 3.8 – *Tg*EDP (TGGT1_301410) localises close to the *trans*-Golgi

Figure 3.8 – *Tg*EDP (TGGT1_301410) localises close to the *trans*-Golgi (previous page)

(**A**) *Tg*EDP (in yellow) does not localise to the *cis*-Golgi body. GRASP-RFP (in magenta) is a *cis*-Golgi marker that was stably inserted into the parasite genome via replacement of the UPRT locus, and subsequent drug selection. Colocalisation experiments were done in triplicate with a minimum of 100 parasites observed per replicate. Colocalisation was never observed. (**B**) SortLR (in yellow), a marker for the *trans*-Golgi, was endogenously tagged with Halo-tag. The protein of interest was seen to localise close to the marker in both extracellular parasites in (B) as well as intracellular parasites in (**C**). (**D**) Orthogonal views of the merged image in (C) show that despite *Tg*EDP and SortLR come in very close proximity, they do not always colocalise. (**E**) A profile plot taken across the red line in the merged image in (A) shows that there is no overlap between GRASP-RFP (magenta) and *Tg*EDP (yellow). (**F**) A profile plot taken across the red line in the merged image in (C) shows that complete overlap between SortLR-Halo (yellow) and TGGT1_301410-mCherry (magenta) was not observed. Prior to obtaining the profile plots in (E) and (F), the merged images in (A) and (C) were first converted to 8-bit to account for variations in signal intensity, thus allowing all intensities to be plotted on the same scale. (**G**) Upon addition of brefeldin A, a drug which causes the Golgi body (SortLR in yellow) to collapse back into the ER, *Tg*EDP (magenta) was similarly mislocalised in all cases (100%). This confirmed that *Tg*EDP's localisation is close to the *trans*-Golgi. All scale bars for intracellular parasites are 5 µm. Scale bar for extracellular parasite is 1 µm.

Figure 3.9 – Colocalisation of *Tg*EDP (TGGT1_301410) with post-Golgi markers (next page)

Confocal colocalisation data of post-Golgi markers (**A**) ProM2AP, (**B**) Syntaxin6, and (**C**) DrpB (all in yellow) tagged endogenously or labelled using antibodies also showed that *Tg*EDP (in magenta) localises close to these compartments. All scale bars are 5 µm. (**D**), (**E**), and (**F**) show profile plots taken across the white lines in the merged images of (A), (B), and (C) respectively. In all cases, colocalisation signals overlap, but not completely. Prior to obtaining the profile plots, all images were converted to 8-bit to account for differences in protein levels and therefore signal intensities.

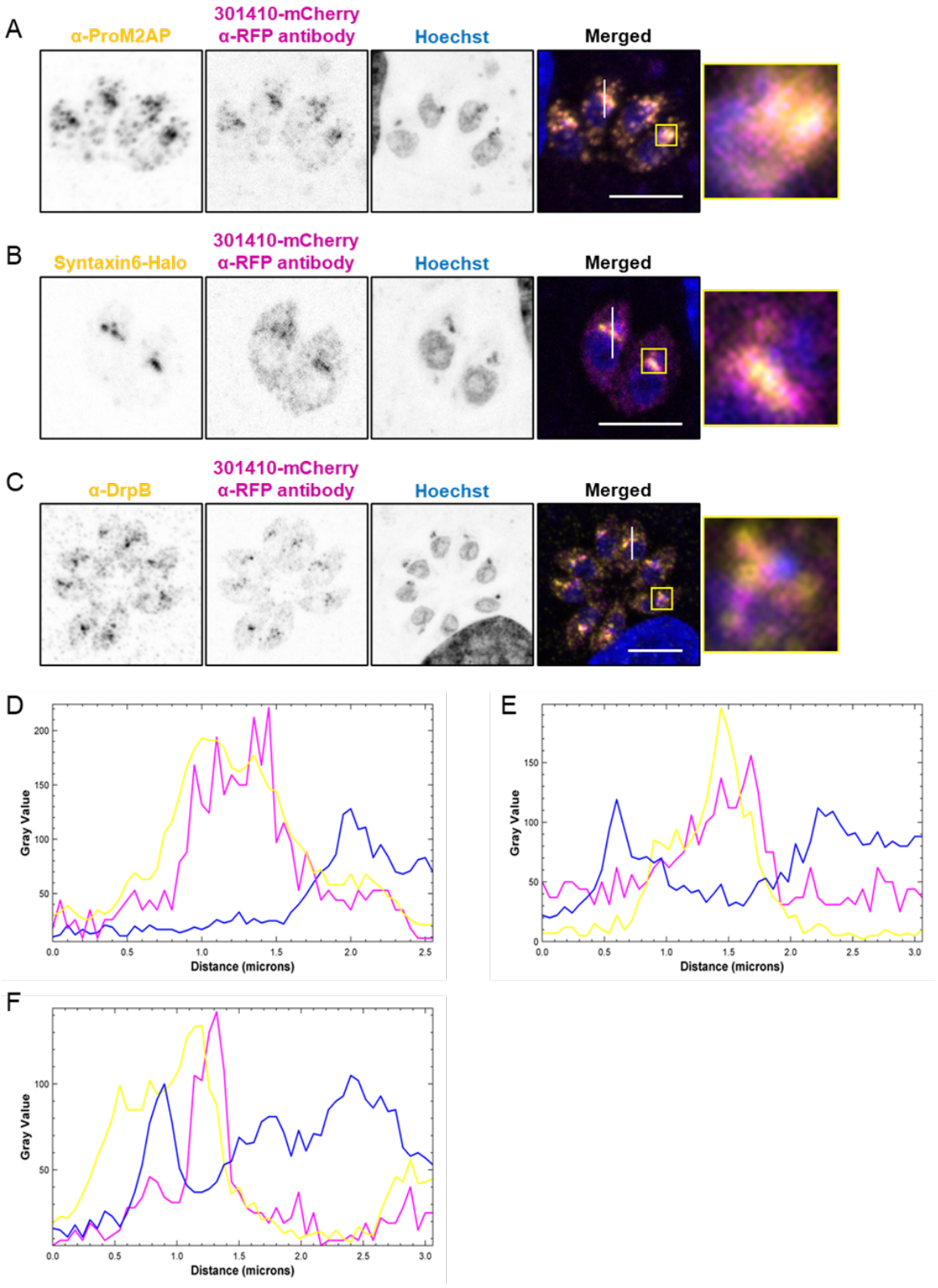

Figure 3.9 – Colocalisation of *Tg*EDP (TGGT1_301410) with post-Golgi markers

Localisation with respect to vesicle membranes – cargo or vesicle-associated

As previously mentioned, *Tg*EDP does not have any identifiable transmembrane domains. This suggested that the entirety of the protein is present on one side of a membrane, that is, either inside of the vesicles it is associated with, or on their outside, possibly being involved in vesicle transport. Therefore, the next step in trying to elucidate the function of the protein was to determine on which side of the membrane the protein resides. In order to do this, a plasmid was constructed wherein a GFP-nanobody (amplified from the addgene plasmid #58370) (S. Lee et al., 2014), which also binds YFP and SYFP2, was fused to a Halo-tag. This construct was then stably inserted into the UPRT locus (Donald & Roos, 1995; Shen et al., 2014) of the parasite (as explained in Figure 2.2), leading to co-expression of the YFP/SYFP2-tagged protein and the nanobody. The GFP-nanobody-Halo construct had no specific target sequences and hence localised to the cytoplasm. This meant that if the protein of interest is present on the cytoplasmic side of the vesicles, it is accessible to and bound by the nanobody (Figure 3.10A). In order to validate the use of this GFP-nanobody construct, both positive and negative controls were used. For this, the GFP-nanobody-Halo construct was also expressed in strains where proteins tagged with YFP/SYFP2 were either accessible or not accessible to the cytoplasm, as well as in a strain where no YFP/SYFP2 was present. The parasite strains used were: 1) a strain expressing Formin2 fused to SYFP2 generated by Dr. Mirko Singer (Stortz et al., 2019), 2) a strain where the surface antigen SAG1 is tagged with YFP directly upstream of the GPI-anchor thus making the tag extracellular, also generated by Dr. Mirko Singer, and 3) the strain where the protein of interest is tagged with mCherry, which is not recognised by the nanobody and therefore serves as negative control (Figure 3.10). Since the expression levels of the nanobody is very high, a caveat of the system can be high background levels, in case the protein of interest has low expression levels. This can be observed in case of the positive control, Formin2-SYFP2. Although the nanobody can be seen to localise at the Golgi-region, a high cytosolic background level can still be detected. Despite this, signal showing SYFP2-bound nanobody was clearly observed in the parasites expressing the cytoplasmically-accessible SYFP2-tagged proteins, that is, the Formin2-SYFP2 strain and the TGGT1_301410-SYFP2 strain. This confirmed that the protein of interest is likely bound to the cytoplasmic side of the Golgi body.

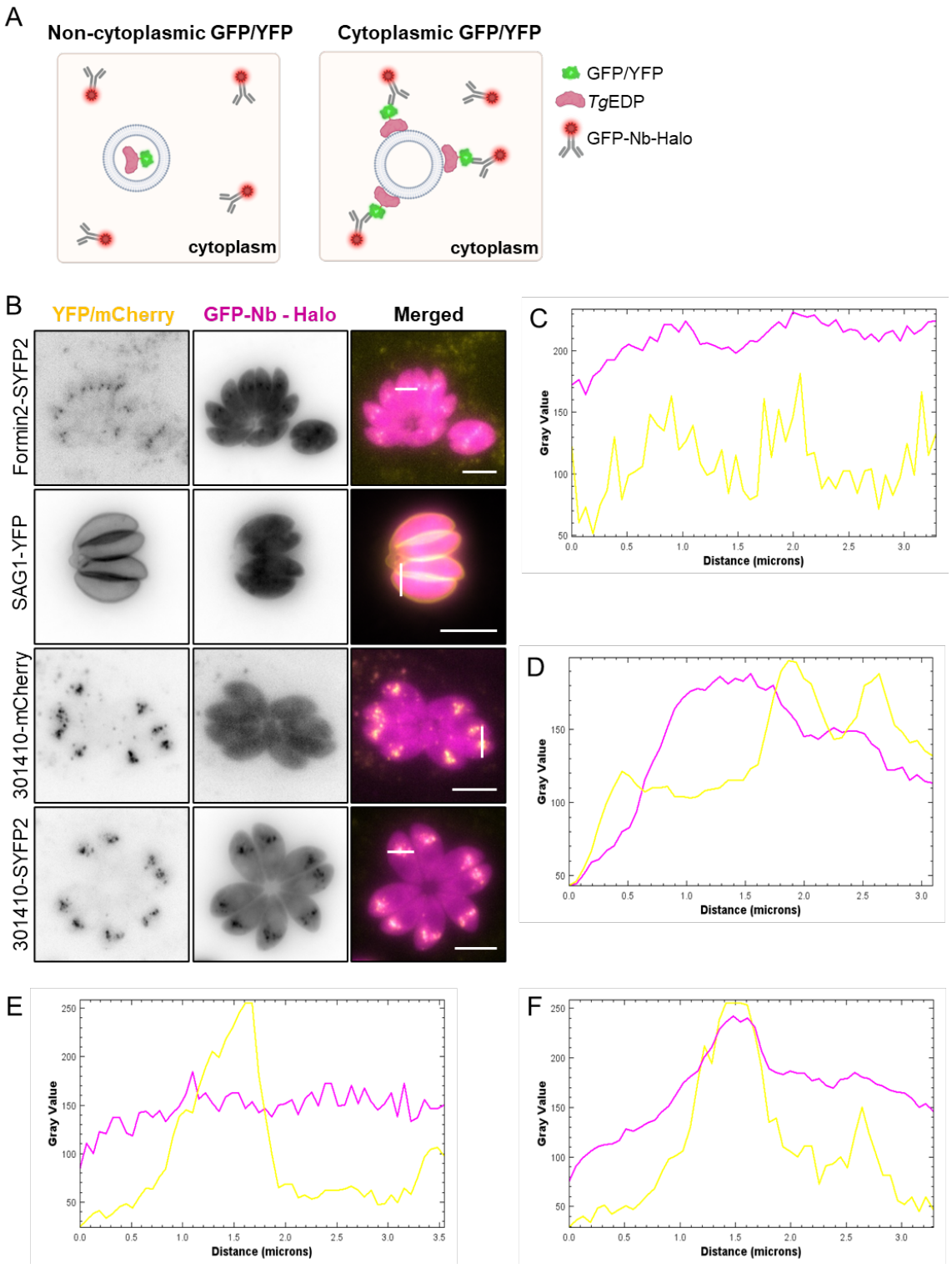

Figure 3.10 – *Tg*EDP (TGGT1_301410) is present within the cytoplasm

(**A**) Scheme of how the GFP-nanobody-Halo construct works. A GFP-nanobody fused to a Halo-tag was stably expressed within the parasites by replacing the UPRT locus. This nanobody has no target sequence and therefore localises within the cytoplasm. In cases where

no GFP, YFP, or SYFP2 are accessible within the cytoplasm, no colocalisation with the nanobody occurs and this nanobody signal remains diffuse within the cytoplasm. However, in cases where GFP, YFP, or SYFP2 are present within the cytoplasm, the nanobody binds to the fluorescent tag, resulting in colocalisation. (**B**) *Tg*EDP-SYFP2 was seen to colocalise with the cytoplasmic GFP-Nanobody-Halo. Formin2-SYFP2 was used as a positive control, while SAG1-YFP and TGGT1_301410-mCherry were used as negative controls. YFP and mCherry tags are shown in yellow, while the GFP-nanobody-Halo is shown in magenta. Scale bars are all 5 µm. (**C**), (**D**), (**E**), (**F**) show the plot profiles across the white lines drawn on the merged images in (B). (C) shows the plot profile of formin2-SYFP2, (D) shows that of SAG1-YFP, (E) shows that of TGGT1_301410-mCherry, and (F) shows that of TGGT1_301410-SYFP2. In all cases, the merged images were first converted to 8-bit images in order to account for variations in protein expression levels leading to differences in intensities. In the cases of TGGT1_301410-SYFP2 and Formin2-SYFP2, peaks in SYFP2 intensity correspond to peaks in Halo intensity. This was in contrast to TGGT1_301410-mCherry and SAG1-YFP, where he peaks in intensities did not correspond.

3.2.3. *The lytic cycle – invasion, replication, egress, essentiality*

Since all genetic modifications were done in a parasite strain which expressed the dimerisable Cre recombinase (Andenmatten et al., 2013; Hunt et al., 2019), flanking of the gene of interest with loxP sequences allowed for the generation of inducible knockouts upon addition of rapamycin (Figure 3.5B). The generated knockouts were used to facilitate characterisation, starting with investigating at which stage of the lytic cycle *Tg*EDP is essential.

*Plaque assays confirm essentiality of Tg*EDP

Plaques assays were initially done in order to confirm the essentiality of *Tg*EDP predicted by the genome-wide screen (Sidik et al., 2016). In a plaque assay, a known number of parasites was used to infect a host cell monolayer, the multiplicity of infection being chosen in a way so as to ensure that the monolayer is not lysed after a week of undisturbed incubation. During this incubation, parasites invaded, replicated, egressed, and reinvaded neighbouring cells, this repetitive process eventually resulting in a ‘plaque’ in the monolayer (Figure 3.11A). In the case of parasites which have reduced fitness, this reduction in fitness is evident in the reduction of the number and size of plaques left in the monolayer. After 7 days of undisturbed incubation in the presence of rapamycin, no plaques were observed on the HFF monolayer, showing that *Tg*EDP is essential (Figure 3.11B).

Invasion, replication, and egress assays suggest metabolic defect

Invasion assays were carried out wherein the parasites were manually egressed following 48 hr of knockout induction, after which they were allowed to invade for 30 minutes, and then fixed with 4% PFA. All parasites which remained extracellular were labelled with anti-SAG1 antibodies in the absence of triton x-100, after which all parasites, both intra- and extracellular, were then permeabilized and labelled with anti-GAP45 antibodies. From the results obtained (Figure 3.11C), there was no significant difference noted between the non-induced and knockout parasites. This suggested that the secretory organelles required for invasion and parasitophorous vacuole formation were unaffected in the knockout mutants.

For the replication assays, the parasites were manually egressed after 48 hr of induction, after which they were allowed to invade for 1 hour. The glass slides were then washed with fresh supplemented DMEM to remove any extracellular parasites, and the invaded parasites allowed to replicated for 24 hours. Following this period of replication, the slides were fixed with 4% PFA, and anti-GAP45 antibodies used to label the parasites. As seen in Figure 3.11D, the knockout parasites seemed to have a growth defect when compared to the non-induced parasites, possibly suggesting a metabolic deficiency.

In the case of the egress assays carried out, the parasites were induced with rapamycin for 24 hours, after which they were manually egressed and allowed 4 hours to invade HFFs grown on IFA slides. The slides were then washed with fresh supplemented DMEM, and the parasites incubated for 36 hours. At the 36 hour timepoint, egress was induced for 5 minutes using calcium ionophore (Caldas et al., 2007; Endo et al., 1982), and the cells were then fixed and the percentage of successfully egressed parasites quantified. (Figure 3.11E). Significantly less parasites were seen to egress successfully after deletion of *Tg*EDP. Given that the knockout parasites also seemed to have a growth defect, it is hypothesised that the failure in egress is a downstream effect of the growth defect or parasite vacuole collapse.

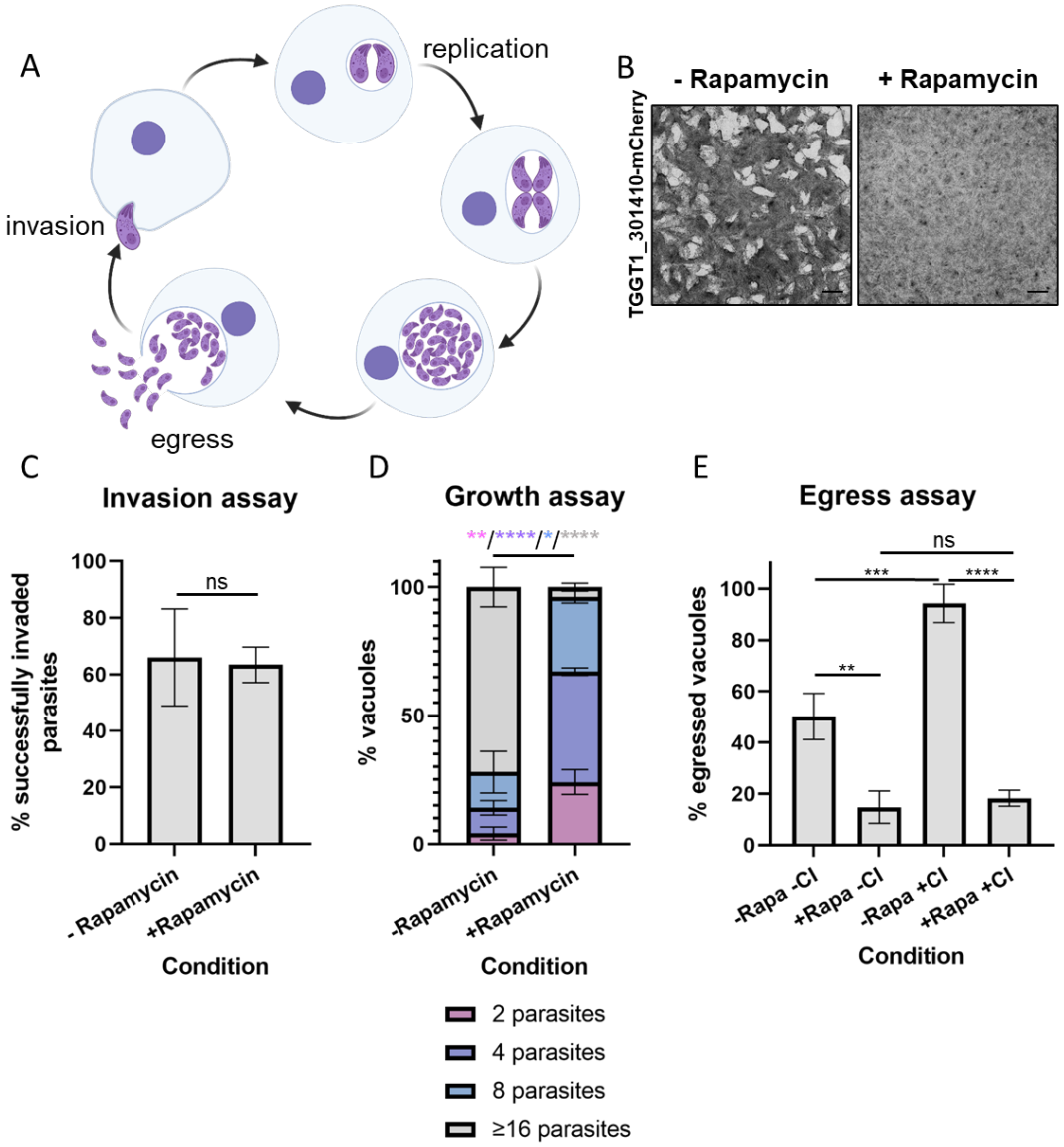

Figure 3.11 – *Tg*EDP (TGGT1_301410) is essential for parasite survival

(**A**) Overview of the parasite's lytic cycle; a tachyzoite attaches to and invades an uninfected host cell, after which it replicates intracellularly. Following several rounds of replication, the parasites then lyse the host cell to egress and reinvade neighbouring host cells. Repeated cycles of invasion, replication, and egress create a plaque in the host cell monolayer. (**B**) Plaque assays were done wherein parasites were left in the presence of 50 nM rapamycin or vehicle control (DMSO) for 7 days of undisturbed incubation. Results showed that, unlike non-knockout parasites, knockout mutants (+ Rapamycin) did not form plaques in the host cell monolayer. The absence of plaques in the well containing the inducible knockout line shows that removal of *Tg*EDP is detrimental to the survival of the parasites. Scale bars are 1.5 mm. (**C**) Invasion assays were done wherein parasites were incubated in the presence of 50 nM rapamycin or DMSO for a period of 48 hrs, after which these were manually egressed and allowed to invade fresh HFFs. The cells were then fixed and the number of successful invasions quantified. The difference in invasion levels between wildtype and knockout

parasites was not significant. (**D**) Growth assays were done wherein parasites were incubated in the presence of 50 nM rapamycin or DMSO for a period of 48 hrs, after which these were manually egressed and allowed to invade fresh HFFs. These were then allowed to replicate for a period of 24 hrs, after which they were fixed and the number of parasites per vacuole quantified. The number of knockout parasites per vacuole was significantly lower than that of wildtype parasites, suggesting a growth retardation. (**E**) Egress assays were done wherein parasites were incubated in the presence of 50 nM rapamycin or DMSO (-/+ Rapa) for a period of 24 hrs, after which these were manually egressed and allowed to invade fresh HFFs. These were then allowed to replicate for a further 36 hrs, after which egress was either allowed to occur naturally or was induced using calcium ionophore A23187 (-/+ CI). The percentage of successfully egressed parasites was significantly lower for the knockout mutants.
All assays were done thrice, with a minimum of 100 parasites/vacuoles quantified per condition per replicate. All data are plotted as mean ± s.d. Unpaired two-tailed Student's t-test was calculated for (C), where p = 0.8193. One-way ANOVA with Tukey's multiple comparison test was done for both (D) and (E). Colour-coded P values in (D) represent the vacuoles compared. P values are represented as follows: ns = >0.05; * = 0.01 - 0.05; ** = 0.001 – 0.01; *** = 0.0001 – 0.001; **** = < 0.0001.

3.2.4. *Knockout phenotypes*

The initial phenotypic characterisation suggested that a) the protein functions at the Golgi, and b) the parasites are affected in replication. Therefore, it was speculated that the protein functions in a critical step of the secretory pathway. Consequently, organelles which are affected upon depletion of the protein were investigated.

The Golgi Body and Post-Golgi compartments

Given that *Tg*EDP localises to the Golgi body, the effect of its knockout on this organelle, as well as the downstream compartments was investigated. The different markers used for colocalisation studies were also used to determine the effect of the knockout of *Tg*EDP.

Upon induction with rapamycin, no change was observed in the *cis*-Golgi marked with GRASP-RFP (Pfluger et al., 2005) (Figure 3.12A). The *trans*-Golgi, however, was observed to vesiculate (Figure 3.12B). This phenotype was seen to start around 48 hours post-induction, and reached almost 100% by 72 hours (Figure 3.12C), at which point the vacuoles had started to collapse.

The same pattern was observed for the dynamin related protein, DrpB (Breinich et al., 2009) and syntaxin6 (Jackson et al., 2013) (Figure 3.14B-D), two of the post-Golgi compartments

investigated. The endosome-like compartment (Harper et al., 2006), on the other hand, was not observed to experience any negative effect and remained unchanged (Figure 3.14A).

Wildtype and knockout parasites were also sent for Transmission Electron Microscopy in order to better understand the changes in the ultrastructures of the parasites. In agreement with IFA data, at the 72hr timepoint following the addition of rapamycin, what seemed to be large electron-lucent vesicles were observed in place of the Golgi body, suggesting that the Golgi body itself expanded (Figure 3.13).

Figure 3.12 – Knockout of *Tg*EDP (TGGT1_301410) results in *trans*-Golgi fragmentation, but does not affect *cis*-Golgi (next page)

(**A**) The *cis*-Golgi marked with GRASP-RFP (in magenta) is unaffected upon knockout of *Tg*EDP (shown in yellow). This was observed in 100% of cases. In the figure, the *cis*-Golgi can be seen replicating normally. (**B**) Upon knockout of *Tg*EDP, the *trans*-Golgi, labelled by endogenously tagging SortLR with Halo-tag (in yellow) was seen to fragment. All scale bars are 5 µm. (**C**) The fragmentation of the *trans*-Golgi in knockout parasites was seen to be significantly higher than that of wildtype parasites after 48 hours post-induction (hpi) with rapamycin. All Immunofluorescence assays were done thrice, with a minimum of 100 parasite vacuoles quantified per condition per replicate. Data is presented as mean ± s.d. One-way ANOVA with Tukey's multiple comparison test was done, with P values being represented as follows: ns = >0.05; **** = < 0.0001.

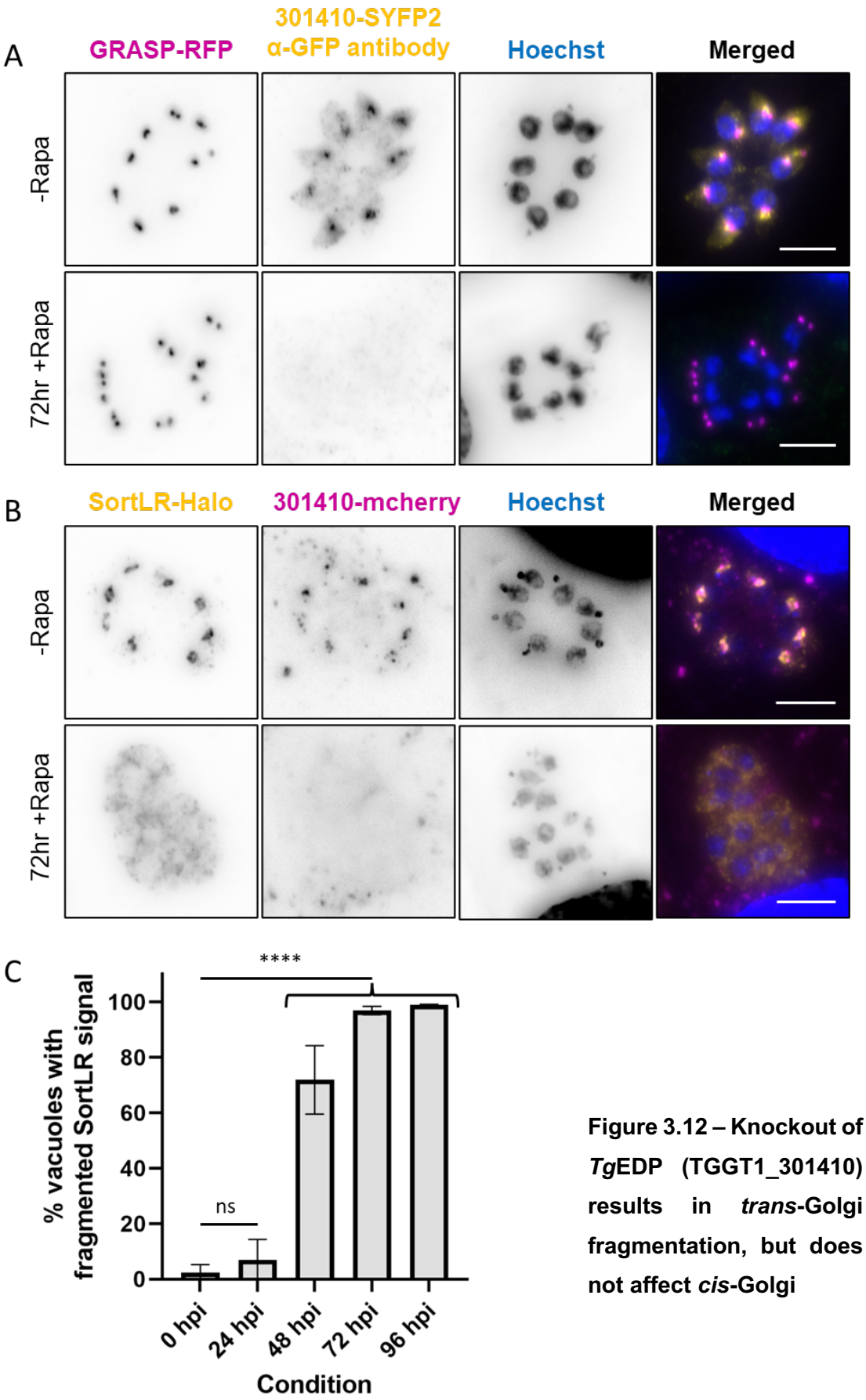

Figure 3.12 – Knockout of *Tg*EDP (TGGT1_301410) results in *trans*-Golgi fragmentation, but does not affect *cis*-Golgi

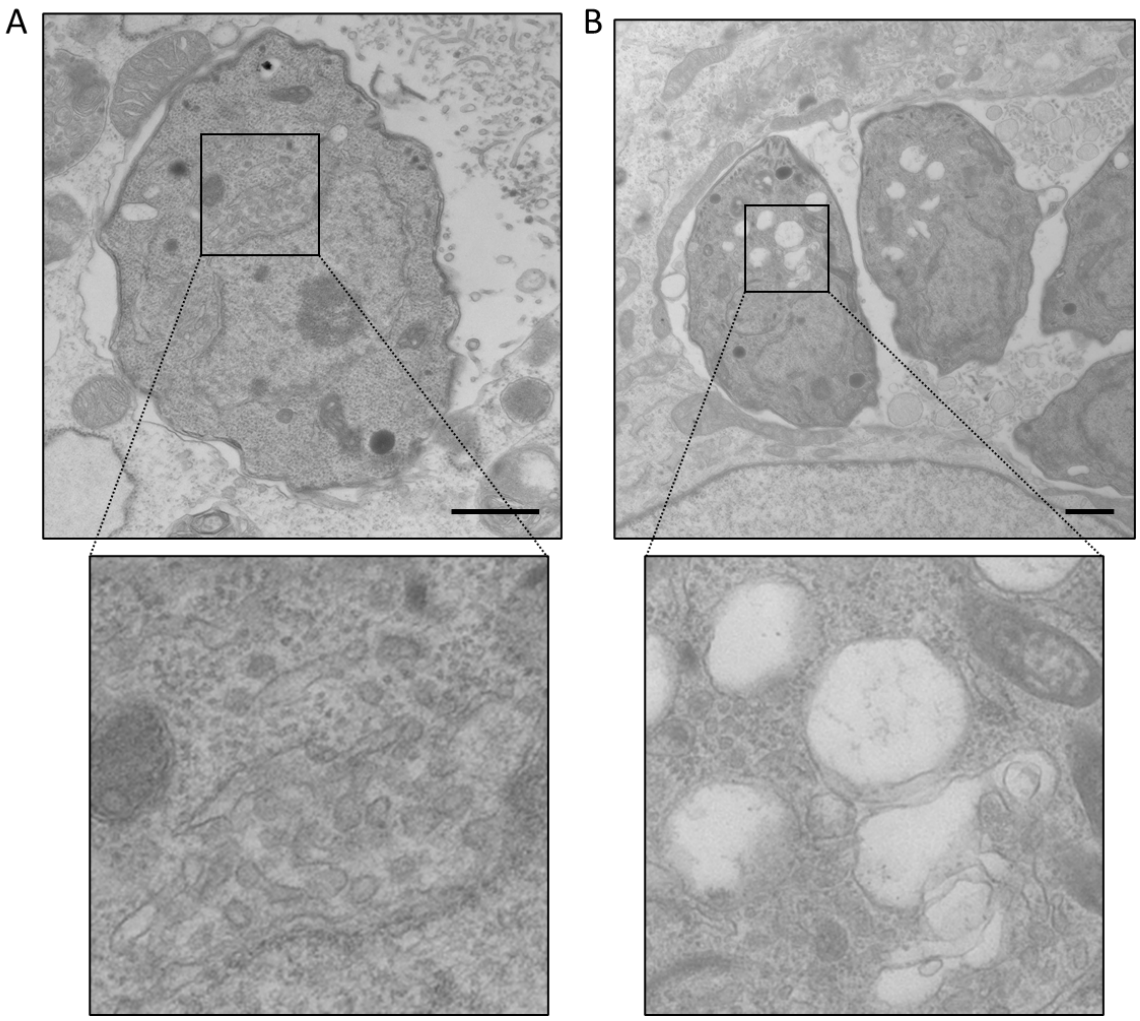

Figure 3.13 – Knockout of *Tg*EDP (TGGT1_301410) results in the swelling of the Golgi

(**A**) shows the wildtype condition, wherein the Golgi stacks are organised adjacent to the nucleus. (**B**) shows parasites at 72 hours after addition of 50 nM rapamycin. Upon knockout of *Tg*EDP, the Golgi body was seen to enlarge, confirming the results observed via IFA. Scale bars are 1 µm.

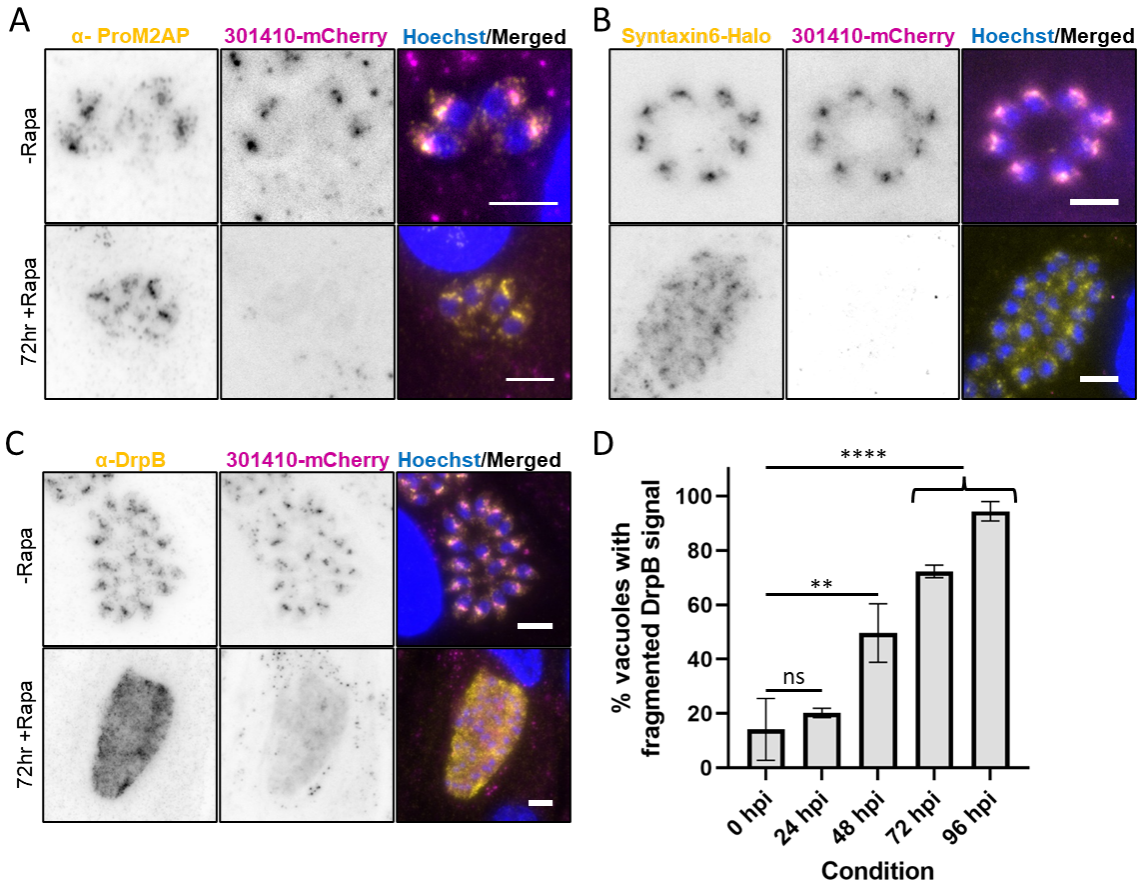

Figure 3.14 – Knockout of *Tg*EDP (TGGT1_301410) results in the fragmentation of some post-Golgi compartments

(**A**) In all parasites observed, knockout of *Tg*EDP (in magenta) was not seen to affect the compartments labelled with anti-ProM2AP antibodies (in yellow). In contrast to this, the compartments marked by syntaxin6 (**B**) and DrpB (**C**) (both in yellow) were seen to fragment upon *Tg*EDP knockout. All scale bars are 5 μm. (**D**) Quantifications showed that in knockout parasites, the fragmentation of the post-Golgi compartment marked by DrpB was significantly higher than that in wildtype parasites after 48 hours post-induction (hpi) with rapamycin. All Immunofluorescence assays were done three times, with a minimum of 100 parasite vacuoles quantified per condition per replicate. Data is presented as mean ± s.d. One-way ANOVA with Tukey's multiple comparison test was done, with P values being represented as follows: ns = >0.05; ** = 0.001 – 0.01; **** = < 0.0001.

The secretory organelles

In order to determine whether *Tg*EDP functions within the secretory pathway, the micronemes, rhoptries, and dense granules were investigated.

MIC8 antibodies were used to look at the trafficking of micronemal proteins. No change in the localisation of these proteins was observed after 96 hours of induction (Figure 3.15A), despite the vacuole itself appearing to collapse, thus implying that the transport of micronemes is unaffected.

The same observation was made when investigating rhoptry and dense granule trafficking by means of ROP2,4 (Figure 3.15B) and Gra1 (Figure 3.15C) visualization respectively - no change was seen upon knockout of *Tg*EDP. These results suggest that unlike other trafficking factors operating at the Golgi (Breinich et al., 2009; Pieperhoff et al., 2013), *Tg*EDP does not seem to be involved in the secretory pathway.

The Inner Membrane Complex and the apicoplast

After determining that knockout of *Tg*EDP does not affect the trafficking of the micronemes, rhoptries, or dense granules, other compartments within the parasite were also investigated. The IMC were observed to be unaffected in the mutant (Figure 3.15D), as was the apicoplast (Figure 3.15E). Antibodies against IMC1 and G2-Trx were used respectively.

Figure 3.15 – Knockout of *Tg*EDP (TGGT1_301410) does not affect the localisation of micronemes, rhoptries, dense granules, IMC, or apicoplast (next page)

IFAs using antibodies against (**A**) micronemes (Mic8), (**B**) rhoptries (Rop2,4), (**C**) dense granules (Gra1), (**D**) IMC (IMC1), and (**E**) apicoplast (G2-Trx) (all in yellow) showed that knockout of *Tg*EDP (tagged with mCherry, shown in magenta) has no effect on their localisation. Any effects observed were deemed to be due to the collapse of the vacuole (shown in DIC). Immunofluorescence assays were done in triplicate, with a minimum number of 100 vacuoles per replicate observed. The nuclei were labelled with Hoechst. All scale bars are 5 µm.

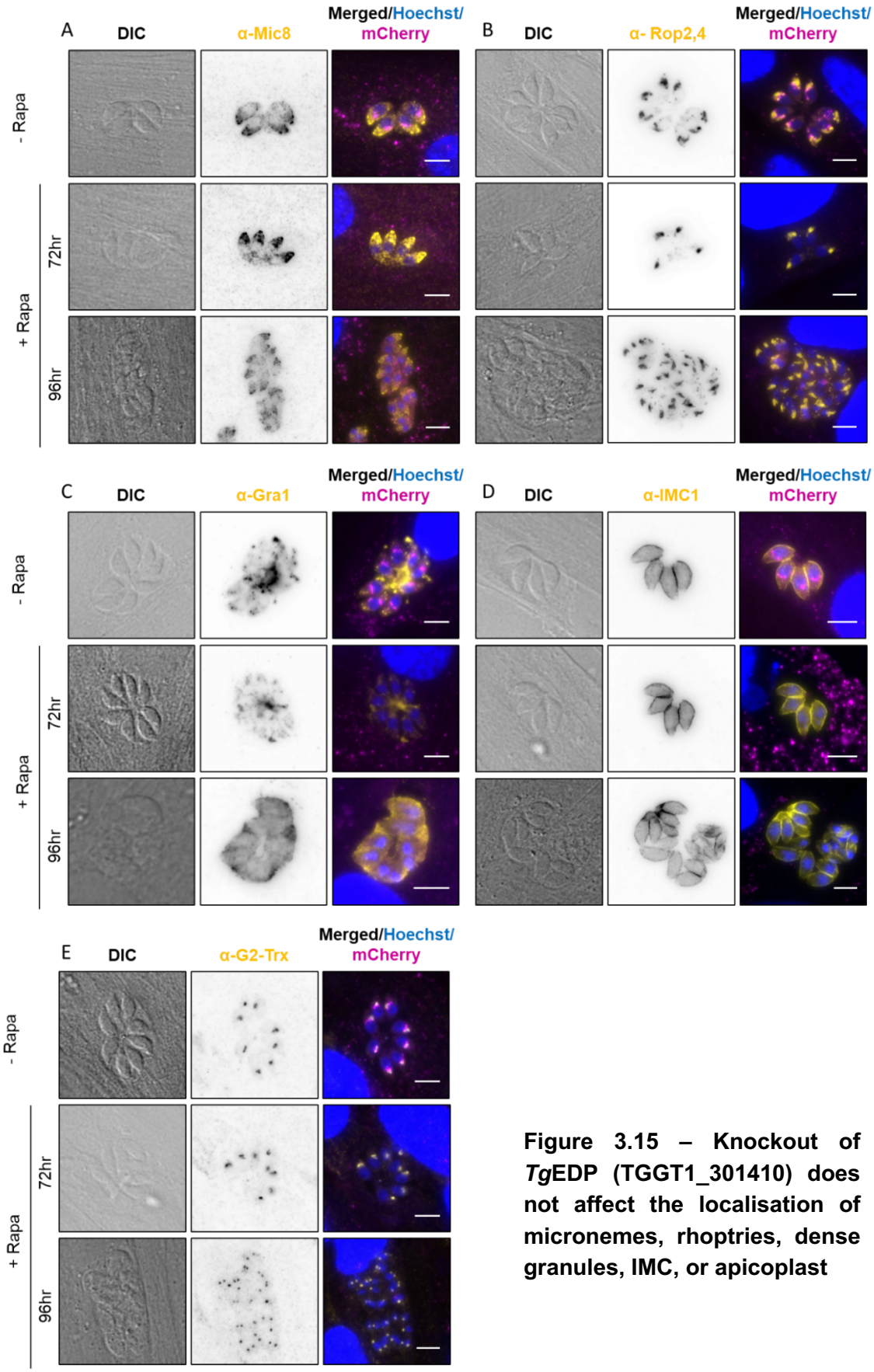

Figure 3.15 – Knockout of *Tg*EDP (TGGT1_301410) does not affect the localisation of micronemes, rhoptries, dense granules, IMC, or apicoplast

The Vacuolar Compartment

The vacuolar compartment (VAC), the parasites' equivalent of the lysosome, was also investigated. Under wildtype intracellular conditions, the VAC, typically observed using antibodies against cathepsin L, is observed to be composed of a number of vesicles which are relatively diffused throughout the cytoplasm of a tachyzoite, these vesicles only fusing together to form a larger structure when the parasites are extracellular, just invaded, or during division (Miranda et al., 2010; Parussini et al., 2010). Upon knockout of *Tg*EDP, the VAC, here also visualized using anti-CPL antibodies, appeared to be enlarged, with the signal also appearing more intense (Figure 3.16A-D). This phenotype was observed to peak at around 48 hours post-induction with rapamycin, after which the structure was seen to fragment and the parasitophorous vacuoles began to collapse (Figure 3.16A-B). This phenotype was also observed in extracellular parasites (Figure 3.16C).

Figure 3.16 – Knockout of *Tg*EDP (TGGT1_301410) results in altered CPL localisation (next page)

(**A**) CPL is found in small cytoplasmic vesicles in intracellular parasites and typically shows a diffuse localisation. Knockout of *Tg*EDP (in magenta) resulted in an accumulation of CPL (shown in yellow). This accumulation was seen to fragment at 72 hr post-induction of *Tg*EDP knockout. Scale bars are 5μm. (**B**) The percentage of parasitophorous vacuoles showing altered CPL localisation was significantly higher in knockout mutants after 48 hr post-induction (hpi) with 50 nM rapamycin. The assay was done three times, with a minimum of 100 vacuoles quantified per condition per replicate. The data is plotted as mean ± s.d. One-way ANOVA with Tukey's multiple comparison test was applied, with P values being represented as follows: ns = >0.05; ** = 0.001 – 0.01; **** = < 0.0001. (**C**) CPL signal, which typically appears more confined to a few structures in extracellular wildtype parasites, also appeared to accumulate in extracellular *Tg*EDP-knockout parasites. Scale bars are 3 μm. (**D**) CPL signal intensity quantifications confirmed an accumulation of CPL, this being significantly higher in knockout parasites after 48 hours post-induction (hpi) with rapamycin. The assay was done three times, with the intensities of a minimum of 15 vacuoles quantified per condition per replicate. The data is plotted as mean ± s.d., with the dots representing the value for each data point. One-way ANOVA with Tukey's multiple comparison test was done. The P values are represented as follows: ns = >0.05; **** = < 0.0001. (**E**) Colocalisation with SortLR-Halo (in magenta) was done in order to determine whether the accumulation of CPL (in yellow) was occurring downstream of the *trans-Golgi* vesiculation upon *Tg*EDP knockout. Immunofluorescence assay images show that CPL colocalises with an intact *trans-Golgi*. Scale bars are 5μm. (**F**), (**G**), and (**H**) show profile plots taken across the white lines in panel (E) (-Rapamycin, 24 hr +Rapamycin, and 48 hr +Rapamycin respectively). (**F**) shows that in wildtype conditions, CPL intensity (yellow) does not correlate with the peak in signal intensity from SortLR-Halo (magenta). (**G**) and (**H**) show that upon *Tg*EDP knockout, CPL signal intensity (yellow) starts to increase and the peak in signal overlaps with that of SortLR-Halo (magenta).

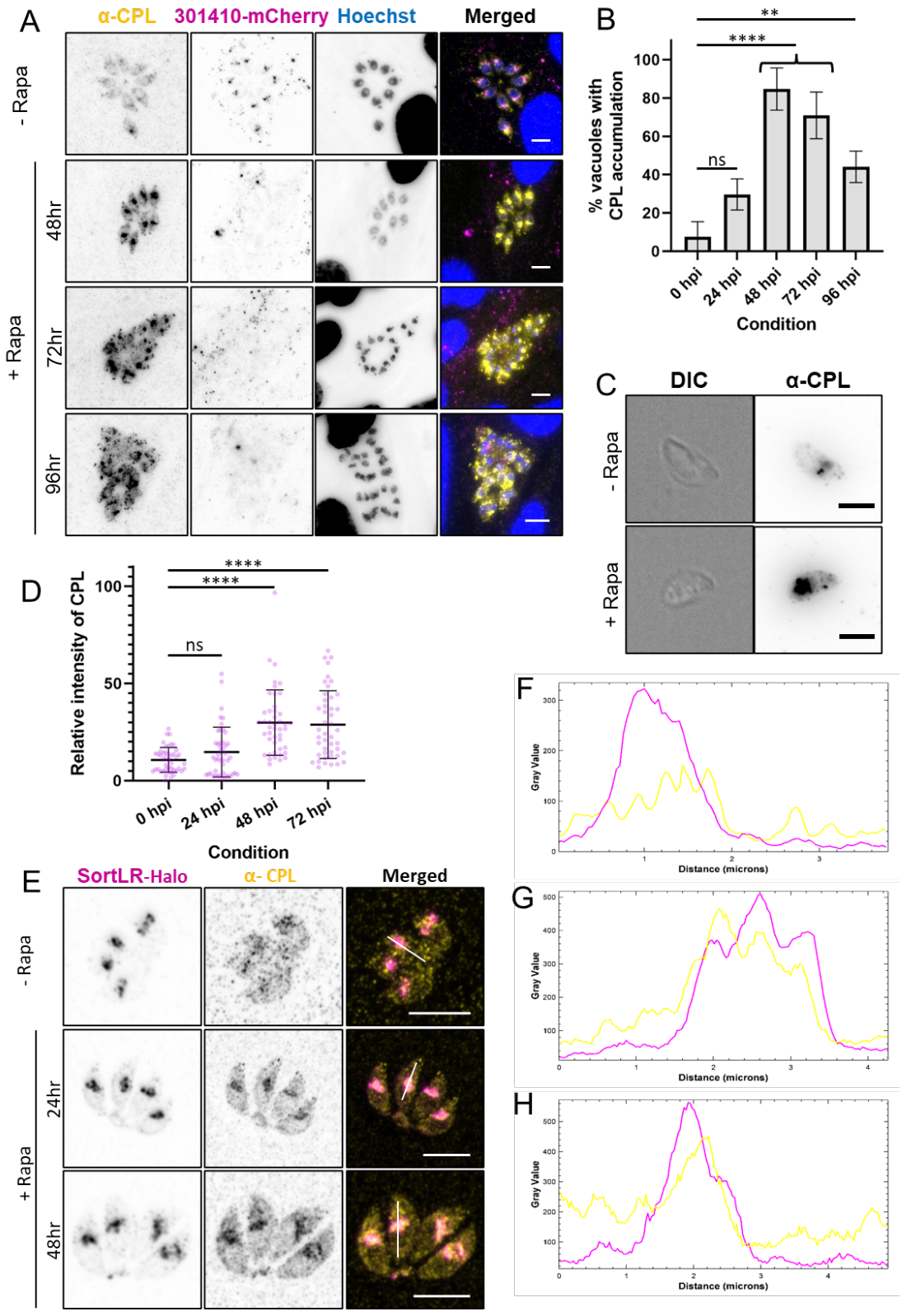

Figure 3.16 - Knockout of *Tg*EDP (TGGT1_301410) results in altered CPL localisation

Since CPL is a protease that is trafficked from the Golgi to the VAC, its localisation upon knockout of *Tg*EDP could possibly indicate a defect in its trafficking. In an attempt to better understand which phenotype is the primary effect, the VAC was visualized in a parasite strain wherein SortLR was endogenously Halo-tagged. During this colocalisation experiment, the signal from CPL appeared to colocalise with that coming from SortLR (Figure 3.16E-H), showing that accumulation of CPL occurs prior to the fragmentation of the Golgi body. This result also suggested that CPL is being retained within the *trans*-Golgi.

The mitochondria

Immunofluorescence assays were done wherein *Tg*EDP was knocked out and the effect on the mitochondria was observed by means of anti-TOM40 antibodies (Figure 3.17). Upon doing so, the mitochondria were seen to fragment. The number of knockout mutant parasitophorous vacuoles exhibiting this aberrant phenotype was significantly higher than that in wildtype parasites after 48 hours post-induction.

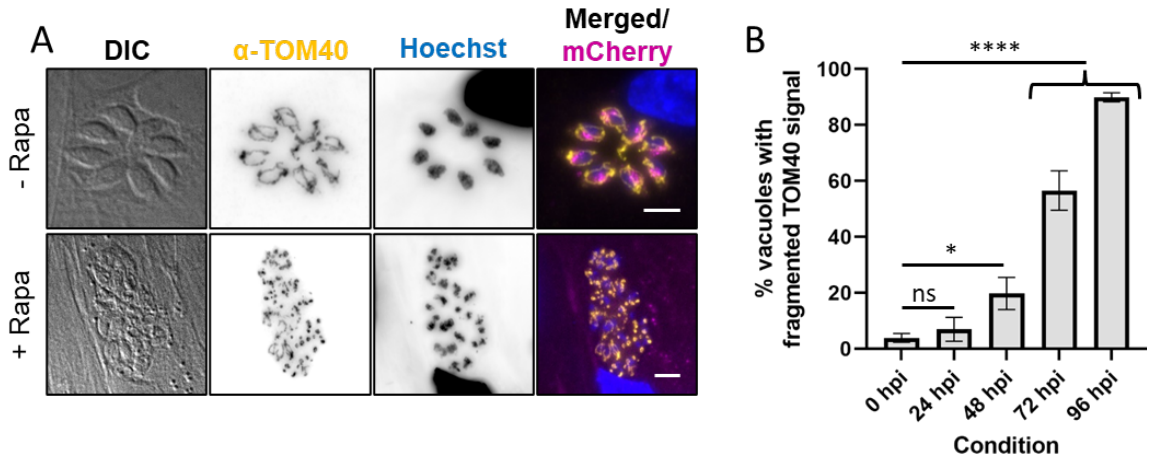

Figure 3.17 – Knockout of *Tg*EDP (TGGT1_301410) causes mitochondrial fragmentation

(**A**) Knockout of *Tg*EDP (in magenta) results in the fragmentation of the mitochondria (marked using the anti-TOM40 antibodies in yellow). Scale bars are 5 μm. (**B**) Mitochondrial fragmentation was seen to be significantly higher in knockout parasites compared to wildtype parasites after 48 hours post-induction (hpi) with rapamycin. Data is presented as mean ± s.d. One-way ANOVA with Tukey's multiple comparison test was done, with P values being represented as follows: ns = >0.05; * = 0.01 - 0.05; **** = < 0.0001.

In order to better understand which was the primary aberrant phenotype upon knockout of *Tg*EDP, the quantification data from Figures 3.12, 3.16, and 3.17 were plotted on the same graph (Figure 3.18). Doing so demonstrated that the number of vacuoles showing abnormal CPL accumulation was significantly higher than those showing *trans*-Golgi or mitochondrial fragmentation at 24 hours post-induction. Furthermore, the number of vacuoles exhibiting abnormal CPL accumulation and Golgi morphology at 48 hours post-induction were not significantly different (P = 0.6885), but were both significantly higher that the number of vacuoles with fragmented mitochondria. Taken together, this data suggests that the primary effect upon knockout of *Tg*EDP is CPL accumulation, while mitochondrial fragmentation occurred downstream of both CPL accumulation and Golgi fragmentation.

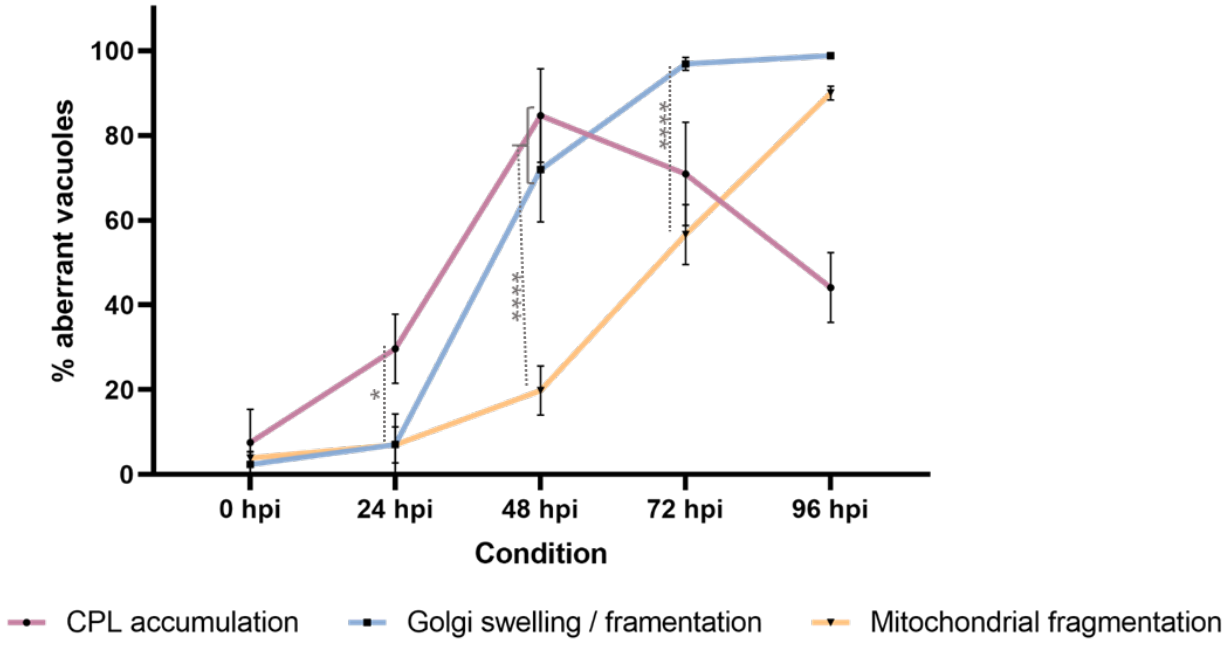

Figure 3.18 – CPL accumulation is the first phenotype evident upon knockout of *Tg*EDP

Phenotype quantifications indicate that the first impact upon knockout of *Tg*EDP was on the localisation of cathepsin L, followed by the compromise of the Golgi structure. Since the negative effects on mitochondrial structure became apparent later, the data suggests that this is a downstream phenotype. Three biological replicates were done for each quantification, with a minimum of 100 vacuoles per condition per replicate counted. All data is presented as mean ± s.d. One-way ANOVA with Tukey's multiple comparison test was performed. P values are represented as follows: ns = >0.05; * = 0.01 - 0.05; **** = < 0.0001.

3.2.5. *Endocytosis and secretion*

In order to further investigate the parasites' trafficking system and determine whether *Tg*EDP knockout parasites were deficient in either endocytosis or secretion, a pulse-chase assay was carried out as has been described in Koreny et al., (2022) and Periz et al., (2019). For this experiment, SAG1 was tagged with a Halo-tag by inserting the tag upstream of the GPI-anchor, thus placing it extracellularly. The parasites were incubated in the presence or absence of rapamycin for 24 hours, after which they were incubated intracellularly in the presence of a cell-permeable Halo-dye for 24 hours. The labelled parasites were then washed thoroughly to remove all unbound dye, and used to infect a fresh monolayer of HFFs. After 24 hours of replication, the parasites were then labelled once more with a different cell-permeable Halo-dye for an hour, after which the dye was again washed off thoroughly and the parasites fixed with 4% PFA. The parasites were then imaged and total relative fluorescence measured using ImageJ and compared to the non-induced condition.

Results showed that under both wildtype as well as *Tg*EDP-knockout conditions, both the newly synthesized as well as the recycled SAG1 were present at the plasma membrane and within vesicles inside the parasites (Figure 3.19A). These results showed that in *Tg*EDP-knockout parasites, SAG1 can still be secreted from the parasite to the plasma membrane, and is still eventually endocytosed. It was noted, however, that SAG1 intensity was marginally higher in the knockout mutants compared to the non-induced strain, suggesting a possible deficiency in SAG1 degradation. Although not statistically significant, this deficiency would be consistent with the parasites' inability to traffic proteases to the VAC.

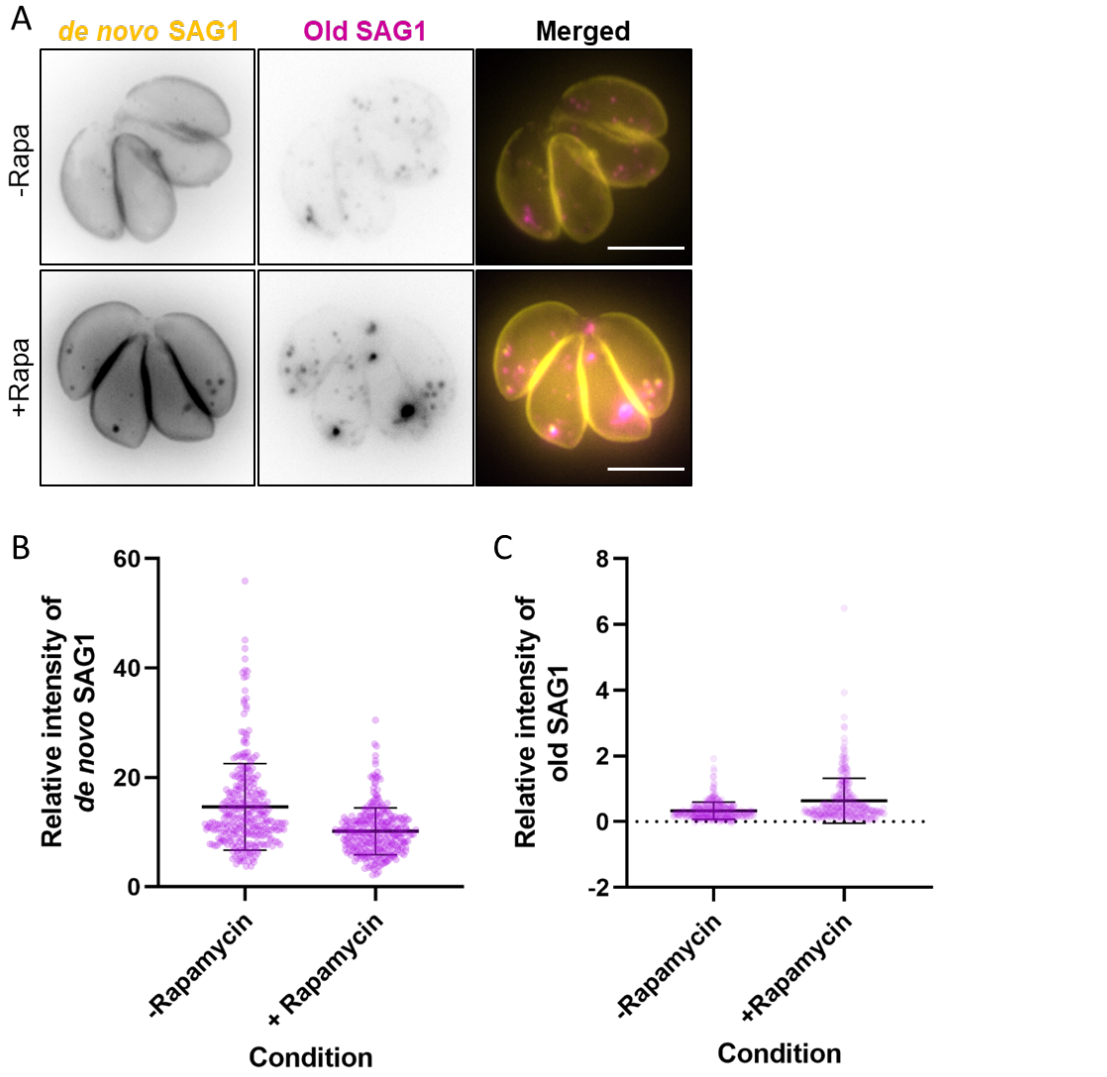

Figure 3.19 – Dual labelling of SAG1-Halo shows no effect on endocytosis or secretion upon *Tg*EDP knockout

(**A**) Halo-tagged SAG1 was labelled with cell-permeable dyes using the dual-labelling system wherein one dye was added for 24 hours, after which it was washed, the parasites allowed to replicate for a further 24 hours, and then labelled with a different dye. The plasma membrane localisation of *de novo* SAG1 (in yellow) shows that there is no defect in SAG1 secretion, whereas the colocalisation of 'old' and *de novo* SAG1 vesicles shows that endocytosis is also unaffected. Scale bars are 5 µm. (**B**) shows the signal intensity quantifications of *de novo* SAG1-Halo in both the wildtype and induced knockout, whereas (**C**) shows the signal intensity quantifications of 'old' SAG1-Halo. Although there seems to be less *de novo* and more 'old' SAG1-Halo in the induced knockout parasites, this difference was not significant (P = >0.9999). Three replicate experiments were done, with the intensities of a minimum of 100 vacuoles quantified per condition per replicate for (B) and (C). The data is presented as mean ± s.d., with the dots representing the value for each data point. One-way ANOVA with Tukey's multiple comparison test was done for both (B) and (C).

3.2.6. *TurboID proximity labelling*

Previous results have shown that *Tg*EDP is on the cytoplasmic side of the Golgi body, suggesting that it is not cargo. The fact that the protein is also not predicted to have a transmembrane domain also suggested it is likely to be bound to the Golgi body via interactions with other proteins. These protein interactions are possibly stable, forming a protein complex. However, there is also a possibility that *Tg*EDP is involved in other transient protein-protein interactions. In an attempt to identify potential interaction partners, both of a stable, as well as of a transient nature, *Tg*EDP was C-terminally tagged with TurboID.

TurboID is an enhanced version of BioID where a highly reactive biotin ligase converts supplemented biotin into the reactive biotin-AMP, which in turn covalently labels proteins which are in close proximity to the biotin ligase (Cho et al., 2020). These biotinylated proteins are then pulled down via their interaction with streptavidin-coupled beads, and sent for mass spectrometry. Due to the highly reactive nature of TurboID versus conventional BioID, higher temporal resolution is permitted (Cho et al., 2020). This temporal resolution was taken advantage of to try to not only identify proteins interacting with *Tg*EDP, but also make the distinction between those which interact transiently and those with which it might form a potentially more stable complex.

In order to both confirm the correct integration of the TurboID tag within the parasite genome, as well as test this temporal resolution, IFAs using streptavidin-coupled antibodies were done. Parasites were used to infect HFF monolayers, and biotin was added for different lengths of time; 30 minutes to capture the stable interactions, and 6 hours to try to capture the transient interactions. The results were as shown below (Figure 3.20A). When biotin was added for 30 minutes, a clear fluorescent signal was seen predominantly at the Golgi body. This clear signal also included signal at the apicoplast, an organelle which is known to have naturally biotinylated proteins (Chen et al., 2015). To exclude that the signal observed around the Golgi is not primarily originating from the apicoplast, co-staining of the apicoplast was done using anti-G2-Trx antibodies, and Δku80 DiCre parasites were used as negative control. As expected, the apicoplast was seen to overlap with fluorescence signal showing biotinylation, but was mostly seen to lie adjacent to the areas of highest intensity. When biotin was added for 6 hours, the fluorescent signal was, however, seen to form a ‘cloud’ around the Golgi region and apicoplast. In addition to this ‘cloud’ of signal seen around the Golgi, signal was also always observed at the periphery and basal end of

the parasites, and occasionally along the connections between the parasites in the parasitophorous vacuole.

Upon confirmation that the gene of interest was correctly endogenously tagged with the TurboID construct, triplicate samples were prepared wherein parasites were used to infect flasks of HFFs, and biotin was added for the abovementioned lengths of time, that is, 30 minutes and 6 hours. The parasites were collected, lysed, and the biotinylated proteins pulled down using streptavidin-coated magnetic beads. In order to confirm that the pulldown was successful, a percentage of the beads were removed from the final collection volume and run on a Western blot (Figure 3.20B). Along with these bead samples, other samples loaded onto the gel included parasite samples which were treated or not treated with biotin, as well as the post-lysis pellets from the samples which were used for the pulldown. Parasite samples were loaded as an input control in order to confirm that the biotinylation was successful, whereas the post-lysis pellets were loaded in order to confirm that the parasite lysis was efficient and no major losses of biotinylated proteins were experienced.

As can be seen in the below Figure 3.20B, biotinylated proteins were pulled down in all samples irrespective of the strain or the presence of biotin. This was due to the presence of biotinylated proteins in the apicoplast as well as the presence of biotin in supplemented DMEM. Unfortunately, there were some inevitable losses incurred by inefficient lysis as can be seen from the presence of biotinylated proteins still present in the post-lysis pellets. However, since the amount of proteins loaded from the post-lysis pellets represents the entire pellet, versus only 3.5% of the beads to be sent for mass spectrometry, these losses were not considered grievous.

The samples were then submitted for mass spectrometric analysis at the LMU Biomedical Centre, Martinsried. Here, the samples were digested, purified, fragmented, and the protein masses were determined. The data obtained was mapped to the Uniprot protein database, and the protein quantities were determined. The data was then plotted using Perseus (Tyanova et al., 2016). As seen from the PCA plots (Figure 3.21), all wildtype (Δku80 DiCre) replicates regardless of biotinylation time were seen to cluster together. On the other hand, as expected given the rough indication obtained from the Western blots, the samples prepared for TGGT1_301410-TurboID were seen to cluster distinctly separate. The replicates for each timepoint clustered together.

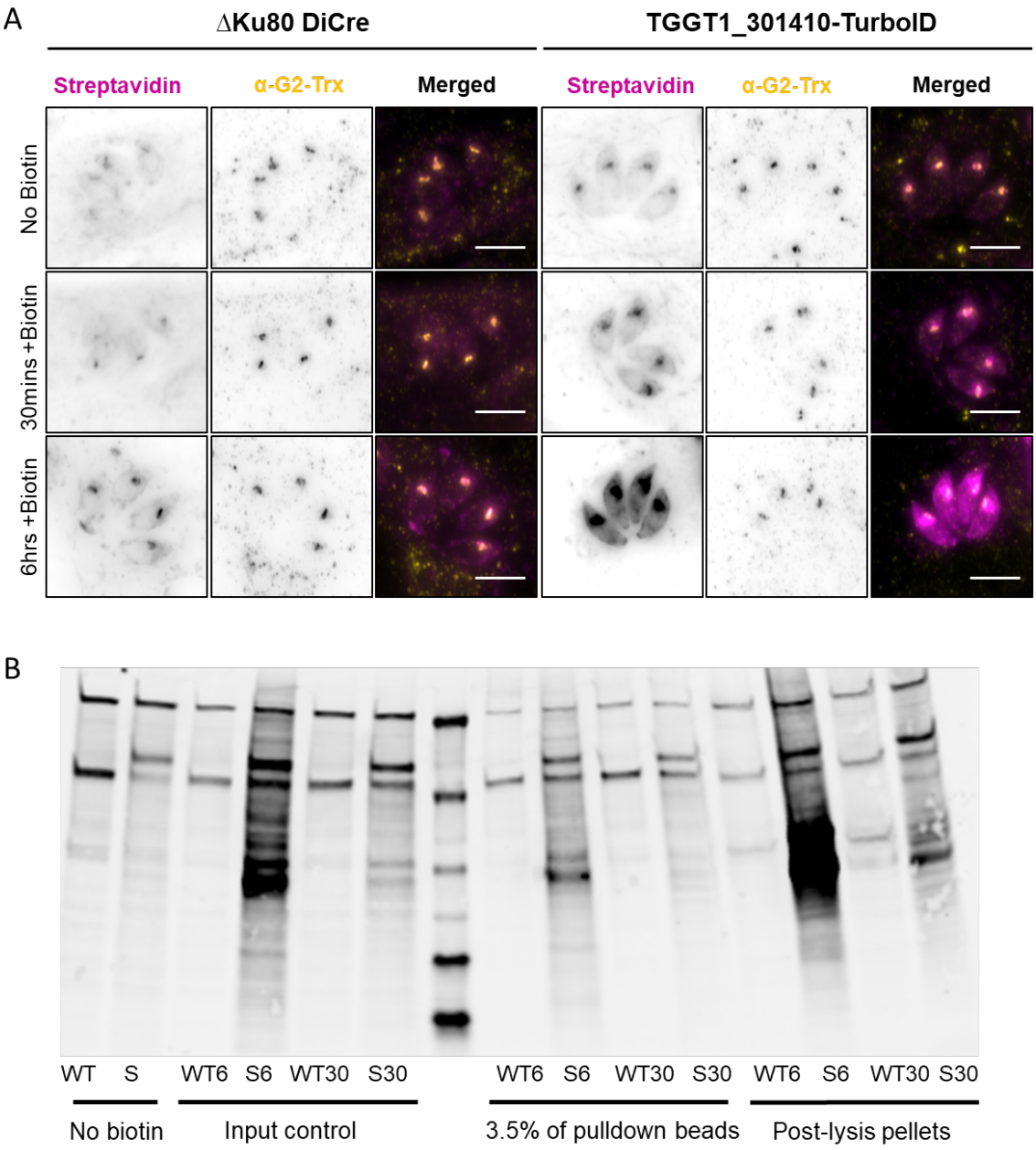

Figure 3.20 – Biotinylated proteins in parasites expressing TurboID-tagged *Tg*EDP

(**A**) Addition of 150 µM biotin to parasites expressing Turbo-ID tagged TGGT1_301410 resulted in the biotinylation of all proteins which come in proximity to the TurboID construct. Immunofluorescence assays using fluorescently conjugated streptavidin show the localisation of these biotinylated proteins (in magenta). Biotinylation for different lengths of time show different intensities and localisations of biotinylated proteins. Naturally occurring biotinylated proteins within the apicoplast are also labelled with the fluorescently conjugated streptavidin. The apicoplast was co-labelled with antibodies against G2-Trx (in yellow). The parental strain, ΔKu80 DiCre, was used as a negative control and only shows naturally occurring biotinylated proteins within the apicoplast. All images are normalised to the parental no-biotin control

image. Scale bars are 5µm. (**B**) ΔKu80 DiCre parasites (wildtype, labelled as 'WT') and mutant parasites (expressing TGGT1_301410-TurboID, labelled as 'S') were incubated in the presence or absence of 150 µM biotin for 30 minutes (WT30 / S30) or 6 hours (WT6 / S6), after which they were harvested. The parasites were then lysed and biotinylated proteins collected via streptavidin-coupled magnetic beads. Western blots were run using 1) "no biotin" control parasites, 2) pre-lysis control parasites ("Input control"), 3) "post-lysis" control pellets, and 4) 3.5% of the pulldown beads collected. Fluorescently conjugated streptavidin was used to label the biotinylated proteins on the blot.

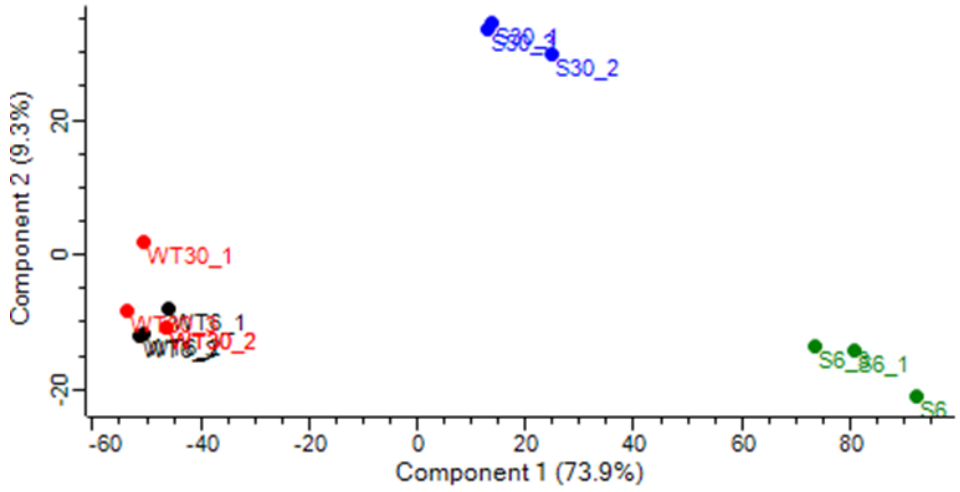

Figure 3.21 – PCA plot showing the clustering for all TurboID sample replicates
All six wildtype replicates (in black and red) cluster together irrespective of the length of incubation time in the presence of biotin. The TurboID sample replicates form separate clusters depending on the length of biotinylation time (30-minute sample shown in blue, 6-hour sample shown in green).

Potential interactors

In order to identify proteins which were significantly enriched relative to the wildtype, volcano plots were prepared using Perseus (Tyanova et al., 2016). Significance was calculated using the t-test, with FDR value set at 0.05 and S0 value of 0.1.

To narrow down the list of candidates and find which ones were most likely to be forming a stable complex with *Tg*EDP, thus anchoring it to vesicles, the 30-minute timepoint dataset was analysed (Figure 3.22A). For this, a set of criteria were established. Firstly, since *Tg*EDP is essential, it was hypothesized that its interactors might similarly be essential.

Although this might not necessarily be the case, this hypothesis was used to facilitate the narrowing down of the extensive list of protein candidates. Therefore, all proteins with a phenotypic score of -1 or more were excluded from the list of potential stable interactors (Sidik et al., 2016). Next, since it was expected that stable interactors would localise to the same sub-cellular compartment as *Tg*EDP, hyperLOPIT was used (Barylyuk et al., 2020). Here, proteins which were observed to cluster far away from *Tg*EDP were excluded. The predicted domains of the candidate proteins were then checked on ToxoDB (Gajria et al., 2008), as well as InterPro (Blum et al., 2021), in order to eliminate proteins which are predicted unlikely to be involved with *Tg*EDP. A large proportion of the proteins which were eliminated at this stage seemed to have predicted RNA-binding domains. The enrichment of such proteins was expected given the cytoplasmic localisation of *Tg*EDP within the cell. In addition to this, proteins with a known function were also excluded at this stage, including proteins like MyoF, DrpB, and many IMC proteins, since their function has already been described in the literature (Breinich et al., 2009; Carmeille et al., 2021) and are therefore unlikely to be anchoring *Tg*EDP to vesicles. This strategy of narrowing down the candidate proteins resulted in a list of proteins which can be found in the appendix section. From this list it was concluded that the most likely interactor acting as anchor for *Tg*EDP was the protein TGGT1_244290, a subunit of the AP-4 complex. This candidate is currently being endogenously tagged and floxed for further investigations, and will be discussed later.

As would be expected, all hits obtained for the 30-minute biotinylation experiment were also enriched during the 6-hour biotinylation experiment (Figure 3.22B,D). In order to find the proteins not present during the 30-minute experiment, and therefore identify the likely transient interactors, the data was normalised and a volcano plot prepared (Figure 3.22C). Similar selection criteria as before were applied in the search for transient interactors; the proteins were selected based on predicted essentiality and hyperLOPIT localisation. Of the three proteins seen to be the most enriched, two were seen to be non-essential. The other protein, on the other hand, was profilin. In addition to this, it was also interesting to see K13 come up as a significantly enriched hit (Koreny et al., 2022). K13 is present at the micropore and is likely the site of endocytosis. This last result suggested that the vesicles *Tg*EDP associates with not only travel to the site of endocytosis where K13 is present, but also come in close enough proximity for K13 to be biotinylated. A number of other interesting proteins were also identified in the datasets. Some were noted to be actin-related (MyoF, formin2, and profilin), while others were noted to be related to the trafficking system (SortLR, DrpB, clathrin heavy and light chain) (Figure 3.22). A protein annotated as being a “Xin

actin-binding repeat-containing protein" was also identified (TGGT1_213392). Since *Tg*EDP was identified from a screen designed to find actin-binding proteins, this candidate was endogenously tagged, and will be discussed in Chapter 4. Its localisation data can be found in the appendix (Figure A.3).

Figure 3.22 – Biotinylated proteins identified by mass-spectrometry (next page) (**A**) shows the difference in protein hits between wildtype and TGGT1_301410-TurboID sample following 30 minutes of biotinylation, whereas (**B**) shows the difference between wildtype and TurboID samples following 6 hours of biotinylation. As expected from both the IFA and the western blot, (B) had a greater number of hits. The bait protein (*Tg*EDP, 'B' in green) was significantly enriched for both timepoints. (**C**) shows the total number of proteins enriched during the 6-hour experiment vs the 30-minute experiment after normalisation of protein abundance. Proteins of particular interest in panels (A) – (C) are numerated and listed in the table in (E). (**D**) All proteins identified at the 30-minute timepoint were also identified at the 6-hour timepoint. Proteins of high interest identified included those typically associated with the Golgi and post-Golgi compartments (in blue), actin-binding proteins (in pink), proteins associated with parasite's micropore (in green), and an uncharacterised AP4 subunit (in orange). (**E**) lists a number of proteins which were of particular interest due to their association with the Golgi compartments, with the acto-myosin system, or with the micropore. An uncharacterised protein (TGGT1_213392) was also listed and will be discussed later.

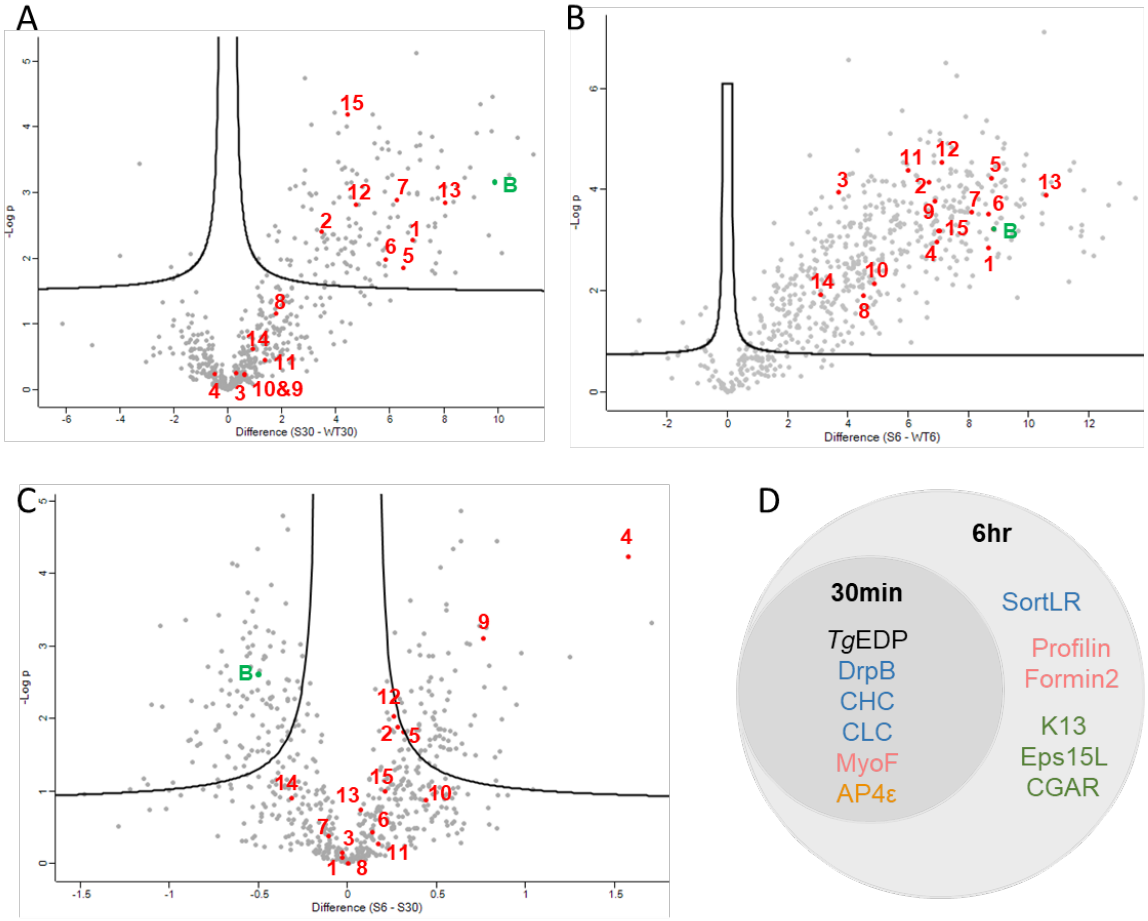

E

Label	Accession number	Protein
1	TGGT1_244290	Adaptor related protein (AP4ε subunit)
2	TGGT1_278870	MyoF
3	TGGT1_206580	Formin2
4	TGGT1_293690	Profilin
5	TGGT1_321620	DrpB
6	TGGT1_290950	Clathrin heavy chain
7	TGGT1_213030	Clathrin light chain
8	TGGT1_290160	SortLR
9	TGGT1_262150	K13
10	TGGT1_227800	EF hand domain-containing protein (Eps15L)
11	TGGT1_297520	proteophosphoglycan PPG1 (CGAR)
12	TGGT1_273370	putative coatomer gamma 2-subunit protein
13	TGGT1_309220	GTPase activating protein for Arf protein
14	TGGT1_235020	Putative COPI protein
15	TGGT1_213392	surface antigen repeat-containing protein
B	TGGT1_301410	Bait – *Tg*EDP

Figure 3.22 – Biotinylated proteins identified by mass-spectrometry

The acto-myosin system; F-actin, Formin2, and MyoF

Since *Tg*EDP was identified in a screen designed to find novel actin-related proteins, its interaction with actin was investigated. This necessitated the insertion of the actin Chromobody-emerald into the parasite strains where *Tg*EDP was already tagged and floxed. Replacement of the UPRT locus with the Chromobody-emerald construct was done as explained in Figure 2.2. The double strand break was induced within the first exon of the UPRT locus, and primers with homology arms were designed in such a way as to still retain the endogenous promoter and 3' UTR. The repair template was generated by PCR amplification from the plasmid used in Periz et al., (2017), this amplification done in such a way as to also include the plasmid promoter and 3' UTR in the PCR product. The signal observed, although weaker than that observed in the library parasites, was consistent with what has been previously reported (Periz et al., 2017).

Live imaging showed that *Tg*EDP is trafficked along actin filaments. These vesicles were not only observed to move along actin filaments around the Golgi region (Figure 3.23A), but also along the periphery and towards the basal end of the parasites (Figure 3.23B).

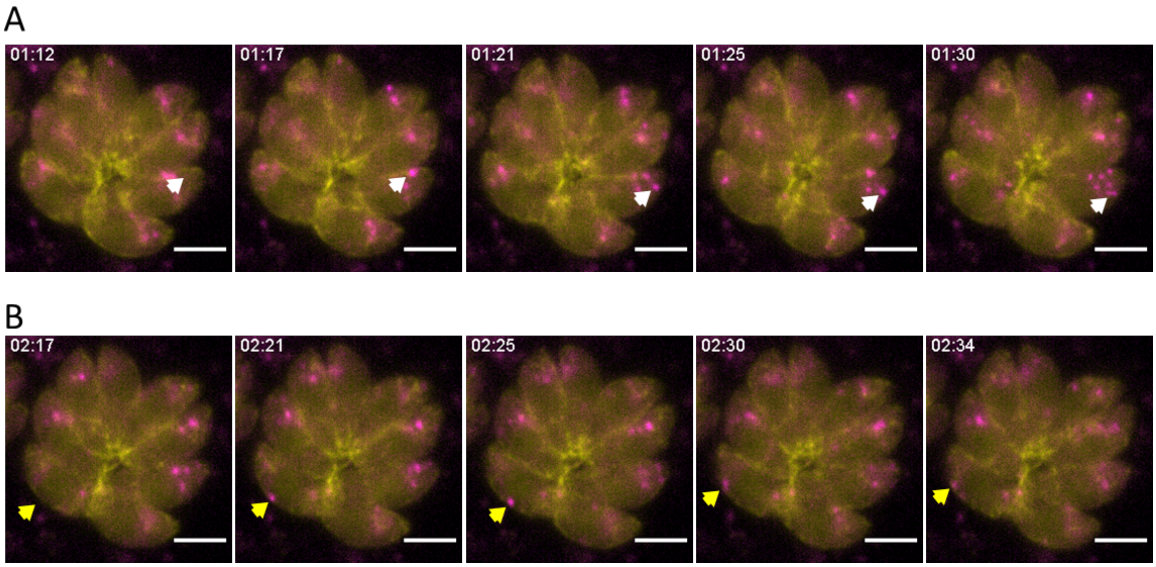

Figure 3.23 – *Tg*EDP moves along actin filaments
In live movies, *Tg*EDP (in magenta) was seen colocalising and moving along actin filaments (marked with the Chromobody-emerald in yellow). (**A**) shows still images taken from the live movies wherein the white arrow indicates vesicles which are moving along actin filaments close to the actin nucleation centre. (**B**) The yellow arrow points towards vesicles which are moving along actin filaments along the periphery of the parasites. The live movies were taken at a rate of 0.233 frames per second (fps). All scale bars are 5 µm.

Three actin-related proteins were enriched in the TurboID data; MyoF, formin2, and profilin. Since both MyoF and formin2 have been documented to exhibit specific knockout phenotypes similar to that of *Tg*EDP, but knockout of profilin showed a more general negative effect, the former two proteins were investigated further.

Upon knockout of *Tg*EDP, MyoF's localisation was seen to be negatively affected. Whereas its typical wildtype localisation is concentrated at the Golgi region and around the periphery of the parasites, its signal became punctate and distributed throughout the parasites (Figure 3.24A). The number of vacuoles exhibiting this phenotype was seen to be significantly higher than wildtype after 48 hours post-induction (Figure 3.24B). In contrast to this, no effect on formin2 localisation was observed upon deletion of *Tg*EDP (Figure 3.24C). Validation of the F-actin phenotype observed in the splitCas9 screen was also done (Figure 3.24D). Here, the actin filaments formed seem to be short and more concentrated towards the basal ends of the parasites, with very few filaments present at the formin2 nucleation centre. The nature of the altered actin filament dynamics is still under investigation. However, given that actin was not enriched in the TurboID data, it is unlikely to be directly interacting with *Tg*EDP. Since formin2 localisation was not affected upon *Tg*EDP knockout, the lack of actin filaments at the nucleation centre upon knockout could therefore be a downstream effect of MyoF aggregation.

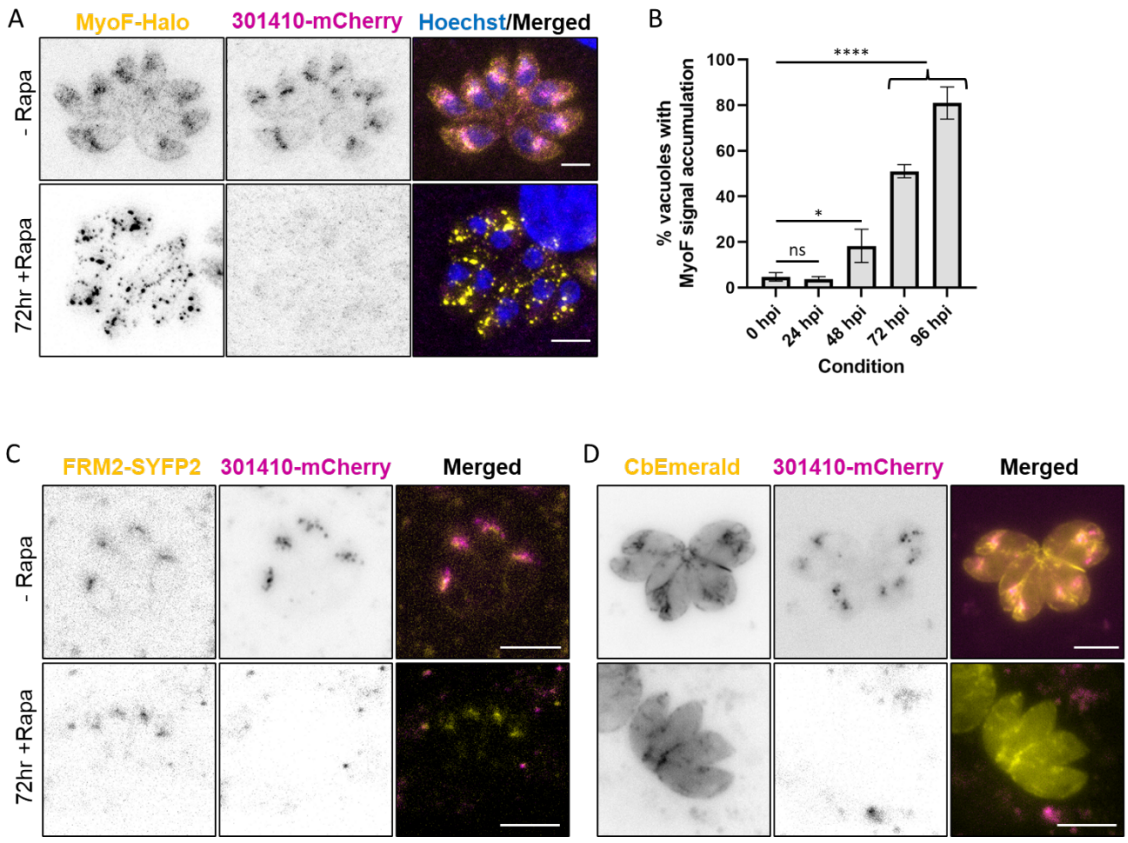

Figure 3.24 – Knockout of *Tg*EDP impacts MyoF and actin filaments but not formin2

(**A**) In wildtype parasites, MyoF is seen to localise around the periphery of the cells and near the actin nucleation centre proximal to the Golgi body. Upon knockout of *Tg*EDP (in magenta), MyoF (in yellow) was seen to aggregate within the parasites. This was observed in both live as well as fixed parasites. MyoF and TGGT1_301410 images were taken with STED while the nuclei (labelled with Hoechst) were taken with the confocal setting. Scale bars are 3 µm. (**B**) The number of parasitophorous vacuoles with altered MyoF localisation was seen to be significantly higher than that in wildtype parasites starting at 48 hours post-induction (hpi) with 50 nM rapamycin. The assay was done thrice, with a minimum of 100 vacuoles quantified per condition per replicate. Data is plotted as mean ± s.d. One-way ANOVA with Tukey's multiple comparison test was applied, with P values being represented as follows: ns = >0.05; * = 0.01 – 0.05; **** = < 0.0001. (**C**) Formin2, typical localising at the Golgi region, seemed unaffected upon knockout of *Tg*EDP. Scale bars in (C) and (D) are 5 µm. (**D**) Knockout of *Tg*EDP (in magenta) resulted in a change in actin filament formation (in yellow). In wildtype parasites, the filaments primarily localise at the actin polymerisation centre near the Golgi body, and connect the parasites within the parasitophorous vacuole at the basal end. Upon knockout of *Tg*EDP, no actin filaments were observed at the actin nucleation centre, and the filaments connecting the parasites appeared more prominent. The dynamics of these filaments in comparison to those in wildtype parasites is still under investigation. Scale bars are 5 µm.

Given that *Tg*EDP moves along actin filaments, and the deletion of formin2 results in the absence of actin filaments at the nucleation centre near the Golgi, the effect of *Tg*EDP upon knockout of formin2 was also investigated. *Tg*EDP was therefore Halo-tagged in a parasite strain wherein formin2 is SYFP2-tagged and floxed (from Stortz et al., 2019). Surprisingly, no change in *Tg*EDP localisation was observed (Figure 3.25). The effect of MyoD knockdown on *Tg*EDP is also currently under investigation and given its documented function, is expected to result in *Tg*EDP mislocalisation.

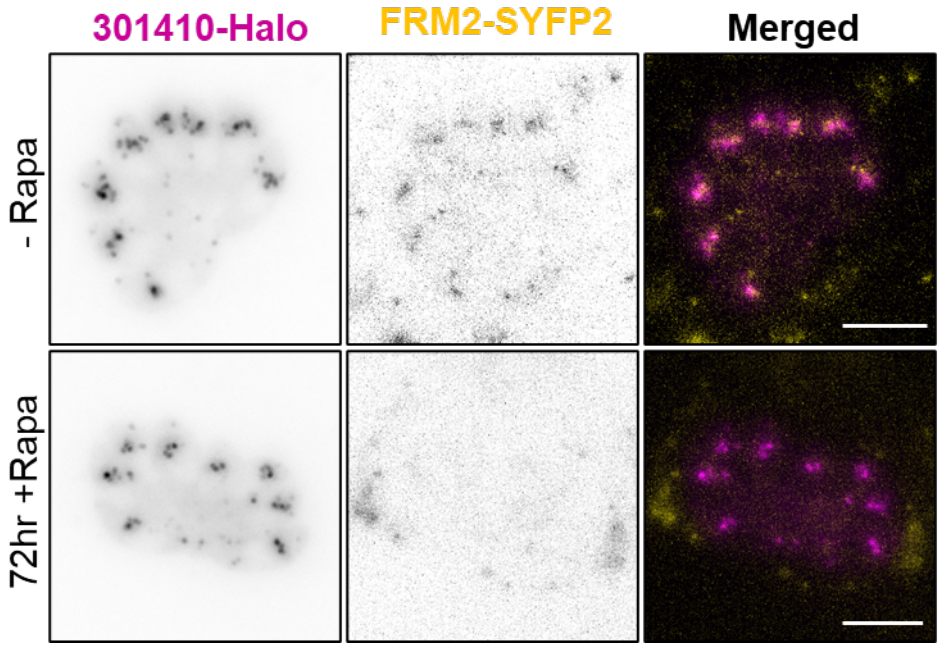

Figure 3.25 – Knockout of formin2 does not affect *Tg*EDP (TGGT1_301410) localisation
Live imaging of formin2 knockout mutant showed no change in *Tg*EDP localisation. *Tg*EDP was endogenously tagged with Halo (in magenta) in the parasite strain used in Stortz et al., (2019) wherein formin2 was endogenously tagged with SYFP2 and floxed (in yellow). Scale bars are 5µm.

Chapter 4. Discussion

The aim of the phenotypic screen was to identify actin regulatory proteins using a novel conditional splitCas9 system that had been previously established in the Meissner lab. Using an indicator strain that allows detection of actin-related phenotypes (actin dynamics, apicoplast maintenance and egress), three proteins were put forward for detailed analysis. While two candidates have been already published (Li et al., 2022), within this thesis the detailed analysis of TGGT1_301410 was performed. Therefore, this discussion will first summarise the phenotypic screen, its applications and results, after which it will discuss the function of TGGT1_301410 in detail.

4.1. The actin and egress phenotypic screens

Actin, as in other eukaryotic organisms, is an essential protein in *Toxoplasma*. Its essentiality has been well studied and the impact of its absence well documented. It has been demonstrated that it is crucial for practically almost every step of the parasite's lytic cycle, including gliding, and both invasion of the parasites into host cells, and later on, egress out of said host cells (Egarter et al., 2014; Whitelaw et al., 2017). While daughter cell assembly during endodyogeny is unaffected in the absence of actin, synchronous division and the final steps of replication, such as closure of the basal pole and apicoplast division, are inhibited (Jacot et al., 2013; Stortz et al., 2019; Whitelaw et al., 2017). Actin has also been shown to be involved in inheritance of micronemes from mother to daughter cells, and trafficking of secretory vesicles including micronemes, and dense granules (Heaslip et al., 2016; Periz et al., 2019). Structural integrity of the Golgi body was also seen to be correlated to actin, with this being dependent on the actin-binding protein myosin F (Carmeille et al., 2021). All of these investigations into actin, actin-binding proteins, and their function could not have been possible without the aid of the actin Chromobody-emerald, established by Dr. Javier Periz (Periz et al., 2017).

Bearing the essentiality of actin in mind, it therefore comes as a great surprise that the number of actin-binding proteins in apicomplexans appears to be significantly reduced when compared to other eukaryotic organisms. While mammalian cells are known to have up to two hundred actin binding proteins, apicomplexans have around twenty that can be identified based on homology criteria (Baum et al., 2006). This was where the phenotypic

screens came in, since we speculated that apicomplexans evolved their own, unique set of actin binding proteins.

4.1.1. The setup of the screens

The primary aim of the phenotypic screens was initially to identify novel actin regulatory proteins. In order to achieve this aim, a reporter strain was used wherein the actin filaments were marked using the Chromobody-emerald, and the apicoplast was marked by inserting an extra copy of an apicoplast protein, FNR, tagged with RFP (Periz et al., 2017; Striepen et al., 2000).

Since the screen carried out was not a genome-wide screen but rather a curated one, the genes targeted were selected to fit specific criteria. One of the criteria for choosing the genes was their predicted essentiality (Sidik et al., 2016). This criterion was set because since actin itself is critical, it was hypothesised that any actin-modulating proteins present would likewise also be essential. In addition to this criterion, the genes included in the screen were also chosen based on their prediction to not possess any signal peptides, with the idea that they would be more likely to function within the cytosol of the cell, where actin resides. The genes to be targeted were also chosen based on their annotation as being absent in other eukaryotes, but conserved within apicomplexans. Based on these three criteria, a list of 320 genes were chosen to be included in the library. Other genes which were also included in the library were GAP40 and profilin. These were used as positive controls for a ‘nuclear/replication’ phenotype and ‘F-actin’ phenotype respectively (Harding et al., 2016; Plattner et al., 2008).

In addition to choosing the genes to be targeted by the phenotypic screen and generating the sgRNAs to target them, it was necessary to establish a system wherein this curated library of sgRNAs could be used within the context of a phenotypic screen. Given that only genes predicted to be essential were to be included in the curated library, an inherent necessity was for the knockout-generating system to be conditional. By using a conditional system, this would prevent the loss of the strains from happening immediately upon integration and expression of the sgRNA constructs. This conditional system would therefore allow proper downstream imaging and analysis of the generated knockout mutants. For this reason, this screen made use of a splitCas9 system (Zetsche et al., 2015)

established within *Toxoplasma* by Dr. Johannes Stortz, a previous PhD student within the Meissner group (Li et al., 2022).

4.1.2. Outcome of the actin screen

Following the insertion of the sgRNA library into the recipient parasites, clonal knockout parasites were generated via the addition of rapamycin, resulting in the reconstitution of an active Cas9 enzyme, and subsequent induction of double-strand breaks. The mutants generated were imaged (Figure 3.2) and the resulting data analysed by myself and another independent researcher within the Meissner group, Dr. Elena Jimenez Ruiz. The phenotypes observed were classified into five main types; 'no phenotype', 'F-actin phenotype', 'apicoplast phenotype', 'egress phenotype', and 'nuclear/replication phenotype' (Figure 3.2). These phenotypes were also graded according to their perceived strength (Table A.1).

A number of clones were selected based on their severely aberrant phenotype. These, however, turned out to be a result of multiple integrations of the sgRNA plasmid into the parasite genome, thus leading to multiple gene knockouts within the same parasite (Figure 3.3). These were not taken into consideration during follow-up analyses.

In addition to the potential candidate genes selected, the positive controls included in the library were also successfully identified (Figure 3.4). GAP40 was picked out for having a 'nuclear/replication phenotype', whereas profilin was picked out for having an 'F-actin phenotype', both of which being consistent with what is already published in literature (Harding et al., 2016; Plattner et al., 2008). The fact that the positive controls used in the screen were correctly identified was a clear indication that the screen served its purposed in being able to properly identify specific phenotypes and their associated proteins.

While none of the mutants were noted as exhibiting a striking F-actin phenotype, a list of candidates was obtained where F-actin appeared to have different localisation or dynamics compared to control parasites. A total of 13 out of 16 genes with the strongest 'F-actin' and/or 'apicoplast phenotypes' were successfully endogenously tagged in order to be able to narrow down the candidate list and facilitate future characterisation. Interestingly, 2 were observed to localise at the perinuclear region, close to the actin nucleation centre. Due to this localisation, and its perceived knockout phenotype, TGGT1_301410 was picked as the

candidate to be followed up, and the characterization of this gene will be discussed later. Of the 13 tagged proteins, 1 was observed to localise to the micronemes, 6 to the nucleus, and 4 to the mitochondria.

Since many of the candidates identified from the screen have a localisation that seems to be rather unrelated to actin, it is possible that these are not direct regulators of actin, and that the effect visualised in the screen may have been a side-effect of interfering with the function of other organelles, such as mitochondria that is known to also lead to collapse of the parasitophorous vacuole. Similarly, disruption of nuclear proteins might be indirectly causing differences in F-actin dynamics due to changes in gene expression or triggering a more general stress response. That said, in other eukaryotes, actin has been observed to interact with the mitochondria (Schiavon et al., 2020) and recent research demonstrates crucial functions of actin in the nucleus, where it is an important co-factor for transcription factors or involved in RNA splicing (Kapoor et al., 2013; Parisis et al., 2017; Viita et al., 2019; Zhang et al., 2019). However, our phenotypic analysis of parasites depleted for F-actin did thus far not identify any function of F-actin in these processes in *Toxoplasma gondii.* It was for this reason, that none of the mitochondrial or nuclear candidates were chosen for in-depth characterization within this study. Therefore, the candidates localised close to the Golgi, where the known actin nucleator formin2 resides, were prioritised.

Despite nuclear and mitochondrial candidates not being followed up during this project, their investigation would still make an interesting research avenue. A colleague in the Meissner lab, Matthew Gow, has recently generated a plasmid which expresses a nuclear-targeted Chromobody-emerald, and attempted to investigate the possibility of nuclear F-actin. This has already been done with successful results in mammalian cells (Abdellatif et al., 2019; Plessner et al., 2015). If this investigation into *Toxoplasma* nuclear F-actin were to be successful, the nuclear candidate proteins identified in this screen could be revisited by future researchers. It is, however, important to bear in mind that the actin phenotype observed could also be based on a downstream effect. If a nuclear protein were to, for example, influence gene expression of already known actin regulators, this would also result in an ‘F-actin’ phenotype. In such cases, one would benefit from also investigating whether these nuclear candidates, particularly the predicted chromatin remodeler TGGT1_229460, bind DNA.

4.1.3. Outcome of the egress screen

In addition to the phenotypic screen designed to identify novel actin regulatory proteins, a screen which set out to identify novel egress factors was also carried out in parallel by Li Wei. This was done using the same curated library of sgRNAs. The same 72-hour post-induction images obtained during the actin screen were used to identify potential egress phenotypes (Figure 3.2). These images were screened for vacuoles which seemed to have an egress phenotype, that is, they did not lyse the host cells within this time frame. The identity of these mutants was determined via sequencing of the sgRNA, after which the results observed in the screen images were validated once more using the sCas9 clones and various egress inducers. After this validation, the candidates were chosen and characterisation was done. One of the candidates chosen, Signalling Linking Factor (SLF) localises to the apical cap and to the residual body, and has been hypothesised to be a component of the signalling platform which has already been described in the literature (Bisio et al., 2019; Ye et al., 2022). Upon knockout of this candidate, the parasites do not disassemble the intravacuolar network, do not lyse the parasitophorous vacuole membrane, do not initiate motility, and therefore fail to egress (Li et al., 2022). The other candidate, Conoid Gliding Protein (CGP) localises to the conoid. Upon its knockout, the parasites are unable to initiate motility for egress despite disassembling the intravacuolar network and lysing the parasitophorous vacuole membrane (Li et al., 2022). Further characterisation of these proteins is currently ongoing.

4.1.4. Limitations of the screen and recommendations for future screens

As with all genetic screens, not all genes involved in a certain process can be identified and, even worse, not all candidates identified are truly involved in the pathway/mechanism for which the screen was designed. This appears especially true for screens aiming to identify new factors involved in F-actin regulation, since this protein can be influenced by many pathways. It is therefore important to prioritise candidates efficiently, based on their location in the cell and the observed phenotype. Here, in order to prioritise the candidates, the severity of the phenotype observed in the screen was first assessed. Those exhibiting the strongest phenotypes were then identified and subsequently endogenously tagged in order to determine to which subcellular compartment they localise. Based on this, the final list of candidates to be followed up was picked. These were then investigated using an alternative

conditional knockout system, thus validating the phenotype obtained from the screen and further enabling characterization. This strategy resulted in the successful identification of two proteins which are critical for egress, and another whose dynamics are dependent on the acto-myosin system.

An alternative approach to merge both a knockdown screening process as well as the process of localising the candidates of interest would be to employ a screen such as that done by Smith et al., (2022). In this study, the genes being targeted were endogenously tagged with a fluorescent marker as well as the auxin-inducible degron construct (AID). While this approach is more efficient in some regards, the drawback is that one might experience difficulty with successfully functionally tagging some proteins. In contrast to this, since our screen based on the splitCas9 acts directly on the genome, there is no limit to the identity and number of genes which can be targeted. Additionally, a splitCas9-based screen also carries no risks of incomplete protein knockdowns, and issues with accessibility to the degradation machinery.

Unfortunately, the main limitation of a splitCas9-based screen, and indeed of any screen using CRISPR/Cas9, is the side-effect wherein some parasites exhibit aberrant nuclear morphology. While it did not hinder our actin and egress screens in any way, it is important not to lose sight of this unintentional artefact and account for it. The GAP40 positive control was easily identified as a nuclear/replication phenotype. This shows that even though the artefact also relates to nuclear deformities, it is relatively easy to account for, and true nuclear/replication phenotypes can still be identified by taking into consideration total number of vacuoles affected. A true nuclear phenotype would likely be observed in more than 70% of parasite vacuoles (Li et al., 2022), whereas a solely (non-specific) aberrant nuclear phenotype affects a much lower percentage (between 20 and 50%), this percentage having been observationally noted to vary depending on the gene being knockout. Furthermore, automated imaging analysis could also be taken advantage of in order to both account for the aberrant nuclear side-effect as well as identify the desired phenotypes (Fisch et al., 2019).

Due to the success of our screen and its versatile design, future screens are currently in the pipeline. By using different recipient parasite strains wherein different cell compartments are labelled, one would be able to adapt the sgRNA library to their specific needs depending on the research question. In fact, in addition to the F-actin and egress screens mentioned in this thesis, another screen has also been carried out using a recipient strain wherein both

actin as well as alpha-tubulin were labelled. This screen has also identified a number of interesting proteins which are currently being followed up. Recipient strains where the IMC, mitochondria, and micronemes are labelled have also been created (Figure 4.1).

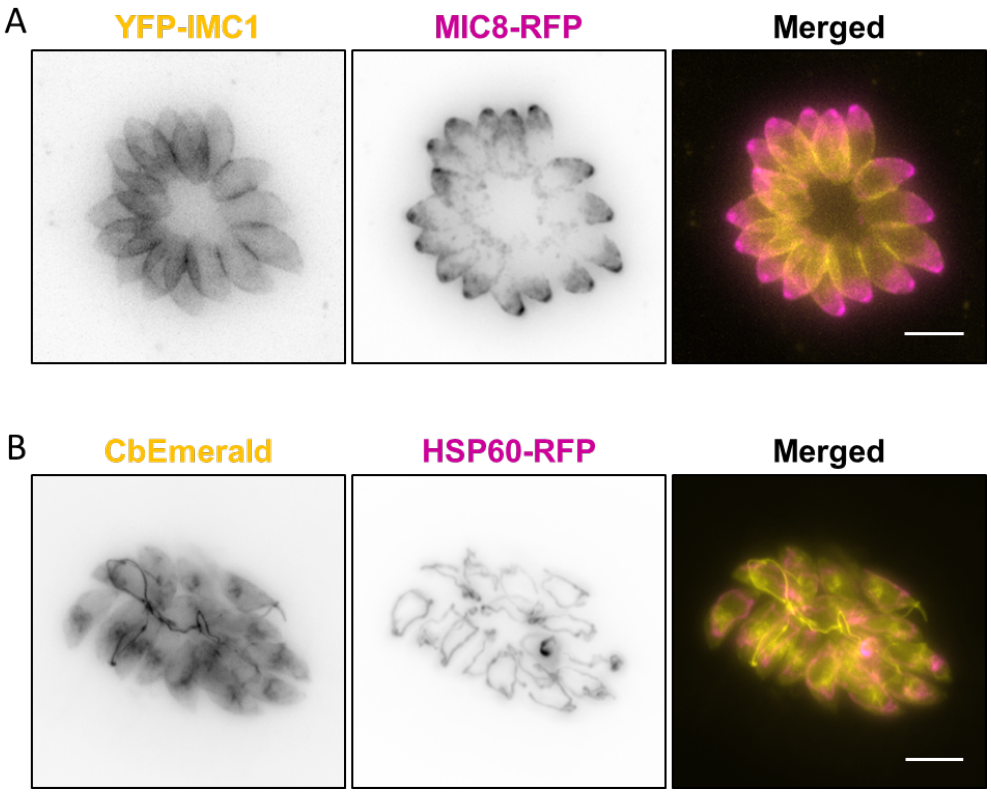

Figure 4.1 – Strains for future screens

New strains have been generated for future screens. (**A**) shows the strain wherein extra copies of IMC1 tagged with YFP and MIC8 tagged with RFP were randomly integrated into the parasite genome, the former labelling the IMC and the latter marking the micronemes. (**B**) shows a parasite strain wherein the construct for the Chromobody-emerald, and an extra copy of HSP60 tagged with RFP were integrated into the genome, the former marking the actin filaments and the latter marking the mitochondria. Scale bars are 5 µm.

*4.2. TGGT1_301410 – ENTH Domain-containing Protein (Tg*EDP*)*

4.2.1. Subcellular localisation of TgEDP

*Tg*EDP was chosen as the protein of interest based on its localisation in proximity to the actin nucleation centre. This protein is a 1033 amino acid protein that, in agreement with its localisation, seems to have a sole ENTH domain predicted to be involved in endocytosis and cytoskeletal machinery (De Camilli et al., 2002). In addition to this localisation, live imaging shows that this protein is highly mobile within the cell, both near the actin nucleation centre but also throughout the entire parasite, reaching the periphery and as far back as the residual body. This pattern of movement suggests that this protein might be located on vesicles which travel throughout the parasite. Colocalisation analyses were done using various Golgi body markers. As a marker for the *cis*-Golgi, the compartment closest to the ER, GRASP-RFP was used (Pfluger et al., 2005). In colocalisation analysis it was evident that this compartment and that occupied by the protein of interest are distinct from each other. As a marker for the *trans*-Golgi compartment, SortLR was Halo-tagged (Sloves et al., 2012). Here, signals obtained were seen to be in closer proximity. However, confocal imaging showed that while these compartments are close, there is no perfect colocalisation. Further colocalisation studies using other post-Golgi markers, including syntaxin6 (Jackson et al., 2013), DrpB (Breinich et al., 2009), and ProM2AP (Harper et al., 2006), all showed the same. In order to definitively confirm that *Tg*EDP is a resident of the Golgi body, images were taken following the addition of Brefeldin A to the parasites. Brefeldin A is a drug that inhibits the flow of material from the ER to the Golgi body (Helms & Rothman, 1992; Sciaky et al., 1997). Since the retrograde flow of material from the Golgi to the ER is not affected, addition of this drug essentially collapses the Golgi body back into the ER. Following said addition of Brefeldin A, relocalisation of *Tg*EDP to the ER was observed, thus confirming that it localises to the Golgi body.

Since the protein's sole predicted domain suggests a possible involvement in cytoskeletal machinery, an inquiry into its exact location with regards to the vesicle cell membrane was necessary. Use of a construct expressing a cytoplasmic GFP-nanobody fused to a Halo-tag was made. The GFP-nanobody targeted to the cytoplasm was seen to colocalise exactly with the SYFP2-tagged protein of interest, thus confirming that the C-terminal SYFP2-tag also localised to the cytoplasm. Since the protein of interest does not have a predicted

transmembrane domain, this implied that the entire protein associates with Golgi and derived vesicles within the cytoplasm.

The pattern of localisation of *Tg*EDP described above suggested that this protein of interest might not inhabit a specific Golgi or post-Golgi compartment, but instead acts as an intermediate and travels between said compartments. Its presence outside of the vesicles with which it is associated further point towards a function in facilitating vesicle formation, fusion, or trafficking. The fact that it has also been observed at the residual body also hinted at a possible involvement in facilitating inter-parasite communication and/or recycling of maternal material (Periz et al., 2019).

4.2.2. Essentiality of TgEDP

*Tg*EDP was seen to be essential via plaque assay since its knockout did not result in the formation of plaques after 7 days of undisturbed incubation. This validated the low phenotypic score obtained from the genome-wide screen (Sidik et al., 2016). Assays done to investigate the different stages of the parasite's lytic cycle showed that at 48 hours post-induction of the knockout, invasion is not significantly affected. However, during the period of time between 48 and 72 hours, growth of the parasites started to become affected. These parasites, while seen to still be capable of normal division, were observed to have delayed growth and replication. This retardation in cell development could be an indicator of lack of sustenance, as has been suggested previously (Koreny et al., 2022).

4.2.3. TgEDP within the context of vesicular trafficking

As expected from the localisation, knockout of the protein of interest severely affected the Golgi body structure resulting in its swelling and vesiculation. Interestingly, this effect was limited to the *trans*-Golgi and the Golgi compartments marked by DrpB and syntaxin6. No effect was seen on the *cis*-Golgi or the endosome-like compartment marked by ProM2AP. Surprisingly, although the Golgi structure was observed to be compromised, this did not appear to affect trafficking of secretory proteins such as the micronemes, the rhoptries, and the dense granules. Other structures such as the IMC and the apicoplast were similarly observed to be largely unaffected following knockout of *Tg*EDP. All these results in combination show that while the structure of the Golgi body is severely affected by the

knockout of the protein of interest, the components mentioned are still able to be trafficked successfully.

In order to investigate other trafficking routes that are unrelated to secretion, CPL was used as a marker of the parasite's vacuolar compartment. As previously described, CPL is a VAC resident protease which has been seen to be non-essential in tachyzoites (Larson et al., 2009) but crucial in bradyzoites (Di Cristina et al., 2017). CPL has been observed to be involved in processing the precursors of the proteins M2AP, MIC3, and MIC6 (Parussini et al., 2010). Upon knockout of *Tg*EDP, CPL, which typically localises to vesicles diffused throughout the cytoplasm (Miranda et al., 2010; Parussini et al., 2010), was seen to accumulate to a more focused location. This accumulation of CPL was seen to peak around 48 hours after induction of the knockout, after which fragmentation starts to occur at around 72 hours. Quantifications showed that this CPL accumulation occurred temporally prior to the fragmentation of the Golgi body. In agreement with this, IFA images showed CPL accumulation in parasites with a still normal *trans*-Golgi. In these images, CPL signal colocalised with the *trans*-Golgi marker. This, therefore, indicated that accumulation of material trafficked to the VAC was the primary phenotype, and so it can be speculated that *Tg*EDP functions in the trafficking of vesicles from the *trans*-Golgi to the VAC.

4.2.4. TgEDP interactors

In an attempt to identify proteins interacting with *Tg*EDP, it was C-terminally tagged with TurboID. TurboID is a version of the BioID tag which has been modified in order to make biotinylation more efficient, thus allowing the reaction to take place within minutes (Branon et al., 2018; Cho et al., 2020). This efficiency was taken advantage of during this experiment by adding biotin to the parasites for two different lengths of time. Biotinylation for a 30-minute duration was done in order to detect protein interactors within the immediate vicinity, whereas biotinylation for 6 hours was done in order to find interactors of a more transient nature. Signal observed in IFAs showed biotinylation throughout the parasites, including the periphery, the basal end and intravacuolar network.

In order to narrow down the potential list of candidate proteins obtained from the TurboID experiments, the proteins chosen as likely interactors were chosen based on their predicted essentiality (Sidik et al., 2016) as well as their predicted domains (Blum et al., 2021; Gajria et al., 2008) and predicted subcellular localisation (Barylyuk et al., 2020). Mass

spectrometry data obtained from the 30-minute biotinylation experiment showed an enrichment in biotinylated Golgi body proteins. These proteins included DrpB (Breinich et al., 2009), clathrin heavy and light chain (Pieperhoff et al., 2013), and SortLR (Sloves et al., 2012), in good agreement with a function of *Tg*EDP at the Golgi. In addition to these proteins, a component of the AP-4 complex, as well as MyoF, were also identified as potential immediate interactors of *Tg*EDP. With regards to the 6-hour biotinylation experiment, three of the most notable proteins identified by mass spectrometry were K13, Eps15L and CGAR. These have been described as being components of the endocytosis machinery found at the periphery of the parasites, integrated into the IMC (Koreny et al., 2022). Two other notable proteins identified were profilin and formin2. The validity of all these proteins as legitimate interactors of *Tg*EDP are still under investigation and the results and implications of these finds will be discussed in the following sections.

4.2.5. TgEDP within the context of actin dynamics

Since the protein of interest was highlighted as a potential actin-binding candidate from the phenotypic screen, and a number of actin-binding proteins were obtained from the TurboID pulldown experiment, these were investigated. A copy of the construct coding for the actin Chromobody-emerald was integrated into the parasite genome via targetted replacement of the UPRT locus (Donald & Roos, 1995; Shen et al., 2014), while both MyoF and formin2 were tagged endogenously.

Knockout of *Tg*EDP was observed to result in abnormal aggregations of MyoF, while it did not seem to have any influence on formin2 localisation. An effect was also observed on actin filament dynamics upon deletion of *Tg*EDP. While this could have been a result of vacuolar collapse, it could also have been a downstream result of MyoF accumulation since the latter has also been shown to influence actin filament dynamics (Sladewski & Heaslip, 2022). Taken together, the data suggests that *Tg*EDP is not a direct actin or formin2 modulator. The reason for the effect on MyoF is, as of yet, undetermined. Since this effect was observed to occur downstream of the other phenotypes, there exists the possibility that it is an indirect downstream effect. In reverse experiments wherein formin2 was knocked out, *Tg*EDP localised similarly to that in wildtype conditions, but observationally appeared less dynamic during live imaging. Investigations into the changes in dynamics are ongoing. MyoF disruption would also be expected to have a negative impact on *Tg*EDP localisation.

The nature of this effect is, however, yet to be seen as investigations are similarly still ongoing.

Given the results obtained, it is unlikely that *Tg*EDP is a direct modulator of actin. It is also unlikely that *Tg*EDP interacts with actin directly since actin was not enriched in any of the TurboID datasets. That being said, the fact that MyoF, formin2, and profilin were all enriched in the TurboID datasets shows that *Tg*EDP does come in very close proximity to these proteins. Since previous data has shown Golgi and post-Golgi vesicles to be dependent on MyoF for their trafficking (Carmeille et al., 2021), it is not implausible to postulate that *Tg*EDP-associated vesicles are likewise dependent on MyoF. Since myosins generally move towards the plus end of actin filaments (Kneussel & Wagner, 2013), it is also an interesting hypothesis that formin2 might be building filaments 'in real time' as MyoF is carrying *Tg*EDP and associated vesicles to the sites of endocytosis. These hypotheses would need to be investigated in any future work.

In model eukaryotic cells, profilin has been shown to be involved in formin-mediated actin polymerisation (Kovar, 2006; Romero et al., 2004). *Toxoplasma* profilin, on the other hand, acts to sequester G-actin and actually inhibits polymerisation (Skillman et al., 2012). While the reason profilin would be so highly enriched in the TurboID data is still a mystery, this result might suggest that a second look at profilin and its function during vesicular transport is warranted.

4.2.6. TgEDP's possible role in parasite nutrition

Components of the K13 endocytosis machinery were identified in the TurboID experiments, and endocytosis was investigated using the assay as described in Koreny et al. (2022). This process was seen to be unaffected in the *Tg*EDP knockout parasites thus ruling out a critical role in endocytosis. However, from normalised IFA images of the endocytosis assay as well as quantifications, an accumulation of SAG1 was observed. This increase in signal suggests a potential reduction in the parasites' ability to degrade endocytosed SAG1, further reinforcing the hypothesis that *Tg*EDP is involved in trafficking proteases from the Golgi body. The fact that components of the endocytosis machinery were identified via TurboID, but no proteins characteristically present on the surface of the VAC were identified (Stasic et al., 2022), suggests that the role *Tg*EDP plays in the whole process only goes as

far as the site of uptake, and is likely not involved in the fusion of endocytosed material to the lysosomes.

An unexpected phenotype which was also observed upon knockout of *Tg*EDP was the fragmentation of the mitochondria. This observation is not typically seen in cases of Golgi body disruption. It has, however, been observed in cases where the parasites suffered nutritional deficiencies (Ghosh et al., 2012). This observation is, therefore, in line with what would be expected from a phenotype that is primarily negatively affecting the parasite's digestive vacuole as described above, and further advocates for a deficiency in degradation. However, this brings into question the cause of parasite death. As previously stated, CPL is not essential in tachyzoites and therefore its seeming retention within the *trans*-Golgi should not be detrimental. It is more likely that the cause of death of the parasites is not an inability to traffic CPL, but an inability to traffic cargo that is co-trafficked with CPL. This will be discussed later on.

4.2.7. Looking at the bigger picture and the outlook

This project, while answering many questions about the function of a novel essential Golgi body protein identified, has brought up even more questions and opened up a multitude of other avenues of research which could, and indeed should, take place. Below are described a number of recommended investigations which would tie up a few loose ends left by this project.

Investigating the possible starvation phenotype

One of the preferred ways to check for host protein uptake and degradation which was attempted during this project was the experiment done by McGovern et al., (2018). Here, a fluorescent protein is expressed in the cytoplasm of host cells, and its uptake by the parasites is monitored and quantified. Unfortunately, it was not possible to reproduce the data by McGovern et al., (2018) in a reliable manner so that meaningful quantification of uptake and digestion could be achieved. While uptake of host cell proteins certainly occurs during the intracellular stage of the parasites, only few parasites appeared to perform this uptake, making proper quantifications complicated. This same observation has also been made in other studies (Koreny et al., 2022).

Another way of potentially investigating starvation is to carry out metabolomics experiments. In these experiments, compounds such as sugars, and amino and fatty acids which have been 13C-labelled are taken up by host cells. Their metabolism within the parasites can then be followed using gas chromatography-mass spectrometry and liquid chromatography-mass spectrometry (J. Kloehn et al., 2016; Joachim Kloehn et al., 2021; MacRae et al., 2012). By doing so, while the exact process with which *Tg*EDP is involved would still be unknown, the results might possibly shed some light on any nutritional deficiencies the knockout mutant parasites could be experiencing.

In addition to these experiments, MitoTracker, the membrane potential-sensitive dye, could be used to investigate the functionality of the fragmented mitochondria in knockout mutants, as has already been done in previous studies relating to starvation (Ghosh et al., 2012).

Identifying the mechanism of action

At the time the curated sgRNA library was generated, and the screen candidates were chosen, no orthologs of *Tg*EDP were known. This protein had only been annotated as having a 'ENTH domain'. However, as the ToxoDB database was updated throughout the progression of the project, a region called 'AP-4 complex accessory subunit tepsin' was then annotated. The similarity between *Tg*EDP and tepsin was further highlighted when submitting the former's protein sequence into HHpred, a Max Planck Institute Bioinformatics toolkit (Gabler et al., 2020; Söding et al., 2005; Zimmermann et al., 2018). Here, the top 13 hits (bar the first one, the *Plasmodium* homolog) all referred to AP-4 complex accessory subunit tepsin. Despite HHpred highlighting tepsin as a possible homolog, STRING-db shows that *Tg*EDP seems relatively apicomplexan-specific (Figure 3.7). The structures of *Tg*EDP and tepsin were compared using AlphaFold (Figure 4.2) (Jumper et al., 2021; Varadi et al., 2022). Both were observed to have helixes towards the centre of the protein, but many disordered regions surrounding these helixes. These disordered region could potentially be responsible for any versatility the protein has with regards to interaction partners (Dyson & Wright, 2005). Tepsin is believed to be responsible for the trafficking of ATG9 (Mattera et al., 2017), a lipid scramblase that is involved in the extension of autophagosomal membranes (Matoba et al., 2020). In *Toxoplasma*, ATG9 was observed to be essential for bradyzoite viability (Nguyen et al., 2017; D. Smith et al., 2021). In these publications it was described how knockout of this protein led to a phenotype wherein the VAC was more electron-dense, suggesting a defect in canonical autophagy. This VAC

phenotype was paired with another phenotype wherein the mitochondria were seen to have an abnormal fragmented or punctate morphology. Despite ATG9 being essential for bradyzoites, this protein was observed to be dispensable for the tachyzoite stage. Therefore, even though *Tg*EDP might potentially have homology with tepsin, their functions likely differ since a defect in ATG9 trafficking would not be detrimental. As described earlier, *Tg*EDP is more likely to be essential with regards to facilitating the transportation of a crucial component of the parasite's digestive system.

With regards to the AP-4 complex, not much is known in terms of its function. However, according to STRING-db (Szklarczyk et al., 2011; von Mering et al., 2003), it is relatively well conserved across eukaryotes. While its interaction with *Tg*EDP would still need to be confirmed via colocalisation and knockout experiments, the predicted AP-4 component identified via TurboID was submitted to HHpred and the structures of the top potential homologs found comparable using AlphaFold. In agreement with the data obtained during this project (Figure A.2), the AP-4 complex has been shown to localise to the perinuclear region, close to the *trans*-Golgi network, and is sensitive to brefeldin-A treatment (Dell'Angelica et al., 1999; Fuji et al., 2016; Hirst et al., 1999). In association with its accessory protein tepsin, it is also currently hypothesized to be involved in transporting the autophagy-related protein ATG9, among other proteins (Davies et al., 2018; De Pace et al., 2018; Fuji et al., 2016; Mattera et al., 2017).

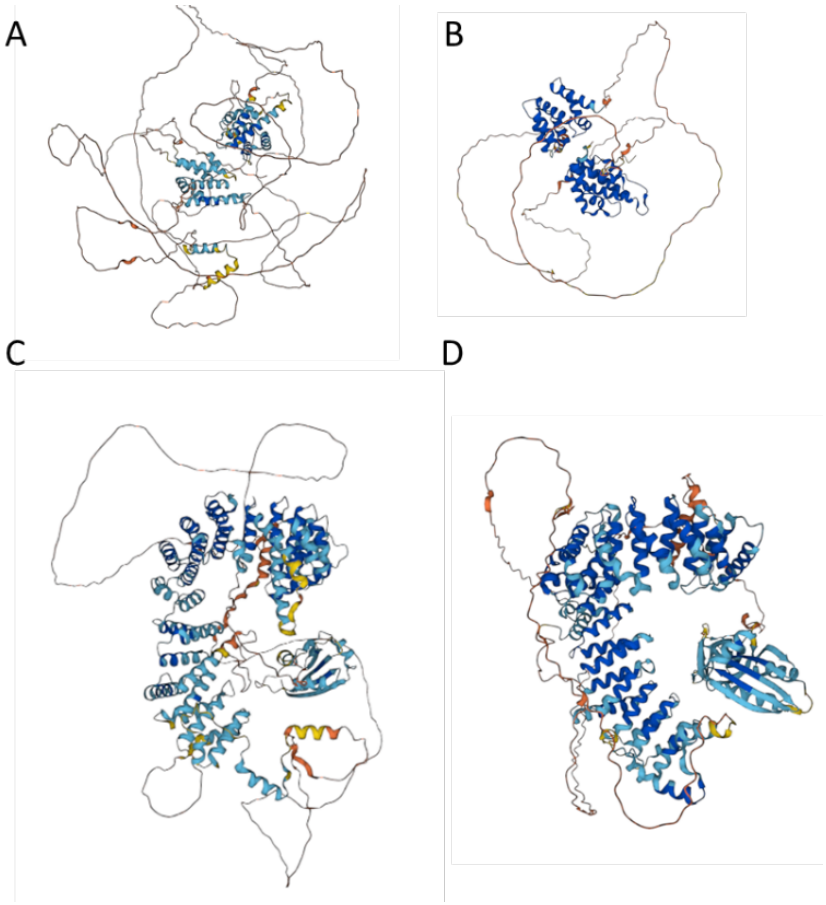

Figure 4.2 – Predicted structures of *Tg*EDP, tepsin, and the AP-4 epsilon subunits of *Toxoplasma* and *Homo sapiens*

(**A**) and (**B**) show the structure of *Tg*EDP and tepsin respectively, while (**C**) and (**D**) show the structure of AP-4 epsilon of *Toxoplasma* and humans respectively, as predicted by AlphaFold.

Identifying the essential cargo

As previously mentioned, CPL is not essential in *Toxoplasma* tachyzoites, meaning that its retention within the *trans*-Golgi in the knockout mutants is likely not the reason for parasite mortality. This could therefore imply that the parasites are either dying as a result of 1) the Golgi body disruption itself, or 2) an essential protein being co-mislocalised with CPL. In the latter case, this hypothetical protein would likely inhabit the same compartment, and is trafficked with CPL. In an attempt to identify this protein, the hyperLOPIT data generated by Barylyuk et al. (2020) was taken advantage of, and CPL was used as 'bait' to identify the cluster of interest.

The proteins clustering close to CPL were identified, and are listed in the appendix. Since the cargo being sought is predicted to be essential, the phenotypic scores were noted (Sidik et al., 2016). From Figure 4.3 (and Table A.4 in the appendix), one can see that the proteins predicted to be essential clustering the closest to CPL (TGME49_321530) are TGME49_247030, TGME49_309930, and TGME49_297420. None of these proteins are predicted to have a signal peptide. TGME49_297420 is annotated as being the putative beta-tubulin cofactor D, making it an unlikely candidate. TGME49_247030, on the other hand, is not annotated as having any known domains. A search for potential homologous proteins on HHpred did not result in any legitimate hits as all of these showed a relatively high E-value, therefore no comment can be made as to whether it is a potential candidate.

The remaining protein clustering relatively close to CPL is TGME49_309930. This is annotated as being a melibiase subfamily protein on ToxoDB (Gajria et al., 2008). According to STRING-db, this protein is a potential ortholog of α-N-acetylgalactosaminidase, an essential protein involved in cleaving glycopeptide and glycolipid α-N-acetylgalactosamine (Clark & Garman, 2009; Szklarczyk et al., 2011; von Mering et al., 2003). Since there is reason to believe that TGME49_309930 might be critically involved in the processes under investigation in this project, it is recommended that future work also determine the function of this protein. Should knockout of this protein result in a phenotype similar to that observed upon knockout of *Tg*EDP, this would confirm the hypothesis.

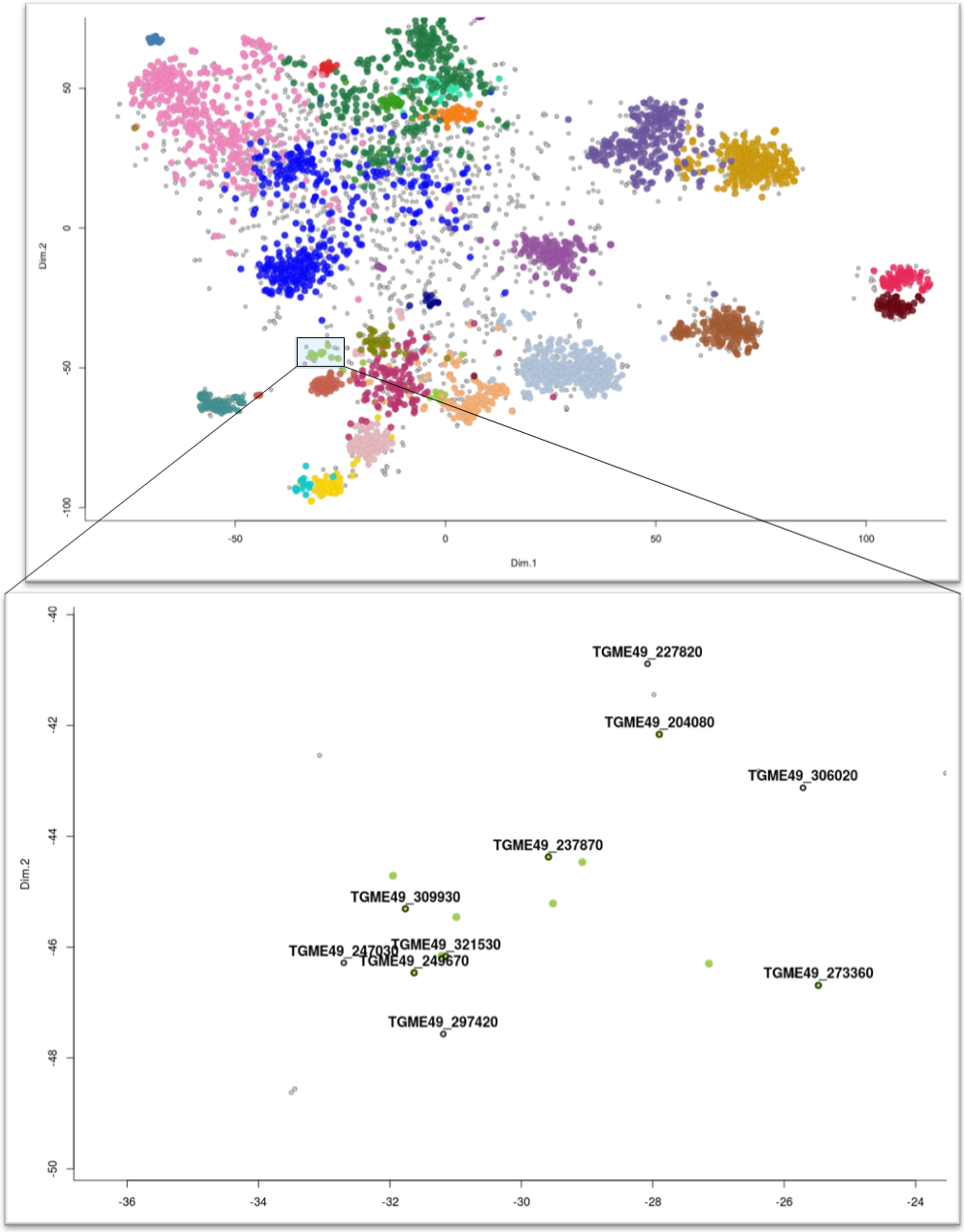

Figure 4.3 – Proteins clustering with CPL within *Toxoplasma* as detected by hyperLOPIT

HyperLOPIT is a system wherein the different subcellular compartments of lysed parasite cells were separated by means of gradient centrifugation, and their contents identified using proteomics (Barylyuk et al., 2020). The proteins clustering with CPL are marked with a box in the top image, are shown in more detail in the below image, and are listed in Table A.4.

Involvement with the acto-myosin system

While quantification data of the phenotypes showed that CPL accumulation occurs first upon knockout of *Tg*EDP, and is therefore likely the primary phenotype, it was nevertheless interesting to observe that MyoF was also affected. Previous studies have shown that knockdown of the myosin resulted in the disruption of the Golgi and post-Golgi compartments (Carmeille et al., 2021). Based on these reports, it would seem that MyoF is critical for Golgi and post-Golgi compartments localisation. However, results obtained during this project showed that the reverse is also true, with a Golgi protein (*Tg*EDP) knockout also negatively affecting MyoF localisation. Knockout of formin2, the actin nucleator present near the Golgi, would also have been expected to result in a disruption of the Golgi, and thus *Tg*EDP. As seen in Figure 3.25, this was not the case. Taken together, both the MyoF phenotype upon *Tg*EDP knockout, and the lack of *Tg*EDP mislocalisation upon FRM2 knockout seem to suggest that the dependence of the Golgi on the acto-myosin system, and vice versa, needs to be more thoroughly investigated.

Along this line of thought, it was interesting to find the protein TGGT1_213392 in both TurboID datasets. This protein is annotated as being a 'Xin actin-binding repeat-containing protein'. Preliminary IFA data shows that it localises close to *Tg*EDP, possibly localising at the *cis*-Golgi. This protein was also identified as a protein of interest by another research group who used proximity labelling to find potential MyoF interactors. Camille Pearce, a member of the Heaslip research group presented preliminary data on this protein at MPM2022 and is currently characterising it (Pearce & Heaslip, 2022).

4.3. General outlook and concluding thoughts

The splitCas9 system for carrying out phenotypic screening established during this project is one which proved useful during this project, and it will prove useful in the future. This system is highly versatile, with slight changes allowing it to be used in many ways to answer a myriad of scientific questions. As mentioned in this thesis, recipient strains wherein the microtubules, mitochondria, IMC, and micronemes are labelled have already been established and have started being used. Their use in the context of a phenotypic screen will likely highlight new candidates which are essential with respect to invasion and egress, as well as with respect to specific organellar structures, specifically the mitochondria, the secretory system, and the cytoskeletal system.

While novel direct actin regulators were not found during this project, several proteins linked to actin function, and which affect F-actin dynamics, were identified. Further work on these proteins and their mechanism of action will undoubtedly continue. Future work on other candidates identified from the F-actin screen is also recommended. The majority of the proteins identified localised to the nucleus or to the mitochondria (Figure 3.6), two organelles which deserve more in-depth study. Since the proteins targeted by the screen are all predicted to be apicomplexan-specific, their investigation is even more important as these might potentially make good candidates for novel intervention strategies. This is especially relevant in the case of *Tg*EDP, the candidate investigated during this project. This essential candidate is not only rather divergent from homologs in other eukaryotes (Figure 3.7), but also seems to be relatively conserved among apicomplexans. According to the model below, *Tg*EDP is involved in protease vesicle trafficking from the *trans*-Golgi network to the micropore, the site of parasite endocytosis (Koreny et al., 2022). Whether *Tg*EDP is involved in the formation of these vesicles, their transport, or their tethering and fusion with endocytosed vesicles is not yet known with certainty. The data obtained points towards it being responsible for binding to MyoF, allowing the protease vesicles to move along the actin filaments. While the ultimate functions of *Tg*EDP and its seemingly distant *Homo sapiens* homolog tepsin differ, it is interesting to speculate whether these proteins achieve their respective functions using the same mechanism given that they seem to have the same binding partner, AP-4.

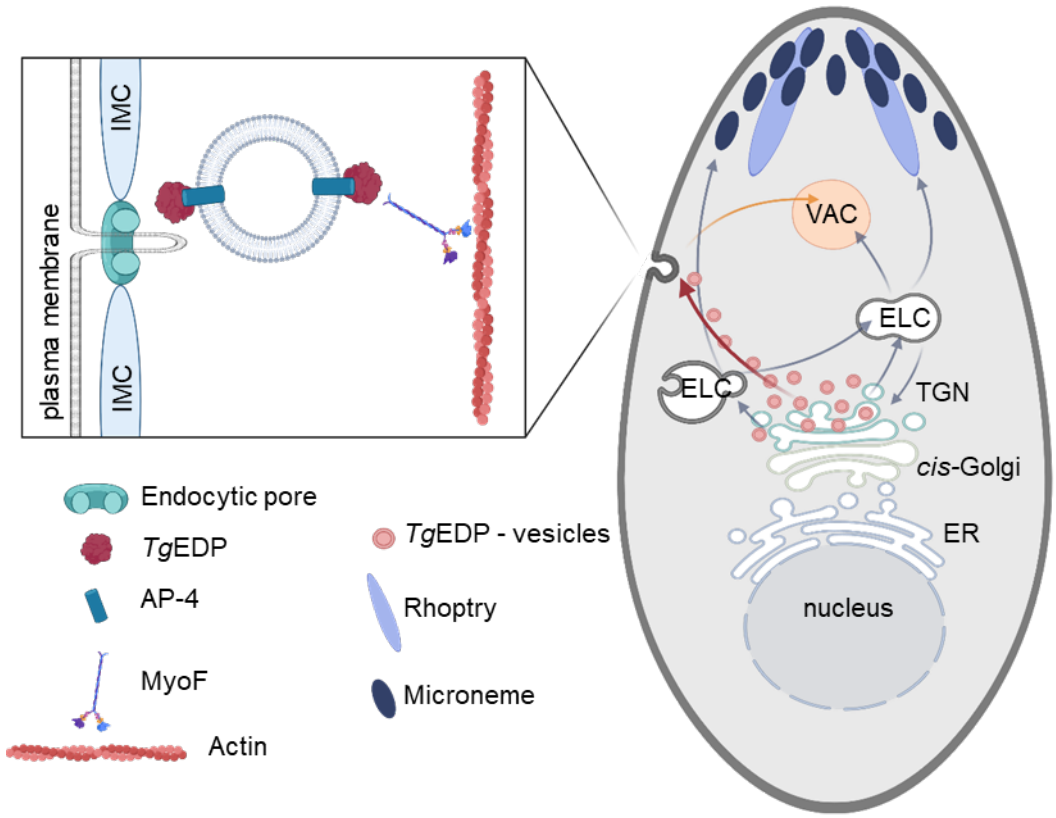

Figure 4.4 – Model illustrating the hypothesised function of *Tg*EDP

According to the proposed model, *Tg*EDP bound to protease vesicles via AP-4 is involved in transporting these said vesicles to the endocytic pore via MyoF and actin (along the red arrow). These protease vesicles then fuse with endocytosed vesicles, and together these are transported to the VAC (along the orange arrow). Knockout of *Tg*EDP results in the retention of proteases within the *trans*-Golgi network resulting in its vesiculation, and possibly a downstream inability for the parasite to metabolise endocytosed nutrients. Despite the structure of the Golgi compartment being compromised, the other secretory pathways (some of which are denoted by the grey arrows) are unaffected.

References

Abdellatif, M. E. A., Hipp, L., Plessner, M., Walther, P., & Knöll, B. (2019). Indirect visualization of endogenous nuclear actin by correlative light and electron microscopy (CLEM) using an actin-directed chromobody. *Histochemistry and Cell Biology*, *152*(2), 133–143. https://doi.org/10.1007/s00418-019-01795-3

Adl, S. M., Bass, D., Lane, C. E., Lukeš, J., Schoch, C. L., Smirnov, A., Agatha, S., Berney, C., Brown, M. W., Burki, F., Cárdenas, P., Čepička, I., Chistyakova, L., del Campo, J., Dunthorn, M., Edvardsen, B., Eglit, Y., Guillou, L., Hampl, V., … Zhang, Q. (2019). Revisions to the Classification, Nomenclature, and Diversity of Eukaryotes. *Journal of Eukaryotic Microbiology*, *66*(1), 4–119. https://doi.org/https://doi.org/10.1111/jeu.12691

Adl, S. M., Leander, B. S., Simpson, A. G. B., Archibald, J. M., Anderson, O. R., Bass, D., Bowser, S. S., Brugerolle, G., Farmer, M. A., Karpov, S., Kolisko, M., Lane, C. E., Lodge, D. J., Mann, D. G., Meisterfeld, R., Mendoza, L., Moestrup, Ø., Mozley-Standridge, S. E., Smirnov, A. V., & Spiegel, F. (2007). Diversity, nomenclature, and taxonomy of protists. *Systematic Biology*, *56*(4), 684–689. https://doi.org/10.1080/10635150701494127

Alexander, D. L., Mital, J., Ward, G. E., Bradley, P., & Boothroyd, J. C. (2005). Identification of the moving junction complex of Toxoplasma gondii: A collaboration between distinct secretory organelles. *PLoS Pathogens*, *1*(2), 0137–0149. https://doi.org/10.1371/journal.ppat.0010017

Andenmatten, N., Egarter, S., Jackson, A. J., Jullien, N., Herman, J. P., & Meissner, M. (2013). Conditional genome engineering in Toxoplasma gondii uncovers alternative invasion mechanisms. *Nature Methods*, *10*(2), 125–127. https://doi.org/10.1038/nmeth.2301

Anderson-White, B., Beck, J. R., Chen, C.-T. T., Meissner, M., Bradley, P. J., & Gubbels, M.-J. J. (2012). Cytoskeleton Assembly in Toxoplasma gondii Cell Division. *International Review of Cell and Molecular Biology*, *298*, 1–31. https://doi.org/10.1016/B978-0-12-394309-5.00001-8

Aparna, P., & Swati, P. (2021). Recognition of Two Distinct Pathways for Trafficking of

Proteins to the Apicoplast. *MBio*, *12*(6), e02634-21. https://doi.org/10.1128/mBio.02634-21

Arisue, N., & Hashimoto, T. (2015). Phylogeny and evolution of apicoplasts and apicomplexan parasites. *Parasitology International*, *64*(3), 254–259. https://doi.org/https://doi.org/10.1016/j.parint.2014.10.005

Arrizabalaga, G., & Boothroyd, J. C. (2004). Role of calcium during Toxoplasma gondii invasion and egress. *International Journal for Parasitology*, *34*(3), 361–368. https://doi.org/10.1016/j.ijpara.2003.11.017

Attias, M., Miranda, K., & De Souza, W. (2019). Development and fate of the residual body of Toxoplasma gondii. *Experimental Parasitology*, *196*, 1–11. https://doi.org/10.1016/j.exppara.2018.11.004

Balderhaar, H. J. kleine, & Ungermann, C. (2013). CORVET and HOPS tethering complexes - coordinators of endosome and lysosome fusion. *Journal of Cell Science*, *126*(Pt 6), 1307–1316. https://doi.org/10.1242/jcs.107805

Barylyuk, K., Koreny, L., Ke, H., Butterworth, S., Crook, O. M., Lassadi, I., Gupta, V., Tromer, E., Mourier, T., Stevens, T. J., Breckels, L. M., Pain, A., Lilley, K. S., & Waller, R. F. (2020). A Comprehensive Subcellular Atlas of the Toxoplasma Proteome via hyperLOPIT Provides Spatial Context for Protein Functions. *Cell Host and Microbe*, *28*(5), 752-766.e9. https://doi.org/10.1016/j.chom.2020.09.011

Baum, J., Papenfuss, A. T., Baum, B., Speed, T. P., & Cowman, A. F. (2006). Regulation of apicomplexan actin-based motility. *Nature Reviews Microbiology*, *4*(8), 621–628. https://doi.org/10.1038/nrmicro1465

Baum, J., Tonkin, C. J., Paul, A. S., Rug, M., Smith, B. J., Gould, S. B., Richard, D., Pollard, T. D., & Cowman, A. F. (2008). A Malaria Parasite Formin Regulates Actin Polymerization and Localizes to the Parasite-Erythrocyte Moving Junction during Invasion. *Cell Host and Microbe*, *3*(3), 188–198. https://doi.org/10.1016/j.chom.2008.02.006

Beck, J. R., Rodriguez-Fernandez, I. A., de Leon, J. C., Huynh, M. H., Carruthers, V. B., Morrissette, N. S., & Bradley, P. J. (2010). A novel family of Toxoplasma IMC proteins displays a hierarchical organization and functions in coordinating parasite division. *PLoS Pathogens*, *6*(9), e1001094. https://doi.org/10.1371/journal.ppat.1001094

Beckers, C. J., Dubremetz, J. F., Mercereau-Puijalon, O., & Joiner, K. A. (1994). The Toxoplasma gondii rhoptry protein ROP 2 is inserted into the parasitophorous vacuole membrane, surrounding the intracellular parasite, and is exposed to the host cell cytoplasm. *The Journal of Cell Biology*, *127*(4), 947–961. https://doi.org/10.1083/jcb.127.4.947

Behnke, M. S., Radke, J. B., Smith, A. T., Sullivan, W. J., & White, M. W. (2008). The transcription of bradyzoite genes in Toxoplasma gondii is controlled by autonomous promoter elements. *Molecular Microbiology*, *68*(6), 1502–1518. https://doi.org/10.1111/j.1365-2958.2008.06249.x

Behnke, M. S., Wootton, J. C., Lehmann, M. M., Radke, J. B., Lucas, O., Nawas, J., Sibley, L. D., & White, M. W. (2010). Coordinated progression through two subtranscriptomes underlies the tachyzoite cycle of Toxoplasma gondii. *PloS One*, *5*(8), e12354. https://doi.org/10.1371/journal.pone.0012354

Belli, S. I., Smith, N. C., & Ferguson, D. J. P. (2006). The coccidian oocyst: a tough nut to crack! *Trends in Parasitology*, *22*(9), 416–423. https://doi.org/10.1016/j.pt.2006.07.004

Benenson, M. W., Takafuji, E. T., Lemon, S. M., Greenup, R. L., & Sulzer, A. J. (1982). Oocyst-Transmitted Toxoplasmosis Associated with Ingestion of Contaminated Water. *New England Journal of Medicine*, *307*(11), 666–669. https://doi.org/10.1056/nejm198209093071107

Besteiro, S., Michelin, A., Poncet, J., Dubremetz, J.-F., & Lebrun, M. (2009). Export of a Toxoplasma gondii rhoptry neck protein complex at the host cell membrane to form the moving junction during invasion. *PLoS Pathogens*, *5*(2), e1000309. https://doi.org/10.1371/journal.ppat.1000309

Béthune, J., Wieland, F., & Moelleken, J. (2006). COPI-mediated Transport. *The Journal of Membrane Biology*, *211*(2), 65–79. https://doi.org/10.1007/s00232-006-0859-7

Bisio, H., Lunghi, M., Brochet, M., & Soldati-Favre, D. (2019). Phosphatidic acid governs natural egress in Toxoplasma gondii via a guanylate cyclase receptor platform. *Nature Microbiology*, *4*(3), 420–428. https://doi.org/10.1038/s41564-018-0339-8

Bisio, H., & Soldati-Favre, D. (2019). Signaling cascades governing entry into and exit from host cells by Toxoplasma gondii. *Annual Review of Microbiology*, *73*(1), 579–599.

https://doi.org/10.1146/annurev-micro-020518-120235

Black, M. W., & Boothroyd, J. C. (2000). Lytic cycle of Toxoplasma gondii. *Microbiology and Molecular Biology Reviews : MMBR*, *64*(3), 607–623. https://doi.org/10.1128/MMBR.64.3.607-623.2000

Blader, I. J., Coleman, B. I., Chen, C.-T. T., & Gubbels, M.-J. J. (2015). Lytic Cycle of Toxoplasma gondii: 15 Years Later. *Annual Review of Microbiology*, *69*(1), 463–485. https://doi.org/10.1146/annurev-micro-091014-104100

Blake, D. P., Knox, J., Dehaeck, B., Huntington, B., Rathinam, T., Ravipati, V., Ayoade, S., Gilbert, W., Adebambo, A. O., Jatau, I. D., Raman, M., Parker, D., Rushton, J., & Tomley, F. M. (2020). Re-calculating the cost of coccidiosis in chickens. *Veterinary Research*, *51*(1), 115. https://doi.org/10.1186/s13567-020-00837-2

Blum, M., Chang, H. Y., Chuguransky, S., Grego, T., Kandasaamy, S., Mitchell, A., Nuka, G., Paysan-Lafosse, T., Qureshi, M., Raj, S., Richardson, L., Salazar, G. A., Williams, L., Bork, P., Bridge, A., Gough, J., Haft, D. H., Letunic, I., Marchler-Bauer, A., … Finn, R. D. (2021). The InterPro protein families and domains database: 20 years on. *Nucleic Acids Research*, *49*(D1), D344–D354. https://doi.org/10.1093/nar/gkaa977

Bonifacino, J. S., & Glick, B. S. (2004). The Mechanisms of Vesicle Budding and Fusion. *Cell*, *116*(2), 153–166. https://doi.org/10.1016/S0092-8674(03)01079-1

Borges-Pereira, L., Budu, A., McKnight, C. A., Moore, C. A., Vella, S. A., Triana, M. A. H., Liu, J., Garcia, C. R. S., Pace, D. A., & Moreno, S. N. J. (2015). Calcium signaling throughout the toxoplasma gondii lytic cycle a study using genetically encoded calcium indicators. *Journal of Biological Chemistry*, *290*(45), 26914–26926. https://doi.org/10.1074/jbc.M115.652511

Bouchut, A., Geiger, J. A., Derocher, A. E., & Parsons, M. (2014). Vesicles bearing toxoplasma apicoplast membrane proteins persist following loss of the relict plastid or golgi body disruption. *PLoS ONE*, *9*(11), e112096. https://doi.org/10.1371/journal.pone.0112096

Bougdour, A., Durandau, E., Brenier-Pinchart, M.-P., Ortet, P., Barakat, M., Kieffer, S., Curt-Varesano, A., Curt-Bertini, R.-L., Bastien, O., Coute, Y., Pelloux, H., & Hakimi, M.-A. (2013). Host cell subversion by Toxoplasma GRA16, an exported dense granule protein that targets the host cell nucleus and alters gene expression. *Cell Host &*

Microbe, *13*(4), 489–500. https://doi.org/10.1016/j.chom.2013.03.002

Bowie, W. R., King, A. S., Werker, D. H., Isaac-Renton, J. L., Bell, A., Eng, S. B., & Marion, S. A. (1997). Outbrak of toxoplasmosis associated with municipal drinking water. *Lancet*, *350*(9072), 173–177. https://doi.org/10.1016/S0140-6736(96)11105-3

Branon, T. C., Bosch, J. A., Sanchez, A. D., Udeshi, N. D., Svinkina, T., Carr, S. A., Feldman, J. L., Perrimon, N., & Ting, A. Y. (2018). Efficient proximity labeling in living cells and organisms with TurboID. *Nature Biotechnology*, *36*(9), 880–898. https://doi.org/10.1038/nbt.4201

Breinich, M. S., Ferguson, D. J. P., Foth, B. J., van Dooren, G. G., Lebrun, M., Quon, D. V., Striepen, B., Bradley, P. J., Frischknecht, F., Carruthers, V. B., & Meissner, M. (2009). A Dynamin Is Required for the Biogenesis of Secretory Organelles in Toxoplasma gondii. *Current Biology*, *19*(4), 277–286. https://doi.org/10.1016/j.cub.2009.01.039

Breitsprecher, D., & Goode, B. L. (2013). Formins at a glance. *Journal of Cell Science*, *126*(Pt 1), 1–7. https://doi.org/10.1242/jcs.107250

Brown, K., Long, S., & Sibley, L. (2018). Conditional Knockdown of Proteins Using Auxin-inducible Degron (AID) Fusions in Toxoplasma gondii. *Bio-Protocol*, *8*(4). https://doi.org/10.21769/bioprotoc.2728

Bullen, H. E., Jia, Y., Yamaryo-Botté, Y., Bisio, H., Zhang, O., Jemelin, N. K., Marq, J. B., Carruthers, V., Botté, C. Y., & Soldati-Favre, D. (2016). Phosphatidic Acid-Mediated Signaling Regulates Microneme Secretion in Toxoplasma. *Cell Host and Microbe*, *19*(3), 349–360. https://doi.org/10.1016/j.chom.2016.02.006

Butterworth, S., Torelli, F., Lockyer, E. J., Wagener, J., Song, O.-R., Broncel, M., Russell, M. R. G., Young, J. C., & Treeck, M. (2022). Toxoplasma gondii ROP1 subverts murine and human innate immune restriction. *BioRxiv*, 2022.03.21.485090. https://doi.org/10.1101/2022.03.21.485090

Caldas, L. A., de Souza, W., & Attias, M. (2007). Calcium ionophore-induced egress of Toxoplasma gondii shortly after host cell invasion. *Veterinary Parasitology*, *147*(3–4), 210–220. https://doi.org/10.1016/j.vetpar.2007.05.012

Carmeille, R., Lomoriello, P. S., Devarakonda, P. M., Kellermeier, J. A., & Heaslip, A. T. (2021). Actin and an unconventional myosin motor, TgMyoF, control the organization

and dynamics of the endomembrane network in Toxoplasma gondii. *PLoS Pathogens*, *17*(2), e1008787. https://doi.org/10.1371/JOURNAL.PPAT.1008787

Carruthers, V. B., Giddings, O. K., & Sibley, L. D. (1999). Secretion of micronemal proteins is associated with toxoplasma invasion of host cells. *Cellular Microbiology*, *1*(3), 225–235. https://doi.org/10.1046/j.1462-5822.1999.00023.x

Castrillon, D. H., & Wasserman, S. A. (1994). Diaphanous is required for cytokinesis in Drosophila and shares domains of similarity with the products of the limb deformity gene. *Development (Cambridge, England)*, *120*(12), 3367–3377. https://doi.org/10.1242/dev.120.12.3367

Chen, A. L., Kim, E. W., Toh, J. Y., Vashisht, A. A., Rashoff, A. Q., Van, C., Huang, A. S., Moon, A. S., Bell, H. N., Bentolila, L. A., Wohlschlegel, J. A., & Bradley, P. J. (2015). Novel components of the toxoplasma inner membrane complex revealed by BioID. *MBio*, *6*(1), e02357-14. https://doi.org/10.1128/mBio.02357-14

Chen, A. L., Moon, A. S., Bell, H. N., Huang, A. S., Vashisht, A. A., Toh, J. Y., Lin, A. H., Nadipuram, S. M., Kim, E. W., Choi, C. P., Wohlschlegel, J. A., & Bradley, P. J. (2017). Novel insights into the composition and function of the Toxoplasma IMC sutures. *Cellular Microbiology*, *19*(4). https://doi.org/10.1111/cmi.12678

Cho, K. F., Branon, T. C., Udeshi, N. D., Myers, S. A., Carr, S. A., & Ting, A. Y. (2020). Proximity labeling in mammalian cells with TurboID and split-TurboID. *Nature Protocols*, *15*(12), 3971–3999. https://doi.org/10.1038/s41596-020-0399-0

Chou, H.-T., Dukovski, D., Chambers, M. G., Reinisch, K. M., & Walz, T. (2016). CATCHR, HOPS and CORVET tethering complexes share a similar architecture. *Nature Structural & Molecular Biology*, *23*(8), 761–763. https://doi.org/10.1038/nsmb.3264

Clark, N. E., & Garman, S. C. (2009). The 1.9 Å Structure of Human α-N-Acetylgalactosaminidase: The Molecular Basis of Schindler and Kanzaki Diseases. *Journal of Molecular Biology*, *393*(2), 435–447. https://doi.org/10.1016/j.jmb.2009.08.021

Cortes, H., Leitão, A., Gottstein, B., & Hemphill, A. (2014). A review on bovine besnoitiosis: A disease with economic impact in herd health management, caused by Besnoitia besnoiti (Franco and Borges,). *Parasitology*, *141*(11), 1406–1417. https://doi.org/10.1017/S0031182014000262

Cowman, A. F., Healer, J., Marapana, D., & Marsh, K. (2016). Malaria: Biology and Disease. *Cell*, *167*(3), 610–624. https://doi.org/10.1016/j.cell.2016.07.055

Curt-Varesano, A., Braun, L., Ranquet, C., Hakimi, M. A., & Bougdour, A. (2016). The aspartyl protease TgASP5 mediates the export of the Toxoplasma GRA16 and GRA24 effectors into host cells. *Cellular Microbiology*, *18*(2), 151–167. https://doi.org/10.1111/cmi.12498

Daher, W., Plattner, F., Carlier, M. F., & Soldati-Favre, D. (2010). Concerted action of two formins in gliding motility and host cell invasion by Toxoplasma gondii. *PLoS Pathogens*, *6*(10), 1–14. https://doi.org/10.1371/journal.ppat.1001132

Davies, A. K., Itzhak, D. N., Edgar, J. R., Archuleta, T. L., Hirst, J., Jackson, L. P., Robinson, M. S., & Borner, G. H. H. (2018). AP-4 vesicles contribute to spatial control of autophagy via RUSC-dependent peripheral delivery of ATG9A. *Nature Communications*, *9*(1), 3958. https://doi.org/10.1038/s41467-018-06172-7

De Camilli, P., Chen, H., Hyman, J., Panepucci, E., Bateman, A., & Brunger, A. T. (2002). The ENTH domain. *FEBS Letters*, *513*(1), 11–18. https://doi.org/10.1016/S0014-5793(01)03306-3

De Castro Corrêa, C., Maximino, L. P., & Weber, S. A. T. (2018). Hearing disorders in congenital toxoplasmosis: A literature review. *International Archives of Otorhinolaryngology*, *22*(3), 330–333. https://doi.org/10.1055/s-0037-1605377

De Pace, R., Skirzewski, M., Damme, M., Mattera, R., Mercurio, J., Foster, A. M., Cuitino, L., Jarnik, M., Hoffmann, V., Morris, H. D., Han, T. U., Mancini, G. M. S., Buonanno, A., & Bonifacino, J. S. (2018). Altered distribution of ATG9A and accumulation of axonal aggregates in neurons from a mouse model of AP-4 deficiency syndrome. *PLoS Genetics*, *14*(4), e1007363. https://doi.org/10.1371/journal.pgen.1007363

Del Carmen, M. G., Mondragón, M., González, S., & Mondragón, R. (2009). Induction and regulation of conoid extrusion in Toxoplasma gondii. *Cellular Microbiology*, *11*(6), 967–982. https://doi.org/https://doi.org/10.1111/j.1462-5822.2009.01304.x

Delbac, F., Sänger, A., Neuhaus, E. M., Stratmann, R., Ajioka, J. W., Toursel, C., Herm-Götz, A., Tomavo, S., Soldati, T., & Soldati, D. (2001). Toxoplasma gondii myosins B/C: One gene, two tails, two localizations, and a role in parasite division. *Journal of Cell Biology*, *155*(4), 613–623. https://doi.org/10.1083/jcb.200012116

Dell'Angelica, E. C., Mullins, C., & Bonifacino, J. S. (1999). AP-4, a novel protein complex related to clathrin adaptors. *The Journal of Biological Chemistry*, *274*(11), 7278–7285. https://doi.org/10.1074/jbc.274.11.7278

Di Cristina, M., Dou, Z., Lunghi, M., Kannan, G., Huynh, M. H., McGovern, O. L., Schultz, T. L., Schultz, A. J., Miller, A. J., Hayes, B. M., Van Der Linden, W., Emiliani, C., Bogyo, M., Besteiro, S., Coppens, I., & Carruthers, V. B. (2017). Toxoplasma depends on lysosomal consumption of autophagosomes for persistent infection. *Nature Microbiology*, *2*, 17096. https://doi.org/10.1038/nmicrobiol.2017.96

Dobrowolski, J. M., Niesman, I. R., & Sibley, L. D. (1997). Actin in the parasite Toxoplasma gondii is encoded by a single copy gene, ACT1 and exists primarily in a globular form. *Cell Motility and the Cytoskeleton*, *37*(3), 253–262. https://doi.org/10.1002/(SICI)1097-0169(1997)37:3<253::AID-CM7>3.0.CO;2-7

Dogga, S. K., Mukherjee, B., Jacot, D., Kockmann, T., Molino, L., Hammoudi, P. M., Hartkoorn, R. C., Hehl, A. B., & Soldati-Favre, D. (2017). A druggable secretory protein maturase of Toxoplasma essential for invasion and egress. *ELife*, *6*, e27480. https://doi.org/10.7554/eLife.27480

Donald, R. G., & Roos, D. S. (1995). Insertional mutagenesis and marker rescue in a protozoan parasite: cloning of the uracil phosphoribosyltransferase locus from Toxoplasma gondii. *Proceedings of the National Academy of Sciences of the United States of America*, *92*(12), 5749–5753. https://doi.org/10.1073/pnas.92.12.5749

Dos Santos Pacheco, N., Brusini, L., Haase, R., Tosetti, N., Maco, B., Brochet, M., Vadas, O., & Soldati-Favre, D. (2022). Conoid extrusion regulates glideosome assembly to control motility and invasion in Apicomplexa. *Nature Microbiology*, *7*(11), 1777–1790. https://doi.org/10.1038/s41564-022-01212-x

Dou, Z., Coppens, I., & Carruthers, V. B. (2013). Non-canonical maturation of two papain-family Proteases in Toxoplasma gondii. *Journal of Biological Chemistry*, *288*(5), 3523–3534. https://doi.org/10.1074/jbc.M112.443697

Dou, Z., McGovern, O. L., Di Cristina, M., & Carruthers, V. B. (2014). Toxoplasma gondii ingests and digests host Cytosolic proteins. *MBio*, *5*(4), e01188-14. https://doi.org/10.1128/mBio.01188-14

Dubey, J. P., Lindsay, D. S., & Speer, C. A. (1998). Structures of Toxoplasma gondii

tachyzoites, bradyzoites, and sporozoites and biology and development of tissue cysts. *Clinical Microbiology Reviews*, *11*(2), 267–299. https://doi.org/10.1128/cmr.11.2.267

Dubremetz, J. F. (2007). Rhoptries are major players in Toxoplasma gondii invasion and host cell interaction. *Cellular Microbiology*, *9*(4), 841–848. https://doi.org/10.1111/j.1462-5822.2007.00909.x

Dyson, H. J., & Wright, P. E. (2005). Intrinsically unstructured proteins and their functions. *Nature Reviews Molecular Cell Biology*, *6*(3), 197–208. https://doi.org/10.1038/nrm1589

Egarter, S., Andenmatten, N., Jackson, A. J., Whitelaw, J. A., Pall, G., Black, J. A., Ferguson, D. J. P., Tardieux, I., Mogilner, A., & Meissner, M. (2014). The toxoplasma Acto-MyoA motor complex is important but not essential for gliding motility and host cell invasion. *PloS One*, *9*(3), e91819. https://doi.org/10.1371/journal.pone.0091819

Endo, T., Sethi, K. K., & Piekarski, G. (1982). Toxoplasma gondii: Calcium Ionophore A23187-mediated exit of trophozoites from infected murine macrophages. *Experimental Parasitology*, *53*(2), 179–188. https://doi.org/10.1016/0014-4894(82)90059-5

Evangelista, M., Blundell, K., Longtine, M. S., Chow, C. J., Adames, N., Pringle, J. R., Peter, M., & Boone, C. (1997). Bni1p, a Yeast Formin Linking Cdc42p and the Actin Cytoskeleton During Polarized Morphogenesis. *Science*, *276*(5309), 118–122. https://doi.org/10.1126/science.276.5309.118

Ferguson, D. J. P., Hutchison, W. M., & Siim, J. C. (1975). the Ultrastructural Development of the Macrogamete and Formation of the Oocyst Wall of Toxoplasma Gondii. *Acta Pathologica Microbiologica Scandinavica Section B Microbiology*, *83 B*(5), 491–505. https://doi.org/10.1111/j.1699-0463.1975.tb00130.x

Fisch, D., Yakimovich, A., Clough, B., Wright, J., Bunyan, M., Howell, M., Mercer, J., & Frickel, E. (2019). Defining host–pathogen interactions employing an artificial intelligence workflow. *ELife*, *8*. https://doi.org/10.7554/eLife.40560

Foth, B. J., Goedecke, M. C., & Soldati, D. (2006). New insights into myosin evolution and classification. *Proceedings of the National Academy of Sciences of the United States of America*, *103*(10), 3681–3686. https://doi.org/10.1073/pnas.0506307103

Fox, B. A., Ristuccia, J. G., Gigley, J. P., & Bzik, D. J. (2009). Efficient gene replacements in Toxoplasma gondii strains deficient for nonhomologous end joining. *Eukaryotic Cell*, *8*(4), 520–529. https://doi.org/10.1128/EC.00357-08

Francia, M. E., & Striepen, B. (2014). Cell division in apicomplexan parasites. *Nature Reviews Microbiology*, *12*(2), 125–136. https://doi.org/10.1038/nrmicro3184

Frénal, K., Dubremetz, J. F., Lebrun, M., & Soldati-Favre, D. (2017). Gliding motility powers invasion and egress in Apicomplexa. *Nature Reviews Microbiology*, *15*(11), 645–660. https://doi.org/10.1038/nrmicro.2017.86

Frénal, K., Jacot, D., Hammoudi, P.-M. M., Graindorge, A., MacO, B., & Soldati-Favre, D. (2017). Myosin-dependent cell-cell communication controls synchronicity of division in acute and chronic stages of Toxoplasma gondii. *Nature Communications*, *8*(1), 15710. https://doi.org/10.1038/ncomms15710

Frénal, K., Polonais, V., Marq, J. B., Stratmann, R., Limenitakis, J., & Soldati-Favre, D. (2010). Functional dissection of the apicomplexan glideosome molecular architecture. *Cell Host and Microbe*, *8*(4), 343–357. https://doi.org/10.1016/j.chom.2010.09.002

Fuji, K., Shirakawa, M., Shimono, Y., Kunieda, T., Fukao, Y., Koumoto, Y., Takahashi, H., Hara-Nishimura, I., & Shimada, T. (2016). The Adaptor Complex AP-4 Regulates Vacuolar Protein Sorting at the trans-Golgi Network by Interacting with VACUOLAR SORTING RECEPTOR1. *Plant Physiology*, *170*(1), 211–219. https://doi.org/10.1104/pp.15.00869

Gabler, F., Nam, S. Z., Till, S., Mirdita, M., Steinegger, M., Söding, J., Lupas, A. N., & Alva, V. (2020). Protein Sequence Analysis Using the MPI Bioinformatics Toolkit. *Current Protocols in Bioinformatics*, *72*(1), e108. https://doi.org/10.1002/cpbi.108

Gajria, B., Bahl, A., Brestelli, J., Dommer, J., Fischer, S., Gao, X., Heiges, M., Iodice, J., Kissinger, J. C., Mackey, A. J., Pinney, D. F., Roos, D. S., Stoeckert, C. J., Wang, H., & Brunk, B. P. (2008). ToxoDB: An integrated toxoplasma gondii database resource. *Nucleic Acids Research*, *36*(SUPPL. 1), D553–D556. https://doi.org/10.1093/nar/gkm981

Galvez, T., Gilleron, J., Zerial, M., & O'Sullivan, G. A. (2012). SnapShot: Mammalian Rab proteins in endocytic trafficking. *Cell*, *151*(1), 234-234.e2. https://doi.org/10.1016/j.cell.2012.09.013

Garcia-Réguet, N., Lebrun, M., Fourmaux, M. N., Mercereau-Puijalon, O., Mann, T., Beckers, C. J., Samyn, B., Van Beeumen, J., Bout, D., & Dubremetz, J. F. (2000). The microneme protein MIC3 of Toxoplasma gondii is a secretory adhesin that binds to both the surface of the host cells and the surface of the parasite. *Cellular Microbiology*, *2*(4), 353–364. https://doi.org/10.1046/j.1462-5822.2000.00064.x

Garneau, J. E., Dupuis, M.-È., Villion, M., Romero, D. A., Barrangou, R., Boyaval, P., Fremaux, C., Horvath, P., Magadán, A. H., & Moineau, S. (2010). The CRISPR/Cas bacterial immune system cleaves bacteriophage and plasmid DNA. *Nature*, *468*(7320), 67–71. https://doi.org/10.1038/nature09523

Gasiunas, G., Barrangou, R., Horvath, P., & Siksnys, V. (2012). Cas9–crRNA ribonucleoprotein complex mediates specific DNA cleavage for adaptive immunity in bacteria. *Proceedings of the National Academy of Sciences*, *109*(39), E2579–E2586. https://doi.org/10.1073/pnas.1208507109

Ghosh, D., Walton, J. L., Roepe, P. D., & Sinai, A. P. (2012). Autophagy is a cell death mechanism in Toxoplasma gondii. *Cellular Microbiology*, *14*(4), 589–607. https://doi.org/10.1111/j.1462-5822.2011.01745.x

Gilbert, W., Bellet, C., Blake, D. P., Tomley, F. M., & Rushton, J. (2020). Revisiting the Economic Impacts of Eimeria and Its Control in European Intensive Broiler Systems With a Recursive Modeling Approach. In *Frontiers in Veterinary Science* (Vol. 7). https://doi.org/10.3389/fvets.2020.558182

Gold, D. A., Kaplan, A. D., Lis, A., Bett, G. C. L., Rosowski, E. E., Cirelli, K. M., Bougdour, A., Sidik, S. M., Beck, J. R., Lourido, S., Egea, P. F., Bradley, P. J., Hakimi, M.-A., Rasmusson, R. L., & Saeij, J. P. J. (2015). The Toxoplasma Dense Granule Proteins GRA17 and GRA23 Mediate the Movement of Small Molecules between the Host and the Parasitophorous Vacuole. *Cell Host & Microbe*, *17*(5), 642–652. https://doi.org/https://doi.org/10.1016/j.chom.2015.04.003

Goode, B. L., & Eck, M. J. (2007). Mechanism and function of formins in the control of actin assembly. *Annual Review of Biochemistry*, *76*, 593–627. https://doi.org/10.1146/annurev.biochem.75.103004.142647

Gordon, J. L., & Sibley, L. D. (2005). Comparative genome analysis reveals a conserved family of actin-like proteins in apicomplexan parasites. *BMC Genomics*, *6*, 179.

https://doi.org/10.1186/1471-2164-6-179

Gould, S. B., Tham, W. H., Cowman, A. F., McFadden, G. I., & Waller, R. F. (2008). Alveolins, a new family of cortical proteins that define the protist infrakingdom Alveolata. *Molecular Biology and Evolution*, *25*(6), 1219–1230. https://doi.org/10.1093/molbev/msn070

Graindorge, A., Frénal, K., Jacot, D., Salamun, J., Marq, J. B., & Soldati-Favre, D. (2016). The Conoid Associated Motor MyoH Is Indispensable for Toxoplasma gondii Entry and Exit from Host Cells. *PLoS Pathogens*, *12*(1), e1005388. https://doi.org/10.1371/journal.ppat.1005388

Gras, S., Jackson, A., Woods, S., Pall, G., Whitelaw, J., Leung, J. M., Ward, G. E., Roberts, C. W., & Meissner, M. (2017). Parasites lacking the micronemal protein MIC2 are deficient in surface attachment and host cell egress, but remain virulent in vivo. *Wellcome Open Research*, *2*, 32. https://doi.org/10.12688/wellcomeopenres.11594.2

Gras, S., Jimenez-Ruiz, E., Klinger, C. M., Schneider, K., Klingl, A., Lemgruber, L., & Meissner, M. (2019). An endocytic-secretory cycle participates in Toxoplasma gondii in motility. *PLoS Biology*, *17*(6). https://doi.org/10.1371/journal.pbio.3000060

Griffith, M. B., Pearce, C. S., & Heaslip, A. T. (2022). Dense granule biogenesis, secretion, and function in Toxoplasma gondii . *Journal of Eukaryotic Microbiology*, *n/a*(n/a), e12904. https://doi.org/10.1111/jeu.12904

Gubbels, M.-J., White, M., & Szatanek, T. (2008). The cell cycle and Toxoplasma gondii cell division: Tightly knit or loosely stitched? *International Journal for Parasitology*, *38*(12), 1343–1358. https://doi.org/https://doi.org/10.1016/j.ijpara.2008.06.004

Haase, S., Zimmermann, D., Olshina, M. A., Wilkinson, M., Fisher, F., Tan, Y. H., Stewart, R. J., Tonkin, C. J., Wong, W., Kovar, D. R., & Baum, J. (2015). Disassembly activity of actin-depolymerizing factor (ADF) is associated with distinct cellular processes in apicomplexan parasites. *Molecular Biology of the Cell*, *26*(17), 3001–3012. https://doi.org/10.1091/mbc.E14-10-1427

Håkansson, S., Morisaki, H., Heuser, J., & Sibley, L. D. (1999). Time-lapse video microscopy of gliding motility in Toxoplasma gondii reveals a novel, biphasic mechanism of cell locomotion. *Molecular Biology of the Cell*, *10*(11), 3539–3547. https://doi.org/10.1091/mbc.10.11.3539

Hakimi, M. A., Olias, P., & Sibley, L. D. (2017). Toxoplasma effectors targeting host signaling and transcription. *Clinical Microbiology Reviews*, *30*(3), 615–644. https://doi.org/10.1128/CMR.00005-17

Hale, C. R., Zhao, P., Olson, S., Duff, M. O., Graveley, B. R., Wells, L., Terns, R. M., & Terns, M. P. (2009). RNA-guided RNA cleavage by a CRISPR RNA-Cas protein complex. *Cell*, *139*(5), 945–956. https://doi.org/10.1016/j.cell.2009.07.040

Han, J., Pluhackova, K., & Böckmann, R. A. (2017). The Multifaceted Role of SNARE Proteins in Membrane Fusion . In *Frontiers in Physiology* (Vol. 8). https://www.frontiersin.org/articles/10.3389/fphys.2017.00005

Harding, C. R., Egarter, S., Gow, M., Jiménez-Ruiz, E., Ferguson, D. J. P., & Meissner, M. (2016). Gliding Associated Proteins Play Essential Roles during the Formation of the Inner Membrane Complex of Toxoplasma gondii. *PLoS Pathogens*, *12*(2), e1005403. https://doi.org/10.1371/journal.ppat.1005403

Harding, C. R., Gow, M., Kang, J. H., Shortt, E., Manalis, S. R., Meissner, M., & Lourido, S. (2019). Alveolar proteins stabilize cortical microtubules in Toxoplasma gondii. *Nature Communications*, *10*(1), 401. https://doi.org/10.1038/s41467-019-08318-7

Harper, J. M., Huynh, M. H., Coppens, I., Parussini, F., Moreno, S., & Carruthers, V. B. (2006). A cleavable propeptide influences Toxoplasma infection by facilitating the trafficking and secretion of the TgMIC2-M2AP invasion complex. *Molecular Biology of the Cell*, *17*(10), 4551–4563. https://doi.org/10.1091/mbc.E06-01-0064

Hartman, M. A., & Spudich, J. A. (2012). The myosin superfamily at a glance. *Journal of Cell Science*, *125*(7), 1627–1632. https://doi.org/10.1242/jcs.094300

Heaslip, A. T., Nelson, S. R., & Warshaw, D. M. (2016). Dense granule trafficking in Toxoplasma gondii requires a unique class 27 myosin and action filaments. *Molecular Biology of the Cell*, *27*(13), 2080–2089. https://doi.org/10.1091/mbc.E15-12-0824

Heissler, S. M., & Sellers, J. R. (2014). Myosin light chains: Teaching old dogs new tricks. *Bioarchitecture*, *4*(6), 169–188. https://doi.org/10.1080/19490992.2015.1054092

Helms, J. B., & Rothman, J. E. (1992). Inhibition by brefeldin a of a Golgi membrane enzyme that catalyses exchange of guanine nucleotide bound to ARF. *Nature*, *360*(6402), 352–354. https://doi.org/10.1038/360352a0

Herm-Götz, A., Agop-Nersesian, C., Münter, S., Grimley, J. S., Wandless, T. J., Frischknecht, F., & Meissner, M. (2007). Rapid control of protein level in the apicomplexan Toxoplasma gondii. *Nature Methods*, *4*(12), 1003–1005. https://doi.org/10.1038/nmeth1134

Hill, D., & Dubey, J. P. (2002). Toxoplasma gondii: transmission, diagnosis and prevention. *Clinical Microbiology and Infection : The Official Publication of the European Society of Clinical Microbiology and Infectious Diseases*, *8*(10), 634–640. https://doi.org/10.1046/j.1469-0691.2002.00485.x

Hirst, J., Bright, N. A., Rous, B., & Robinson, M. S. (1999). Characterization of a fourth adaptor-related protein complex. *Molecular Biology of the Cell*, *10*(8), 2787–2802. https://doi.org/10.1091/mbc.10.8.2787

Hsu, V. W., Lee, S. Y., & Yang, J. S. (2009). The evolving understanding of COPI vesicle formation. *Nature Reviews Molecular Cell Biology*, *10*(5), 360–364. https://doi.org/10.1038/nrm2663

Hu, K., Roos, D. S., & Murray, J. M. (2002). A novel polymer of tubulin forms the conoid of Toxoplasma gondii. *Journal of Cell Biology*, *156*(6), 1039–1050. https://doi.org/10.1083/jcb.200112086

Hunt, A., Russell, M. R. G., Wagener, J., Kent, R., Carmeille, R., Peddie, C. J., Collinson, L., Heaslip, A., Ward, G. E., & Treeck, M. (2019). Differential requirements for cyclase-associated protein (CAP) in actin-dependent processes of toxoplasma gondii. *ELife*, *8*, e50598. https://doi.org/10.7554/eLife.50598

Hunter, C. A., & Sibley, L. D. (2012). Modulation of innate immunity by Toxoplasma gondii virulence effectors. *Nature Reviews Microbiology*, *10*(11), 766–778. https://doi.org/10.1038/nrmicro2858

Huynh, M. H., & Carruthers, V. B. (2009). Tagging of endogenous genes in a Toxoplasma gondii strain lacking Ku80. *Eukaryotic Cell*, *8*(4), 530–539. https://doi.org/10.1128/EC.00358-08

Itakura, S., Yamakawa, H., Toyoshima, Y. Y., Ishijima, A., Kojima, T., Harada, Y., Yanagida, T., Wakabayashi, T., & Sutoh, K. (1993). Force-generating domain of myosin motor. *Biochemical and Biophysical Research Communications*, *196*(3), 1504–1510. https://doi.org/10.1006/bbrc.1993.2422

Jackson, A. J., Clucas, C., Mamczur, N. J., Ferguson, D. J., & Meissner, M. (2013). Toxoplasma gondii Syntaxin 6 Is Required for Vesicular Transport Between Endosomal-Like Compartments and the Golgi Complex. *Traffic*, *14*(11), 1166–1181. https://doi.org/10.1111/tra.12102

Jacot, D., Daher, W., & Soldati-Favre, D. (2013). Toxoplasma gondii myosin F, an essential motor for centrosomes positioning and apicoplast inheritance. *EMBO Journal*, *32*(12), 1702–1716. https://doi.org/10.1038/emboj.2013.113

Jacot, D., Tosetti, N., Pires, I., Stock, J., Graindorge, A., Hung, Y. F., Han, H., Tewari, R., Kursula, I., & Soldati-Favre, D. (2016). An Apicomplexan Actin-Binding Protein Serves as a Connector and Lipid Sensor to Coordinate Motility and Invasion. *Cell Host and Microbe*, *20*(6), 731–743. https://doi.org/10.1016/j.chom.2016.10.020

Jiménez-Ruiz, E., Wong, E. H., Pall, G. S., & Meissner, M. (2014). Advantages and disadvantages of conditional systems for characterization of essential genes in Toxoplasma gondii. *Parasitology*, *141*(11), 1390–1398. https://doi.org/10.1017/S0031182014000559

Jinek, M., Chylinski, K., Fonfara, I., Hauer, M., Doudna, J. A., & Charpentier, E. (2012). A programmable dual-RNA-guided DNA endonuclease in adaptive bacterial immunity. *Science (New York, N.Y.)*, *337*(6096), 816–821. https://doi.org/10.1126/science.1225829

Jones, J., Lopez, A., & Wilson, M. (2003). Congenital toxoplasmosis. *American Family Physician*, *67*(10), 2131–2138.

Joshua, M., B., G. R., Yolanda, R.-C., Vincent, T., Tadakimi, T., D., R. J., Leslie, G.-C., Simone, S., Isabelle, C., B., C. V., & M., W. L. (2022). Dense Granule Protein GRA64 Interacts with Host Cell ESCRT Proteins during Toxoplasma gondii Infection. *MBio*, *13*(4), e01442-22. https://doi.org/10.1128/mbio.01442-22

Jumper, J., Evans, R., Pritzel, A., Green, T., Figurnov, M., Ronneberger, O., Tunyasuvunakool, K., Bates, R., Žídek, A., Potapenko, A., Bridgland, A., Meyer, C., Kohl, S. A. A., Ballard, A. J., Cowie, A., Romera-Paredes, B., Nikolov, S., Jain, R., Adler, J., … Hassabis, D. (2021). Highly accurate protein structure prediction with AlphaFold. *Nature*, *596*(7873), 583–589. https://doi.org/10.1038/s41586-021-03819-2

Kapoor, P., Chen, M., Winkler, D. D., Luger, K., & Shen, X. (2013). Evidence for monomeric

actin function in INO80 chromatin remodeling. *Nature Structural and Molecular Biology*, *20*(4), 426–432. https://doi.org/10.1038/nsmb.2529

Kessler, H., Herm-Götz, A., Hegge, S., Rauch, M., Soldati-Favre, D., Frischknecht, F., & Meissner, M. (2008). Microneme protein 8 - A new essential invasion factor in Toxoplasma gondii. *Journal of Cell Science*, *121*(7), 947–956. https://doi.org/10.1242/jcs.022350

Kloehn, J., Blume, M., Cobbold, S. A., Saunders, E. C., Dagley, M. J., & McConville, M. J. (2016). Using metabolomics to dissect host–parasite interactions. *Current Opinion in Microbiology*, *32*, 59–65. https://doi.org/10.1016/j.mib.2016.04.019

Kloehn, Joachim, Lunghi, M., Varesio, E., Dubois, D., & Soldati-favre, D. (2021). Untargeted metabolomics uncovers the essential lysine transporter in toxoplasma gondii. *Metabolites*, *11*(8). https://doi.org/10.3390/metabo11080476

Kneussel, M., & Wagner, W. (2013). Myosin motors at neuronal synapses: Drivers of membrane transport and actin dynamics. *Nature Reviews Neuroscience*, *14*(4), 233–247. https://doi.org/10.1038/nrn3445

Konstantinovic, N., Guegan, H., Stäjner, T., Belaz, S., & Robert-Gangneux, F. (2019). Treatment of toxoplasmosis: Current options and future perspectives. *Food and Waterborne Parasitology*, *15*, e00036. https://doi.org/10.1016/j.fawpar.2019.e00036

Koreny, L., Mercado-Saavedra, B. N., Klinger, C. M., Barylyuk, K., Butterworth, S., Hirst, J., Rivera-Cuevas, Y., Zaccai, N. R., Holzer, V. J. C., Klingl, A., Dacks, J. B., Carruthers, V. B., Robinson, M. S., Gras, S., & Waller, R. F. (2022). Stable and ancient endocytic structures navigate the complex pellicle of apicomplexan parasites. *BioRxiv*, 2022.06.02.494549. https://doi.org/10.1101/2022.06.02.494549

Koreny, L., Zeeshan, M., Barylyuk, K., Tromer, E. C., van Hooff, J. J. E. E., Brady, D., Ke, H., Chelaghma, S., Ferguson, D. J. P. P., Eme, L., Tewari, R., & Waller, R. F. (2021). Molecular characterization of the conoid complex in Toxoplasma reveals its conservation in all apicomplexans, including Plasmodium species. *PLoS Biology*, *19*(3), e3001081. https://doi.org/10.1371/journal.pbio.3001081

Kovar, D. R. (2006). Molecular details of formin-mediated actin assembly. *Current Opinion in Cell Biology*, *18*(1), 11–17. https://doi.org/10.1016/j.ceb.2005.12.011

Kremer, K., Kamin, D., Rittweger, E., Wilkes, J., Flammer, H., Mahler, S., Heng, J., Tonkin, C. J., Langsley, G., Hell, S. W., Carruthers, V. B., Ferguson, D. J. P., & Meissner, M. (2013). An Overexpression Screen of Toxoplasma gondii Rab-GTPases Reveals Distinct Transport Routes to the Micronemes. *PLoS Pathogens*, *9*(3), e1003213. https://doi.org/10.1371/journal.ppat.1003213

Krogh, A., Larsson, B., Von Heijne, G., & Sonnhammer, E. L. L. (2001). Predicting transmembrane protein topology with a hidden Markov model: Application to complete genomes. *Journal of Molecular Biology*, *305*(3), 567–580. https://doi.org/10.1006/jmbi.2000.4315

Kühner, S., & Fischer, S. (2011). Structural mechanism of the ATP-induced dissociation of rigor myosin from actin. *Proceedings of the National Academy of Sciences of the United States of America*, *108*(19), 7793–7798. https://doi.org/10.1073/pnas.1018420108

Larson, E. T., Parussini, F., Huynh, M.-H., Giebel, J. D., Kelley, A. M., Zhang, L., Bogyo, M., Merritt, E. A., & Carruthers, V. B. (2009). Toxoplasma gondii cathepsin L is the primary target of the invasion-inhibitory compound morpholinurea-leucyl-homophenyl-vinyl sulfone phenyl. *The Journal of Biological Chemistry*, *284*(39), 26839–26850. https://doi.org/10.1074/jbc.M109.003780

Lebrun, M., Michelin, A., El Hajj, H., Poncet, J. J., Bradley, P. J., Vial, H., & Dubremetz, J. F. (2005). The rhoptry neck protein RON4 re-localizes at the moving junction during Toxoplasma gondii invasion. *Cellular Microbiology*, *7*(12), 1823–1833. https://doi.org/10.1111/j.1462-5822.2005.00646.x

Lee, M. C. S., Miller, E. A., Goldberg, J., Orci, L., & Schekman, R. (2004). Bi-directional protein transport between the ER and Golgi. *Annual Review of Cell and Developmental Biology*, *20*, 87–123. https://doi.org/10.1146/annurev.cellbio.20.010403.105307

Lee, S., Park, H., Kyung, T., Kim, N. Y., Kim, S., Kim, J., & Heo, W. Do. (2014). Reversible protein inactivation by optogenetic trapping in cells. *Nature Methods*, *11*(6), 633–636. https://doi.org/10.1038/nmeth.2940

Lentini, G., Ben Chaabene, R., Vadas, O., Ramakrishnan, C., Mukherjee, B., Mehta, V., Lunghi, M., Grossmann, J., Maco, B., Visentin, R., Hehl, A. B., Korkhov, V. M., & Soldati-Favre, D. (2021). Structural insights into an atypical secretory pathway kinase

crucial for Toxoplasma gondii invasion. *Nature Communications*, *12*(1), 3788. https://doi.org/10.1038/s41467-021-24083-y

Leung, J. M., He, Y., Zhang, F., Hwang, Y.-C. C., Nagayasu, E., Liu, J., Murray, J. M., & Hu, K. (2017). Stability and function of a putative microtubule-organizing center in the human parasite Toxoplasma gondii. *Molecular Biology of the Cell*, *28*(10), 1361–1378. https://doi.org/10.1091/mbc.E17-01-0045

Li, W., Grech, J., Stortz, J. F., Gow, M., Periz, J., Meissner, M., & Jimenez-Ruiz, E. (2022). A splitCas9 phenotypic screen in Toxoplasma gondii identifies proteins involved in host cell egress and invasion. *Nature Microbiology*, *7*(6), 882–895. https://doi.org/10.1038/s41564-022-01114-y

Lima, T. S., & Lodoen, M. B. (2019). Mechanisms of human innate immune evasion by Toxoplasma gondii. *Frontiers in Cellular and Infection Microbiology*, *9*(MAR), 103. https://doi.org/10.3389/fcimb.2019.00103

Liu, J., Pace, D., Dou, Z., King, T. P., Guidot, D., Li, Z. H., Carruthers, V. B., & Moreno, S. N. J. (2014). A vacuolar-H+-pyrophosphatase (TgVP1) is required for microneme secretion, host cell invasion, and extracellular survival of Toxoplasma gondii. *Molecular Microbiology*, *93*(4), 698–712. https://doi.org/10.1111/mmi.12685

Lourido, S., Tang, K., & David Sibley, L. (2012). Distinct signalling pathways control Toxoplasma egress and host-cell invasion. *EMBO Journal*, *31*(24), 4524–4534. https://doi.org/10.1038/emboj.2012.299

MacRae, J. I., Sheiner, L., Nahid, A., Tonkin, C., Striepen, B., & McConville, M. J. (2012). Mitochondrial metabolism of glucose and glutamine is required for intracellular growth of toxoplasma gondii. *Cell Host and Microbe*, *12*(5), 682–692. https://doi.org/10.1016/j.chom.2012.09.013

Mallo, N., Ovciarikova, J., Martins-Duarte, E. S., Baehr, S. C., Biddau, M., Wilde, M. L., Uboldi, A. D., Lemgruber, L., Tonkin, C. J., Wideman, J. G., Harding, C. R., & Sheiner, L. (2021). Depletion of a toxoplasma porin leads to defects in mitochondrial morphology and contacts with the endoplasmic reticulum. *Journal of Cell Science*, *134*(20). https://doi.org/10.1242/jcs.255299

Mann, T., & Beckers, C. (2001). Characterization of the subpellicular network, a filamentous membrane skeletal component in the parasite Toxoplasma gondii. *Molecular and*

Biochemical Parasitology, *115*(2), 257–268. https://doi.org/10.1016/s0166-6851(01)00289-4

Marilyn, P., Anuradha, K., E., F. J., & Amy, D. (2007). Protein Trafficking to the Apicoplast: Deciphering the Apicomplexan Solution to Secondary Endosymbiosis. *Eukaryotic Cell*, *6*(7), 1081–1088. https://doi.org/10.1128/EC.00102-07

Matoba, K., Kotani, T., Tsutsumi, A., Tsuji, T., Mori, T., Noshiro, D., Sugita, Y., Nomura, N., Iwata, S., Ohsumi, Y., Fujimoto, T., Nakatogawa, H., Kikkawa, M., & Noda, N. N. (2020). Atg9 is a lipid scramblase that mediates autophagosomal membrane expansion. *Nature Structural and Molecular Biology*, *27*(12), 1185–1193. https://doi.org/10.1038/s41594-020-00518-w

Mattera, R., Park, S. Y., De Pace, R., Guardia, C. M., & Bonifacino, J. S. (2017). AP-4 mediates export of ATG9A from the trans-Golgi network to promote autophagosome formation. *Proceedings of the National Academy of Sciences of the United States of America*, *114*(50), E10697–E10706. https://doi.org/10.1073/pnas.1717327114

Mazumdar, J., Wilson, E. H., Masek, K., Hunter, C. A., & Striepen, B. (2006). Apicoplast fatty acid synthesis is essential for organelle biogenesis and parasite survival in Toxoplasma gondii. *Proceedings of the National Academy of Sciences of the United States of America*, *103*(35), 13192–13197. https://doi.org/10.1073/pnas.0603391103

McAuley, J. B. (2014). Congenital toxoplasmosis. *Journal of the Pediatric Infectious Diseases Society*, *3*(SUPPL1), S30-5. https://doi.org/10.1093/jpids/piu077

McGovern, O. L., Rivera-Cuevas, Y., Kannan, G., Narwold, A. J., & Carruthers, V. B. (2018). Intersection of endocytic and exocytic systems in Toxoplasma gondii. *Traffic*, *19*(5), 336–353. https://doi.org/10.1111/tra.12556

Mehta, S., & Sibley, L. D. (2011). Actin depolymerizing factor controls actin turnover and gliding motility in Toxoplasma gondii. *Molecular Biology of the Cell*, *22*(8), 1290–1299. https://doi.org/10.1091/mbc.E10-12-0939

Meissner, M., Schlüter, D., & Soldati, D. (2002). Role of Toxoplasma gondii myosin a in powering parasite gliding and host cell invasion. *Science*, *298*(5594), 837–840. https://doi.org/10.1126/science.1074553

Mercier, C., Dubremetz, J. F., Rauscher, B., Lecordier, L., Sibley, L. D., & Cesbron-Delauw,

M. F. (2002). Biogenesis of nanotubular network in Toxoplasma parasitophorous vacuole induced by parasite proteins. *Molecular Biology of the Cell*, *13*(7), 2397–2409. https://doi.org/10.1091/mbc.E02-01-0021

Mermall, V., Post, P. L., & Mooseker, M. S. (1998). Unconventional Myosins in Cell Movement, Membrane Traffic, and Signal Transduction. *Science*, *279*(5350), 527–533. https://doi.org/10.1126/science.279.5350.527

Miranda, K., Pace, D. A., Cintron, R., Rodrigues, J. C. F., Fang, J., Smith, A., Rohloff, P., Coelho, E., De Haas, F., De Souza, W., Coppens, I., Sibley, L. D., & Moreno, S. N. J. (2010). Characterization of a novel organelle in Toxoplasma gondii with similar composition and function to the plant vacuole. *Molecular Microbiology*, *76*(6), 1358–1375. https://doi.org/10.1111/j.1365-2958.2010.07165.x

Moon, A., & Drubin, D. G. (1995). The ADF/cofilin proteins: stimulus-responsive modulators of actin dynamics. *Molecular Biology of the Cell*, *6*(11), 1423–1431. https://doi.org/10.1091/mbc.6.11.1423

Morlon-Guyot, J., El Hajj, H., Martin, K., Fois, A., Carrillo, A., Berry, L., Burchmore, R., Meissner, M., Lebrun, M., & Daher, W. (2018). A proteomic analysis unravels novel CORVET and HOPS proteins involved in Toxoplasma gondii secretory organelles biogenesis. *Cellular Microbiology*, *20*(11). https://doi.org/10.1111/cmi.12870

Morlon-Guyot, J., Pastore, S., Berry, L., Lebrun, M., & Daher, W. (2015). Toxoplasma gondii Vps11, a subunit of HOPS and CORVET tethering complexes, is essential for the biogenesis of secretory organelles. *Cellular Microbiology*, *17*(8), 1157–1178. https://doi.org/10.1111/cmi.12426

Morrissette, N. S., Murray, J. M., & Roos, D. S. (1997). Subpellicular microtubules associate with an intramembranous particle lattice in the protozoan parasite Toxoplasma gondii. *Journal of Cell Science*, *110*(1), 35–42. https://doi.org/10.1242/jcs.110.1.35

Morrissette, N. S., & Sibley, L. D. (2002a). Cytoskeleton of Apicomplexan Parasites. *Microbiology and Molecular Biology Reviews*, *66*(1), 21–38. https://doi.org/10.1128/mmbr.66.1.21-38.2002

Morrissette, N. S., & Sibley, L. D. (2002b). Disruption of microtubules uncouples budding and nuclear division in Toxoplasma gondii. *Journal of Cell Science*, *115*(Pt 5), 1017–1025. https://doi.org/10.1242/jcs.115.5.1017

Mullins, R. D., Stafford, W. F., & Pollard, T. D. (1997). Structure, subunit topology, and actin-binding activity of the Arp2/3 complex from Acanthamoeba. *The Journal of Cell Biology*, *136*(2), 331–343. https://doi.org/10.1083/jcb.136.2.331

Munera Lopez, J., Tengganu, I. F., Liu, J., Murray, J. M., Arias Padilla, L. F., Zhang, Y., Brown, P. T., Florens, L., & Hu, K. (2022). An apical protein, Pcr2, is required for persistent movement by the human parasite Toxoplasma gondii. *PLoS Pathogens*, *18*(8), e1010776. https://doi.org/10.1371/journal.ppat.1010776

Munson, M. (2009). Tip20p reaches out to Dsl1p to tether membranes. *Nature Structural and Molecular Biology*, *16*(2), 100–102. https://doi.org/10.1038/nsmb0209-100

Nair, S. C., Brooks, C. F., Goodman, C. D., Strurm, A., McFadden, G. I., Sundriyal, S., Anglin, J. L., Song, Y., Moreno, S. N. J., & Striepen, B. (2011). Apicoplast isoprenoid precursor synthesis and the molecular basis of fosmidomycin resistance in Toxoplasma gondii. *Journal of Experimental Medicine*, *208*(7), 1547–1559. https://doi.org/10.1084/jem.20110039

Nguyen, H. M., El Hajj, H., El Hajj, R., Tawil, N., Berry, L., Lebrun, M., Bordat, Y., & Besteiro, S. (2017). Toxoplasma gondii autophagy-related protein ATG9 is crucial for the survival of parasites in their host. *Cellular Microbiology*, *19*(6). https://doi.org/10.1111/cmi.12712

Nichols, B. A., & Chiappino, M. L. (1987). Cytoskeleton of Toxoplasma gondii. *The Journal of Protozoology*, *34*(2), 217–226. https://doi.org/10.1111/j.1550-7408.1987.tb03162.x

Niedelman, W., Gold, D. A., Rosowski, E. E., Sprokholt, J. K., Lim, D., Arenas, A. F., Melo, M. B., Spooner, E., Yaffe, M. B., & Saeij, J. P. J. (2012). The rhoptry proteins ROP18 and ROP5 mediate Toxoplasma gondii evasion of the murine, but not the human, interferon-gamma response. *PLoS Pathogens*, *8*(6), e1002784. https://doi.org/10.1371/journal.ppat.1002784

Nihongaki, Y., Kawano, F., Nakajima, T., & Sato, M. (2015). Photoactivatable CRISPR-Cas9 for optogenetic genome editing. *Nature Biotechnology*, *33*(7), 755–760. https://doi.org/10.1038/nbt.3245

Nishi, M., Hu, K., Murray, J. M., & Roos, D. S. (2008). Organellar dynamics during the cell cycle of Toxoplasma gondii. *Journal of Cell Science*, *121*(9), 1559–1568. https://doi.org/10.1242/jcs.021089

Oda, T., Iwasa, M., Aihara, T., Maéda, Y., & Narita, A. (2009). The nature of the globular- to fibrous-actin transition. *Nature*, *457*(7228), 441–445. https://doi.org/10.1038/nature07685

Odronitz, F., & Kollmar, M. (2007). Drawing the tree of eukaryotic life based on the analysis of 2,269 manually annotated myosins from 328 species. *Genome Biology*, *8*(9), R196. https://doi.org/10.1186/gb-2007-8-9-r196

Opitz, C., Di Cristina, M., Reiss, M., Ruppert, T., Crisanti, A., & Soldati, D. (2002). Intramembrane cleavage of microneme proteins at the surface of the apicomplexan parasite Toxoplasma gondii. *The EMBO Journal*, *21*(7), 1577–1585. https://doi.org/10.1093/emboj/21.7.1577

Ovciarikova, J., Lemgruber, L., Stilger, K. L., Sullivan, W. J., & Sheiner, L. (2017). Mitochondrial behaviour throughout the lytic cycle of Toxoplasma gondii. *Scientific Reports*, *7*, 42746. https://doi.org/10.1038/srep42746

Parisis, N., Krasinska, L., Harker, B., Urbach, S., Rossignol, M., Camasses, A., Dewar, J., Morin, N., & Fisher, D. (2017). Initiation of DNA replication requires actin dynamics and formin activity . *The EMBO Journal*, *36*(21), 3212–3231. https://doi.org/10.15252/embj.201796585

Park, Y. H., & Nam, H. W. (2013). Clinical features and treatment of ocular toxoplasmosis. *Korean Journal of Parasitology*, *51*(4), 393–399. https://doi.org/10.3347/kjp.2013.51.4.393

Parussini, F., Coppens, I., Shah, P. P., Diamond, S. L., & Carruthers, V. B. (2010). Cathepsin L occupies a vacuolar compartment and is a protein maturase within the endo/exocytic system of Toxoplasma gondii. *Molecular Microbiology*, *76*(6), 1340–1357. https://doi.org/10.1111/j.1365-2958.2010.07181.x

Pearce, C. S., & Heaslip, A. T. (2022). No Determining the Role of a Golgi-Localized Protein in the Secretory Pathway of T. gondii. *Poster Presentation at MPMXXXIII, 18-22 September*. https://www.parasitesrule.com/mpm-xxxiii/mpmabstractbook

Peng, D., & Tarleton, R. (2015). Eupagdt: A web tool tailored to design crispr guide rnas for eukaryotic pathogens. *Microbial Genomics*, *1*(4), e000033–e000033. https://doi.org/10.1099/MGEN.0.000033

Periz, J., Del Rosario, M., McStea, A., Gras, S., Loney, C., Wang, L., Martin-Fernandez, M. L., & Meissner, M. (2019). A highly dynamic F-actin network regulates transport and recycling of micronemes in Toxoplasma gondii vacuoles. *Nature Communications*, *10*(1), 4183. https://doi.org/10.1038/s41467-019-12136-2

Periz, J., Whitelaw, J., Harding, C., Gras, S., Minina, M. I. D. R., Latorre-Barragan, F., Lemgruber, L., Reimer, M. A., Insall, R., Heaslip, A., & Meissner, M. (2017). Toxoplasma gondii F-actin forms an extensive filamentous network required for material exchange and parasite maturation. *ELife*, *6*. https://doi.org/10.7554/eLife.24119

Pfluger, S. L., Goodson, H. V., Moran, J. M., Ruggiero, C. J., Ye, X., Emmons, K. M., & Hager, K. M. (2005). Receptor for retrograde transport in the apicomplexan parasite Toxoplasma gondii. *Eukaryotic Cell*, *4*(2), 432–442. https://doi.org/10.1128/EC.4.2.432-442.2005

Pieperhoff, M. S., Pall, G. S., Jiménez-Ruiz, E., Das, S., Melatti, C., Gow, M., Wong, E. H., Heng, J., Müller, S., Blackman, M. J., & Meissner, M. (2015). Conditional U1 gene silencing in Toxoplasma gondii. *PLoS ONE*, *10*(6), e0130356. https://doi.org/10.1371/journal.pone.0130356

Pieperhoff, M. S., Schmitt, M., Ferguson, D. J. P., & Meissner, M. (2013). The Role of Clathrin in Post-Golgi Trafficking in Toxoplasma gondii. *PLoS ONE*, *8*(10), e77620. https://doi.org/10.1371/journal.pone.0077620

Plattner, F., Yarovinsky, F., Romero, S., Didry, D., Carlier, M. F., Sher, A., & Soldati-Favre, D. (2008). Toxoplasma Profilin Is Essential for Host Cell Invasion and TLR11-Dependent Induction of an Interleukin-12 Response. *Cell Host and Microbe*, *3*(2), 77–87. https://doi.org/10.1016/j.chom.2008.01.001

Plessner, M., Melak, M., Chinchilla, P., Baarlink, C., & Grosse, R. (2015). Nuclear F-actin formation and reorganization upon cell spreading. *Journal of Biological Chemistry*, *290*(18), 11209–11216. https://doi.org/10.1074/jbc.M114.627166

Pollard, T. D. (2016). Actin and actin-binding proteins. *Cold Spring Harbor Perspectives in Biology*, *8*(8). https://doi.org/10.1101/cshperspect.a018226

Pollard, T. D., & Borisy, G. G. (2003). Cellular motility driven by assembly and disassembly of actin filaments. *Cell*, *112*(4), 453–465. https://doi.org/10.1016/S0092-

8674(03)00120-X

Pollard, T. D., & Cooper, J. A. (2009). Actin, a central player in cell shape and movement. *Science (New York, N.Y.)*, *326*(5957), 1208–1212. https://doi.org/10.1126/science.1175862

Polstein, L. R., & Gersbach, C. A. (2015). A light-inducible CRISPR-Cas9 system for control of endogenous gene activation. *Nature Chemical Biology*, *11*(3), 198–200. https://doi.org/10.1038/nchembio.1753

Poupel, O., & Tardieux, I. (1999). Toxoplasma gondii motility and host cell invasiveness are drastically impaired by jasplakinolide, a cyclic peptide stabilizing F-actin. *Microbes and Infection*, *1*(9), 653–662. https://doi.org/https://doi.org/10.1016/S1286-4579(99)80066-5

Prasad, A., Mastud, P., & Patankar, S. (2021). Dually localised proteins found in both the apicoplast and mitochondrion utilize the Golgi-dependent pathway for apicoplast targeting in Toxoplasma gondii. *Biology of the Cell*, *113*(1), 58–78. https://doi.org/10.1111/boc.202000050

Pruyne, D., Evangelista, M., Yang, C., Bi, E., Zigmond, S., Bretscher, A., & Boone, C. (2002). Role of Formins in Actin Assembly: Nucleation and Barbed-End Association. *Science*, *297*(5581), 612–615. https://doi.org/10.1126/science.1072309

Pucadyil, T. J., & Schmid, S. L. (2009). Conserved functions of membrane active GTPases in coated vesicle formation. *Science (New York, N.Y.)*, *325*(5945), 1217–1220. https://doi.org/10.1126/science.1171004

Quinlan, M. E., Heuser, J. E., Kerkhoff, E., & Mullins, R. D. (2005). Drosophila Spire is an actin nucleation factor. *Nature*, *433*(7024), 382–388. https://doi.org/10.1038/nature03241

Ren, J., Wen, L., Gao, X., Jin, C., Xue, Y., & Yao, X. (2009). DOG 1.0: illustrator of protein domain structures. In *Cell research* (Vol. 19, Issue 2, pp. 271–273). https://doi.org/10.1038/cr.2009.6

Robert-Gangneux, F., & Dardé, M.-L. (2012). Epidemiology of and diagnostic strategies for toxoplasmosis. *Clinical Microbiology Reviews*, *25*(2), 264–296. https://doi.org/10.1128/CMR.05013-11

Rohn, W. M., Rouillé, Y., Waguri, S., & Hoflack, B. (2000). Bi-directional trafficking between the trans-Golgi network and the endosomal/lysosomal system. *Journal of Cell Science*, *113 (Pt 1*, 2093–2101. https://doi.org/10.1242/jcs.113.12.2093

Romero, S., Le Clainche, C., Didry, D., Egile, C., Pantaloni, D., & Carlier, M.-F. (2004). Formin is a processive motor that requires profilin to accelerate actin assembly and associated ATP hydrolysis. *Cell*, *119*(3), 419–429. https://doi.org/10.1016/j.cell.2004.09.039

Ruggiero, M. A., Gordon, D. P., Orrell, T. M., Bailly, N., Bourgoin, T., Brusca, R. C., Cavalier-Smith, T., Guiry, M. D., & Kirk, P. M. (2015). A Higher Level Classification of All Living Organisms. *PLOS ONE*, *10*(4), e0119248. https://doi.org/10.1371/journal.pone.0119248

Russell, D. G., & Burns, R. G. (1984). The polar ring of coccidian sporozoites: a unique microtubule-organizing centre. *Journal of Cell Science*, *65*, 193–207. https://doi.org/10.1242/jcs.65.1.193

Sagot, I., Rodal, A. A., Moseley, J., Goode, B. L., & Pellman, D. (2002). An actin nucleation mechanism mediated by Bni1 and profilin. *Nature Cell Biology*, *4*(8), 626–631. https://doi.org/10.1038/ncb834

Sahoo, N., Beatty, W., Heuser, J., Sept, D., & Sibley, L. D. (2005). Unusual Kinetic and Structural Properties Control Rapid Assembly and Turnover of Actin in the Parasite Toxoplasma gondii. *Molecular Biology of the Cell*, *17*(2), 895–906. https://doi.org/10.1091/mbc.e05-06-0512

Sakura, T., Sindikubwabo, F., Oesterlin, L. K., Bousquet, H., Slomianny, C., Hakimi, M. A., Langsley, G., & Tomavo, S. (2016). A Critical Role for Toxoplasma gondii Vacuolar Protein Sorting VPS9 in Secretory Organelle Biogenesis and Host Infection. *Scientific Reports*, *6*, 38842. https://doi.org/10.1038/srep38842

Schiavon, C. R., Zhang, T., Zhao, B., Moore, A. S., Wales, P., Andrade, L. R., Wu, M., Sung, T. C., Dayn, Y., Feng, J. W., Quintero, O. A., Shadel, G. S., Grosse, R., & Manor, U. (2020). Actin chromobody imaging reveals sub-organellar actin dynamics. *Nature Methods*, *17*(9), 917–921. https://doi.org/10.1038/s41592-020-0926-5

Schindelin, J., Arganda-Carreras, I., Frise, E., Kaynig, V., Longair, M., Pietzsch, T., Preibisch, S., Rueden, C., Saalfeld, S., Schmid, B., Tinevez, J. Y., White, D. J.,

Hartenstein, V., Eliceiri, K., Tomancak, P., & Cardona, A. (2012). Fiji: An open-source platform for biological-image analysis. *Nature Methods*, *9*(7), 676–682. https://doi.org/10.1038/nmeth.2019

Schlacht, A., Herman, E. K., Klute, M. J., Field, M. C., & Dacks, J. B. (2014). Missing pieces of an ancient puzzle: evolution of the eukaryotic membrane-trafficking system. *Cold Spring Harbor Perspectives in Biology*, *6*(10), a016048. https://doi.org/10.1101/cshperspect.a016048

Schmid, S. L. (1997). Clathrin-coated vesicle formation and protein sorting: an integrated process. *Annual Review of Biochemistry*, *66*, 511–548. https://doi.org/10.1146/annurev.biochem.66.1.511

Sciaky, N., Presley, J., Smith, C., Zaal, K. J. M., Cole, N., Moreira, J. E., Terasaki, M., Siggia, E., & Lippincott-Schwartz, J. (1997). Golgi tubule traffic and the effects of brefeldin A visualized in living cells. *Journal of Cell Biology*, *139*(5), 1137–1155. https://doi.org/10.1083/jcb.139.5.1137

Sellers, J. R. (2000). Myosins: A diverse superfamily. *Biochimica et Biophysica Acta - Molecular Cell Research*, *1496*(1), 3–22. https://doi.org/10.1016/S0167-4889(00)00005-7

Serpeloni, M., Jiménez-Ruiz, E., Vidal, N. M., Kroeber, C., Andenmatten, N., Lemgruber, L., Mörking, P., Pall, G. S., Meissner, M., & Ávila, A. R. (2016). UAP56 is a conserved crucial component of a divergent mRNA export pathway in Toxoplasma gondii. *Molecular Microbiology*, *102*(4), 672–689. https://doi.org/10.1111/mmi.13485

Sheffield, H. G., & Melton, M. L. (1968). The fine structure and reproduction of Toxoplasma gondii. *The Journal of Parasitology*, *54*(2), 209–226. https://doi.org/10.2307/3276925

Sheiner, L., Demerly, J. L., Poulsen, N., Beatty, W. L., Lucas, O., Behnke, M. S., White, M. W., & Striepen, B. (2011). A Systematic Screen to Discover and Analyze Apicoplast Proteins Identifies a Conserved and Essential Protein Import Factor. *PLOS Pathogens*, *7*(12), e1002392. https://doi.org/10.1371/journal.ppat.1002392

Shen, B., Brown, K. M., Lee, T. D., & Sibley, L. D. (2014). Efficient gene disruption in diverse strains of Toxoplasma gondii using CRISPR/CAS9. *MBio*, *5*(3), e01114-14. https://doi.org/10.1128/mBio.01114-14

Sibley, L. D., Khan, A., Ajioka, J. W., & Rosenthal, B. M. (2009). Genetic diversity of Toxoplasma gondii in animals and humans. *Philosophical Transactions of the Royal Society of London. Series B, Biological Sciences*, *364*(1530), 2749–2761. https://doi.org/10.1098/rstb.2009.0087

Sidik, S. M., Hackett, C. G., Tran, F., Westwood, N. J., & Lourido, S. (2014). Efficient Genome Engineering of Toxoplasma gondii Using CRISPR/Cas9. *PLOS ONE*, *9*(6), e100450. https://doi.org/10.1371/journal.pone.0100450

Sidik, S. M., Huet, D., Ganesan, S. M., Huynh, M. H., Wang, T., Nasamu, A. S., Thiru, P., Saeij, J. P. J., Carruthers, V. B., Niles, J. C., & Lourido, S. (2016). A Genome-wide CRISPR Screen in Toxoplasma Identifies Essential Apicomplexan Genes. *Cell*, *166*(6), 1423-1435.e12. https://doi.org/10.1016/j.cell.2016.08.019

Sidik, S. M., Huet, D., & Lourido, S. (2018). CRISPR-Cas9-based genome-wide screening of toxoplasma gondii. *Nature Protocols*, *13*(1), 307–323. https://doi.org/10.1038/nprot.2017.131

Sievers, F., Wilm, A., Dineen, D., Gibson, T. J., Karplus, K., Li, W., Lopez, R., McWilliam, H., Remmert, M., Söding, J., Thompson, J. D., & Higgins, D. G. (2011). Fast, scalable generation of high-quality protein multiple sequence alignments using Clustal Omega. *Molecular Systems Biology*, *7*(1), 539. https://doi.org/10.1038/msb.2011.75

Sinai, A. P., & Joiner, K. A. (2001). The Toxoplasma gondii protein ROP2 mediates host organelle association with the parasitophorous vacuole membrane. *The Journal of Cell Biology*, *154*(1), 95–108. https://doi.org/10.1083/jcb.200101073

Singer, M., Simon, K., Forné, I., & Meissner, M. (2023). A central CRMP complex essential for invasion in Toxoplasma gondii. *PLOS Biology 21(1):* e3001937. https://doi.org/10.1371/journal.pbio.3001937

Skillman, K. M., Daher, W., Ma, C. I., Soldati-Favre, D., & Sibley, L. D. (2012). Toxoplasma gondii profilin acts primarily to sequester G-actin while formins efficiently nucleate actin filament formation in vitro. *Biochemistry*, *51*(12), 2486–2495. https://doi.org/10.1021/bi201704y

Skillman, K. M., Diraviyam, K., Khan, A., Tang, K., Sept, D., & Sibley, L. D. (2011). Evolutionarily Divergent, Unstable Filamentous Actin Is Essential for Gliding Motility in Apicomplexan Parasites. *PLOS Pathogens*, *7*(10), e1002280.

https://doi.org/10.1371/journal.ppat.1002280

Skillman, K. M., Ma, C. I., Fremont, D. H., Diraviyam, K., Cooper, J. A., Sept, D., & Sibley, L. D. (2013). The unusual dynamics of parasite actin result from isodesmic polymerization. *Nature Communications*, *4*(1), 2285. https://doi.org/10.1038/ncomms3285

Sladewski, T. E., & Heaslip, A. T. (2022). Reconstituting actomyosin dynamics in T. gondii from recombinantly purified actin and myosin F. *Oral Presentation at MPMXXXIII, 18-22 September*. https://www.parasitesrule.com/mpm-xxxiii/mpmabstractbook

Sloves, P. J., Delhaye, S., Mouveaux, T., Werkmeister, E., Slomianny, C., Hovasse, A., Dilezitoko Alayi, T., Callebaut, I., Gaji, R. Y., Schaeffer-Reiss, C., Van Dorsselear, A., Carruthers, V. B., & Tomavo, S. (2012). Toxoplasma sortilin-like receptor regulates protein transport and is essential for apical secretory organelle biogenesis and host infection. *Cell Host and Microbe*, *11*(5), 515–527. https://doi.org/10.1016/j.chom.2012.03.006

Smith, C. J., & Pearse, B. M. F. (1999). Clathrin: anatomy of a coat protein. *Trends in Cell Biology*, *9*(9), 335–338. https://doi.org/10.1016/S0962-8924(99)01631-1

Smith, D., Kannan, G., Coppens, I., Wang, F., Nguyen, H. M., Cerutti, A., Olafsson, E. B., Rimple, P. A., Schultz, T. L., Soto, N. M. M., Di Cristina, M., Besteiro, S., & Carruthers, V. B. (2021). Toxoplasma tgatg9 is critical for autophagy and long-term persistence in tissue cysts. *ELife*, *10*, e59384. https://doi.org/10.7554/ELIFE.59384

Smith, T. A., Lopez-Perez, G. S., Herneisen, A. L., Shortt, E., & Lourido, S. (2022). Screening the Toxoplasma kinome with high-throughput tagging identifies a regulator of invasion and egress. *Nature Microbiology*, *7*(6), 868–881. https://doi.org/10.1038/s41564-022-01104-0

Söding, J., Biegert, A., & Lupas, A. N. (2005). The HHpred interactive server for protein homology detection and structure prediction. *Nucleic Acids Research*, *33*(SUPPL. 2), W244-8. https://doi.org/10.1093/nar/gki408

Soldati, D., Dubremetz, J. F., & Lebrun, M. (2001). Microneme proteins: Structural and functional requirements to promote adhesion and invasion by the apicomplexan parasite Toxoplasma gondii. *International Journal for Parasitology*, *31*(12), 1293–1302. https://doi.org/10.1016/S0020-7519(01)00257-0

Sparvoli, D., Delabre, J., Penarete-Vargas, D. M., Kumar Mageswaran, S., Tsypin, L. M., Heckendorn, J., Theveny, L., Maynadier, M., Mendonça Cova, M., Berry-Sterkers, L., Guérin, A., Dubremetz, J.-F., Urbach, S., Striepen, B., Turkewitz, A. P., Chang, Y.-W., & Lebrun, M. (2022). An apical membrane complex for triggering rhoptry exocytosis and invasion in Toxoplasma. *The EMBO Journal*, e111158. https://doi.org/10.15252/embj.2022111158

Speer, C. A., Clark, S., & Dubey, J. P. (1998). Ultrastructure of the oocysts, sporocysts, and sporozoites of Toxoplasma gondii. *Journal of Parasitology*, *84*(3), 505–512. https://doi.org/10.2307/3284713

Stadler, R. V, Nelson, S. R., Warshaw, D. M., & Ward, G. E. (2022). A circular zone of attachment to the extracellular matrix acts as a guidance system for Toxoplasma gondii 3D motility. *BioRxiv*, 2022.06.08.495400. https://doi.org/10.1101/2022.06.08.495400

Stasic, A. J., Chasen, N. M., Dykes, E. J., Vella, S. A., Asady, B., Starai, V. J., & Moreno, S. N. J. (2019). The Toxoplasma Vacuolar H+-ATPase Regulates Intracellular pH and Impacts the Maturation of Essential Secretory Proteins. *Cell Reports*, *27*(7), 2132-2146.e7. https://doi.org/10.1016/j.celrep.2019.04.038

Stasic, A. J., Moreno, S. N. J., Carruthers, V. B., & Dou, Z. (2022). The Toxoplasma plant-like vacuolar compartment (PLVAC). *The Journal of Eukaryotic Microbiology*, e12951. https://doi.org/10.1111/jeu.12951

Stenmark, H. (2009). Rab GTPases as coordinators of vesicle traffic. *Nature Reviews Molecular Cell Biology*, *10*(8), 513–525. https://doi.org/10.1038/nrm2728

Stortz, J. F., Del Rosario, M., Singer, M., Wilkes, J. M., Meissner, M., & Das, S. (2019). Formin-2 drives polymerisation of actin filaments enabling segregation of apicoplasts and cytokinesis in Plasmodium Falciparum. *ELife*, *8*. https://doi.org/10.7554/eLife.49030

Straub, K. W., Peng, E. D., Hajagos, B. E., Tyler, J. S., & Bradley, P. J. (2011). The Moving Junction Protein RON8 Facilitates Firm Attachment and Host Cell Invasion in Toxoplasma gondii. *PLOS Pathogens*, *7*(3), e1002007. https://doi.org/10.1371/journal.ppat.1002007

Striepen, B. (2013). Time to tackle cryptosporidiosis. *Nature*, *503*(7475), 189–191. https://doi.org/10.1038/503189a

Striepen, B., Crawford, M. J., Shaw, M. K., Tilney, L. G., Seeber, F., & Roos, D. S. (2000). The plastid of Toxoplasma gondii is divided by association with the centrosomes. *Journal of Cell Biology*, *151*(7), 1423–1434. https://doi.org/10.1083/jcb.151.7.1423

Suss-Toby, E., Zimmerberg, J., & Ward, G. E. (1996). Toxoplasma invasion: the parasitophorous vacuole is formed from host cell plasma membrane and pinches off via a fission pore. *Proceedings of the National Academy of Sciences*, *93*(16), 8413–8418. https://doi.org/10.1073/pnas.93.16.8413

Szklarczyk, D., Franceschini, A., Kuhn, M., Simonovic, M., Roth, A., Minguez, P., Doerks, T., Stark, M., Muller, J., Bork, P., Jensen, L. J., & Von Mering, C. (2011). The STRING database in 2011: Functional interaction networks of proteins, globally integrated and scored. *Nucleic Acids Research*, *39*(SUPPL. 1), D561-8. https://doi.org/10.1093/nar/gkq973

Thornton, L. B., Teehan, P., Floyd, K., Cochrane, C., Bergmann, A., Riegel, B., Stasic, A. J., Di Cristina, M., Moreno, S. N. J., Roepe, P. D., & Dou, Z. (2019). An ortholog of Plasmodium falciparum chloroquine resistance transporter (PfCRT) plays a key role in maintaining the integrity of the endolysosomal system in toxoplasma gondii to facilitate host invasion. *PLoS Pathogens*, *15*(6). https://doi.org/10.1371/journal.ppat.1007775

Tomova, C., Humbel, B. M., Geerts, W. J. C., Entzeroth, R., Holthuis, J. C. M., & Verkleij, A. J. (2009). Membrane contact sites between apicoplast and ER in Toxoplasma gondii revealed by electron tomography. *Traffic (Copenhagen, Denmark)*, *10*(10), 1471–1480. https://doi.org/10.1111/j.1600-0854.2009.00954.x

Tosetti, N., Pacheco, N. D. S., Favre, D. S., & Jacot, D. (2019). Three f-actin assembly centers regulate organelle inheritance, cell-cell communication and motility in toxoplasma gondii. *ELife*, *8*. https://doi.org/10.7554/eLife.42669

Tosetti, N., Pacheco, N. dos S., Bertiaux, E., Maco, B., Bournonville, L., Hamel, V., Guichard, P., & Soldati-Favre, D. (2020). Essential function of the alveolin network in the subpellicular microtubules and conoid assembly in Toxoplasma gondii. *ELife*, *9*, 1–22. https://doi.org/10.7554/eLife.56635

Tyanova, S., Temu, T., Sinitcyn, P., Carlson, A., Hein, M. Y., Geiger, T., Mann, M., & Cox, J. (2016). The Perseus computational platform for comprehensive analysis of (prote)omics data. *Nature Methods*, *13*(9), 731–740.

https://doi.org/10.1038/nmeth.3901

Van Dooren, G. G., Kennedy, A. T., & McFadden, G. I. (2012). The use and abuse of heme in apicomplexan parasites. *Antioxidants and Redox Signaling*, *17*(4), 634–656. https://doi.org/10.1089/ars.2012.4539

van Dooren, G. G., & Striepen, B. (2013). The algal past and parasite present of the apicoplast. *Annual Review of Microbiology*, *67*, 271–289. https://doi.org/10.1146/annurev-micro-092412-155741

Varadi, M., Anyango, S., Deshpande, M., Nair, S., Natassia, C., Yordanova, G., Yuan, D., Stroe, O., Wood, G., Laydon, A., Zídek, A., Green, T., Tunyasuvunakool, K., Petersen, S., Jumper, J., Clancy, E., Green, R., Vora, A., Lutfi, M., … Velankar, S. (2022). AlphaFold Protein Structure Database: Massively expanding the structural coverage of protein-sequence space with high-accuracy models. *Nucleic Acids Research*, *50*(D1), D439–D444. https://doi.org/10.1093/nar/gkab1061

Vella, S. A., Moore, C. A., Li, Z. H., Hortua Triana, M. A., Potapenko, E., & Moreno, S. N. J. (2021). The role of potassium and host calcium signaling in Toxoplasma gondii egress. *Cell Calcium*, *94*. https://doi.org/10.1016/j.ceca.2020.102337

Venugopal, K., Werkmeister, E., Barois, N., Saliou, J. M., Poncet, A., Huot, L., Sindikubwabo, F., Hakimi, M. A., Langsley, G., Lafont, F., & Marion, S. (2017). Dual role of the Toxoplasma gondii clathrin adaptor AP1 in the sorting of rhoptry and microneme proteins and in parasite division. *PLoS Pathogens*, *13*(4), e1006331. https://doi.org/10.1371/journal.ppat.1006331

Viita, T., Kyheröinen, S., Prajapati, B., Virtanen, J., Frilander, M. J., Varjosalo, M., & Vartiainen, M. K. (2019). Nuclear actin interactome analysis links actin to KAT14 histone acetyl transferase and mRNA splicing. *Journal of Cell Science*, *132*(8). https://doi.org/10.1242/jcs.226852

Viotti, C., Bubeck, J., Stierhof, Y. D., Krebs, M., Langhans, M., van den Berg, W., van Dongen, W., Richter, S., Geldner, N., Takano, J., Jürgens, G., de Vries, S. C., Robinson, D. G., & Schumacher, K. (2010). Endocytic and secretory traffic in Arabidopsis merge in the trans-golgi network/early endosome, an independent and highly dynamic organelle. *Plant Cell*, *22*(4), 1344–1357. https://doi.org/10.1105/tpc.109.072637

von Mering, C., Huynen, M., Jaeggi, D., Schmidt, S., Bork, P., & Snel, B. (2003). STRING: A database of predicted functional associations between proteins. *Nucleic Acids Research*, *31*(1), 258–261. https://doi.org/10.1093/nar/gkg034

Waller, R. F., Reed, M. B., Cowman, A. F., & McFadden, G. I. (2000). Protein trafficking to the plastid of Plasmodium falciparum is via the secretory pathway. *The EMBO Journal*, *19*(8), 1794–1802. https://doi.org/10.1093/emboj/19.8.1794

Warring, S. D., Dou, Z., Carruthers, V. B., Mcfadden, G. I., & Van Dooren, G. G. (2014). Characterization of the chloroquine resistance transporter homologue in Toxoplasma gondii. *Eukaryotic Cell*, *13*(11), 1360–1370. https://doi.org/10.1128/EC.00027-14

Wegner, A. (1976). Head to tail polymerization of actin. *Journal of Molecular Biology*, *108*(1), 139–150. https://doi.org/10.1016/S0022-2836(76)80100-3

Welch, M. D., Iwamatsu, A., & Mitchison, T. J. (1997). Actin polymerization is induced by Arp2/3 protein complex at the surface of Listeria monocytogenes. *Nature*, *385*(6613), 265–269. https://doi.org/10.1038/385265a0

White, N. J., Pukrittayakamee, S., Hien, T. T., Faiz, M. A., Mokuolu, O. A., & Dondorp, A. M. (2014). Malaria. *The Lancet*, *383*(9918), 723–735. https://doi.org/10.1016/S0140-6736(13)60024-0

Whitelaw, J. A. (2017). *The dynamic nature and functions of actin in Toxoplasma gondii*. Doctoral dissertation, University of Glasgow.

Whitelaw, Jamie A., Latorre-Barragan, F., Gras, S., Pall, G. S., Leung, J. M., Heaslip, A., Egarter, S., Andenmatten, N., Nelson, S. R., Warshaw, D. M., Ward, G. E., & Meissner, M. (2017). Surface attachment, promoted by the actomyosin system of Toxoplasma gondii is important for efficient gliding motility and invasion. *BMC Biology*, *15*(1), 1. https://doi.org/10.1186/s12915-016-0343-5

Woo, Y. H., Ansari, H., Otto, T. D., Klinger, C. M., Kolisko, M., Michálek, J., Saxena, A., Shanmugam, D., Tayyrov, A., Veluchamy, A., Ali, S., Bernal, A., del Campo, J., Cihlář, J., Flegontov, P., Gornik, S. G., Hajdušková, E., Horák, A., Janouškovec, J., … Pain, A. (2015a). Chromerid genomes reveal the evolutionary path from photosynthetic algae to obligate intracellular parasites. *ELife*, *4*, e06974. https://doi.org/10.7554/eLife.06974

Woo, Y. H., Ansari, H., Otto, T. D., Klinger, C. M., Kolisko, M., Michálek, J., Saxena, A., Shanmugam, D., Tayyrov, A., Veluchamy, A., Ali, S., Bernal, A., del Campo, J., Cihlář, J., Flegontov, P., Gornik, S. G., Hajdušková, E., Horák, A., Janouškovec, J., … Pain, A. (2015b). Chromerid genomes reveal the evolutionary path from photosynthetic algae to obligate intracellular parasites. *ELife*, *4*, e06974. https://doi.org/10.7554/eLife.06974

Xu, D., & Esko, J. D. (2009). A Golgi-on-a-chip for glycan synthesis. *Nature Chemical Biology*, *5*(9), 612–613. https://doi.org/10.1038/nchembio0909-612

Ye, S., Lunghi, M., & Soldati-Favre, D. (2022). A Signaling Factor Linked to Toxoplasma gondii Guanylate Cyclase Complex Controls Invasion and Egress during Acute and Chronic Infection. *MBio*, *13*(5), e0196522. https://doi.org/10.1128/mbio.01965-22

Yeoh, S., Pope, B., Mannherz, H. G., & Weeds, A. (2002). Determining the differences in actin binding by human ADF and cofilin. *Journal of Molecular Biology*, *315*(4), 911–925. https://doi.org/10.1006/jmbi.2001.5280

Yilmaz, S. M., & Hopkins, S. H. (1972). Effects of different conditions on duration of infectivity of Toxoplasma gondii oocysts. *The Journal of Parasitology*, *58*(5), 938–939. https://doi.org/10.2307/3286589

Zetsche, B., Volz, S. E., & Zhang, F. (2015). A split-Cas9 architecture for inducible genome editing and transcription modulation. *Nature Biotechnology*, *33*(2), 139–142. https://doi.org/10.1038/nbt.3149

Zhang, X., Wang, X., Zhang, Z., & Cai, G. (2019). Structure and functional interactions of INO80 actin/Arp module. *Journal of Molecular Cell Biology*, *11*(5), 345–355. https://doi.org/10.1093/jmcb/mjy062

Zimmermann, L., Stephens, A., Nam, S. Z., Rau, D., Kübler, J., Lozajic, M., Gabler, F., Söding, J., Lupas, A. N., & Alva, V. (2018). A Completely Reimplemented MPI Bioinformatics Toolkit with a New HHpred Server at its Core. *Journal of Molecular Biology*, *430*(15), 2237–2243. https://doi.org/10.1016/j.jmb.2017.12.007

Zintl, A., Mulcahy, G., Skerrett, H. E., Taylor, S. M., & Gray, J. S. (2003). Babesia divergens, a Bovine Blood Parasite of Veterinary and Zoonotic Importance. *Clinical Microbiology Reviews*, *16*(4), 622–636. https://doi.org/10.1128/CMR.16.4.622-636.2003

Appendix

Supplementary results

Table A.1 - Table of phenotypes observed during the phenotypic screen

Accession no.	Name	No. of times picked	Investigator 1	Investigator 2
201270	hypothetical protein	x1	F_1	
202500	GAPM1a	x1	A_1	
203170	OB-fold nucleic acid binding domain-containing protein	x1	R_2	A_2
205540	DEAD/DEAH box helicase domain-containing protein	x2	F_1 A_1 / F_1 R_1	
207820	putative cell-cycle-associated protein kinase MAPK	x1	R_3	R_2
208420	Sodium:neurotransmitter symporter family protein	x3	F_3/F_3 E_4	F_2 A_2
208820	1-deoxy-D-xylulose-5-phosphate synthase	x1	F_1 A_1	A_2
209100	PUB domain-containing protein	X2	E_3	
209550	hypothetical protein	x2	A_1 / F_1 A_3	F_2 A_2
209900	hypothetical protein	x2	F_1 E_1	E_2
210230	hypothetical protein	x1	E_2	
210490	hypothetical protein	x1	E_2	F_2A_2
211060	hypothetical protein	x1	F_1	A_2
214250	hypothetical protein	x1	F_1	
214560	hypothetical protein	x1	F_1 A_3 R_3 E_2	N_2 E_2
214620	putative hypoxia- inducible factor prolyl hydroxylase (phd2)	x1	F_3	F_2
214790	glycoprotein	x1	E_4	
215610	hypothetical protein	x2	R_3 / R_1	R_2 / A_2
216000	alveolin domain containing intermediate filament IMC3	x2	F_1 A_3/ A_2 N_2 E_1	N_2 / F_2 A_2 N_2
216040	putative 30S ribosomal protein S15	x1	E_1	E_2
216080	apical complex lysine methyltransferase	x1	A_4	A_2 R_2
216530	ribosome recycling factor protein	x2	R_3 / R_1	F_2 A_2 / F_2 A_2 N_2
216820	transporter, major facilitator family protein	x1	A_3 R_3	F_4
218280	putative eukaryotic porin	x1	A_3	R_2
221600	hypothetical protein	x3	R_3 / R_3 E_2	F_2 A_2 N_2 /A_2 E_1
222990	putative ribosomal protein S18	x1	A_3 R_3	R_2
223040	hypothetical protein	x1	R_3	A_4
223940	GAP45 protein	x1	R_3	R_2 E_2

224720	SPOC domain-containing protein	x1	R_3	F_2 A_2 N_2
225510	RAP domain-containing protein	x1	R_1	A_2
226280	putative ribosomal protein L28	x3	R_3 / R_3 / R_3	N_2 / R_2 / R_2
226320	hypothetical protein	x1	A_3 R_2	F_2A_2
229460	SWI2/SNF2-containing protein	x1	F_4	F_2A_2
229620	hypothetical protein	x2	R_3 /F_3	R_2
229740	hypothetical protein	x1	R_3 E_3	A_2 E_1
230210	alveolin domain containing intermediate filament IMC10	x2	R_3 / A_2 N_2	F_2 A_2 R_2
235398	hypothetical protein	x1	R_3	
237010	hypothetical protein	x1	A_3 E_4	E_2
238000	peptidyl-prolyl isomerase	x1	R_2	R_2
240380	hypothetical protein	x1	E_3	
240910	hypothetical protein	x1	E_2	E_2
242840	membrane protein	x1	R_3	R_2
244430	putative pseudouridylate synthase	x1	E_2	E_1
248640	regulator of chromosome condensation (RCC1) repeat-containing protein	From colony picking	E_2	
248490	hypothetical protein	From colony picking		F_4 A_2
248660	hypothetical protein	x2	R_3	E3
249480	tetratricopeptide repeat-containing protein	x1		E_1
249850	GAP40 protein	x3	R_4 / F_4 A_3 N_3 / F_4 A_3 N_3	N_4 / F_2 A_2 N_2 / N_2
249970	hypothetical protein	x1	F_3 A_3 E_2	E_2
252465	radical SAM domain-containing protein	From colony picking	E_2	
253360	hypothetical protein	x2	F_4 A_3 N_3 /residual body	N_2
253510	transporter/permease protein	x1	A_3	
253830	hypothetical protein	x1	E_2	E_1
254230	hypothetical protein	x1	F_2 A_2	F_2 A_4
254600	ubiquitin family protein	x1	E_4	E4
255920	putative GINS complex subunit Psf3	x1	R_1	R_2F_2
257350	putative eukaryotic translation initiation factor	x1	R_4	F_4
257530	transporter, major facilitator family protein	x1	R_1	R_2
259720	hypothetical protein	x2	A_3 / F_2 E_1	A_2 / A_2 E_2
260320	Noc2p family protein	x2	R_3 / R_3 A_3	R_2 / A_2 R_4
261440	ARM repeats containing protein	x1	A_1	A_2
262430	4-hydroxy-3-methylbut-2-en-1-yl diphosphate synthase	x1	N_3	A_2 R_2
262640	Cg8 family protein	x1	A_4	A_2

263300	eukaryotic porin protein	x3	F_2 N_2 / R_3 / R_1	R_2 i/F_2 A_2 N_2
263580	bromodomain-containing protein	x1	A_3	A_2
263680	hypothetical protein	x1	F_1	F_2 A_2
267510	hypothetical protein	x1	R_3	
268400	hypothetical protein	x1	F_3	F_2 A_2
268685	mitochondrial large subunit ribosomal protein	x1	A_3 N_3	
269330	hypothetical protein	x1	A_1 E_4	E_2
269700	NLI interacting factor family phosphatase	x4	F_3 R_1 E_2	F_2 A_2
271970	glideosome-associated protein with multiple-membrane spans GAPM3	x2	F_4 N_3 / F_3 N_3	F_2 N_2 / F_2 N_2
273100	3'-5' exonuclease domain-containing protein	x1	E_3	
273445	sufB/sufD domain-containing protein	x1	R_2	A_2
286790	nuclear factor NF2	x1	F_1	F_2
288270	hypothetical protein	x1	A_1	A_2 R_2
289950	hypothetical protein	x1		F_1 A_2 N_3
293570	putative translocation protein sec62	x1	R_3	R_2
293690	profilin	x1	F_4 / R_3	F_4 / R_2
294250	WD domain, G-beta repeat-containing protein	x1		F_2 A_2
294902	hypothetical protein	x1	F_1	
294930	leucine rich repeat-containing protein	x3	A_2 / F_1 E_4	F_4
297780	ATPase/histidine kinase/DNA gyrase B/HSP90 domain-containing protein	x1	R_1	A_2
299080	VTC domain-containing protein	x1	F_1	A_2
301410	hypothetical protein	x1	F_3 E_2	F_2 A_2 E_2
305340	corepressor complex CRC230	x2	A_2 N_3 E_2	R_2
306640	hypothetical protein	x1	E_2	E_2
308920	splicing factor U2AF protein	x1	R_2	A_4
309170	TAF7-like RNA polymerase II TAF7L	x1	A_1	
310360	hypothetical protein	x1	R_3	R_2
310430	Hsp90 domain-containing protein	x5	R_2 / F_1 R_3 / A_2 R_2 E_2	A_2 / A_2 E_2
310500	hypothetical protein	x1	A_3 E_2	A_2 E_2
310850	MYND finger domain-containing protein	x1	F_1 A_3	
310930	hypothetical protein	x1	E_2	
312390	hypothetical protein	x1	F_1	F_2 A_2
312650	hypothetical protein	x1	A_1	A_2
313160	hypothetical protein	x1	R_2	R_2
318420	putative 30S ribosomal protein S16	x1	A_2 E_3	A_2
320020	transporter, major facilitator family protein	x2	R_3 / R_4	R_2 / R_2

Table A.2 - List of screen candidates followed up

Accession No.	F-actin	Apicoplast	Nuclear / Division	Natural Egress in screen	Induced egress
TGGT1_208420	✓	✓		✓	✓
TGGT1_209100				✓	
TGGT1_209900				✓	
TGGT1_210230				✓	
TGGT1_210490	✓		✓	✓	
TGGT1_214560				✓	
TGGT1_214790				✓	
TGGT1_216000				✓	
TGGT1_216040				✓	
TGGT1_221600				✓	
TGGT1_226320	✓	✓	✓		
TGGT1_229460	✓	✓			
TGGT1_229740				✓	
TGGT1_237010				✓	
TGGT1_240380				✓	✓
TGGT1_240910				✓	
TGGT1_244430				✓	
TGGT1_248490	✓	✓			
TGGT1_248640				✓	✓
TGGT1_248660				✓	
TGGT1_249970	✓	✓		✓	
TGGT1_252465				✓	✓
TGGT1_253830				✓	
TGGT1_254230	✓	✓			
TGGT1_254600				✓	
TGGT1_255920	✓		✓		
TGGT1_259720	✓	✓		✓	
TGGT1_263300	✓	✓	✓		
TGGT1_263680	✓	✓			
TGGT1_269330				✓	
TGGT1_269700	✓	✓		✓	
TGGT1_273100				✓	
TGGT1_286790	✓		✓		
TGGT1_289950	✓	✓	✓		
TGGT1_294930	✓	✓		✓	
TGGT1_301410	✓	✓		✓	
TGGT1_305340				✓	

TGGT1_306640				✓	
TGGT1_310430				✓	
TGGT1_310500				✓	
TGGT1_310930				✓	
TGGT1_318420				✓	

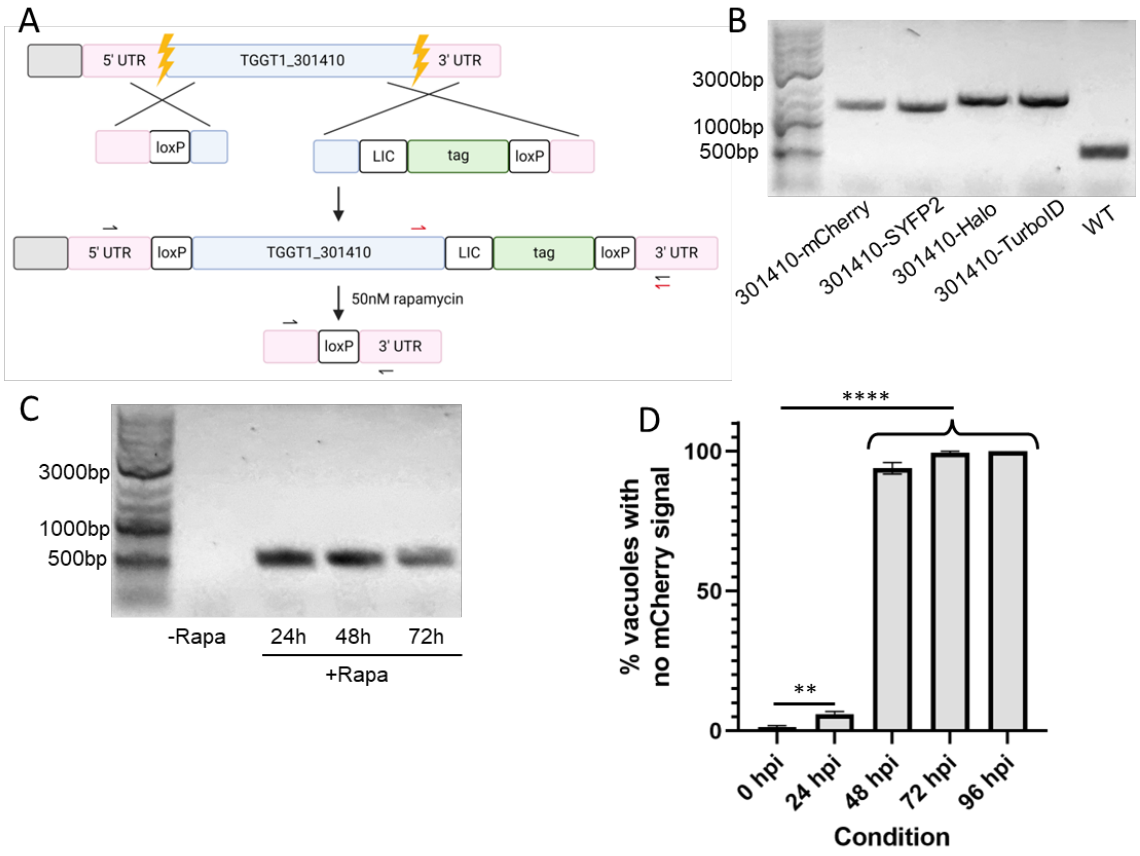

Figure A.1 – Genotyping and knockout of *Tg*EDP (TGGT1_301410)

(**A**) shows the tagging and floxing strategy of TGGT1_301410. Addition of 50 nM rapamycin results in the excision of the tagged gene of interest and one loxP sequence. (**B**) Genotyping of the wildtype (WT) (524bp) parasite strain as well as parasite strains obtained wherein TGGT1_301410 is endogenously tagged with mCherry (1290bp), SYFP2 (1299bp), Halo (1529bp), and TurboID (1557bp). Primer design corresponds to the red arrows in panel (A). (**C**) Knockout of tagged TGGT1_301410 results in a band size of 514bp. The floxed, endogenously tagged protein (-Rapa) could not be amplified. Primer design corresponds to the black arrows in panel (A). (**D**) The clone expressing TGGT1_301410-mCherry was used to quantify loss of protein via IFA. 95% of parasite vacuoles lost the protein by 48 hpi. Data is presented as mean ± s.d. One-way ANOVA with Tukey's multiple comparison test was done, with P values being represented as follows: ns = >0.05; ** = 0.001 – 0.01; **** = < 0.0001.

Table A.3 - Highest enriched proteins obtained from TurboID experiment, selected based on phenotypic score, predicted localisation, and domain prediction (listed in ascending order of phenotypic score)

Accession No.	Name	Phenotypic score	HyperLOPIT localisation	Domains
TGGT1_213392	Surface antigen repeat-containing protein	-5.02	nucleus - chromatin	XIRP1/XIRP2 Xin actin-binding repeat-containing protein
TGGT1_230940	Uncharacterized protein	-4.92	nucleus - chromatin	
TGGT1_244290	Adapter-related protein	-4.87	nucleus - chromatin	Armadillo-type fold, AP4E1_C AP-4 complex subunit epsilon-1, C-terminal
TGGT1_291180	Uncharacterized protein	-4.69	nucleus - chromatin	VPS13 Vacuolar protein sorting-associated protein 13
TGGT1_272910	T-complex protein 1 subunit delta	-4.41	cytosol	GroEL-intermediate domain like TCP-1-like chaperonin intermediate domain
TGGT1_309220	GTPase activating protein for Arf protein	-4.23	cytosol	ArfGap Arf GTPase activating protein
TGGT1_301410	Uncharacterized protein – **bait protein**	-4.16	nucleus - chromatin	
TGGT1_243200	Uncharacterized protein	-3.95	dense granules	
TGGT1_220090	DIX domain-containing protein	-3.67	cytosol	Ubiquitin-like domain
TGGT1_222380	Importin-beta N-terminal domain-containing protein	-3.51	cytosol	ARM repeat Armadillo-type fold, importin, exportin
TGGT1_273370	Coatomer subunit gamma	-3.26	cytosol	Clathrin/coatomer_adapt-like_N Clathrin/coatomer adaptor, adaptin-like, N-terminal
TGGT1_298610	GYF domain-containing protein	-2.16	nucleus - chromatin	GYF-like domain
TGGT1_240220	Uncharacterized protein	-2.1	cytosol	
TGGT1_293220	DHHC zinc finger domain-containing protein	-2.06	Golgi	DHHC Palmitoyltransferase, DHHC domain, TM
TGGT1_228150	Uncharacterized protein	-1.48	nucleus - chromatin	

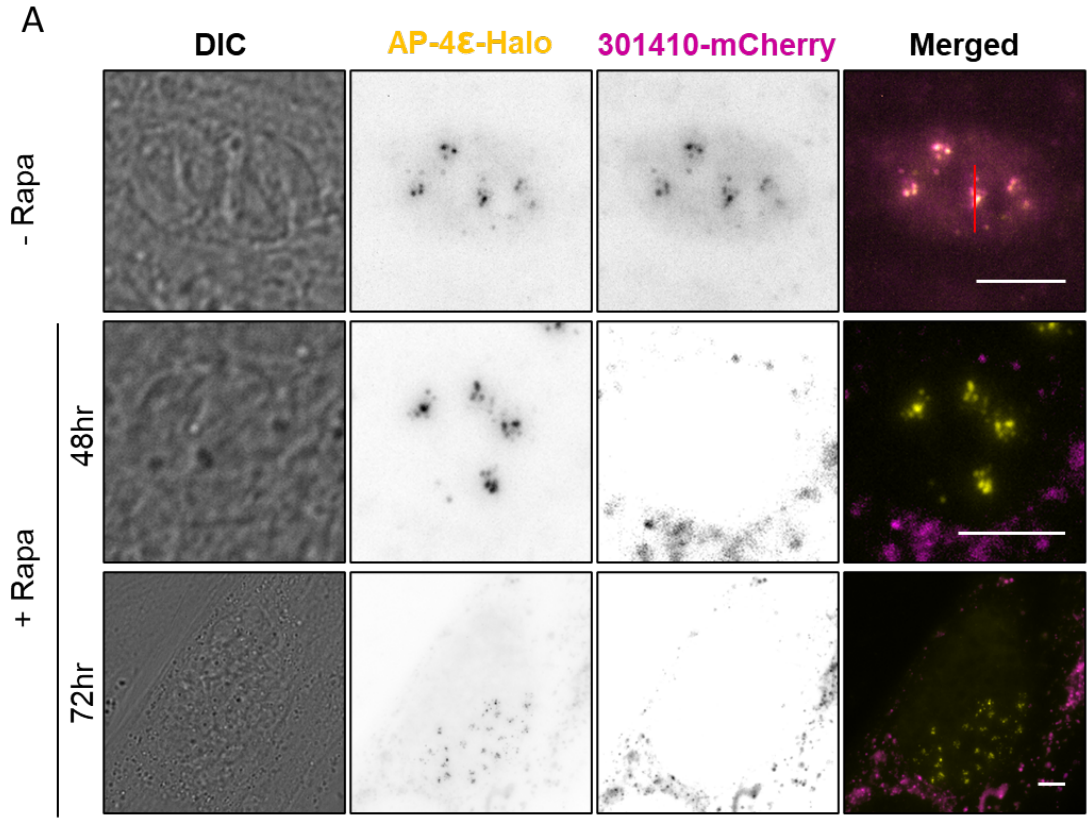

Figure A.2 - Colocalisation of *Tg*EDP with AP-4

(**A**) Colocalisation experiments show that Halo-tagged AP-4ε colocalises with mCherry-tagged *Tg*EDP. Upon addition of 50 nM rapamycin and knockout of *Tg*EDP, AP-4ε is unaffected until the parasitophorous vacuole starts to collapse (at 72 hours). Scale bars are all 5 µm. (**B**) shows the plot profile across the red line drawn on the merged image in (A). The merged image was first converted to 8-bit image in order to account for variations in protein expression levels leading to differences in intensities. The intensity peaks for Halo correspond to peaks in mCherry intensity, showing that *Tg*EDP colocalises with AP-4ε.

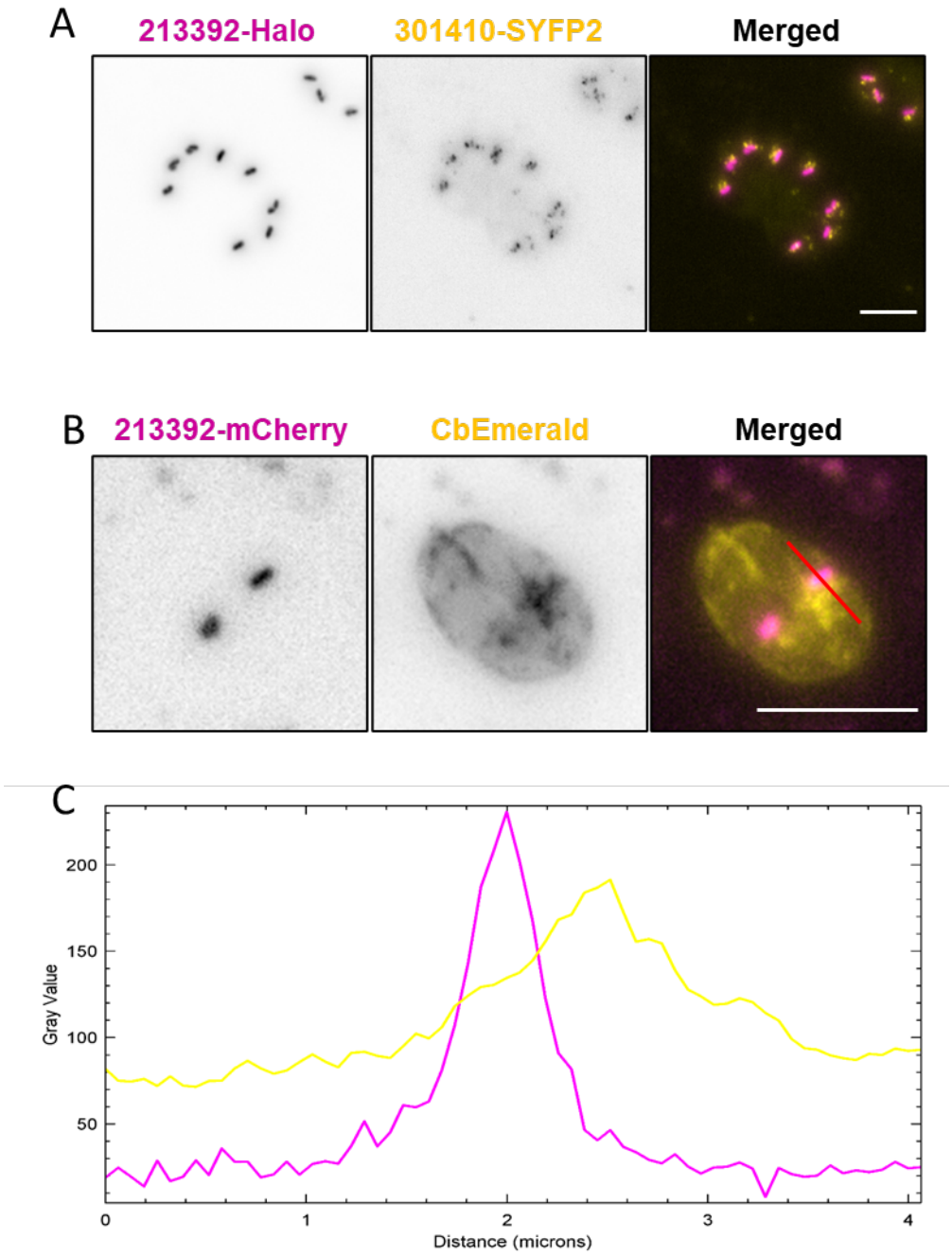

Figure A.3 - TGGT1_213392 does not colocalise with TGGT1_301410

(**A**) Assays wherein TGGT1_213392 was endogenously tagged with Halo (in magenta) showed that it does not colocalise with *Tg*EDP (in yellow). (**B**) Due to its predicted actin-binding domain, the Chromobody-Emerald was expressed in the strain co-expressing TGGT1_213392-mCherry. No colocalisation of the actin nucleation centre with TGGT1_213392 was observed. Scale bars are 5µm. (**C**) shows a profile plot taken across the red line in the merged image of (B). Intensity signals show no colocalization. Prior to obtaining the profile plots, the image was converted to 8-bit to account for differences in protein levels and therefore signal intensities.

Table A.4 - List of proteins clustering with CPL according to hyperLOPIT, arranged in ascending order of phenotypic score

Accession No.	Name	Phenotypic score
TGME49_227820	hypothetical protein	-5.01
TGME49_297420	beta-tubulin cofactor D, putative	-4.45
TGME49_306020	hypothetical protein	-3.25
TGME49_204080	histidine acid phosphatase superfamily protein	-1.99
TGME49_247030	hypothetical protein	-1.51
TGME49_237870	FYVE zinc finger domain-containing protein	-1.4
TGME49_309930	melibiase subfamily protein	-1.13
TGME49_201840	aspartyl protease ASP1	-0.36
TGME49_226072	Ser/Thr phosphatase family protein	-0.32
TGME49_315710	hypothetical protein	-0.2
TGME49_273360	ABC transporter transmembrane region domain-containing protein	-0.17
TGME49_243350	gamma-glutamyl hydrolase	0.45
TGME49_272420	phosphatidylcholine-sterol O-acyltransferase, putative	0.57
TGME49_291600	gamma interferon inducible lysosomal thiol reductase (GILT) protein	0.6
TGME49_254010	serine carboxypeptidase s28 protein	0.64
TGME49_321530	CPL	0.68
TGME49_249670	CPB	0.95
TGME49_208730	microneme protein, putative	1.09
TGME49_255330	hypothetical protein	1.13

Oligos

Table A.5 - Curated library of sgRNAs used for the phenotypic screen

Target	sgRNA no. in Sidik et al., 2016	sgRNA sequence with overhangs for cloning
TGGT1_293690	sgTGGT1_293690_3	TGGGGATGTCAAGTTGCGGCGGCTGATGATGATGAGTTTTAGAGCTAGAA
TGGT1_201220	sgTGGT1_201220_10	TGGGGATGTCAAGTTGAGACAGCTCGAGCTTCAGAGTTTTAGAGCTAGAA
TGGT1_201270	sgTGGT1_201270_9	TGGGGATGTCAAGTTGATGGGTGGAAGAGCTAACCGGTTTTAGAGCTAGAA
TGGT1_201380	sgTGGT1_201380_3	TGGGGATGTCAAGTTGCCGTGTTTCGACAAAGTGGGTTTTAGAGCTAGAA
TGGT1_201830	sgTGGT1_201830_9	TGGGGATGTCAAGTTGCAGACTCAGGAGGATCCCGGGTTTTAGAGCTAGAA
TGGT1_201880	sgTGGT1_201880_2	TGGGGATGTCAAGTTGTGTGGCGCCGCATTAACAAGTTTTAGAGCTAGAA
TGGT1_202120	sgTGGT1_202120_9	TGGGGATGTCAAGTTGCGCGTGGAGAAACTGACTCGGTTTTAGAGCTAGAA
TGGT1_202290	sgTGGT1_202290_9	TGGGGATGTCAAGTTGATTTAACTAGGCAACCAAGGGTTTTAGAGCTAGAA
TGGT1_202460	sgTGGT1_202460_2	TGGGGATGTCAAGTTGCAGAACCAACCTCCCGCACGTTTTAGAGCTAGAA
TGGT1_202500	sgTGGT1_202500_1	TGGGGATGTCAAGTTGGTACGCAGACAATTGCACGGTTTTAGAGCTAGAA
TGGT1_202840	sgTGGT1_202840_10	TGGGGATGTCAAGTTGATAGCGAGAAATTGAGACGTGTTTTAGAGCTAGAA
TGGT1_202880	sgTGGT1_202880_2	TGGGGATGTCAAGTTGAGAGACGACGAGGAAGGTGAGTTTTAGAGCTAGAA
TGGT1_202920	sgTGGT1_202920_4	TGGGGATGTCAAGTTGTAAGTAACTACCTCTCCCAGGTTTTAGAGCTAGAA
TGGT1_203020	sgTGGT1_203020_9	TGGGGATGTCAAGTTGGAGAGAGGGAAACATCCAGGTTTTAGAGCTAGAA
TGGT1_203170	sgTGGT1_203170_1	TGGGGATGTCAAGTTGAAACTCGTGGAGAACGGCGGTTTTAGAGCTAGAA
TGGT1_203358	sgTGGT1_203358_5	TGGGGATGTCAAGTTGATAGAGAAGCAACCCACAGGTTTTAGAGCTAGAA
TGGT1_203362	sgTGGT1_203362_3	TGGGGATGTCAAGTTGAATGACTCTCGAAGAAGCAGGTTTTAGAGCTAGAA
TGGT1_203620	sgTGGT1_203620_4	TGGGGATGTCAAGTTGCTTCCTCCAATTCGTCTGGGTTTTAGAGCTAGAA
TGGT1_204480	sgTGGT1_204480_9	TGGGGATGTCAAGTTGACAGCGAGGCGCATCTCCAGGTTTTAGAGCTAGAA
TGGT1_205540	sgTGGT1_205540_10	TGGGGATGTCAAGTTGCAACGCAAAGGCGGTCGCGGTTTTAGAGCTAGAA
TGGT1_205670	sgTGGT1_205670_10	TGGGGATGTCAAGTTGAGTTGCAAGCGATGAAAAGGTTTTAGAGCTAGAA

TGGT1_206490	sgTGGT1_206490_3	TGGGGATGTCAAGTTGACATGAGCAGGAGGAGGCGGGTTTTAGAGCTAGAA
TGGT1_207020	sgTGGT1_207020_1	TGGGGATGTCAAGTTGCTCTCAGGAGGATCATCGAGTTTTAGAGCTAGAA
TGGT1_207800	sgTGGT1_207800_7	TGGGGATGTCAAGTTGATATGCCTGCGGTATGCCAGTTTTAGAGCTAGAA
TGGT1_207820	sgTGGT1_207820_10	TGGGGATGTCAAGTTGATTGGGGACTCCGAGTGAGGGTTTTAGAGCTAGAA
TGGT1_207910	sgTGGT1_207910_9	TGGGGATGTCAAGTTGAAGAACTCGCACTCCACACGTTTTAGAGCTAGAA
TGGT1_207940	sgTGGT1_207940_1	TGGGGATGTCAAGTTGACACGAGAGGAAGGCGGGGGTTTTAGAGCTAGAA
TGGT1_208420	sgTGGT1_208420_7	TGGGGATGTCAAGTTGGCCTCGCCAGATATAGGCAGTTTTAGAGCTAGAA
TGGT1_208800	sgTGGT1_208800_10	TGGGGATGTCAAGTTGAGGCACTCTTGTGAAGAAGGGTTTTAGAGCTAGAA
TGGT1_208820	sgTGGT1_208820_9	TGGGGATGTCAAGTTGCGAAACAGGAGAGAAACAGGGTTTTAGAGCTAGAA
TGGT1_209100	sgTGGT1_209100_1	TGGGGATGTCAAGTTGCAGCGAGAACAACTCCTCGGTTTTAGAGCTAGAA
TGGT1_209550	sgTGGT1_209550_5	TGGGGATGTCAAGTTGCGACATGGCCGGAATGGAGGTTTTAGAGCTAGAA
TGGT1_209900	sgTGGT1_209900_3	TGGGGATGTCAAGTTGAAGTGCCGATACGCTTCGTGTTTTAGAGCTAGAA
TGGT1_210230	sgTGGT1_210230_6	TGGGGATGTCAAGTTGTGTCGCACCCCAGTAGGCGAGTTTTAGAGCTAGAA
TGGT1_210280	sgTGGT1_210280_3	TGGGGATGTCAAGTTGACGGAGGTCGGAAAGACTGGGTTTTAGAGCTAGAA
TGGT1_210490	sgTGGT1_210490_2	TGGGGATGTCAAGTTGTGGAAGAGAAGACTACCCCGGTTTTAGAGCTAGAA
TGGT1_210800	sgTGGT1_210800_1	TGGGGATGTCAAGTTGGCGCGCCTGCAGATACTCGGTTTTAGAGCTAGAA
TGGT1_211060	sgTGGT1_211060_9	TGGGGATGTCAAGTTGCCATACGACAAGTGTGACCAGTTTTAGAGCTAGAA
TGGT1_212960A	sgTGGT1_212960A_6	TGGGGATGTCAAGTTGCAAGTGATCGCAGAGCACAGTTTTAGAGCTAGAA
TGGT1_213100	sgTGGT1_213100_1	TGGGGATGTCAAGTTGAGGATGGTGATGAACGAGGGTTTTAGAGCTAGAA
TGGT1_213420	sgTGGT1_213420_5	TGGGGATGTCAAGTTGAGAAGAGTCAGAGGATGCAGGTTTTAGAGCTAGAA
TGGT1_213910	sgTGGT1_213910_3	TGGGGATGTCAAGTTGGACGAACTGCGGGGAGAGGGTTTTAGAGCTAGAA
TGGT1_214250	sgTGGT1_214250_4	TGGGGATGTCAAGTTGGGCATCTTCGCTATGTGGAGTTTTAGAGCTAGAA
TGGT1_214340	sgTGGT1_214340_7	TGGGGATGTCAAGTTGCGTTTGAGCGCTTCTGCGCGTTTTAGAGCTAGAA
TGGT1_214520	sgTGGT1_214520_7	TGGGGATGTCAAGTTGTACGGGCGCAGCAGGCGGAGTTTTAGAGCTAGAA

TGGT1_214560	sgTGGT1_214560_3	TGGGGATGTCAAGTTGAAGGCGAAGAGATCCGCGGGTTTTAGAGCTAGAA
TGGT1_214620	sgTGGT1_214620_7	TGGGGATGTCAAGTTGAGACACGATGTGCTTAAGGGTTTTAGAGCTAGAA
TGGT1_214790	sgTGGT1_214790_1	TGGGGATGTCAAGTTGTCTTTCAGGCAAGAAGGTGGGTTTTAGAGCTAGAA
TGGT1_215020	sgTGGT1_215020_7	TGGGGATGTCAAGTTGAGGGAGTTCCATGAGAGGGGTTTTAGAGCTAGAA
TGGT1_215070	sgTGGT1_215070_3	TGGGGATGTCAAGTTGAAGGAGCAGGACGAACTCGGTTTTAGAGCTAGAA
TGGT1_215370	sgTGGT1_215370_2	TGGGGATGTCAAGTTGAAGCCTTGCGAGGCAGACGGGTTTTAGAGCTAGAA
TGGT1_215610	sgTGGT1_215610_1	TGGGGATGTCAAGTTGCGCCATCAACCCAGTGCAGGTTTTAGAGCTAGAA
TGGT1_216000	sgTGGT1_216000_9	TGGGGATGTCAAGTTGACGGGTACGGAACTTCGGCGGTTTTAGAGCTAGAA
TGGT1_216040	sgTGGT1_216040_6	TGGGGATGTCAAGTTGCGATCTCCGTCCACAGCAAGTTTTAGAGCTAGAA
TGGT1_216080	sgTGGT1_216080_8	TGGGGATGTCAAGTTGACAGGAGGAGAACATGAGGGTTTTAGAGCTAGAA
TGGT1_216530	sgTGGT1_216530_3	TGGGGATGTCAAGTTGAGAAGGCGAGGAAGAAGGCGGTTTTAGAGCTAGAA
TGGT1_216670	sgTGGT1_216670_10	TGGGGATGTCAAGTTGACTATGGCCCGCAAGAAGAGGTTTTAGAGCTAGAA
TGGT1_216820	sgTGGT1_216820_10	TGGGGATGTCAAGTTGAGAATGATAACGATGGACGGTTTTAGAGCTAGAA
TGGT1_217010	sgTGGT1_217010_1	TGGGGATGTCAAGTTGGAGATGTGCGTGGAGGCGGGTTTTAGAGCTAGAA
TGGT1_217450	sgTGGT1_217450_6	TGGGGATGTCAAGTTGCTGCAGCGACCCGCCAACGAGTTTTAGAGCTAGAA
TGGT1_217900	sgTGGT1_217900_4	TGGGGATGTCAAGTTGAGAATTTGGCAGGGAACCAGGTTTTAGAGCTAGAA
TGGT1_218280	sgTGGT1_218280_1	TGGGGATGTCAAGTTGGGTTCTCCAATCACCAGCGGTTTTAGAGCTAGAA
TGGT1_218550	sgTGGT1_218550_7	TGGGGATGTCAAGTTGCGAAAGGGAAAACCAGGAAGGTTTTAGAGCTAGAA
TGGT1_218880	sgTGGT1_218880_9	TGGGGATGTCAAGTTGGCGCACGAGGAGATGGAAGGTTTTAGAGCTAGAA
TGGT1_218940	sgTGGT1_218940_5	TGGGGATGTCAAGTTGAAGCGAGGAGGACGGAAAGGTTTTAGAGCTAGAA
TGGT1_219280	sgTGGT1_219280_8	TGGGGATGTCAAGTTGGAGCGCTTTTACCCTCCAGGTTTTAGAGCTAGAA
TGGT1_220090	sgTGGT1_220090_6	TGGGGATGTCAAGTTGAGATCTACGGGGTCAGCCAGTTTTAGAGCTAGAA
TGGT1_220270	sgTGGT1_220270_8	TGGGGATGTCAAGTTGAAGTTCGTTGACAAAGTCGGTTTTAGAGCTAGAA
TGGT1_220930	sgTGGT1_220930_5	TGGGGATGTCAAGTTGAGAACTCCGGAGAGCCCTGGTTTTAGAGCTAGAA

TGGT1_221600	sgTGGT1_221600_5	TGGGGATGTCAAGTTGAGGGCTGTGAGGACGCCGAGTTTTAGAGCTAGAA
TGGT1_222180	sgTGGT1_222180_8	TGGGGATGTCAAGTTGTGAAGGCTTGGCGCCAGCGGTTTTAGAGCTAGAA
TGGT1_222390	sgTGGT1_222390_6	TGGGGATGTCAAGTTGAGAAACGGCGGGGAAGCGAGTTTTAGAGCTAGAA
TGGT1_222410	sgTGGT1_222410_3	TGGGGATGTCAAGTTGCTGCGGTCCCAGCAAGGCGGTTTTAGAGCTAGAA
TGGT1_222990	sgTGGT1_222990_9	TGGGGATGTCAAGTTGAAGAGGTCAGCGGGTTGCCGGTTTTAGAGCTAGAA
TGGT1_223040	sgTGGT1_223040_6	TGGGGATGTCAAGTTGCAAGTGCCTTCAGTCTGCGCGTTTTAGAGCTAGAA
TGGT1_223580	sgTGGT1_223580_4	TGGGGATGTCAAGTTGGATTCAGACGAAGCAGCGTGTTTTAGAGCTAGAA
TGGT1_223940	sgTGGT1_223940_3	TGGGGATGTCAAGTTGAAGGAGCGGCAGGAGCGGGGTTTTAGAGCTAGAA
TGGT1_224720	sgTGGT1_224720_5	TGGGGATGTCAAGTTGAGGGAACTCGAAGCCGGGCGTTTTAGAGCTAGAA
TGGT1_225360	sgTGGT1_225360_10	TGGGGATGTCAAGTTGGAGACACGCATATGTGTGGGTTTTAGAGCTAGAA
TGGT1_225380	sgTGGT1_225380_10	TGGGGATGTCAAGTTGCGTACCCAACTGAGCAAGGGTTTTAGAGCTAGAA
TGGT1_225510	sgTGGT1_225510_9	TGGGGATGTCAAGTTGTCCGCATCTGGTGAACGGCGGTTTTAGAGCTAGAA
TGGT1_225730	sgTGGT1_225730_2	TGGGGATGTCAAGTTGAAGGAGACGTGAACAGAAAGGTTTTAGAGCTAGAA
TGGT1_225800	sgTGGT1_225800_6	TGGGGATGTCAAGTTGAGAGGTGGTGGAGGAAAGCGGTTTTAGAGCTAGAA
TGGT1_226068	sgTGGT1_226068_5	TGGGGATGTCAAGTTGAAAGGCAGCAAAGTCCCCAGTTTTAGAGCTAGAA
TGGT1_226220	sgTGGT1_226220_5	TGGGGATGTCAAGTTGTCAAGGAGAGAGACGGCGAGTTTTAGAGCTAGAA
TGGT1_226280	sgTGGT1_226280_4	TGGGGATGTCAAGTTGTACAACCCGGTCTGTGACGGTTTTAGAGCTAGAA
TGGT1_226320	sgTGGT1_226320_5	TGGGGATGTCAAGTTGTGGCGCCGGAACGTCGCGTGTTTTAGAGCTAGAA
TGGT1_226510	sgTGGT1_226510_5	TGGGGATGTCAAGTTGCAGGGGCAGGGTAACGGTGGTTTTAGAGCTAGAA
TGGT1_226550	sgTGGT1_226550_7	TGGGGATGTCAAGTTGTCCGCGTTTCGGTTAAGCAGGTTTTAGAGCTAGAA
TGGT1_226580	sgTGGT1_226580_9	TGGGGATGTCAAGTTGCAACGAAAGTAGCATGCGTGTTTTAGAGCTAGAA
TGGT1_226980	sgTGGT1_226980_10	TGGGGATGTCAAGTTGCTCTCGCCGAGAAGATGCGGGTTTTAGAGCTAGAA
TGGT1_227420	sgTGGT1_227420_9	TGGGGATGTCAAGTTGAGGAGGAGGGGCAGTGAGAGTTTTAGAGCTAGAA
TGGT1_227860	sgTGGT1_227860_3	TGGGGATGTCAAGTTGCAGCAGCAGAAGGAGAAGAGTTTTAGAGCTAGAA

TGGT1_228750	sgTGGT1_228750_7	TGGGGATGTCAAGTTGAGTCGCGCAAGCAGTGGGTGTTTTAGAGCTAGAA
TGGT1_229020	sgTGGT1_229020_9	TGGGGATGTCAAGTTGAAGAAAGGCGAGACCGTTGGTTTTAGAGCTAGAA
TGGT1_229030	sgTGGT1_229030_4	TGGGGATGTCAAGTTGAGCCGCTATGCAGCAAGCGAGTTTTAGAGCTAGAA
TGGT1_229460	sgTGGT1_229460_5	TGGGGATGTCAAGTTGCAGAAGAGGAAGGGGAAGGGTTTTAGAGCTAGAA
TGGT1_229490	sgTGGT1_229490_8	TGGGGATGTCAAGTTGTGGTGTCAGGACCTCATGGGTTTTAGAGCTAGAA
TGGT1_229620	sgTGGT1_229620_1	TGGGGATGTCAAGTTGAGAAGGGCAAGGAACACGGGTTTTAGAGCTAGAA
TGGT1_229740	sgTGGT1_229740_10	TGGGGATGTCAAGTTGACGGGCGACACCGGAAGAAGGTTTTAGAGCTAGAA
TGGT1_229900	sgTGGT1_229900_7	TGGGGATGTCAAGTTGGACACGAGACGAACGCCAGGTTTTAGAGCTAGAA
TGGT1_229940	sgTGGT1_229940_2	TGGGGATGTCAAGTTGCAGAGAAGAAGGCGCGCGAGTTTTAGAGCTAGAA
TGGT1_230210	sgTGGT1_230210_5	TGGGGATGTCAAGTTGAACATCCGGAGACATGCTGGTTTTAGAGCTAGAA
TGGT1_230350	sgTGGT1_230350_2	TGGGGATGTCAAGTTGCAGCCGGAAAAGAGAACGAGTTTTAGAGCTAGAA
TGGT1_230710	sgTGGT1_230710_7	TGGGGATGTCAAGTTGATAGGGGAGGACTTTACGCGTTTTAGAGCTAGAA
TGGT1_231120	sgTGGT1_231120_5	TGGGGATGTCAAGTTGGCTTTCACTGCTCATGGGCGTTTTAGAGCTAGAA
TGGT1_231410	sgTGGT1_231410_3	TGGGGATGTCAAGTTGAAGAATGGCTACACAGACAGTTTTAGAGCTAGAA
TGGT1_231630	sgTGGT1_231630_4	TGGGGATGTCAAGTTGCAACAACTCCAGAAACGAGGGTTTTAGAGCTAGAA
TGGT1_231640	sgTGGT1_231640_1	TGGGGATGTCAAGTTGTTGAAGGAAAAGGAGGCGAGTTTTAGAGCTAGAA
TGGT1_232050	sgTGGT1_232050_10	TGGGGATGTCAAGTTGAAGAGCAGAAAGACCAGAGGTTTTAGAGCTAGAA
TGGT1_232815	sgTGGT1_232815_3	TGGGGATGTCAAGTTGAAGATCCGTGCAACGCGCAGGTTTTAGAGCTAGAA
TGGT1_233170	sgTGGT1_233170_3	TGGGGATGTCAAGTTGGAGGACTGCGCAGCGACGGGTTTTAGAGCTAGAA
TGGT1_235398	sgTGGT1_235398_3	TGGGGATGTCAAGTTGAATTCCGGAAGAAAGGCGAGTTTTAGAGCTAGAA
TGGT1_236520	sgTGGT1_236520_9	TGGGGATGTCAAGTTGTGAAGCTGACAGTGACCCTGTTTTAGAGCTAGAA
TGGT1_236550	sgTGGT1_236550_1	TGGGGATGTCAAGTTGACCCGCTTGCGAAAAGGGGGTTTTAGAGCTAGAA
TGGT1_236570	sgTGGT1_236570_5	TGGGGATGTCAAGTTGATGATGGAAGCCGGAAACAGGTTTTAGAGCTAGAA
TGGT1_236820	sgTGGT1_236820_9	TGGGGATGTCAAGTTGTCGAGACACCGGAACGCAGGTTTTAGAGCTAGAA

TGGT1_237010	sgTGGT1_237010_2	TGGGGATGTCAAGTTGAACGCGGTCTACAGACCAGGGTTTTAGAGCTAGAA
TGGT1_237820	sgTGGT1_237820_10	TGGGGATGTCAAGTTGAACGAGTAGACTGCTCGGCCGTTTTAGAGCTAGAA
TGGT1_238000	sgTGGT1_238000_6	TGGGGATGTCAAGTTGATCCCACGAGAGGCACCAGGTTTTAGAGCTAGAA
TGGT1_239748	sgTGGT1_239748_2	TGGGGATGTCAAGTTGACAAAGTGGGAAGACAGCGCGTTTTAGAGCTAGAA
TGGT1_240270	sgTGGT1_240270_6	TGGGGATGTCAAGTTGTCGACGGCGTCTTCAAACGCGTTTTAGAGCTAGAA
TGGT1_240380	sgTGGT1_240380_1	TGGGGATGTCAAGTTGGAGGCACCCACAGAGGCAGGTTTTAGAGCTAGAA
TGGT1_240600	sgTGGT1_240600_8	TGGGGATGTCAAGTTGATGCGTCAACTGCTCAAAGGTTTTAGAGCTAGAA
TGGT1_240780	sgTGGT1_240780_5	TGGGGATGTCAAGTTGCCGATTGTCTGCGGAGAGAGGTTTTAGAGCTAGAA
TGGT1_240910	sgTGGT1_240910_5	TGGGGATGTCAAGTTGTGTCTGCACACAGGAGCGCGTTTTAGAGCTAGAA
TGGT1_242840	sgTGGT1_242840_2	TGGGGATGTCAAGTTGTGAGACGACGGGATGAGCGGGTTTTAGAGCTAGAA
TGGT1_243530	sgTGGT1_243530_5	TGGGGATGTCAAGTTGATCGACGAACACGAACTGAGTTTTAGAGCTAGAA
TGGT1_244430	sgTGGT1_244430_9	TGGGGATGTCAAGTTGACACCGTAGAGGTTGGGAGGTTTTAGAGCTAGAA
TGGT1_245450	sgTGGT1_245450_1	TGGGGATGTCAAGTTGGAGGCCTCTCAGAGCGAGAGTTTTAGAGCTAGAA
TGGT1_246000	sgTGGT1_246000_4	TGGGGATGTCAAGTTGCGAGCGCTTGGGGACTCTCGGTTTTAGAGCTAGAA
TGGT1_246050	sgTGGT1_246050_7	TGGGGATGTCAAGTTGAGGGCGGCTGAGAGCACGGGTTTTAGAGCTAGAA
TGGT1_246740	sgTGGT1_246740_5	TGGGGATGTCAAGTTGTTGTCTCACCTGCATGCGCGTTTTAGAGCTAGAA
TGGT1_247380	sgTGGT1_247380_7	TGGGGATGTCAAGTTGAAGAGGAAGAAGGAGAGCGAGTTTTAGAGCTAGAA
TGGT1_247410	sgTGGT1_247410_6	TGGGGATGTCAAGTTGTACCTGCTCCGACACCAAAGGTTTTAGAGCTAGAA
TGGT1_247770	sgTGGT1_247770_7	TGGGGATGTCAAGTTGTGAAGTCGTGGAAACGGCCGGTTTTAGAGCTAGAA
TGGT1_248490	sgTGGT1_248490_5	TGGGGATGTCAAGTTGCCAAGGTGAGGAAAAGCCGTGTTTTAGAGCTAGAA
TGGT1_248640	sgTGGT1_248640_2	TGGGGATGTCAAGTTGGAGCAGGCACAGACGGGGAGTTTTAGAGCTAGAA
TGGT1_248660	sgTGGT1_248660_1	TGGGGATGTCAAGTTGACTCTGGATGGGACAAGAGTGTTTTAGAGCTAGAA
TGGT1_248950	sgTGGT1_248950_10	TGGGGATGTCAAGTTGAGAGTGCCGAAGACGAGCAGGTTTTAGAGCTAGAA
TGGT1_249480	sgTGGT1_249480_6	TGGGGATGTCAAGTTGCAGGCGGCGCAGTTCGACGGTTTTAGAGCTAGAA

TGGT1_249790	sgTGGT1_249790_7	TGGGGATGTCAAGTTGACCAACCTTTGAAAGAGCCTGTTTTAGAGCTAGAA
TGGT1_249850	sgTGGT1_249850_5	TGGGGATGTCAAGTTGTAGGCAGCACGGAAGGCTGGTTTTAGAGCTAGAA
TGGT1_249970	sgTGGT1_249970_3	TGGGGATGTCAAGTTGACAGAAAGAAGCCTTCTGGGTTTTAGAGCTAGAA
TGGT1_250010	sgTGGT1_250010_1	TGGGGATGTCAAGTTGGAGCAGCGGAGGAACGCGGGTTTTAGAGCTAGAA
TGGT1_250340	sgTGGT1_250340_10	TGGGGATGTCAAGTTGCGATCATTTGATAGATCGTGTTTTAGAGCTAGAA
TGGT1_251570B	sgTGGT1_251570B_2	TGGGGATGTCAAGTTGAAAGAACTCGCAACTTACGGGTTTTAGAGCTAGAA
TGGT1_252465	sgTGGT1_252465_4	TGGGGATGTCAAGTTGGAGAAGAGGACCAAGGGAGGTTTTAGAGCTAGAA
TGGT1_253360	sgTGGT1_253360_3	TGGGGATGTCAAGTTGCAAACGCACAGCAGTTGCCGGTTTTAGAGCTAGAA
TGGT1_253510	sgTGGT1_253510_5	TGGGGATGTCAAGTTGAATTAGCAGCGACAACAGGGGTTTTAGAGCTAGAA
TGGT1_253830	sgTGGT1_253830_3	TGGGGATGTCAAGTTGGAACGCTTATCTGGGACAAGTTTTAGAGCTAGAA
TGGT1_253860	sgTGGT1_253860_1	TGGGGATGTCAAGTTGAAGGTACGACACGAAGAAGGTTTTAGAGCTAGAA
TGGT1_254230	sgTGGT1_254230_2	TGGGGATGTCAAGTTGAGCAATGGCATGACCGAGGGTTTTAGAGCTAGAA
TGGT1_254370	sgTGGT1_254370_4	TGGGGATGTCAAGTTGAAGATTGGAGGCAGACACCGGTTTTAGAGCTAGAA
TGGT1_254420	sgTGGT1_254420_7	TGGGGATGTCAAGTTGAAGGCGAAGAAGATAACGAGTTTTAGAGCTAGAA
TGGT1_254600	sgTGGT1_254600_5	TGGGGATGTCAAGTTGCCCAGGCTGCACGATACACAGTTTTAGAGCTAGAA
TGGT1_255920	sgTGGT1_255920_6	TGGGGATGTCAAGTTGAGCAGCGAGGTCGACGGTGGTTTTAGAGCTAGAA
TGGT1_256010	sgTGGT1_256010_2	TGGGGATGTCAAGTTGGCCAGAATGAGGGATGCGAGTTTTAGAGCTAGAA
TGGT1_256030	sgTGGT1_256030_10	TGGGGATGTCAAGTTGACGAGTTCGGAAATGGTAGGTTTTAGAGCTAGAA
TGGT1_256070	sgTGGT1_256070_2	TGGGGATGTCAAGTTGCCTCGTGGGAAGAACCCTGGTTTTAGAGCTAGAA
TGGT1_256820	sgTGGT1_256820_5	TGGGGATGTCAAGTTGTAGAGGTGGGCAGTAGTAGGTTTTAGAGCTAGAA
TGGT1_257310	sgTGGT1_257310_5	TGGGGATGTCAAGTTGAAGAGATGGACGCAGGCGAGTTTTAGAGCTAGAA
TGGT1_257350	sgTGGT1_257350_3	TGGGGATGTCAAGTTGAGAGCTGGACCGCACAGTGAGTTTTAGAGCTAGAA
TGGT1_257530	sgTGGT1_257530_8	TGGGGATGTCAAGTTGTACGGGAACAGCGGCAGGAGTTTTAGAGCTAGAA
TGGT1_258130	sgTGGT1_258130_8	TGGGGATGTCAAGTTGAATGCGATCAACGTGGACGGTTTTAGAGCTAGAA

TGGT1_258700	sgTGGT1_258700_8	TGGGGATGTCAAGTTGTCGAGGCTTCAGGACGCGAGTTTTAGAGCTAGAA
TGGT1_259520	sgTGGT1_259520_1	TGGGGATGTCAAGTTGGCGCTGCTCAACTATGAAGGTTTTAGAGCTAGAA
TGGT1_259720	sgTGGT1_259720_1	TGGGGATGTCAAGTTGGAGAGCGGAGACGAGGCGAGTTTTAGAGCTAGAA
TGGT1_259850	sgTGGT1_259850_4	TGGGGATGTCAAGTTGCAGTCGGATGGCCTCCCTGGTTTTAGAGCTAGAA
TGGT1_260180	sgTGGT1_260180_9	TGGGGATGTCAAGTTGAAAGTGGACGAACGGTAGGAGTTTTAGAGCTAGAA
TGGT1_260250	sgTGGT1_260250_8	TGGGGATGTCAAGTTGCCAGACAACCTGGAAGCCGGTTTTAGAGCTAGAA
TGGT1_260320	sgTGGT1_260320_2	TGGGGATGTCAAGTTGGGGAGAGAAATCTCAGGGAGTTTTAGAGCTAGAA
TGGT1_260360	sgTGGT1_260360_6	TGGGGATGTCAAGTTGAAGCACCGCAAAGATAACGAGTTTTAGAGCTAGAA
TGGT1_260470	sgTGGT1_260470_2	TGGGGATGTCAAGTTGGAGGAAGTTCTCGAGGAAGGTTTTAGAGCTAGAA
TGGT1_260500	sgTGGT1_260500_6	TGGGGATGTCAAGTTGCAATGTGGGCAGCTGACGTGTTTTAGAGCTAGAA
TGGT1_260660	sgTGGT1_260660_8	TGGGGATGTCAAGTTGCTGCGGTCTTCGATAGAACGTTTTAGAGCTAGAA
TGGT1_260790	sgTGGT1_260790_7	TGGGGATGTCAAGTTGCTGTTGCCAGACGGGCGGGGTTTTAGAGCTAGAA
TGGT1_261080	sgTGGT1_261080_7	TGGGGATGTCAAGTTGAGAAGCTTCTCGCCGAGGGGTTTTAGAGCTAGAA
TGGT1_261440	sgTGGT1_261440_3	TGGGGATGTCAAGTTGGAGGAGCGCATGCACCCGTGTTTTAGAGCTAGAA
TGGT1_262100	sgTGGT1_262100_9	TGGGGATGTCAAGTTGCCTGGGCCAACGAAAGGAGGTTTTAGAGCTAGAA
TGGT1_262150	sgTGGT1_262150_7	TGGGGATGTCAAGTTGAGGGTCTGCAGACGACGCACGTTTTAGAGCTAGAA
TGGT1_262430	sgTGGT1_262430_3	TGGGGATGTCAAGTTGCGGTACGGAGACACCCCGCGTTTTAGAGCTAGAA
TGGT1_262640	sgTGGT1_262640_1	TGGGGATGTCAAGTTGGTGTGGTACTGAAGAAGGAGTTTTAGAGCTAGAA
TGGT1_262710	sgTGGT1_262710_2	TGGGGATGTCAAGTTGCGAAGGACTTTCAGAACGAGTTTTAGAGCTAGAA
TGGT1_263110	sgTGGT1_263110_6	TGGGGATGTCAAGTTGGAGAAACGAGAGAGCGAAGGTTTTAGAGCTAGAA
TGGT1_263300	sgTGGT1_263300_8	TGGGGATGTCAAGTTGAAGGATAGCCTCGACATCGGTTTTAGAGCTAGAA
TGGT1_263310	sgTGGT1_263310_5	TGGGGATGTCAAGTTGAAACCGGAAGAGGCAACGAGGTTTTAGAGCTAGAA
TGGT1_263550	sgTGGT1_263550_6	TGGGGATGTCAAGTTGTGAGGCACTCGAGACGCGCGTTTTAGAGCTAGAA
TGGT1_263580	sgTGGT1_263580_8	TGGGGATGTCAAGTTGATGCATGCAGATACGAGGGGTTTTAGAGCTAGAA

TGGT1_263680	sgTGGT1_263680_9	TGGGGATGTCAAGTTGGAAACTCACTGGTGAGAGTGTTTTAGAGCTAGAA
TGGT1_264640	sgTGGT1_264640_6	TGGGGATGTCAAGTTGAAGCCTCTGCAGGTCCAAGGTTTTAGAGCTAGAA
TGGT1_264710	sgTGGT1_264710_5	TGGGGATGTCAAGTTGTGCCAAGAAGGCAGAAGCAGGTTTTAGAGCTAGAA
TGGT1_264720	sgTGGT1_264720_2	TGGGGATGTCAAGTTGTAGACGACTGGAGCTCGAGGGTTTTAGAGCTAGAA
TGGT1_264730	sgTGGT1_264730_6	TGGGGATGTCAAGTTGTTAGCTCGTCGATGTAAGGCGTTTTAGAGCTAGAA
TGGT1_265040	sgTGGT1_265040_1	TGGGGATGTCAAGTTGGCACAGGGAAACATAGCAGGTTTTAGAGCTAGAA
TGGT1_265470	sgTGGT1_265470_6	TGGGGATGTCAAGTTGAGCACTCCGAGAAGCACCGGTTTTAGAGCTAGAA
TGGT1_265510	sgTGGT1_265510_2	TGGGGATGTCAAGTTGAGTTCAGTTCAGAGCCAGAGTTTTAGAGCTAGAA
TGGT1_266372	sgTGGT1_266372_6	TGGGGATGTCAAGTTGAAACTGCTAAGCGCAGAGCGTTTTAGAGCTAGAA
TGGT1_266630	sgTGGT1_266630_6	TGGGGATGTCAAGTTGTCTGAGGGAAGAGGGAATGGGTTTTAGAGCTAGAA
TGGT1_266810	sgTGGT1_266810_2	TGGGGATGTCAAGTTGCCAGGTGAACACCGATGAAGGTTTTAGAGCTAGAA
TGGT1_267040	sgTGGT1_267040_8	TGGGGATGTCAAGTTGAGATGCTTCTGAAACGCGAGTTTTAGAGCTAGAA
TGGT1_267340	sgTGGT1_267340_4	TGGGGATGTCAAGTTGCAGAGTGACCAATATCGCCGTTTTAGAGCTAGAA
TGGT1_267430	sgTGGT1_267430_3	TGGGGATGTCAAGTTGTATCGCAAGACCGAAGCGGGTTTTAGAGCTAGAA
TGGT1_267510	sgTGGT1_267510_8	TGGGGATGTCAAGTTGAGGGAGTTCAAGACGCGAAGTTTTAGAGCTAGAA
TGGT1_268210	sgTGGT1_268210_5	TGGGGATGTCAAGTTGGTGGATAATTCCTTTGGAGGTTTTAGAGCTAGAA
TGGT1_268400	sgTGGT1_268400_3	TGGGGATGTCAAGTTGAGAAGGGAGAAGCAGAGGGGTTTTAGAGCTAGAA
TGGT1_268685	sgTGGT1_268685_1	TGGGGATGTCAAGTTGCAGATTCTCAAATCGGAGTGTTTTAGAGCTAGAA
TGGT1_268835	sgTGGT1_268835_9	TGGGGATGTCAAGTTGCGGCATCTCAGGGAAGAAGGTTTTAGAGCTAGAA
TGGT1_269330	sgTGGT1_269330_8	TGGGGATGTCAAGTTGCGACGCGGTGAAATCTGAGGGTTTTAGAGCTAGAA
TGGT1_269700	sgTGGT1_269700_3	TGGGGATGTCAAGTTGCGTACGGGAAGGCTCTCCGGGTTTTAGAGCTAGAA
TGGT1_270100	sgTGGT1_270100_7	TGGGGATGTCAAGTTGCGTCTGGTCGACAAAGGAAGTTTTAGAGCTAGAA
TGGT1_270330	sgTGGT1_270330_2	TGGGGATGTCAAGTTGAGTGATGCGAGAAATCGAGGGTTTTAGAGCTAGAA
TGGT1_270690	sgTGGT1_270690_7	TGGGGATGTCAAGTTGTCAGCGAGCGAACCTGAAGAGTTTTAGAGCTAGAA

TGGT1_270880	sgTGGT1_270880_6	TGGGGATGTCAAGTTGCCAGAGATGAAGACCGACGGTTTTAGAGCTAGAA
TGGT1_270910	sgTGGT1_270910_1	TGGGGATGTCAAGTTGCGAAGGCTGGGGAAGCCGAGTTTTAGAGCTAGAA
TGGT1_271780	sgTGGT1_271780_10	TGGGGATGTCAAGTTGGAACAATCAGACGACGAAGGTTTTAGAGCTAGAA
TGGT1_271840	sgTGGT1_271840_2	TGGGGATGTCAAGTTGCCGACGCTGGCGAAAACAGGTTTTAGAGCTAGAA
TGGT1_271970	sgTGGT1_271970_2	TGGGGATGTCAAGTTGGTCGCCAGCACCTTCGTCGGTTTTAGAGCTAGAA
TGGT1_273060	sgTGGT1_273060_1	TGGGGATGTCAAGTTGAAAGTGTGGGCACACGACGGTTTTAGAGCTAGAA
TGGT1_273100	sgTGGT1_273100_1	TGGGGATGTCAAGTTGTGTTGGTGAAGAAGCGCAGGTTTTAGAGCTAGAA
TGGT1_273380	sgTGGT1_273380_2	TGGGGATGTCAAGTTGAAAAGGCCAGGAAGGAACCGGTTTTAGAGCTAGAA
TGGT1_273445	sgTGGT1_273445_5	TGGGGATGTCAAGTTGACGTGGTGGAGCTCTGCGTGTTTTAGAGCTAGAA
TGGT1_273630	sgTGGT1_273630_6	TGGGGATGTCAAGTTGCGGAGCAGCGCATGAGGAAGTTTTAGAGCTAGAA
TGGT1_273830	sgTGGT1_273830_8	TGGGGATGTCAAGTTGTCAGCGAGCTCGACAAAAGAGTTTTAGAGCTAGAA
TGGT1_274160	sgTGGT1_274160_2	TGGGGATGTCAAGTTGCAGAGGTTGACTCTCGGGGGTTTTAGAGCTAGAA
TGGT1_276170	sgTGGT1_276170_5	TGGGGATGTCAAGTTGATGAATCTCGACCGAAACGAGTTTTAGAGCTAGAA
TGGT1_277700	sgTGGT1_277700_4	TGGGGATGTCAAGTTGACTTCGACATACCTTATTGGTTTTAGAGCTAGAA
TGGT1_278975	sgTGGT1_278975_8	TGGGGATGTCAAGTTGTTGTCTGAAGGGGAAGCGAGTTTTAGAGCTAGAA
TGGT1_280440	sgTGGT1_280440_8	TGGGGATGTCAAGTTGACGTAGTGGAGGTTCCACGCGTTTTAGAGCTAGAA
TGGT1_282180	sgTGGT1_282180_10	TGGGGATGTCAAGTTGCAGGACATCACCTCGCTGCGTTTTAGAGCTAGAA
TGGT1_284570	sgTGGT1_284570_1	TGGGGATGTCAAGTTGCAGCACATGTGCAACCCGGGTTTTAGAGCTAGAA
TGGT1_284590	sgTGGT1_284590_10	TGGGGATGTCAAGTTGTGCGGGAGACGCGACAGCCGGTTTTAGAGCTAGAA
TGGT1_285272	sgTGGT1_285272_3	TGGGGATGTCAAGTTGCAGCCGGACAAGCACGAGAGTTTTAGAGCTAGAA
TGGT1_286070	sgTGGT1_286070_5	TGGGGATGTCAAGTTGCACTGCATCACGTTGCGGAGTTTTAGAGCTAGAA
TGGT1_286410	sgTGGT1_286410_5	TGGGGATGTCAAGTTGCAGGCACAACAGAGAGCTGGTTTTAGAGCTAGAA
TGGT1_286440	sgTGGT1_286440_5	TGGGGATGTCAAGTTGTCAAGCACAAACGCAAACAGGTTTTAGAGCTAGAA
TGGT1_286790	sgTGGT1_286790_10	TGGGGATGTCAAGTTGGAGCGTGTTGCTCAGAAGCGTTTTAGAGCTAGAA

TGGT1_288270	sgTGGT1_288270_3	TGGGGATGTCAAGTTGAAGAAGGCGAAGAGCGGCGGTTTTAGAGCTAGAA
TGGT1_288990	sgTGGT1_288990_6	TGGGGATGTCAAGTTGCGGGAAAATGAAGAAAACGAGTTTTAGAGCTAGAA
TGGT1_289100	sgTGGT1_289100_8	TGGGGATGTCAAGTTGAAACACGAGAAAGGCTCCGGGTTTTAGAGCTAGAA
TGGT1_289200	sgTGGT1_289200_7	TGGGGATGTCAAGTTGTGTGAGCTCGCGAATAGACGGTTTTAGAGCTAGAA
TGGT1_289640	sgTGGT1_289640_10	TGGGGATGTCAAGTTGCAGTTGCCCCAGTTAAGGCGTTTTAGAGCTAGAA
TGGT1_289950	sgTGGT1_289950_10	TGGGGATGTCAAGTTGTGGCGTTGCTGAGAAGAAGGTTTTAGAGCTAGAA
TGGT1_290020	sgTGGT1_290020_8	TGGGGATGTCAAGTTGCAGAGCGGCACAGACGACGGTTTTAGAGCTAGAA
TGGT1_290170	sgTGGT1_290170_6	TGGGGATGTCAAGTTGCAACCACCATCAGAACGCGGTTTTAGAGCTAGAA
TGGT1_290180	sgTGGT1_290180_7	TGGGGATGTCAAGTTGAAAGTCTCGACAGCCGCCCAGTTTTAGAGCTAGAA
TGGT1_290460	sgTGGT1_290460_3	TGGGGATGTCAAGTTGATGGTCGACGACAAAGACGGTTTTAGAGCTAGAA
TGGT1_291080	sgTGGT1_291080_9	TGGGGATGTCAAGTTGCACAAACGGTGCAGCTCCGGTTTTAGAGCTAGAA
TGGT1_292020	sgTGGT1_292020_5	TGGGGATGTCAAGTTGTTGTGGAGGGGTCGACCGGGTTTTAGAGCTAGAA
TGGT1_292170	sgTGGT1_292170_7	TGGGGATGTCAAGTTGGAGCAGGCGACAAAAGTGCGTTTTAGAGCTAGAA
TGGT1_292200	sgTGGT1_292200_10	TGGGGATGTCAAGTTGGAGAAGGAGAAGGCTCCCGGTTTTAGAGCTAGAA
TGGT1_293170	sgTGGT1_293170_10	TGGGGATGTCAAGTTGAGCTCGAAACAGACACCAGGTTTTAGAGCTAGAA
TGGT1_293380	sgTGGT1_293380_1	TGGGGATGTCAAGTTGGTGTACGGACAGCCGGAGGGTTTTAGAGCTAGAA
TGGT1_293570	sgTGGT1_293570_6	TGGGGATGTCAAGTTGCAACACTGGAACGAGCCGCGTTTTAGAGCTAGAA
TGGT1_293610	sgTGGT1_293610_5	TGGGGATGTCAAGTTGCGGCGCTGAATCGGAGCCGGTTTTAGAGCTAGAA
TGGT1_294190	sgTGGT1_294190_7	TGGGGATGTCAAGTTGAGTGTCGGAGCGCGAAGCCGGTTTTAGAGCTAGAA
TGGT1_294230	sgTGGT1_294230_9	TGGGGATGTCAAGTTGCCGGCCAGTCCGTTTGCTGAGTTTTAGAGCTAGAA
TGGT1_294250	sgTGGT1_294250_9	TGGGGATGTCAAGTTGGACCGCCGCCGGTTTCGAGGTTTTAGAGCTAGAA
TGGT1_294310	sgTGGT1_294310_3	TGGGGATGTCAAGTTGTTCTGACATTGCAGAGCGGGTTTTAGAGCTAGAA
TGGT1_294902	sgTGGT1_294902_5	TGGGGATGTCAAGTTGCTGTTTGACCGGAACGCGGGTTTTAGAGCTAGAA
TGGT1_294930	sgTGGT1_294930_5	TGGGGATGTCAAGTTGCGCCTGAGCCCACCGACAGGGTTTTAGAGCTAGAA

TGGT1_297170	sgTGGT1_297170_5	TGGGGATGTCAAGTTGTCGAAACCCACAGGACGCGCGTTTTAGAGCTAGAA
TGGT1_297780	sgTGGT1_297780_10	TGGGGATGTCAAGTTGAGAGAAGGGATGCAGACGGGTTTTAGAGCTAGAA
TGGT1_297810	sgTGGT1_297810_8	TGGGGATGTCAAGTTGATGTTCTCGCCGCTCCACGGTTTTAGAGCTAGAA
TGGT1_297960B	sgTGGT1_297960B_3	TGGGGATGTCAAGTTGACCAGAAACAAGGTAGTGGGTTTTAGAGCTAGAA
TGGT1_298030	sgTGGT1_298030_9	TGGGGATGTCAAGTTGACGATCCCAGAGCAAGGACGTTTTAGAGCTAGAA
TGGT1_298630	sgTGGT1_298630_2	TGGGGATGTCAAGTTGGGTCACGAAGACGGAGGGGGTTTTAGAGCTAGAA
TGGT1_299070	sgTGGT1_299070_2	TGGGGATGTCAAGTTGCTGCGACGGGAACTCCGGGGTTTTAGAGCTAGAA
TGGT1_299080	sgTGGT1_299080_5	TGGGGATGTCAAGTTGCAGAACGTCCAGAAGAGCGAGTTTTAGAGCTAGAA
TGGT1_301380	sgTGGT1_301380_10	TGGGGATGTCAAGTTGAAGGGGAAGAACAAGGAAAGTTTTAGAGCTAGAA
TGGT1_301410	sgTGGT1_301410_5	TGGGGATGTCAAGTTGCTGCAGCGCCTGAAGACCGGTTTTAGAGCTAGAA
TGGT1_304890	sgTGGT1_304890_9	TGGGGATGTCAAGTTGCATCGACGACAGCCAGGCAGGTTTTAGAGCTAGAA
TGGT1_304990	sgTGGT1_304990_6	TGGGGATGTCAAGTTGCGAGGAGACTAGAGAAGCGAGTTTTAGAGCTAGAA
TGGT1_305140	sgTGGT1_305140_6	TGGGGATGTCAAGTTGAAAGTGGATGAGAAGCTGGGTTTTAGAGCTAGAA
TGGT1_305340	sgTGGT1_305340_1	TGGGGATGTCAAGTTGGGGAGCCTTGCCTACGGGGGTTTTAGAGCTAGAA
TGGT1_305470	sgTGGT1_305470_2	TGGGGATGTCAAGTTGAGTCGAGGAGGCGAGACGGGTTTTAGAGCTAGAA
TGGT1_306280	sgTGGT1_306280_9	TGGGGATGTCAAGTTGAAGTCTTTCACCGGTTCTGGGTTTTAGAGCTAGAA
TGGT1_306640	sgTGGT1_306640_8	TGGGGATGTCAAGTTGAGTAAAGAGGACCGATACGAGTTTTAGAGCTAGAA
TGGT1_306670	sgTGGT1_306670_6	TGGGGATGTCAAGTTGGAGTGTGTTCACGTACTGAGTTTTAGAGCTAGAA
TGGT1_308920	sgTGGT1_308920_3	TGGGGATGTCAAGTTGGAGTACGAGGATATCGTGGGTTTTAGAGCTAGAA
TGGT1_309170	sgTGGT1_309170_9	TGGGGATGTCAAGTTGTGCAGCCTGGCGGTCCCGAGTTTTAGAGCTAGAA
TGGT1_309380	sgTGGT1_309380_10	TGGGGATGTCAAGTTGCATGTGGAGAGAGCCGCAGCGTTTTAGAGCTAGAA
TGGT1_309390	sgTGGT1_309390_10	TGGGGATGTCAAGTTGAGCACAACCGCCGAAAACGCGTTTTAGAGCTAGAA
TGGT1_309420	sgTGGT1_309420_3	TGGGGATGTCAAGTTGAGAACGACTTGCCTCCGCGGGTTTTAGAGCTAGAA
TGGT1_309580	sgTGGT1_309580_8	TGGGGATGTCAAGTTGCACCAGCCAAAGTAGAGGGGTTTTAGAGCTAGAA

TGGT1_310080	sgTGGT1_310080_9	TGGGGATGTCAAGTTGTTTGACGAAGCTGACGAGAGTTTTAGAGCTAGAA
TGGT1_310118	sgTGGT1_310118_10	TGGGGATGTCAAGTTGATAGGAGTAATGCTGAGGAGTTTTAGAGCTAGAA
TGGT1_310290	sgTGGT1_310290_7	TGGGGATGTCAAGTTGCGCGCAAGACAGGACGACGGTTTTAGAGCTAGAA
TGGT1_310360	sgTGGT1_310360_3	TGGGGATGTCAAGTTGCAGCCGACAGGAACTGGGTGTTTTAGAGCTAGAA
TGGT1_310430A	sgTGGT1_310430A_1	TGGGGATGTCAAGTTGCTGAGGCCGAACTCGCCGGGTTTTAGAGCTAGAA
TGGT1_310430B	sgTGGT1_310430B_4	TGGGGATGTCAAGTTGCGTGACGGACCCGAAAGCGAGTTTTAGAGCTAGAA
TGGT1_310500	sgTGGT1_310500_8	TGGGGATGTCAAGTTGGAGGCTACGGGACGAGACGGTTTTAGAGCTAGAA
TGGT1_310850	sgTGGT1_310850_10	TGGGGATGTCAAGTTGAATGCGTACATCGACAGCATGTTTTAGAGCTAGAA
TGGT1_310930	sgTGGT1_310930_7	TGGGGATGTCAAGTTGGGAGGGAAGGGAGACGCTGGTTTTAGAGCTAGAA
TGGT1_312390	sgTGGT1_312390_4	TGGGGATGTCAAGTTGTCAAGCCCGACTCGCGAGGGTTTTAGAGCTAGAA
TGGT1_312500	sgTGGT1_312500_10	TGGGGATGTCAAGTTGCAGGAGGAGGGAGGAGACGAGTTTTAGAGCTAGAA
TGGT1_312618	sgTGGT1_312618_6	TGGGGATGTCAAGTTGAGACGCTTGGCACACCACAGGTTTTAGAGCTAGAA
TGGT1_312622	sgTGGT1_312622_3	TGGGGATGTCAAGTTGATGACGGTCCGCGCGACCGGGTTTTAGAGCTAGAA
TGGT1_312630	sgTGGT1_312630_1	TGGGGATGTCAAGTTGATCGCCGCAGAGACAGCGGGTTTTAGAGCTAGAA
TGGT1_312650	sgTGGT1_312650_8	TGGGGATGTCAAGTTGCAGAAGTTCCGACAGGCAGGTTTTAGAGCTAGAA
TGGT1_313160	sgTGGT1_313160_5	TGGGGATGTCAAGTTGTCAGCAGCGAGATGCCGAGGTTTTAGAGCTAGAA
TGGT1_313310	sgTGGT1_313310_3	TGGGGATGTCAAGTTGACTGAAGGTGAAGAGGGCGAGTTTTAGAGCTAGAA
TGGT1_313380	sgTGGT1_313380_8	TGGGGATGTCAAGTTGTGAGCGATGAGCCGCAGCACGTTTTAGAGCTAGAA
TGGT1_313570	sgTGGT1_313570_9	TGGGGATGTCAAGTTGACGCGGCTGAGCGTCCCCAGTTTTAGAGCTAGAA
TGGT1_313960	sgTGGT1_313960_3	TGGGGATGTCAAGTTGAAAGACGAGAGACAACGCGTGTTTTAGAGCTAGAA
TGGT1_314415	sgTGGT1_314415_5	TGGGGATGTCAAGTTGGAGGATGAGGAAGAAGAATGTTTTAGAGCTAGAA
TGGT1_314970	sgTGGT1_314970_3	TGGGGATGTCAAGTTGAGGAGTTCTCGAACGCAGGGTTTTAGAGCTAGAA
TGGT1_315190	sgTGGT1_315190_6	TGGGGATGTCAAGTTGGCGAGGGCGAACGAAGAGGGTTTTAGAGCTAGAA
TGGT1_315930	sgTGGT1_315930_2	TGGGGATGTCAAGTTGTTGGAGGAGAAACAGACTGGTTTTAGAGCTAGAA

TGGT1_316140	sgTGGT1_316140_4	TGGGGATGTCAAGTTGGAAGAAGAGGACGACGTGGGTTTTAGAGCTAGAA
TGGT1_316760	sgTGGT1_316760_9	TGGGGATGTCAAGTTGCTGTGCCGCAGAAGCCAGGGTTTTAGAGCTAGAA
TGGT1_291180	sgTGGT1_291180_4	TGGGGATGTCAAGTTGGTTCGTGTGGATCTGACGGGTTTTAGAGCTAGAA
TGGT1_318420	sgTGGT1_318420_1	TGGGGATGTCAAGTTGTGCGCCAGCCGAACATCGGGTTTTAGAGCTAGAA
TGGT1_319850	sgTGGT1_319850_2	TGGGGATGTCAAGTTGCAGAAACTGGCAGACAGCGAGTTTTAGAGCTAGAA
TGGT1_319960	sgTGGT1_319960_7	TGGGGATGTCAAGTTGAAGATGGCAGGAATGATGCGGTTTTAGAGCTAGAA
TGGT1_320020	sgTGGT1_320020_1	TGGGGATGTCAAGTTGCCTGGAAACAGATTCGCCAGTTTTAGAGCTAGAA
TGGT1_320470	sgTGGT1_320470_2	TGGGGATGTCAAGTTGGATGCTGCAGAGAGGACAGGTTTTAGAGCTAGAA
TGGT1_320480	sgTGGT1_320480_6	TGGGGATGTCAAGTTGGTTGGGAACAAACTCGACTGTTTTAGAGCTAGAA
TGGT1_320700	sgTGGT1_320700_8	TGGGGATGTCAAGTTGGGCGAAGTACAAGGAGAAGGTTTTAGAGCTAGAA
TGGT1_359190	sgTGGT1_359190_9	TGGGGATGTCAAGTTGCCAGGCACCAACAGCGCCGGTTTTAGAGCTAGAA

Table A.6 - List of sgRNAs used for downstream characterisation of the screen candidates

Designer	sgRNA sequence with overhangs for cloning	Target
Dr. Singer	AAGTTGTGGAGTTTGCCGGGGCTGCAG	SAG1 internal tagging sgRNA fwd
Janessa	AAGTTGTGTAGAGCGCGTACTGTGTGG	TGGT1-320020 3' tagging sgRNA fwd
Dr. Gras	AAGTTGCAGGGAACCGAAGGTTGTGG	TGGT1-248490 3' tagging sgRNA fwd
Dr. Gras	AAGTTGAACGCTTCAGCGCTGTTTCAG	TGGT1-263680 3' tagging sgRNA fwd
Janessa	AAGTTGGCGAGACAGACTCGACACTG	TGGT1_294930 3' tagging sgRNA fwd
Janessa	AAGTTGTTCTTCGACCGAATGCAGAGG	TGGT1_254230 3' tagging sgRNA fwd
Janessa	AAGTTGCCCGGAAGCGACTCTCCCTG	TGGT1_263300 3' tagging sgRNA fwd
Janessa	AAGTTGACAAATCGAAGACTTGAACG	TGGT1_229460 3' tagging sgRNA fwd
Janessa	AAGTTGTCCAATGTACAGAGAACTCGG	TGGT1_286790 3' tagging sgRNA fwd
Janessa	AAGTTGCGGTGTCCCAGGAGCTGCGG	TGGT1_249970 3' tagging sgRNA fwd
Janessa	AAGTTACATTTCTTGTCTAACAGAGG	TGGT1_210490 3' tagging sgRNA fwd
Janessa	AAGTTGTGAGGAGTTCTTGTTGGGCGG	TGGT1_301410 5' loxP sgRNA fwd
Janessa	AAGTTGCAGTTGACCTCGAGAGAAGG	TGGT1_301410 3' tagging sgRNA fwd
Janessa	AAGTTGCATCCGCCAAATGGGCCTCGG	TGGT1_255920 3' tagging sgRNA fwd
Janessa	AAGTTGTCACACACCGAAGGTATCTGG	TGGT1_226320 3' tagging sgRNA fwd
Janessa	AAGTTGCATGAAGCCGCTGCGACTGGG	TGGT1_269700 3' tagging sgRNA fwd
Janessa	AAGTTGCATGGATGCCACTCGCCTTG	TGGT1_289950 3' tagging sgRNA fwd
Janessa	AAGTTATTGCAAAAGAGAAAAGACTG	TGGT1_259720 3' tagging sgRNA fwd
Janessa	AAGTTGGGAAAATTAAAAACAGGGAG	TGGT1_213392 3' tagging sgRNA fwd
Janessa	AAGTTGCGCGAGGTCGAGCTGTCTGG	MyoF 3' tagging sgRNA fwd
Janessa	AAGTT ATCATCACGTAGCAGCAGAA G	Syntaxin6 3' tagging sgRNA fwd
Dr. Gras	AAGTTGCTCCTACAGAGCTGCAAGAG	SortLR 3' tagging sgRNA fwd
Dr. Singer	AAGTTAATAGGGGTCTGTAGGTTAAG	Formin2 3' tagging sgRNA fwd
Janessa	AAGTTGCCAGGAAGAAAGCATTCTCCG	UPRT 1st exon sgRNA fwd
Janessa	AAGTTGCATGCGCACTCAGAGCCTTG	AP-4E 3' tagging sgRNA fwd

Table A.7 - List of oligos designed for downstream characterisation of the screen candidates

Designer	Primer	Purpose
Janessa	AAGTTGTGTAGAGCGCGTACTGTGTGG	TGGT1-320020 3' tagging sgRNA fwd
Janessa	AAAACCACACAGTACGCGCTCTACACA	TGGT1-320020 3' tagging sgRNA rvs
Janessa	AAGAGCCAGCGGACGAAGACCCGCGTGCACCGAGTCCAGAGGTCGCTGTG GCTAAAATTGGAAGTGGAGG	TGGT1-320020 3' tagging homology primer fwd
Janessa	TTCGACTCTGTGCGTTGAGGGCTTTCGACACACCACACACAGTACGCGCTATAACTTCGTATAA TGTATGCTATACG	TGGT1-320020 3' tagging homology primer rvs
Janessa	CTGTCTTCCGAGACCCTCATC	TGGT1-320020 3' tagging analytical primer fwd
Janessa	GCTGTATCCTCGTGTCGCT	TGGT1-3200203' tagging analytical primer rvs
Dr. Gras	AAGTTGCAGGGAACCGAAGGTTGTGG	TGGT1-248490 3' tagging sgRNA fwd
Dr. Gras	AAAACCACAACCTTCGGTTCCCTGCA	TGGT1-248490 3' tagging sgRNA rvs
Dr. Gras	GTGTTCCACTCACACGAAGAAAGAAACGAGCAGGGAACCGAAGGTTGTGA GCTAAAATTGGAAGTGGAGG	TGGT1-248490 3' tagging homology primer fwd
Dr. Gras	TCGCCAGAAGCAGTCGAGAATTTGTCCAAGTTCGCTCTAGAGTCGCCTCA ATAACTTCGTATAATGTATGCTATACG	TGGT1-248490 3' tagging homology primer rvs
Dr. Gras	CATCCCATCACGAGAACTCC	TGGT1-248490 3' tagging analytical primer fwd
Dr. Gras	CTACAACACATTCGCAACACC	TGGT1-248490 3' tagging analytical primer rvs
Dr. Gras	AAGTTGAACGCTTCAGCGCTGTTTCA G	TGGT1-263680 3' tagging sgRNA fwd
Dr. Gras	AAAACTGAAACAGCGCTGAAGCGTTCA	TGGT1-263680 3' tagging sgRNA rvs
Dr. Gras	TGGACCTCAGAGAAGACCCAGTGTCCTTCCCCTTCACCTTGAAACAGCGC GCTAAAATTGGAAGTGGAGG	TGGT1-263680 3' tagging homology primer fwd
Dr. Gras	GGAAAACGCAGAGACGGACCTGGCGCGACTGGGGTCCTTCGAACGCTTCA ATAACTTCGTATAATGTATGCTATACG	TGGT1-263680 3' tagging homology primer rvs
Dr. Gras	GTTCACTCGCCATGTCTCTG	TGGT1-263680 3' tagging analytical primer fwd
Dr. Gras	GAAGAGCGAAGGAGACAACG	TGGT1-263680 3' tagging analytical primer rvs
Janessa	AAGTT GGCGAGACAGACTCGACACT G	TGGT1_294930 3' tagging sgRNA fwd

Janessa	AAAAC AGTGTCGAGTCTGTCTCGCC A	TGGT1_294930 3' tagging sgRNA rvs
Janessa	AGCGTCCTGCGCCGAGCGTGGAGTCTGTCTCGCCGAAAAAGAAGAAAGTTGCTAAAATTGGA AGTGGAGG	TGGT1_294930 3' tagging homology primer fwd
Janessa	TCTCTACCCTGCGTTCCTCTCCCAGTTCTCTCCCAGTTCTTGAAAAAATTATAACTTCGTATAAT GTATGCTATACG	TGGT1_294930 3' tagging homology primer rvs
Janessa	AAGAAAAACGTGCGAAGGCC	TGGT1_294930 3' tagging analytical primer fwd
Janessa	CTCCCAGTTCTCTCCCAGTTC	TGGT1_294930 3' tagging analytical primer rvs
Janessa	AAGTT G TTCTTCGACCGAATGCAGAG G	TGGT1_254230 3' tagging sgRNA fwd
Janessa	AAAAC CTCTGCATTCGGTCGAAGAAC A	TGGT1_254230 3' tagging sgRNA rvs
Janessa	AGGACGCAAACGCGCCGCAGACGCCCTGGGGAACGCACTCGATATGGGGGGCTAAAATTGG AAGTGGAGG	TGGT1_254230 3' tagging homology primer fwd
Janessa	TGCACCTGCACCCGCGTGGTGACCGTGCCTCCAAAGCGTCTCTCCCGCTCATAACTTCGTATAA TGTATGCTATACG	TGGT1_254230 3' tagging homology primer rvs
Janessa	GAAACGAAACAGGGAACGTCG	TGGT1_254230 3' tagging analytical primer fwd
Janessa	GGAACAAAACCGGTCGCAAAT	TGGT1_254230 3' tagging analytical primer rvs
Janessa	AAGTTGCCCGGAAGCGACTCTCCCTG	TGGT1_263300 3' tagging sgRNA fwd
Janessa	AAAACAGGGAGAGTCGCTTCCGGGCA	TGGT1_263300 3' tagging sgRNA rvs
Janessa	CGAGCAATCCTGACGCGGTGAAGCACGGTTTGAAGCTCGAGATCTGTGCCGCTAAAATTGGA AGTGGAGG	TGGT1_263300 3' tagging homology primer fwd
Janessa	CGTCCCAGCGGGTTCATTGCTGCCTTGCTGAGGGTGGGTGGCTTCCGGGC ATAACTTCGTATAATGTATGCTATACG	TGGT1_263300 3' tagging homology primer rvs
Janessa	GACCACGGACAACAAGTCGG	TGGT1_263300 3' tagging analytical primer fwd
Janessa	GCACATAGAGGTTGACCGCC	TGGT1_263300 3' tagging analytical primer rvs
Janessa	AAGTTGACAAATCGAAGACTTGAACG	TGGT1_229460 3' tagging sgRNA fwd
Janessa	AAAACGTTCAAGTCTTCGATTTGTCA	TGGT1_229460 3' tagging sgRNA rvs
Janessa	ACTCTTTGAATGTTCTGTCACGCGAGGACGCGCTCGACAAATCGAAGACTGCTAAAATTGGAA GTGGAGG	TGGT1_229460 3' tagging homology primer fwd

Janessa	TGTGTGTATGGACGGCGGAAGAGAGGACACGATGGGGAGGGCATCCGGTT ATAACTTCGTATAATGTATGCTATACG	TGGT1_229460 3' tagging homology primer rvs
Janessa	TACGTCCGTTCATTGTGTTCGTA	TGGT1_229460 3' tagging analytical primer fwd
Janessa	TCTGGACAGAATGCCACAACAG	TGGT1_229460 3' tagging analytical primer rvs
Janessa	AAGTTGTCCAATGTACAGAGAACTCGG	TGGT1_286790 3' tagging sgRNA fwd
Janessa	AAAACCGAGTTCTCTGTACATTGGACA	TGGT1_286790 3' tagging sgRNA rvs
Janessa	TCTCTGCAGACTCGGATGACGCGAGCGACAAAGTATCTGAGACGAAAAGCGCTAAAATTGGA AGTGGAGG	TGGT1_286790 3' tagging homology primer fwd
Janessa	CACTCCAAGCGACCCAGACATGGCCAATTCACAGTACATTGGAGCGTCAGATAACTTCGTATA ATGTATGCTATACG	TGGT1_286790 3' tagging homology primer rvs
Janessa	CGCTTGTTCAGACGAAAATCGAG	TGGT1_286790 3' tagging analytical primer fwd
Janessa	GTAACGAGAGGCTGCCCTT	TGGT1_286790 3' tagging analytical primer rvs
Janessa	AAGTTGCGGTGTCCCAGGAGCTGCGG	TGGT1_249970 3' tagging sgRNA fwd
Janessa	AAAACCGCAGCTCCTGGGACACCGCA	TGGT1_249970 3' tagging sgRNA rvs
Janessa	AGAGCTGGCAAGAACAGATTCAGTCCCTGATGAAGTTCATGTCGATGAAAGCTAAAATTGGA AGTGGAGG	TGGT1_249970 3' tagging homology primer fwd
Janessa	TCAAGAAGAGCCAGAATAAACCGCGGCTTCTGGGACACCGCTCAAAATGC ATAACTTCGTATAATGTATGCTATACG	TGGT1_249970 3' tagging homology primer rvs
Janessa	GAGGAGAAAGGACATGCGAATT	TGGT1_249970 3' tagging analytical primer fwd
Janessa	CAAAGTGGCCCAGAACACTC	TGGT1_249970 3' tagging analytical primer rvs
Janessa	AAGTTACATTTCTTGTCTAACAGAGG	TGGT1_210490 3' tagging sgRNA fwd
Janessa	AAAACCTCTGTTAGACAAGAAATGTA	TGGT1_210490 3' tagging sgRNA rvs
Janessa	GAAAGCTTGCTCCGAGTCTCCCGAATTTTCGTTTCCTTGAGCACTGTCTAGCTAAAATTGGAAG TGGAGG	TGGT1_210490 3' tagging homology primer fwd
Janessa	GTCTCCAGACAGCGGTCCTAAACAAAAATGACTGTGGTAGGCAAGAAATG ATAACTTCGTATAATGTATGCTATACG	TGGT1_210490 3' tagging homology primer rvs
Janessa	GCTCATTTCCCATACTGACAGGA	TGGT1_210490 3' tagging analytical primer fwd

Janessa	CATTGCGTGTTGCTCCACAG	TGGT1_210490 3' tagging analytical primer rvs
Janessa	AAGTTGTGAGGAGTTCTTGTTGGGCGG	TGGT1_301410 5' loxP sgRNA fwd
Janessa	AAAACCGCCCAACAAGAACTCCTCACA	TGGT1_301410 5' loxP sgRNA fwd
Janessa	CGGACCTCGTCGTCTGCAGCCGACGCGCCTCGCATAACTTCGTATAGCATACATTATACGAAG TTATCCAACAAGAACTCCTCAAAATGGACAGAACTCT	TGGT1_301410 5' loxP
Janessa	CGAACCGTGTCCAGCCA	TGGT1_301410 5' loxP fwd analytical primer
Janessa	GGAGTTCTTGTTGGATAACTTCGTATAATG	TGGT1_301410 5' loxP rvs analytical primer
Janessa	ACGCTGACTGCCCTACG	TGGT1_301410 5' loxP rvs analytical for sequencing
Janessa	AAGTTGCAGTTGACCTCGAGAGAAGG	TGGT1_301410 3' tagging sgRNA fwd
Janessa	AAAACCTTCTCTCGAGGTCAACTGCA	TGGT1_301410 3' tagging sgRNA rvs
Janessa	TCGAGAGTCGGAATGCAGAGGCGAGAACGAAGTTTGCGTTCGTCACGAGCGCTAAAATTGG AAGTGGAGG	TGGT1_301410 3' tagging homology primer fwd
Janessa	GTAAGTCGCGGCCACCATTGGCTACTATCGATGTCAACTGCGCTTCTCTT ATAACTTCGTATAATGTATGCTATACG	TGGT1_301410 3' tagging homology primer rvs
Janessa	CTTCTCCAGGAAGGACGGAATG	TGGT1_301410 3' tagging analytical primer fwd
Janessa	CGTTGTCTTGGAATCTGACTGC	TGGT1_301410 3' tagging analytical primer rvs
Janessa	AAGTT GCATCCGCCAAATGGGCCTCGG	TGGT1_255920 3' tagging sgRNA fwd
Janessa	AAAACCGAGGCCCATTTGGCGGATGCA	TGGT1_255920 3' tagging sgRNA rvs
Janessa	TGAAAGAACTTCAGAAGGATCAAGCAGGTCCGCGCGGACCGTTCGGAGGTGCTAAAATTGGA AGTGGAGG	TGGT1_255920 3' tagging homology primer fwd
Janessa	CCGGCGCTCATCCTGAACTTCCAGACCGGCGCTCATCCGCCAAATGGGCCATAACTTCGTATA ATGTATGCTATACG	TGGT1_255920 3' tagging homology primer rvs
Janessa	GAAAAGCAGTTTATTGGGCGC	TGGT1_255920 3' tagging analytical primer fwd
Janessa	CGTTGAGAGTATCGGCTTGCA	TGGT1_255920 3' tagging analytical primer rvs
Janessa	AAGTTGTCACACACCGAAGGTATCTGG	TGGT1_226320 3' tagging sgRNA fwd
Janessa	AAAACCAGATACCTTCGGTGTGTGACA	TGGT1_226320 3' tagging sgRNA rvs

Janessa	GCGACAGCGGCGCCAGAGGGCGAGGCAGCGTAGGGCGGGGCGAAGGCCGTGCTAAAATTG GAAGTGGAGG	TGGT1_226320 3' tagging homology primer fwd
Janessa	TCTGTGAATTGAGGCACAGAGTGACAAATAACCTCGGTGTGTGACGCTCC ATAACTTCGTATAATGTATGCTATACG	TGGT1_226320 3' tagging homology primer rvs
Janessa	GGGCAGACGACGAGTAGG	TGGT1_226320 3' tagging analytical primer fwd
Janessa	CCCAACAAGTTCGCCGTC	TGGT1_226320 3' tagging analytical primer rvs
Janessa	AAGTTGCATGAAGCCGCTGCGACTGGG	TGGT1_269700 3' tagging sgRNA fwd
Janessa	AAAACCCAGTCGCAGCGGCTTCATGCA	TGGT1_269700 3' tagging sgRNA rvs
Janessa	AGGGCATGATTGGTGCCACTTCCCATCCGCAATCGCAGCGGCTTCATGCCGCTAAAATTGGAA GTGGAGG	TGGT1_269700 3' tagging homology primer fwd
Janessa	ACTGTGGGTCACGGCAGAATATTGCAGTCTAGGCATGAAGCCGCTGCGAC ATAACTTCGTATAATGTATGCTATACG	TGGT1_269700 3' tagging homology primer rvs
Janessa	GCCGTACGAGGAGTTGTTGT	TGGT1_269700 3' tagging analytical primer fwd
Janessa	CGATGTGGCTACCTAAAAAGTGT	TGGT1_269700 3' tagging analytical primer rvs
Janessa	AAGTTGCATGGATGCCACTCGCCTTG	TGGT1_289950 3' tagging sgRNA fwd
Janessa	AAAACAAGGCGAGTGGCATCCATGCA	TGGT1_289950 3' tagging sgRNA rvs
Janessa	CAACGGAAGACAAGCAGAAATTCATTATTCTGAAGCCTGAATATCGCATGGCTAAAATTGGAA GTGGAGG	TGGT1_289950 3' tagging homology primer fwd
Janessa	GGAGGTGAGCAAGCAGAGATAGATGGAGATTGGCATCCATGCTTTCTTCT ATAACTTCGTATAATGTATGCTATACG	TGGT1_289950 3' tagging homology primer rvs
Janessa	GGAAGTGACTCTCCGCCG	TGGT1_289950 3' tagging analytical primer fwd
Janessa	CTGGGAAGGAGGATCGGAAAT	TGGT1_289950 3' tagging analytical primer rvs
Janessa	AAGTTATTGCAAAAGAGAAAAGACTG	TGGT1_259720 3' tagging sgRNA fwd
Janessa	AAAACAGTCTTTTCTCTTTTGCAATA	TGGT1_259720 3' tagging sgRNA rvs
Janessa	ACGACGAGACATTGCAAAAGAGAAAGGATTCCG AGAGGATCGGCTCTTTTGCTAAAATTGGA AGTGGAGG	TGGT1_259720 3' tagging homology primer fwd

Janessa	TGTCACGTTCGTCTGCGCTTCTCATCAAAAAGAGCCGATCCTCTCCGAGT ATAACTTCGTATAATGTATGCTATACG	TGGT1_259720 3' tagging homology primer rvs
Janessa	GGCTCGGATTCTTCTTCAAGG	TGGT1_259720 3' tagging analytical primer fwd
Janessa	CCTGTGTCTCCTCTTCTCATGT	TGGT1_259720 3' tagging analytical primer rvs
Janessa	AAGTTGGGAAAATTAAAAACAGGGAG	TGGT1_213392 3' tagging sgRNA fwd
Janessa	AAAACTCCCTGTTTTTAATTTTCCCA	TGGT1_213392 3' tagging sgRNA rvs
Janessa	GCGCCGGCGCGTCGGGAGGGCCTTTGCAGGGTGTGGGGGCGGGGGAAAATGCTAAAATTG GAAGTGGAGG	TGGT1_213392 3' tagging homology primer fwd
Janessa	TCTATCCATCCGAGCTCATTCGAGTCACACCCGCTGCCCGGGAGCCCTCCATAACTTCGTATAA TGTATGCTATACG	TGGT1_213392 3' tagging homology primer rvs
Janessa	CAGATGTCTCCGTTGCCAGC	TGGT1_213392 3' tagging analytical primer fwd
Janessa	CAAGTGGACGTGAGGCGCT	TGGT1_213392 3' tagging analytical primer rvs
Janessa	AAGTTGCGCGAGGTCGAGCTGTCTGG	TGGT1_278870 myoF 3' tagging sgRNA fwd
Janessa	AAAACCAGACAGCTCGACCTCGCGCA	TGGT1_278870 myoF 3' tagging sgRNA rvs
Janessa	ATTTCTCTGCCGCTGGCGGCGGCGCCGGGGGGGCGCGAGGTCGAGCTGTCGCTAAAATTGG AAGTGGAGG	TGGT1_278870 myoF 3' tagging homology primer fwd
Janessa	GAGATTGTCCCGGAAGCTTCAACAGTTTTTTACAGCGCCGGCAGCCTCAGATAACTTCGTATA ATGTATGCTATACG	TGGT1_278870 myoF 3' tagging homology primer rvs
Janessa	GAACTTGCAAGACACTTTGTTGG	TGGT1_278870 myoF 3' tagging analytical primer fwd
Janessa	AGTCGACAGCTCGTTGACG	TGGT1_278870 myoF 3' tagging analytical primer rvs
Janessa	AAGTT ATCATCACGTAGCAGCAGAA G	syntaxin6 3' tagging sgRNA fwd
Janessa	AAAAC TTCTGCTGCTACGTGATGAT A	syntaxin6 3' tagging sgRNA fwd
Janessa	TCTGGCTGTCATGCATTGCCTTGTTACTTTTTCTTCTGCTCATCATCACG GCTAAAATTGGAAGTGGAGG	syntaxin6 3' tagging homology primer fwd
Janessa	GAGAAACCTGAAGTCTCACGCGCAACAGAAATCGCGGTGCTTCCCCTTTC ATAACTTCGTATAATGTATGCTATACG	syntaxin6 3' tagging homology primer rvs
Janessa	GCGTCGTTGGAGACATGACT	syntaxin6 3' tagging analytical primer fwd

Janessa	CAGTCGGCAGAGCCTGAA	syntaxin6 3' tagging analytical primer rvs
Dr. Gras	AAGTTGCTCCTACAGAGCTGCAAGAG	SortLR 3' tagging sgRNA fwd
Dr. Gras	AAAACTCTTGCAGCTCTGTAGGAGCA	SortLR 3' tagging sgRNA rvs
Dr. Gras	TTCCGCGTCTGGCGCCGCCGCGATTCGACGAGGATAACGTCGAACTTCTTGCTAAAATTGGAAGTGGAGG	SortLR 3' tagging homology primer fwd
Dr. Gras	AAAGACATGCGAGACACGAAAGAGAGCCGTCTTCGGCGGAAGCTCCTACAATAACTTCGTATAATGTATGCTATACG	SortLR 3' tagging homology primer rvs
Dr. Gras	CTGAGCAGGAGACGTCTCT	SortLR 3' tagging analytical primer fwd
Dr. Gras	AGATTTCCTTTGCAGGCACA	SortLR 3' tagging analytical primer rvs
Janessa	CAGGTCCCAGCGAGCGGAAAGCTCCTTGTCGATCCCCGATATTCGACAAACGACCAGGAAGAAAGCATTCTGCCTGCATTGGGTGCG	GRASP-RFP fwd homology into UPRT locus
Janessa	GTTTATCCTCTTGAGGCGTGCTTTTTCCAGTCCGCGATTCCGTCAGCGGTCTGTCAAAAAAACTAGAGACCGCGGCTTATCTAGTTAAGGGAG	GRASP-RFP rvs homology into UPRT locus
Dr. Singer	AAGTTAATAGGGGTCTGTAGGTTAAG	formin2 3' tagging sgRNA fwd
Dr. Singer	AAAACTTAACCTACAGACCCCTATTA	formin2 3' tagging sgRNA rvs
Dr. Singer	CGCCACACACTTCGCCTGTGAGGCCTCCACCTGCGACGAATAGGGGTCTGGCTAAAATTGGAAGTGGAGGA	formin2 3' tagging homology primer fwd
Dr. Singer	AAGAAGTTAACAGAGGCGGGAAATCCGAGACATTTGATAGTTGGCCCTTAATAACTTCGTATAATGTATGCTA	formin2 3' tagging homology primer rvs
Dr. Singer	GGTGAAAGTTGTTCCCTCG	formin2 3' tagging analytical primer fwd
Dr. Singer	ATCCCTTTCCCTGCAGGAG	formin2 3' tagging analytical primer rvs
Janessa	AAGTTGCCAGGAAGAAAGCATTCTCCG	UPRT 1st exon sgRNA fwd
Janessa	AAAACGGAGAATGCTTTCTTCCTGGCA	UPRT 1st exon sgRNA rvs
Dr. Singer	AAGTTGTGGAGTTTGCCGGGGCTGCAG	SAG1 internal tagging sgRNA fwd
Dr. Singer	AAAACTGCAGCCCCGGCAAACTCCACA	SAG1 internal tagging sgRNA rvs
Dr. Singer	GGGGATCGCCTGAGAAGCATCACTGTACCGTGAAACTGGAGTTTGCCGGGGCTAAAATTGGAAGTGGAGGA	SAG1 internal tag homology primer fwd

Dr. Singer	ATGGAAACGTGACTGGCTGTTCCCGCAGCCGATTTTGCTGACCCTGCAGCCTTGTCGTCATCG TCTTTGTAGTCACCGGAAATCTCCAGAGTAGAC	SAG1 internal tag homology primer rvs
Janessa	CAGGTCCCAGCGAGCGGAAAGCTCCTTGTCGATCCCCGATATTCGACAAACGACCAGGAAGA AAGCATTCCCCCCTCGAGGTCGACG	CbEmerald for UPRT locus fwd
Janessa	GTTTATCCTCTTGAGGCGTGCTTTTTCCAGTCCGCGATTCCGTCAGCGGTCTGTCAAAAAAACT AGAGACGTGTCACTGTAGCCTGCCA	CbEmerald for UPRT locus rvs
Janessa	ATGCAGGAGCAGAAGCTCATCTCCGAGGAGGACCTGGCCATGGCCATGCATGGATCCGAAAT CGGTACTGG	Generation of GFP-Nanobody-Halo plasmid
Janessa	CACCACCACCTGAACCACCCCCTCCGCCTCCCCCACTGTAACCGGAAATCTCCAGAGTAGAC	Generation of GFP-Nanobody-Halo plasmid
Janessa	ATGCAGGAGCAGAAGCTCATCTCCGAGGAGGACCTGGCCATGGCCATGCATGTCCAACTGGT GGAGTCTGG	Generation of GFP-Nanobody-Halo plasmid
Janessa	ACGAAGTGTGTTTCCTTTGTCGATTTGAGAAGTGAGCACAACGGTGATTAATTAATTATTATTA GCTGGAGACGGTGACC	Generation of GFP-Nanobody-Halo plasmid
Janessa	CTCCACCAGTTGGACTTGATCCATGGCTCGAGATCTGAGTCCGGAGCCTCCCGAACCACCACC ACCACCACCACCTGAACCGGAAATCTCCAGAGTAGAC	Generation of GFP-Nanobody-Halo plasmid
Janessa	AAGTTCTTGCGGAAAACTACTCGTTGGCATTTTTTCTTGAATTCATGGCCATGCATGGATCCGA AATCGGTACTGG	Generation of GFP-Nanobody-Halo plasmid
Janessa	AAGTTGCATGCGCACTCAGAGCCTTG	AP4E 3' tagging sgRNA fwd
Janessa	AAAACAAGGCTCTGAGTGCGCATGCA	AP4E 3' tagging sgRNA rvs
Janessa	CTTCGACGGCGCAGCTGGCGGAGGCTGTAGCGGCGGCATGCCAAAGGCTCGCTAAAATTGG AAGTGGAGG	AP4E 3' tagging homology primer fwd
Janessa	TAGAGGCCTGGACGAGCAAAGAGAGAAACAAAGCGCTGCATGCGCACTCAATAACTTCGTAT AATGTATGCTATACG	AP4E 3' tagging homology primer rvs
Janessa	GCGGCACAGACACCTCTCG	AP4E 3' tagging analytical primer fwd
Janessa	GCGGTTGATCGACGCAGAAGA	AP4E 3' tagging analytical primer rvs

Acknowledgements

I would like to thank my supervisor, Prof. Markus Meiβner, for allowing me to do a PhD in your lab. Your excitement for science is infectious, and the daring with which you question everything is both admirable and enviable. I sincerely appreciate all our scientific discussions. Thank you.

I would like to thank Prof. Michael Boshart for generously accepting to be my Doktorvater, for all the level-headed advice and guidance you provided both during and outside of the TAC meetings.

Thank you also to Dr. Lilach Sheiner, my thesis advisor, and MSc. supervisor. I fell in love with *Toxoplasma* thanks to you, and decided to do a PhD at your encouragement. I am eternally grateful for your kind guidance and confidence in my abilities. Thank you also to all members of the Sheiner lab from 2017, especially Dr. Jana Ovciarikova and Dr. Alice Lacombe, for giving me the best introduction to, and teaching me how to take care of, this annoying, beautiful parasite.

Thank you to Prof. Nicolai Siegel, your sound advice and gentle words of wisdom were always appreciated, more than I can accurately convey here. Thank you for being one of my thesis advisors.

I would also like to thank our collaborators for their scientific support, and expertise, Prof. Dr. Andreas Klingl, and Dr. Ignasi Forne.

To all of the Meiβner lab; Elena, Simon, Mirko, Sujaan, Matthew, Mirjam, Julia, Miriam, Yuan, Peipei, Maresa, Javier, and Wei – for the wonderful lunch conversations, and for being amazing lab mates. Your kind words of advice will forever be cherished, and your tolerance of my complaining will forever be appreciated. Marzena, Angelika, and Heidi, for organizing all things lab, LMU, and boss-related, without whom we would not function. Pedro, the cutest, fluffiest, four-legged Meissner lab member, for the emotional support and puppy-dog eyes.

Thank you to everyone at BioDNA Laboratory services Ltd., but especially Dr. Marisa Cassar, and Dr. Claire Bartolo for guiding my first steps in the lab.

Dorita, Ritianne, Pauline, for your amazing friendships, laughs, listening ears, and shoulders to lean on for almost twenty years, thank you. Swathi, for walking this road with me since our MSc. days, thank you. Jasmine, for your attentive friendship, support, and confidence in me, thank you. Anna, Reinhold, Irene, for reminding me that there is more to life than work.

Thank you to my parents, my brother, and my grandmother, for your love, unwavering support, patience, and words of wisdom. I am here thanks to you. I dedicate this to you. I love you.

Curriculum Vitae

janessa.grech@para.vetmed.uni-muenchen.de / janessa.grech@gmail.com

EDUCATION and RESEARCH

2018 – present	**PhD.** Experimental Parasitology - Ludwig Maximilian University, Munich **Project:** A splitCas9-based screen identifies an essential actin-dependent Golgi protein
2016 – 2017	**MSc. Infection Biology (with Distinction)** University of Glasgow **Project:** Localising Ups2 and Mdm35 to the mitochondria of *Toxoplasma gondii*, and generating tools to study mitochondrial membrane contact sites
2008 – 2012	**BSc. (Hons) Biology and Chemistry (2:2)** University of Malta **Project:** Allele frequencies of a novel set of microsatellites to be used in forensic DNA analysis.

EMPLOYMENT

2012 – 2016	BioDNA Laboratory Services Ltd.

CONFERENCES

01-02/11/2018	ToxoUK – poster presentation ("A phenotypic screen to identify actin regulatory proteins")
19-22/06/2019	International Toxoplasma Congress (Toxo XV) – oral presentation ("A phenotypic screen to identify actin regulatory proteins")
05-06/05/2022	SPP2225 EXIT strategies for intracellular pathogens workshop – oral presentation ("A splitCas9 phenotypic screen in Toxoplasma gondii identifies proteins involved in host cell egress and invasion")
18-22/09/2022	Molecular Parasitology Meeting XXXIII (2022) – oral presentation ("Phenotypic screen identifies essential Golgi protein")

PUBLICATIONS

May 2022	Li W*, **Grech J***, Stortz JF*, Gow M, Periz J, Meissner M, Jimenez-Ruiz E. A splitCas9 phenotypic screen in *Toxoplasma gondii* identifies proteins involved in host cell egress and invasion. Nat Microbiol. 2022 May 10. doi: 10.1038/s41564-022-01114-y. PMID: 35538310. * - equal contributors
April 2022	Kehrer J, Formaglio P, Muthinja JM, Weber S, Baltissen D, Lance C, Ripp J, **Grech J**, Meissner M, Funaya C, Amino R, Frischknecht F. *Plasmodium* sporozoite disintegration during skin passage limits malaria parasite transmission. EMBO Rep. 2022 Apr 11:e54719. doi: 10.15252/embr.202254719. PMID: 35403820.